

Status of Thesis

Title of thesis

An Integrated Approach for Scheduling and Real-time Optimization in a Refrigerated Gas Plant

I **NOORYUSMIZA YUSOFF** (Matric No.: G1030258) hereby allow my thesis to be placed at the Information Resource Center (IRC) of Universiti Teknologi PETRONAS (UTP) with the following conditions:

1. The thesis becomes the property of UTP.
2. The IRC of UTP may make copies of the thesis for academic purposes only.
3. This thesis is classified as:

☒ Non-confidential

☐ Confidential. *Please fill in the following:*

If this thesis is confidential, please state the reason(s):

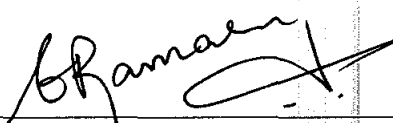
The contents of the thesis will remain confidential for {no. of years}

Remarks on disclosure:



Nooryusmiza Yusoff

Date: 28.09.2009



AP Dr M Ramasamy

Date: 28.09.2009


DR. M. RAMASAMY
Associate Professor
Chemical Engineering Department
Universiti Teknologi PETRONAS

UNIVERSITI TEKNOLOGI PETRONAS

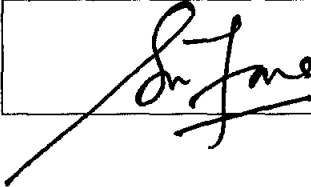
Approval by Supervisors

The undersigned certify that they have read, and recommend to the Postgraduate Studies Program for acceptance, a thesis entitle “**An Integrated Approach for Scheduling and Real-time Optimization in a Refrigerated Gas Plant**” by **Nooryusmiza Yusoff** for the fulfillment of the requirements for the degree of Doctor of Philosophy (PhD) in Chemical Engineering.

AP Dr. Marappagounder Ramasamy
Department of Chemical Engineering
Universiti Teknologi PETRONAS



AP Dr. Suzana Yusup
Department of Chemical Engineering
Universiti Teknologi PETRONAS



Date: 28.09.2009

UNIVERSITI TEKNOLOGI PETRONAS

**An Integrated Approach
for Scheduling and Real-time Optimization
in a Refrigerated Gas Plant**

By

Nooryusmiza Yusoff

A THESIS

SUBMITTED TO THE POSTGRADUATE STUDIES PROGRAM

AS A REQUIREMENT FOR THE

DEGREE OF DOCTOR OF PHILOSOPHY

IN CHEMICAL ENGINEERING

BANDAR SERI ISKANDAR

PERAK

SEPTEMBER 2009

Declaration of Originality

I hereby declare that the thesis is based on my original work except for quotations and citations, which have been duly acknowledged. I also declare that, to the best of my knowledge, it has not been previously or concurrently submitted for any other degree at UTP or other institutions.



Nooryusmiza Yusoff

Date: 28.09.2009

Acknowledgements

Reminiscing the early days of my journey, a master plan for my PhD study was only realized after several weeks of discussion with Prof. Dr. VR Radhakrishnan. He was my supervisor for almost a year. Unfortunately, our journey together was cut short when he passed away in late 2006. As if it was fated, I found a replacement in the form of AP Dr. M. Ramasamy who was incidentally recruited earlier by the late Prof. Radha. Jointly, Dr. Ramasamy and I continued the thesis work as charted *a priori*. In the middle of my journey, I came across an unfamiliar but a useful subject for my research work. The subject is called Taguchi method for design of experiment. With valuable inputs from AP Dr. Suzana Yusup, I managed to identify significance of optimization variables for applications in both model predictive control (MPC) and real-time optimization (RTO) studies.

To strengthen my practical knowledge, I endured four-month industrial training at Kerteh, Terengganu. There, I was attached at the Technical and Engineering Services Department helmed by Abdul Ghani. The training was wonderful as I gained first-hand experience in plant operation. On top of that, I had the opportunity to meet new acquaintance in Gas Processing Plant (GPP) of PETRONAS Gas Berhad. I treasured camaraderie with Wan Nasser, Manaf and Aishah who were instrumental in executing advanced process control (APC) project; Adam and Shahril who were experts in GPP process simulation; Zainuddin who was in charged of energy and loss management system (ELMS) project; Semail who took me to Yokogawa's Vigilant Plant Rollout at Kuantan, Pahang; Azhar and others who showed me around the Main Control Room; Aidi and Airi, old buddies from my undergraduate years in the U.S., who helped me gathering plant information; and last but not least, Charles, Zafran, Hafeez, Ikram, Joon-leong and Fauzi, who were my former students at Department of Chemical Engineering, UTP. In addition, I cherished advice from Prakash, Afifi and Lim on APC implementation issues during a two-day sharing trip to PETRONAS Penapisan Melaka.

I also wish to thank UTP management for granting me an opportunity to pursue PhD here. They could have sent me overseas just like they did to some of my colleagues.

However, I might have to pay the ‘price’ later by starting research afresh when I rejoin the faculty. On another note, it would have been difficult to complete this thesis work without encouragement and understanding of Dr. Shuhaimi Mahadzir who heads the Department of Chemical Engineering, UTP. I highly appreciate his empathy in supporting my six-month study extension.

Finally, I am grateful for moral support of my mother Aminah and mother-in-law Pura. Their daily prayers provide me strength and courage. Now that I seem to have accomplished my short-term goal, I would like to share words of wisdom of Imam Ahmad al-Hambali (780-855 A.D.) who contemplated that:

“A knowledgeable person who is aware of his knowledge and practices it, follow him.

A knowledgeable person who does not practice his knowledge, remind him.

A person who realizes that he lacks of knowledge but relentlessly seeking for it, guide him.

Someone who is ignorant but pretending to be a knowledgeable person, curse be upon him.”

Abstrak

Loji penyejukan gas (RGP) menghadapi cabaran-cabaran operasi melalui tiga cara iaitu: 1) di aliran masuk, gas mentah berbilang aliran dicampur-aduk hingga menyebabkan naik-turun dalam kadar aliran dan kandungan gas; 2) di dalam RGP, penutupan tidak berjadual sering terjadi akibat kepincangan peralatan; 3) di hiliran, kualiti produk yang ketat dikuatkuasakan oleh pelanggan-pelanggannya. Dari sudut perniagaan, RGP menandatangani pelbagai perjanjian dengan pengeluar-pengeluar gas mentah. Harga gas mentah berubah bergantung kepada kualiti gas dan tempoh kontrak. Harga-harga gas asli cecair yakni etana, propana, butana dan hasil pemeluwapan diapung kepada nilai-nilai pasaran. Sebaliknya, harga gas asli ditentukan oleh kerajaan.

Cabaran-cabaran ini memaksa RGP untuk meningkatkan kecekapan dan seterusnya mempertahankan keuntungan. Satu bidang yang dikenalpasti dalam peningkatan kecekapan ialah semasa perancangan pengendalian. Perancangan sebegini mengemukakan masalah penjadualan jangka pendek dan selanjut di mana sasaran-sasaran dilaksanakan secara langsung oleh alat-alat kawalan regulatori. Walaupun amalan ini diterimapakai sekarang, faedah ekonomi boleh dipertingkatkan dengan kekerapan penilaian semula sasaran-sasaran loji melalui pengoptimuman masa-nyata (RTO). Oleh kerana penjadualan diusahakan pada skala masa yang lebih panjang (hari-minggu) berbanding dengan RTO (jam-hari) dan kawalan (saat-minit), integrasi ketiga-tiga lapisan automasi ini adalah sukar.

Tesis ini mencadangkan satu rangkakerja yang menyepadukan penjadualan dan RTO untuk RGP. Pada lapisan atas, satu model dinamik RGP dikemukakan kepada tiga jenis masalah penjadualan yakni aliran masuk, beban, dan mod. Penjadualan aliran masuk merujuk kepada pencampuran pecahan-pecahan tertentu gas mentah yang rendah dan tinggi dengan kandungan hidrokarbon pada kadar loji biasa iaitu 280 tan/jam. Penjadualan beban merujuk kepada mempelbagaikan kadar aliran gas mentah rendah kandungan hidrokarbon sebanyak ± 30 tan/jam. Penjadualan mod merujuk kepada mengubah mod pengendalian loji daripada gas asli kepada gas asli cecair, dan sebaliknya.

Sasaran-sasaran daripada lapisan penjadualan dinamik dihulurkan kepada lapisan RTO berkeadaan mantap. Ketidakteraturan antara model dan loji dikurangkan dengan cara menggantikan nilai-nilai pembolehubah utama antara model berdinamik dan model

berkeadaan mantap. Trajektori-trajektori optimum diperolehi menggunakan algoritma pemrograman kuadratik berjujukan dengan kekangan. Trajektori-trajektori ini dilaksanakan secara berasingan oleh skim kawalan ramalan bermodel (MPC) dan alat-alat kawalan berkadar-kamiran (PI) untuk perbandingan. Lapan kajian kes bagi setiap masalah penjadualan dipersembah untuk menunjukkan kemujaraban teknik yang dicadangkan.

Abstract

A refrigerated gas plant (RGP) faces operational challenges on three fronts namely: 1) at inlet, multiple feed gas streams are mixed causing fluctuation in flow and composition; 2) within RGP, unscheduled shutdowns due to equipment malfunction often occur; 3) at outlet, strict product specifications are enforced by its customers. In business aspect, RGP enters into diverse agreements with producers. Prices of feed gas vary depending upon quality of gas and tenure of contracts. Prices of liquids namely ethane, propane, butane and condensates are floated to market values. In contrast, price of sales gas is tightly regulated by government.

These challenges forces RGP to improve its efficiency in order to sustain profitability. An identified area of improvement is during operational planning. This type of planning poses a short-term and continuous scheduling problem in which preconfigured setpoints are directly implemented by regulatory controllers. While this practice is currently accepted, economic benefits can be further realized by frequent reevaluation of plant states through real-time optimization (RTO). Since scheduling is performed at a much larger time-scale (days-weeks) as compared with RTO (hours-days) and control (seconds-minutes), integration of these three automation layers is difficult.

This thesis proposes an integrated framework of scheduling and RTO of the RGP. At top layer, a dynamic model of RGP is subjected to three types of scheduling problems namely input, load, and mode. Input scheduling refers to mixing of certain fractions of lean and rich feed gas streams at normal plant load of 280 ton/h. Load scheduling refers to varying flow rate of lean feed gas stream by ± 30 ton/h. Mode scheduling refers to change of plant operating mode from sales gas to natural gas liquids, and vice-versa. Setpoints from dynamic scheduling layer are passed to steady-state RTO layer. Modeling mismatch is minimized by rigorously exchanging values of key variables between dynamic and steady-state models. Optimal trajectories of setpoints are obtained using sequential quadratic programming algorithm with constraints. These trajectories are disjointedly implemented by model predictive control scheme and proportional-integral controllers for comparison. Eight case studies for each scheduling problem are performed to illustrate efficacy of the proposed approach.

TABLE OF CONTENTS

Status of Thesis	i
Approval by Supervisors	ii
Title	iii
Declaration of Originality	iv
Dedication	v
Acknowledgment	vi
Abstrak (in <i>Bahasa Malaysia</i>)	viii
Abstract (in <i>English</i>)	x
Table of Contents	xi
List of Tables	xv
List of Figures	xviii
List of Symbols	xxiii
CHAPTER 1: INTRODUCTION	
1.1 Overview	1
1.2 Motivation	2
1.3 Issues with Integrated Framework of Scheduling and RTO	4
1.4 Thesis Objectives and Outline	6
CHAPTER 2: LITERATURE REVIEW	
2.1 Plant Automation	13
2.1.1 Integration at Higher Decision-making Levels	15
2.1.2 Integration at Lower Decision-making Levels	18
2.1.3 Integration between Top and Middle Decision-making Levels	22
2.2 Concluding Remarks	24

CHAPTER 3: RGP MODELING AND CONTROL

3.1	Introduction	26
3.2	Process Description	28
3.3	Modeling	29
3.3.1	Steady-state Modeling	29
3.3.2	Dynamic Modeling	35
3.4	RGP Control Philosophies	46
3.4.1	Plant load control	46
3.4.2	Demethanizer overhead pressure control	48
3.4.3	Sales Gas Quality Control	49
3.4.4	Plant Temperature Control	51
3.5	Model Predictive Control	53
3.5.1	System Identification	56
3.5.1.1	Step Test	56
3.5.1.2	PRBS Test	61
3.5.2	MPC Design	67
3.5.2.1	MPC Formulation	67
3.5.2.2	Design and Tuning Parameters	68
3.5.2.3	Set Point Tracking	69
3.6	Concluding Remarks	74

CHAPTER 4: REAL-TIME OPTIMIZATION

4.1	Introduction	75
4.2	RTO Problem Formulation	75
4.3	Parametric Design	81
4.3.1	Taguchi Method	82

4.3.2	Analyses of Taguchi Results	87
4.3.2.1	Effect of Noise Factors	89
4.3.2.2	Average Profit Analysis	89
4.3.2.3	Signal-to-Noise Ratio (SNR) Analysis	93
4.3.3	Validation	98
4.3.4	Summary of Parametric Design	105
4.4	RTO Case Study	108
4.4.1	RTO Results and Discussion	110
4.4.1.1	Economics	110
4.4.1.2	Process	114
4.5	Concluding Remarks	118

CHAPTER 5: INTEGRATED APPROACH FOR SCHEDULING AND RTO

5.1	Introduction	120
5.2	Integration of Scheduling and RTO	121
5.3	Mode Scheduling	124
5.3.1	Scheduling from NGLs to SG Mode (Case A)	124
5.3.1.1	Process	124
5.3.1.2	Economics	129
5.3.2	Scheduling from SG to NGLs Mode (Case B)	130
5.3.2.1	Process	130
5.3.2.2	Economics	134
5.4	Load Scheduling	135
5.4.1	Load scheduling from 280 to 250 ton/h (Case C)	136
5.4.1.1	Process	136
5.4.1.2	Economics	137

5.4.2	Load scheduling from 280 to 310 ton/h (Case D)	138
5.4.2.1	Process	138
5.4.2.2	Economics	138
5.5	Input Scheduling	139
5.5.1	Input scheduling of feed gas streams A and B (Case E)	140
5.5.1.1	Process	140
5.5.1.2	Economics	141
5.5.2	Input scheduling of feed gas streams A and C (Case F)	141
5.5.2.1	Process	141
5.5.2.2	Economics	142
5.6	Concluding Remarks	143
CHAPTER 6: CONTRIBUTIONS AND FUTURE RESEARCH AVENUES		
6.1	Contributions	144
6.2	Future Research Avenues	152
REFERENCES		155
APPENDICES		
A	Peng-Robinson Equation of State (EOS)	166
B	Additional Results from Chapter 5	168
C	List of Publications and Presentations	186

LIST OF TABLES

Table 3.1	Compositions of feed gas streams	29
Table 3.2	Steady-state specifications and normal operating conditions (NOC) around major equipment	31
Table 3.3	Sizing of demethanizer C-101 column and reboiler E-104	36
Table 3.4	Sizing of absorber C-102 column	37
Table 3.5	Sizing of refrigeration cooler E-102 and air cooler E-106	38
Table 3.6	Dynamic specifications of coldboxes E-101, E-103 and E-105	39
Table 3.7	Suggested tuning parameter settings	44
Table 3.8	Control and tuning parameters	47
Table 3.9a	Control and tuning parameters	49
Table 3.9b	Surge control parameters	49
Table 3.10	Control and tuning parameters	51
Table 3.11	Control and tuning parameters	53
Table 3.12	Open-loop responses with u_1 move	59
Table 3.13	Open-loop responses with u_2 move	59
Table 3.14	FOPTD model parameters	61
Table 3.15	Design parameters of PRBS inputs	63
Table 3.16	Process gains K_p of FOPTD, ARX and state-space (SS) models.	65
Table 3.17	MPC design and tuning parameters	68
Table 3.18	Nominal input and output values	69
Table 3.19	Ranges of actual input duty values	69
Table 3.20	Integral of Squared Errors (ISEs) [$(^\circ\text{C})^2 \cdot \text{min}$] for different set point changes	70
Table 3.21	Average input duties (kW/min) for different set point changes	70
Table 4.1	Economic data	77

Table 4.2	Values and bounds of constraint variables	78
Table 4.3	Compositions of feed gas streams used for parametric design	80
Table 4.4	Description of factors and levels for RGP	83
Table 4.5	Taguchi internal arrays showing levels of controllable factors	84
Table 4.6	Taguchi external arrays showing levels of noise factors	84
Table 4.7	Results of Taguchi crossed-orthogonal-array experiments	88
Table 4.8	Analysis of means for average profit	90
Table 4.9	Analysis of variance for average profit	91
Table 4.10	Results of signal-to-noise ratio (SNR) analysis	94
Table 4.11	Analysis of means (ANOM) for SNR	96
Table 4.12	Analysis of variance (ANOVA) for SNR	96
Table 4.13	Maximum differences of averages of controllable factors for Cases 1 to 9	99
Table 4.14	RGP profit values from experiments (HYSYS) and Taguchi method (ANOM) at optimal conditions	102
Table 4.15	Bounds and description of optimization variables	110
Table 4.16	Values (RM/min) of economic parameters for base and RTO case studies	111
Table 4.17	Values of optimization variables for base and RTO case studies	114
Table 4.18	Values of constraint variables for base and RTO case studies	115
Table 4.19	Values of selected plant model outputs for base and RTO case studies	116
Table 5.1	Values of target variables for base and RTO cases in sales gas mode	125
Table 5.2	Average values (RM/min) of economic parameters over 510 min simulation time	129
Table 5.3	Values of target variables for base and RTO cases in natural gas liquids mode	131

Table 5.4	Average values (RM/min) of economic parameters over 510 min simulation time (Case B)	134
Table 5.5	Values of target variables for base and RTO cases under 250 ton/h load	137
Table 5.6	Average values (RM/min) of economic parameters over 510 min simulation time (Case C)	137
Table 5.7	Values of target variables for base and RTO cases (Case D)	138
Table 5.8	Average values (RM/min) of economic parameters over 510 min simulation time	139
Table 5.9	Values of target variables for base and RTO cases (Case E)	140
Table 5.10	Average values (RM/min) of economic parameters for Case E over 510 min simulation time	141
Table 5.11	Values of target variables for base and RTO case studies (Case F)	142
Table 5.12	Average values (RM/min) of economic parameters over 510 min simulation time	143
Table B.1	Values of optimization variables for Case A	168
Table B.2	Values of constraint variables for Case A	168
Table B.3	Values of optimization variables for Case B	169
Table B.4	Values of constraint variables for Case B	169
Table B.5	Values of optimization variables for Case C	170
Table B.6	Values of constraint variables for Case C	170
Table B.7	Values of optimization variables for Case D	171
Table B.8	Values of constraint variables for Case D	171
Table B.9	Values of optimization variables for Case E	172
Table B.10	Values of constraint variables for Case E	172
Table B.11	Values of optimization variables for Case F	173
Table B.12	Values of constraint variables for Case F	173

LIST OF FIGURES

Figure 1.1	Plant automation pyramid	2
Figure 1.2	Flowchart of case studies for three scheduling problems	8
Figure 1.3	A simplified diagram of a gas processing plant	10
Figure 2.1	Integrated planning and scheduling	16
Figure 2.2	Integration of RTO and MPC	18
Figure 2.3	Integrated scheduling and RTO	23
Figure 3.1	Process flow diagram of RGP	28
Figure 3.2	Composite curves at the coldboxes	32
Figure 3.3	Temperature profile of demethanizer C-101. Square markers denote plant data. Solid line represents simulated values	33
Figure 3.4	Head (a) and efficiency (b) curves of booster compressor K-102. Current operating point is shown as a solid circle	40
Figure 3.5	Head (a) and efficiency (b) curves of demethanizer bottom pump P-101. Current operating point is shown as a solid circle	41
Figure 3.6	Head (a) and efficiency (b) curves of absorber bottom pump P-102. Current operating point is shown as a solid circle	42
Figure 3.7	Process and instrumentation diagram of RGP	45
Figure 3.8	Plant load control scheme	47
Figure 3.9	SRC-101 split range setup	47
Figure 3.10	Demethanizer overhead pressure control scheme	48
Figure 3.11	Sales gas quality control scheme	50
Figure 3.12	SRC-102 split range setup	50
Figure 3.13	Plant temperature control scheme	52
Figure 3.14	SRC-103 split range setup	52
Figure 3.15	Open-loop step responses of outputs y_1 (top) and y_2 (bottom) due to various moves of input u_1	57

Figure 3.16	Open-loop step responses of outputs y_1 (top) and y_2 (bottom) due to various moves of input u_2	58
Figure 3.17	Variation of process gains (K_p) with respect to changes in cooler duty (u_1) and reboiler duty (u_2) from nominal value.	60
Figure 3.18	Variation of process time constants (τ_p) with respect to changes in cooler duty (u_1) and reboiler duty (u_2) from nominal value.	60
Figure 3.19	Variation of process time delays (τ_d) with respect to changes in cooler duty (u_1) and reboiler duty (u_2) from nominal value.	60
Figure 3.20	PRBS signals on inputs u_1 (cooler E-102 duty) and u_2 (reboiler E-104 duty), as well as measured input disturbance u_3 (plant load). Only the first 300 out of 1248 samples are illustrated for clarity.	64
Figure 3.21	Responses of outputs y_1 (after cooler E-102 stream temperature) and y_2 (demethanizer tray 35 temperature) due to PRBS signals. Only the first 300 out of 1248 samples are illustrated for clarity.	65
Figure 3.22	Step responses of process models: ARX (dotted) and state-space (solid)	66
Figure 3.23	Closed-loop responses for a change in y_1 (Case 1) using ARX (thin line) and state-space (thick line) models as compared with output setpoints and input nominal values (dotted line)	71
Figure 3.24	Closed-loop responses for a change in y_2 (Case 2) using ARX (thin line) and state-space (thick line) models as compared with output setpoints and input nominal values (dotted line)	72
Figure 3.25	Closed-loop responses for simultaneous changes in y_1 and y_2 (Case 3) using ARX (thin line) and state-space (thick line) models as compared with output setpoints and input nominal values (dotted line)	73
Figure 4.1	Modeling and optimization process flowchart	76
Figure 4.2	Flow diagram of Taguchi method	82
Figure 4.3	Response plot for average profit analysis	101
Figure 4.4	Response plot for SNR analysis	103
Figure 4.5	RGP profits under optimal configurations for Cases 1 to 9	107
Figure 4.6	RGP revenue due to sales gas (SG), ethane (C2), propane (C3), butane (C4) and condensates (C5+)	112

Figure 4.7	RGP expenses due to costs of feed gas (FG) streams A, B and C, and duties of cooler E-102Q, demethanizer reboiler E-104Q, compressor K-102Q and turboexpander KT-101Q	113
Figure 5.1	Structure of integrated scheduling and real-time optimization (RTO) approach. Set points may be implemented via model predictive control (MPC) scheme or, alternatively, regulatory controllers.	122
Figure 5.2	Closed-loop responses of PI (thin line) and MPC (thick line) controllers on temperature of feed gas stream exiting cooler E-102 (y_2) and temperature of demethanizer C-101 tray 35 (y_4) for Cases A1 and A2 (scheduling only); u_2 =cooler E-102 duty in %; u_4 =reboiler E-104 duty in %	127
Figure 5.3	Closed-loop responses of PI (thin line) and MPC (thick line) controllers on temperature of feed gas stream exiting cooler E-102 (y_2) and temperature of demethanizer C-101 tray 35 (y_4) for Cases A3 and A4 (integrated approach); u_2 =cooler E-102 duty in %; u_4 =reboiler E-104 duty in %	128
Figure 5.4	Dynamic trajectories of RGP profit for Case A	130
Figure 5.5	Closed-loop responses of PI (thin line) and MPC (thick line) controllers on temperature of feed gas stream exiting cooler E-102 (y_2) and temperature of demethanizer C-101 tray 35 (y_4) for Cases B1 and B2 (scheduling only); E-102Q=cooler E-102 duty in %; E-104Q=reboiler E-104 duty in %	132
Figure 5.6	Closed-loop responses of PI (thin line) and MPC (thick line) controllers on temperature of feed gas stream exiting cooler E-102 (y_2) and temperature of demethanizer C-101 tray 35 (y_4) for Cases B3 and B4 (integrated approach); E-102Q=cooler E-102 duty in %; E-104Q=reboiler E-104 duty in %	133
Figure 5.7	Dynamic trajectories of RGP profit for Case B	135
Figure 6.1	Relative profit margins of Cases A to F as compared with respective base cases	149
Figure 6.2	Case-average profit values (RM/min) for Cases A to F	150

Figure B.1	Closed-loop responses of PI (thin line) and MPC (thick line) controllers on temperature of feed gas stream exiting cooler E-102 (y_2) and temperature of demethanizer C-101 tray 35 (y_4) for Cases C1 and C2 (scheduling only); u_2 =cooler E-102 duty in %; u_4 =reboiler E-104 duty in %	174
Figure B.2	Closed-loop responses of PI (thin line) and MPC (thick line) controllers on temperature of feed gas stream exiting cooler E-102 (y_2) and temperature of demethanizer C-101 tray 35 (y_4) for Cases C3 and C4 (integrated approach); u_2 =cooler E-102 duty in %; u_4 =reboiler E-104 duty in %	175
Figure B.3	Closed-loop responses of PI (thin line) and MPC (thick line) controllers on temperature of feed gas stream exiting cooler E-102 (y_2) and temperature of demethanizer C-101 tray 35 (y_4) for Cases D1 and D2 (scheduling only); E-102Q=cooler E-102 duty in %; E-104Q=reboiler E-104 duty in %	176
Figure B.4	Closed-loop responses of PI (thin line) and MPC (thick line) controllers on temperature of feed gas stream exiting cooler E-102 (y_2) and temperature of demethanizer C-101 tray 35 (y_4) for Cases D3 and D4 (integrated approach); E-102Q=cooler E-102 duty in %; E-104Q=reboiler E-104 duty in %	177
Figure B.5	Closed-loop responses of PI (thin line) and MPC (thick line) controllers on temperature of feed gas stream exiting cooler E-102 (y_2) and temperature of demethanizer C-101 tray 35 (y_4) for Cases E1 and E2 (scheduling only); u_2 =cooler E-102 duty in %; u_4 =reboiler E-104 duty in %	178
Figure B.6	Closed-loop responses of PI (thin line) and MPC (thick line) controllers on temperature of feed gas stream exiting cooler E-102 (y_2) and temperature of demethanizer C-101 tray 35 (y_4) for Cases E3 and E4 (integrated approach); u_2 =cooler E-102 duty in %; u_4 =reboiler E-104 duty in %	179
Figure B.7	Closed-loop responses of PI (thin line) and MPC (thick line) controllers on temperature of feed gas stream exiting cooler E-102 (y_2) and temperature of demethanizer C-101 tray 35 (y_4) for Cases F1 and F2 (scheduling only); E-102Q=cooler E-102 duty in %; E-104Q=reboiler E-104 duty in %	180
Figure B.8	Closed-loop responses of PI (thin line) and MPC (thick line) controllers on temperature of feed gas stream exiting cooler E-102 (y_2) and temperature of demethanizer C-101 tray 35 (y_4) for Cases F3 and F4 (integrated approach); E-102Q=cooler E-102 duty in %; E-104Q=reboiler E-104 duty in %	181

Figure B.9	Dynamic trajectories of RGP profit for Case C	182
Figure B.10	Dynamic trajectories of RGP profit for Case D	183
Figure B.11	Dynamic trajectories of RGP profit for Case E	184
Figure B.12	Dynamic trajectories of RGP profit for Case F	185

LIST OF SYMBOLS

Nomenclature

α	filter constant
α_s	a multiplier between closed-loop and open-loop response times
β_s	a factor representing frequency of an input
c	constraint variables
C_k^m	percentage contribution of factor k in case m
C_v	valve sizing coefficient
D	delayed factor
ΔP	frictional pressure loss, which is pressure drop minus static head
$\Delta \mathbf{u}_k$	first input moves
$\Delta \mathbf{u}_{k+j}$	predicted input moves
E	expenses
E^m	error for case m
\mathbf{e}_{k+j}^u	deviations of future inputs from desired steady-state inputs
\mathbf{e}_{k+j}^y	deviations of future model outputs from a reference trajectory
f_E	an economic objective function
f_m	steady-state plant model
F	flow rate
g_E	a set of inequality constraints
k	conductance or reciprocal of resistance
K_c	controller gain
K_p	process gain
L	number of levels
M	number of experiments in external array (Taguchi method) or length of control horizon (MPC)
N	number of experiments in internal arrays
N_R	number of repeated level
n_r	number of shift registers
n_u	number of inputs
n_y	number of outputs
\mathbf{p}	constant plant parameters
P	length of prediction horizon (MPC) or profit (RTO)
P_s	period
\mathbf{Q}, \mathbf{R} and \mathbf{S}	positive semi-definite weighting matrices
R	revenues
R_k	ranking of factor k
S_k	sum of squares of profit due factor k
t_{OLST}^{\max}	maximum open-loop settling time
t_{sw}	switching time
τ_i	integral time constant
τ_d	derivative time constant
τ_{dom}	dominant time constants

u	manipulated variables or inputs
u _{<i>k+j</i>}	future inputs
u ^{<i>s</i>}	desired steady-state inputs
v	measured disturbance variables or input noise
w	unmeasured disturbance variables or process noise
V _{<i>k</i>} ^{<i>m</i>}	variance of factor <i>k</i> in case <i>m</i>
ω	frequency
x	state variables
\bar{x} ^{<i>m</i>}	average of profit in case <i>m</i>
\bar{x} _{<i>kl</i>} ^{<i>m</i>}	average of profit due to factor <i>k</i> at level <i>l</i> in case <i>m</i>
\bar{x} _{<i>k</i>} ^{<i>m</i>}	average of profit due to factor <i>k</i> over all levels <i>L</i> in each case <i>m</i>
x _{<i>opt</i>} ^{<i>m</i>}	optimal profit in case <i>m</i>
ξ	measurement noise
y	controlled variables or outputs
y _{<i>k+j</i>}	future model outputs
y _{<i>k</i>} ^{<i>m</i>}	measured outputs
y _{<i>k+j</i>} ^{<i>r</i>}	reference trajectory
y _{<i>k</i>} ^{<i>sp</i>}	setpoints/targets
z	algebraic state variables

Indices

<i>j</i>	prediction instant (MPC)
<i>k</i>	factor (Taguchi method) or sampling time (MPC)
<i>l</i>	level (Taguchi method)
<i>m</i>	column in external array or case number (Taguchi method)
<i>n</i>	row in internal array or experiment number (Taguchi method)

Abbreviations

AGRU	acid-gas removal unit
ANOM	analysis of means
ANOVA	analysis of variance
APC	advanced process control
ARX	autoregressive exogenous
COM	component object module
CTU	condensate treatment unit
CV	controlled variable
DAE	differential algebraic equation
DOF	degrees of freedom
EKF	extended Kalman filter
ERP	enterprise resource planning

FC	flow controller
FG	feed gas stream
FOPTD	first order plus time delay
GHV	gross heating value
GMN	generalized multi-level noise
GPP	gas processing plant
GSP	gas subcooled process
IPOPT	Interior-Point OPTimizer
ISE	integral of squared error
J-T	Joule-Thompson
KKT	Karush-Kuhn-Tucker
LMTD	log-mean temperature difference
LNG	liquefied natural gas
LTSU	low temperature separation unit
MIDO	mixed integer dynamic optimization
MILP	mixed integer linear programming
MIMO	multi-input-multi-output
MINLP	mixed integer nonlinear programming
MIP	mixed integer programming
MMbtu	million British thermal units
MPC	model predictive control
MSD	mean squared deviation
NCO	necessary conditions of optimality
NLP	nonlinear programming
OPC	object-link-embedded for process control
OPEX	operational expenses
OR	operations research
P&ID	process and instrumentation diagram
PC	pressure controller
PFD	process flow diagram
PFD	process flow diagram
PID	proportional-integral-derivative
PID	proportional-integral-derivative
PRBS	pseudo-random binary sequence
PRU	product recovery unit
PRU	product recovery unit
PSE	process systems engineering
RC	ratio controller
RGP	refrigerated gas plant
RM	Ringgit Malaysia
RTO	real-time optimization
SC	surge controller
SCM	supply chain management
SGCU	sales gas compression unit
SNOPT	Sparse Nonlinear OPTimizer
SNR	signal-to-noise ratio
SP	setpoint

SQP	sequential quadratic programming
SRC	split-range controller
SS	state space
TC	temperature controller

CHAPTER 1

INTRODUCTION

1.1 Overview

Planning is a prerequisite for completing work on time. An old adage “If you fail to plan, you plan to fail” is useful and still valid. There are three levels of planning namely strategic, tactical and operational. Planning differs from forecasting in the sense that the former largely relies on facts and contractual agreements whereas the latter involves an element of speculation. Strategic planning deals with process of making major business decisions such as contractual agreement, joint venture, merger and acquisition. The time horizon varies from months to years. Tactical planning is a company-wide strategy that set operating performance targets, and coordinates manufacture, sales and distribution of products. These activities take weeks to months of planning. Operational planning, often called scheduling, is a plantwide strategy that decides on timing of certain activities and processing of specific raw materials in order to cope with demands. This type of planning can be executed within days to weeks.

The relatively shorter timeframe of scheduling makes it a good candidate for integration with lower levels of decision-making tasks. Economic benefits are enormous depending on the levels of integration and types of industry. For a very large plant, integration of planning, scheduling and control strategies can increase profitability to as high as US\$10 for every ton of feed (Shobrys and White, 2000). Previous efforts on integration are limited due to five technical limitations namely: 1) immature capabilities on analytical techniques, 2) relatively slow computer speed, 3) underdeveloped system of information management, 4) unfriendly user interface, and 5) difficult connectivity between applications. Despite all of these, the economic incentive is large enough to generate strong research interests for studying integration of some, if not all, layers of process automation hierarchy.

1.2 Motivation

The current work is motivated by the ultimate desire of process systems engineering researchers to integrate all levels of plant automation (Figure 1.1) as a single-level control (Tousain, 2002). With the measurement and actuation processes denoted as level 0, the remaining levels are: 1) regulatory control, 2) advanced process control (APC), 3) real-time optimization (RTO) and 4) enterprise resource planning (ERP). Early emphasis was given to integration of regulatory control and APC due to proximity of their respective time scales as well as potential benefits in economics and plant stability. Here, an APC strategy called model predictive control (MPC) scheme overtakes all control calculations and passes optimal targets to regulatory controllers for implementation. Direct execution of targets from an MPC scheme to control valves is currently prohibited due to safety and reliability concerns (Tatjewski, 2008).

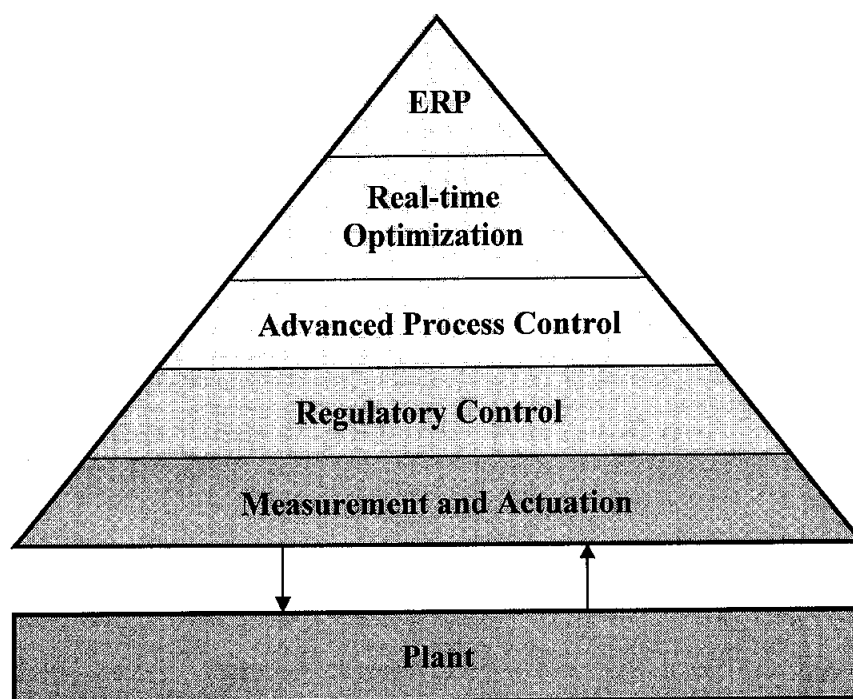


Figure 1.1: Plant automation pyramid

Integration of MPC and RTO brings in additional benefits to process industries. This approach entails combining process modeling, process control and plantwide economic optimization into a single platform. Operational disturbances are handled

by MPC whereas external disturbances such as market swing are taken care of by RTO in a unified way. If both MPC and RTO are to be solved simultaneously, the resulting problem is a dynamic optimization problem. For a relatively difficult process involving a two-phase reactor such as the Tennessee Eastman challenge (Downs and Vogel, 1993), the dynamic optimization problem can be transformed into a large-scale nonlinear programming and solved using standard solvers such as Sparse Nonlinear OPTimizer (SNOPT) or Interior-Point OPTimizer (IPOPT). However, for a highly nonlinear and much larger-scale problem, the simultaneous approach may face computational intractability. For industrial cases such as natural gas processing, a formulation of static RTO problem is more practical because a gas processing plant is essentially intended to operate in steady states.

At the ERP level, integration of production planning and scheduling is a popular subject in operations research field. The emphasis is on logistics and distributions, which typically involve linear and steady-state models (Grossmann, 2005). At planning sublevel, a so-called master problem is formulated for supply chain management based on a *big-bucket* time grid (e.g., 1 week). Targets from the master problem are processed at the more detailed scheduling sublevel based on a *small-bucket* time grid (e.g., 1 hour). A link between planning and scheduling is made through constraints on production resources, operational events, raw materials and market demands (Amaro and Barbosa-Povoa, 2008; Maravelias and Sung, 2009). These constraints are used for enforcing production targets at the end of a scheduling horizon (e.g., 1 week) in each planning period. The scheduling decisions are performed repeatedly when a new set of targets are specified at each subsequent planning period until the end of a planning horizon (e.g., 1 month).

Currently, the production targets are implemented using MPC schemes and/or regulatory controllers. This top-down approach is hierarchical in the sense that production targets are executed sequentially with manual feedbacks from operation personnel. The feedbacks are important to ascertain whether operating setpoints that are determined at the end of a scheduling horizon are practical based on some heuristics and/or design specifications. It is also important to ensure that the operating setpoints such as flow rates, temperatures and pressures are globally optimal. The optimal setpoints can only be determined by executing an RTO procedure based on

scheduling decisions. If scheduling and RTO problems are solved simultaneously, tremendous benefits in the range of 0.10-0.15 US\$/barrel for a typical refinery can be achieved (Moro, 2003). However, several challenges must be overcome in order to solve an integrated problem of this magnitude.

1.3 Issues with Integrated Framework of Scheduling and RTO

A scheduling problem is typically formulated as a mixed integer programming (MIP) problem due to presence of binary decision variables. On the other hand, an RTO problem can be formulated as either a steady-state or dynamic optimization problem. If the latter approach is selected, the integrated framework of scheduling and RTO leads to a mixed integer dynamic optimization (MIDO) problem. A strategy to solve a small MIDO problem has been demonstrated in, for example, calculations of optimal grade transition policies and control configurations for a continuous polymerization reactor (Chatzidoukas et al., 2003). Here, the MIDO problem is transformed into a mixed integer linear programming (MILP) problem that is solved using standard methods such as generalized Benders decomposition.

In a nutshell, the production targets at the end of a scheduling horizon are not implemented immediately. They are passed down to the RTO layer for online optimization of operating setpoints. This sequential approach links production and economic objectives as well as plant operations through a nonlinear first-principle model of an operating unit. In other words, the optimization is performed locally at an individual unit instead of globally at plantwide scale. It should be noted that a typical plant comprises several large and small operating units. The objectives of these individual units are often conflicting. A set of solutions to multiple MILP problems based on several single units can thus result in suboptimal solutions or infeasible operations for the entire plant (Pinto et al., 2000).

To overcome this issue, the production targets must be implemented based on an integrated framework of scheduling and RTO with the latter being performed using a plantwide model that constitutes the entire network of individual units. However, applicability of this strategy to a large-scale integrated plant is hindered with the following limitations:

1. *Difficulties in developing rigorous dynamic models of large process units:* A rigorous first-principle dynamic model for a large unit is difficult to develop. In fact, some of the operating units such as liquefied natural gas (LNG) heat exchangers, polymerization reactors and fluid catalytic crackers are process specific. It is also common for these units to adopt proprietary technologies from third parties and thus making them more expensive to be modeled. On the other hand, even if dynamic models of these units are available in open literature, customization of these units to suit the current process is generally required.

2. *Difficult connectivity among various applications and dynamic models of large individual units into a single process flowsheet:* There are two aspects on this issue. First, a simulation platform may be useful for modeling the processes but it may be lacking an optimization routine. As a result, another application from a different platform is required for this purpose. The second aspect relates to integration of various dynamic models of small, medium and large process units into a single flowsheet. In many cases, some medium and large operating units have to be modeled in a different software environment due to the following factors: 1) unavailability of built-in models in the current platform, 2) the requirement of more rigorous models for certain units like air coolers and shell-and-tube heat exchangers, and 3) the need for employing different thermodynamic property packages for different processes. The connectivity issue must be resolved *a priori* before solving any global optimization problem at the RTO level.

3. *High computational load in executing an online optimization procedure, especially for large-scale nonlinear problems:* In literature, it is common to solve MIDO problems based on mathematical programming approaches. Here, the first-principle dynamic models are used for estimating process parameters and calculating optimal targets of the plant. For process industries, the dynamic models normally take the form of stiff and high order differential algebraic equations (DAEs). As the number of DAEs increases to a certain extent, the computational load may increase exponentially depending on:

1) degrees of nonlinearity of the models, and 2) techniques used for speeding up the convergence rate. This situation renders the optimization problems intractable and therefore preventing the implementation of optimal targets at the control level.

4. *Concerns on model and process uncertainties:* In process industries, uncertainties can be instigated from various sources. As such, a suitable classification of uncertainties was proposed by Pistikopoulos (1995) as follows: 1) model-inherent uncertainty such as physical properties, kinetic constants and mass/heat transfer coefficients, 2) process-inherent uncertainty such as flow rate, temperature, pressure, steam quality and processing time, 3) external uncertainty such as feed stream availability, product demands, prices of feed stocks and products as well as environmental factors, and 4) discrete uncertainty such as equipment availability and absence of operation personnel. These aspects of uncertainties are often left out during a deterministic optimization procedure, which only considers known parameters.

1.4 Thesis Objectives and Outline

The main goal of this thesis is to provide a means for an integrated framework of scheduling and RTO. Out of the four technical limitations discussed in Section 1.3, the current integrated approach attempts to address the first three. To overcome the first two limitations, rigorous steady-state and dynamic first-principle models of all process units are developed in a single HYSYS simulation platform. The dynamic model is built on top of the high-fidelity steady-state model. Dimensions of operating units are specified mostly based on information retrieved from Mechanical Engineering Handbooks and Technical Datasheets of the actual plant. Mismatch between the steady-state and dynamic models is minimized by sufficiently transferring values of key variables. This approach eliminates potential errors that could arise from transferring data manually. Communication between different simulation packages is executed via component object module (COM) technology.

Another issue that hinders the adoption of integrated approach of scheduling and RTO is computing speed when handling online calculations. This is true, especially for large-scale mixed-integer and nonlinear optimization problems. To circumvent this issue, the scheduling problem is formulated as a continuous instead of a batch decision-making process. This way, no discrete variables are involved to give rise to the MIP problem. Hence the scheduling problem can be formulated as a nonlinear programming (NLP) problem. To further reduce uncertainty during data reconciliation step, the scheduling decisions are initially executed using a dynamic model. Thus, setpoints are updated based on the future plant responses. These setpoints are optimized at the RTO level prior to actual implementation.

The RTO procedure employs a steady-state model in order to significantly reduce computational load. Optimal setpoints are obtained by maximizing a profit function, which is subjected to steady-state model convergence and operational constraints. A solution is obtained using a standard sequential quadratic programming (SQP) algorithm. The optimal setpoints are enforced on another dynamic model (a virtual plant), which is kept at the state prior to scheduling. The implementation of these setpoints is performed disjointedly using HYSYS built-in regulatory controllers or an external MPC scheme. In this work, MPC actions are calculated using Model Predictive Control Toolbox in MATLAB. The MPC moves are passed to a HYSYS spreadsheet via COM link. For parameter estimation, process outputs from the dynamic model are forwarded to MATLAB in a similar manner.

To demonstrate the efficacy of the proposed integrated approach, a fairly large-scale integrated plant in the form of a refrigerated gas plant (RGP) is used as a test bed. The RGP is made out of three LNG heat exchangers, a propane-refrigerated cooler, two flash separators, a 40-tray distillation column, a packed-bed absorber, a Joule-Thompson valve, a mechanically-linked turboexpander-compressor, two centrifugal pumps, a booster compressor and an air-fan cooler. The dynamic model of RGP containing 770 stiff DAEs is subjected to three cases of scheduling problems namely: 1) mode, 2) load, and 3) input. Each case is further divided into several sub-cases as illustrated in Figure 1.2. In total, twenty-four case studies are conducted.

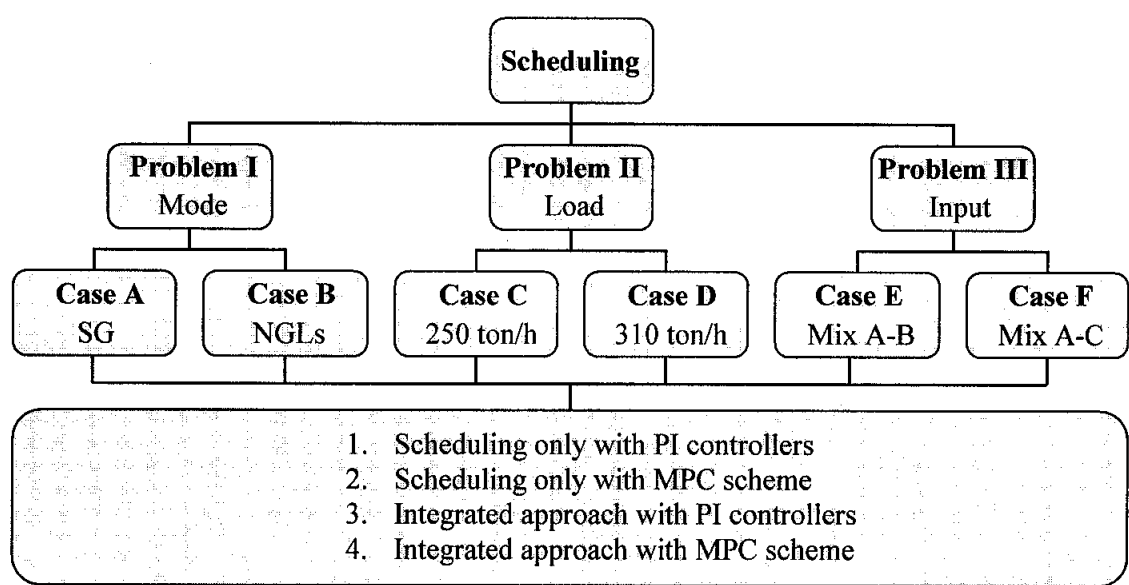


Figure 1.2: Flowchart of case studies for three scheduling problems. Each problem is divided into two cases and each case is further divided into four sub-cases. *Note:* SG=sales gas; NGLs=natural gas liquids; Mix A-B denotes mixing of 130 and 150 ton/h of feed gas streams A and B, respectively; Mix A-C denotes mixing of 180 and 100 ton/h of feed gas streams A and C, respectively.

Following the introductory remarks, the remaining discussions of this thesis are organized as follows:

- Chapter 2 presents reviews of past work on ERP, RTO and MPC as well as integration between different levels of plant automation. The current research work deals with operational planning, which is also known as scheduling. In normal situation, scheduling targets are executed by MPC schemes and/or regulatory controllers. However, it is more beneficial if scheduling can be integrated with RTO before implementation of targets. Integration of scheduling and RTO is difficult due to multi-temporal scales of the two problems. A proposed approach to the integrated framework is the main subject of this thesis.
- To illustrate efficacy of this concept, a refrigerated gas plant (RGP) is used as a test bed. The RGP is essentially a combination of two major units of a gas processing plant (GPP) namely low temperature separation unit (LTSU) and sales gas compression unit (SGCU) as shown in Figure 1.3. The main product is sales gas containing mostly methane and traces of ethane. Quality

of sales gas is strictly upheld according to product specifications. MPC and/or regulatory controllers are employed to sustain production of sales gas and maintain stability of plant. The by-products are natural gas liquids consisting of ethane, propane, butane and condensates. Natural gas liquids are forwarded to product recovery unit (PRU) for further processing into individual hydrocarbon components. Developments of RGP steady-state and dynamic models as well as control schemes are presented in Chapter 3.

- In Chapter 4, an RTO procedure is discussed and a case study is presented. A steady-state RGP model is used for this purpose due to highly complex and nonlinear nature of the process. An economic parameter in the form of RGP profit is chosen as an objective function. The optimization goal is to maximize profit, which is defined as revenues less expenses. Revenues are drawn from values of sales gas and natural gas liquids. Expenses are incurred due to costs of feed gas and utilities especially on refrigeration cooler duty, demethanizer reboiler duty, compressor fuel gas consumption, turboexpander-compressor maintenance and electricity usage on pumping actions. The RTO case study centers on balancing flow rates of feed gas streams A, B and C. Feed gas stream A is the leanest in terms of hydrocarbon gross heating value whereas feed gas streams B and C are rich and richest, respectively. Carbon dioxide content also varies with increasing level from feed gas stream A to C. Maximization of profit is carried out by manipulating ten optimization variables subject to thirty-four constraints on operational parameters. The case study serves as a basis for a subsequent discussion on integrated framework of scheduling and RTO.

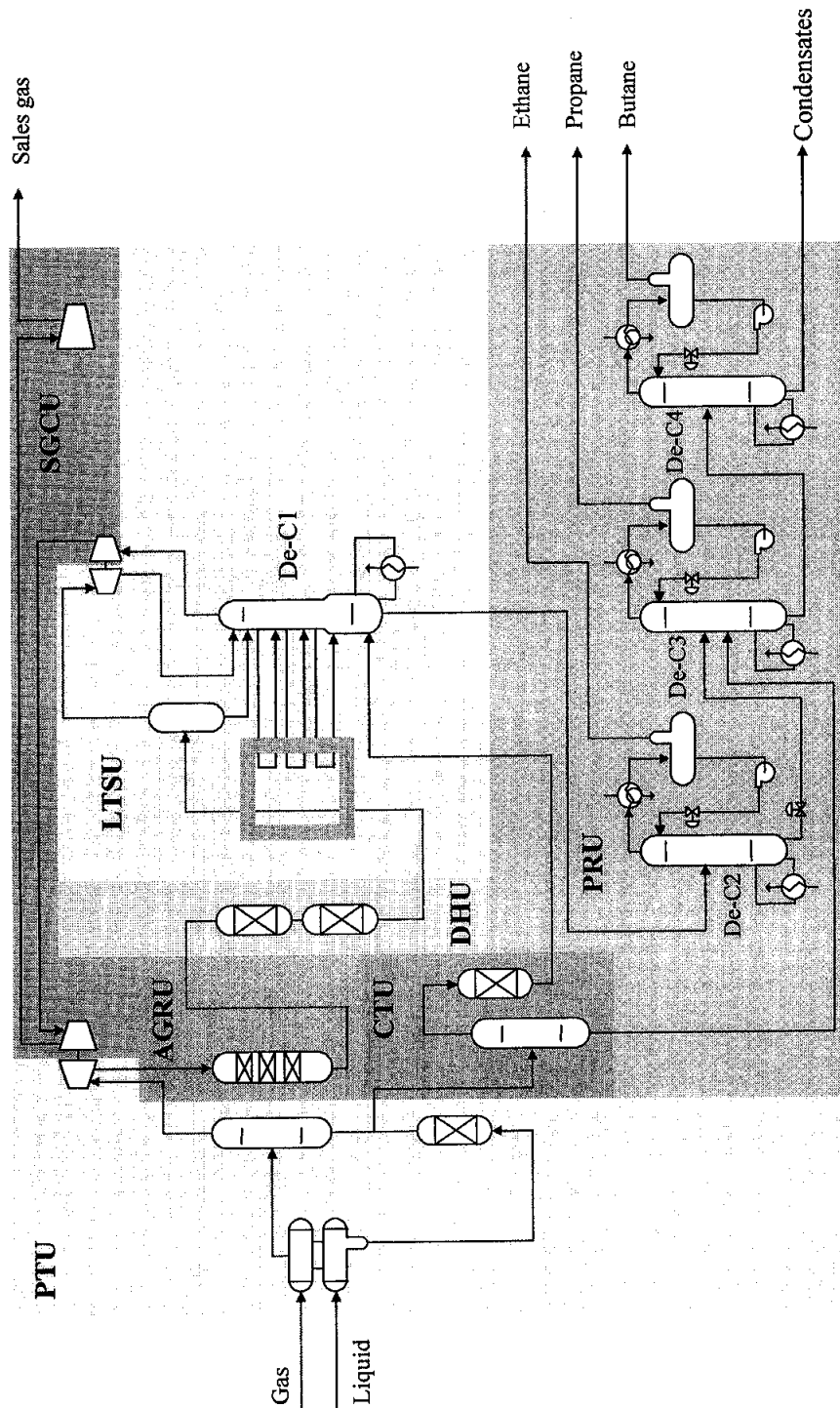


Figure 1.3: A simplified diagram of a gas processing plant depicting pre-treatment unit (PRU), acid-gas removal unit (AGRU), condensate treatment unit (CTU), dehydration unit (DHU), low-temperature separation unit (LTSU), sales gas compression unit (SGCU) and product recovery unit (PRU). Main fractionators are demethanizer (De-C1), deethanizer (De-C2), depropanizer (De-C3) and debutanizer (De-C4). Coldbox is shown as a thick box at the center of LTSU. Other major unit operations are also illustrated but their descriptions are omitted to avoid cluttering up the diagram.

- Chapter 5 presents the main work of this thesis. Here, a procedure for the proposed integration of scheduling and RTO is elucidated. The proposed integrated framework is applied to three scheduling problems. Problem I is scheduling of RGP operational mode from natural gas liquids to sales gas (Case A), and vice-versa (Case B). Mode scheduling is important for RGP to manage production subject to present conditions at both sides of its boundary. Problem II involves varying RGP load by ± 30 ton/h from a normal plant load of 280 ton/h (Cases C and D). Load scheduling is often carried out due to the following reasons: 1) section cleanups, 2) unscheduled equipment shutdown or simply malfunction, 3) low supply of feed gas from producers, and 4) abnormally high demand of sales gas from customers. Problem III deals with mixing specific amounts of lean and rich feed gas streams at the normal load. This case, termed input scheduling, gives RGP an option to explore whether it is beneficial to process rich feed gas streams given operational and contractual constraints. Input scheduling case in this chapter differs from that in Chapter 4, in which RGP can freely choose the combination and quantity of feed gas streams to be processed. In Chapter 5, mixing of feed gas streams A and B (Case E) as well as feed gas streams A and C (Case F) are pre-specified according to *a priori* agreement between RGP and producers.
- In Chapter 6, four major contributions of this thesis work are highlighted. The contributions are: 1) development of steady-state and dynamic models of RGP on a single HYSYS platform to be used as test beds for the proposed integrated approach, 2) systematic identification of the dynamic model of RGP using step and pseudo-random binary sequence (PRBS) input signals to be deployed in MPC scheme, 3) RTO assessment of profit margin by forcing RGP to consider processing additional feed gas streams, and most importantly, 4) proposition of an integrated framework of scheduling and RTO with realistic applications on three scheduling problems namely mode, load and input. Efficacy of the proposed approach is revealed by comparing relative profit margins and case-average profit values of all case studies. In

addition, potential solutions to the challenges faced in the current work are recommended as future research avenues.

- Finally, three appendices are included at the end of this thesis to show Peng-Robinson thermodynamic equations of state used in modeling the hydrocarbon properties (Appendix A), values of optimization and constraint variables for Cases A to F (Appendix B), and a list of publications related to this work (Appendix C).

CHAPTER 2

LITERATURE REVIEW

2.1 Plant Automation

Plant automation refers to a series of activities that are planned and executed in order to meet business and engineering objectives. Previously, plant automation is classified into five levels namely: 1) regulatory control, 2) advanced process control (APC), 3) real-time optimization (RTO), 4) production scheduling, and 5) production planning. In a very recent literature (Harjunkski et al., 2009), production planning and production scheduling levels have been grouped together as part of a single enterprise resource planning (ERP) level whereas the rest are kept as standalone levels. This decision is made due to time-scale: 1) similarities in executing tasks at the highest level, and 2) dissimilarities in carrying out activities at the other levels. The subject of plant automation has received great interest from process systems engineering (PSE) community. Its ultimate aim is to achieve full integration of all levels of plant automation into a single one (Tousain, 2002).

Execution of the multi-temporal activities in a single integrated framework is a daunting challenge. Among major challenges that must be addressed are (Grossmann, 2005):

1. *The modeling challenge*: Traditionally, problems at various levels of plant automation are solved based on different modeling approaches. At the top level, steady-state business and plant conditions are assumed. Linear process models are commonly employed for simplicity. Often, mixed integer problems are formulated due to presence of discrete variables in the decision-making processes. At the bottom level, linear or nonlinear dynamic models are used to address the highly transient processes. Hence an effective modeling technique, possibly, based on a hybrid system of mathematical programming and logic is required to encapsulate all types of process complexity.
2. *The multiscale optimization challenge*: For an integrated problem of two similar levels, a feasible but not necessarily an optimal solution can be

obtained through functional, spatial and/or temporal decompositions. However, coordination of various activities across all levels of plant automation results in a very large-scale optimization problem. Given the first modeling challenge, an efficient optimization method is required to solve the multiscale integrated problem of all levels. The solution time horizons for each of these levels vary as follows: planning (weeks to years), scheduling (days to weeks), RTO (hours to days), APC (minutes to hours) and regulatory control (seconds to minutes).

3. *The uncertainty challenge*: Uncertainty is a critical issue in plant automation. The nature of uncertainties varies dramatically from the highest decision-making level to the lowest implementation level. For example, at the ERP level, uncertainties may arise from order cancellations, processing times or equipment reliability/availability. At the RTO level, uncertainties may take place in the forms of measurement, process, model and market variations. At the APC and regulatory control levels, uncertainties may occur due to random disturbances. A meaningful stochastic technique based on heuristics and meta-heuristics is required to address these issues in a unified way.
4. *The computational challenge*: Depending on how the above three challenges are addressed, the large-scale optimization problem may become intractable due to very high computational load. A feasible and optimal solution may not be found in time for execution at the lower levels. This challenge needs to be tackled from two aspects namely: 1) development of an efficacious algorithm, and 2) overcoming hardware limitations. Both aspects are intertwined in the sense that the latter may become a non-issue if the former is very efficient in solving the optimization problem, or the former may be overlooked if a super computing architecture is available.

Based on the aforementioned challenges, previous and on-going research works focus on integrating two decision-making levels at a time. The existing frameworks can be classified into: 1) higher-level integration, and 2) lower-level integration. All two integrated frameworks share more or less similar challenges.

2.1.1 Integration at Higher Decision-making Levels

Enterprise resource planning (ERP), often called supply chain management (SCM), involves planning and scheduling activities for the whole plant. As such, ERP deals with key business decisions for activities such as marketing, sales, distribution and transportation as well as top-level engineering decisions for activities like production and storage. In reality, business decisions take the longest time to execute due to, among others, lengthy contract negotiations and procurement processes as well as environmental, safety, social and, to some extent, political considerations. The time horizons are on the order of months to years for strategic planning, weeks to months for tactical planning and days to weeks for operational planning. Strategic planning is a highly business-driven activity and thus will not be covered in this thesis. On the other hand, tactical and operational planning deal with mostly engineering-oriented activities that are tightly related to plant processes. In literature, these activities are referred to as production planning and scheduling, respectively.

Production planning and scheduling have been interesting subjects in operations research (OR) and process systems engineering (PSE). Excellent reviews on this subject have been published by Floudas and Lin (2004), Shah (2005) and Mendez et al. (2006). In general, planning and scheduling deal with the timely allotment of company/plant resources to execute a set of tasks. In the context of PSE community, planning and scheduling refer to specific strategies of assigning equipment, exploiting utilities and managing manpower to perform processing tasks required to manufacture single or multiple products.

In typical OR literature (Stadtler, 2005; Varma et al., 2007), planning and scheduling are treated as independent entities due to their dissimilar time scales and complexity levels. The separate treatment of planning and scheduling often leads to inefficient allocation of resources. For example, Shah (2005) highlighted that: 1) stock levels in the entire plant are typically in the range of 30-90% of annual demand, 2) supply chain cycle times, defined as time-elapsd between materials entering a plant as feedstock and leaving it as products, can vary from 1000-8000 hours, and 3) less than 10% of fine chemical and pharmaceutical intermediates that are being processed ends up as final products.

There are strong overlaps within both planning and scheduling activities. As such, an integration of planning and scheduling into a large-scale problem makes sense (Figure 2.1). The integrated framework can enhance plant profitability and reduce capital expenditure associated with maintaining inventories. For examples, Exxon Chemicals estimated 2% annual reduction in operating costs and another 20% reduction in inventory and, similarly, Du Pont reported a reduction of inventory-related working capital from US\$160 million to US\$95 million for a polymer facility (Shobrys and White, 2002).

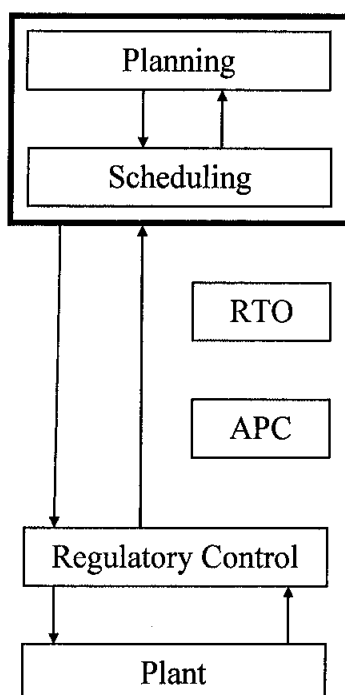


Figure 2.1: Integrated planning and scheduling

Realizing a huge potential for the integrated framework of planning and scheduling, many researchers and practitioners started to work in this emerging area. Modeling approaches and solution strategies for the integrated framework have been discussed by Bassett et al. (1996), Kallrath (2000, 2002), Grossmann and co-workers (2002, 2005) as well as Maravelias and Sung (2009). Early attempts to formulate this problem are based on a simultaneous modeling approach with applications in multipurpose batch plants (Birewar and Grossmann, 1990; Shah and Pantelides, 1991). It should be noted, however, that the simultaneous approach could potentially result in an intractable optimization problem. Thus, Papageorgiou and Pantelides

(1996) proposed a mathematical formulation and a two-stage decomposition approach with applications on batch and semicontinuous plants. The higher level problem is solved cyclically in order to choose a planning campaign whereas the lower level problem is used to generate scheduling operations iteratively. At each iteration, an integer cut is added to avoid a repeat solution of the same planning campaign.

Alternatively, a full-space approach is proposed for solving the integrated planning and scheduling problem for an oil refinery (Pinto et al., 2000), a hydrogen supply network (van den Heever and Grossmann, 2003), petroleum and petrochemical plants (Kelly, 2004) and a fruit packaging plant (Blanco et al., 2005). In general, links between planning and scheduling problems are made through constraints. This means that, at the upper sublevel, production targets in each planning period is tied up to the orders at the end of the relevant scheduling horizon. At the lower sublevel, a detailed scheduling model that incorporates resource constraints and production costs is used. Lagrangian relaxation is applied to a master problem in order to separate soft from hard constraints resulting in the formation of more tractable subproblems.

The above approaches require detailed scheduling formulation for the whole time horizon and thus significantly increases computation load. A more efficient approach is based on a rolling horizon scheme (Dimitriadis et al., 1997). Here, detailed scheduling models are employed in the first few periods because production targets are implemented exactly. Aggregate models are used for the later periods when targets are updated as the horizon rolls. Lin et al. (2002) discussed a three-level integrated model for multi-stage production scheduling of a multiproduct batch plants. At the first level, length of rolling horizon is optimized based on certain production targets. At the second level, a short-term scheduling model is formulated based on customer orders, inventories and processing recipes. Finally, the scheduling model is solved by iteratively maximizing throughput of specified products. A downside of the rolling horizon approach is that global optimality cannot be guaranteed for the entire scheduling operations.

2.1.2 Integration at Lower Decision-making Levels

The decisions related to the operation of a process plant are typically made at three different levels. At the highest level, production planning and scheduling provide coordination of activities over a long time horizon (weeks to months). At the lowest level, APC handles setpoint tracking and disturbance rejection by optimally adjusting plant inputs over a short time scale (minutes to hours). A well-known strategy to establish a link between the highest and lowest level of decision making is RTO. The RTO system optimizes plant economics over a medium time scale (hours to days). Efforts to integrate RTO and MPC (Figure 2.2) have been long carried out by the PSE community.

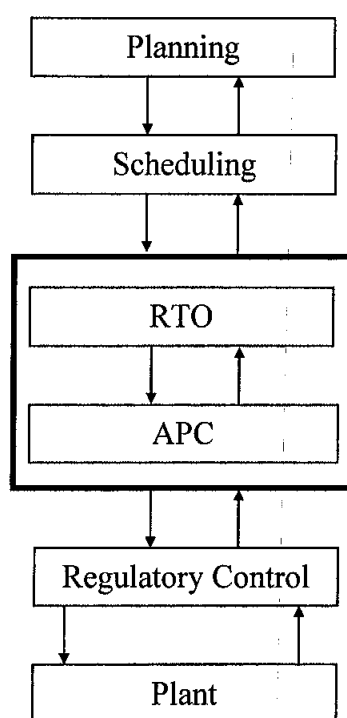


Figure 2.2: Integration of RTO and MPC

This idea was first realized by Cutler and Perry (1983) who proposed a hierarchical approach of RTO and APC. Here, online optimization was performed based on a steady-state plant model and the resulting optimal targets were passed to the controllers for execution at the actual plant. The authors argued that an economic benefit in the range of 6-10% of a given process value could have been achieved via online optimization. As compared with the traditional offline procedure, this approach

provides improvements in abilities: 1) to know the current plant state precisely, 2) to operate the plant at or near constraints, and 3) to obtain direct feedback on the validity of the predictions. A major drawback for this hierarchical approach is the low frequency of RTO sampling time.

The RTO sampling time may be as fast as hours or as slow as days depending on: 1) sensitivity of spot-market prices of feedstock and products, 2) settling time of the entire plant, and 3) the inconsistency between the underlying process models of RTO and APC. The first reason actually depends on the terms and conditions in the contractual agreement between plant and its customers. On one hand, prices of feedstock and products might have been agreed upon long-term basis; hence insensitive to market conditions. On the other hand, prices of products such as oil derivatives (naphtha, gasoline, kerosene), natural gas liquids (ethane, propane, butane) and chemicals (methanol, MTBE, PVC) are subject to daily revisions. In this case, it may be more meaningful to perform RTO calculations once a day or whenever price updates are available.

While the first reason involves business decisions, the last two reasons are caused by technical limitations. The second reason is due to a requirement that the plant must be near a steady state before an RTO procedure, which comprises data reconciliation, parameter estimation and optimization, can be triggered (Darby and White, 1988). In practice, a plant settling time may vary remarkably from one to another. For example, a crude distillation unit takes 1-2 hours to settle (Basak et al., 2002) while others like a propane-propylene splitter requires 2-3 days to reach a new steady state once it is perturbed (Alsop and Ferrer, 2006).

A plant could also be in a highly transient state due to, among others, the presence of random disturbances. In this situation, it is difficult to perform data reconciliation because of potentially large plant-model mismatch. One way to reduce the gap between the low frequency RTO procedure and the fast APC execution time is through a two-stage APC structure (Ying and Joseph, 1999). The upper APC stage computes setpoints for control variables by solving a constrained linear or quadratic optimization problem based on economic information and constraints from the RTO level. The setpoints are passed to the lower APC stage for calculating optimal input

moves that are subsequently sent to the plant. As compared to the hierarchical approach, an integrated framework of steady-state RTO and a two-stage dynamic MPC structure is more superior in the following issues:

- Setpoints can be updated faster after a disturbance enters the plant
- Inconsistency between nonlinear steady-state RTO model and dynamic APC model is significantly reduced
- Instability that results from large setpoint changes is avoided
- Distribution of offsets is explicitly controlled and optimized

In an industrial application, Zanin et al. (2000, 2002) reported the formulation, solution and implementation of a one-layer RTO-APC scheme for a fluidized-bed catalytic cracker unit of a PetroBras plant in Brazil. The unit had seven process inputs and six outputs. Maximization of liquefied petroleum gas (LPG) throughput was used as an economic criterion subject to input and output bounds. The authors found out that tremendous economic performance was achieved for the integrated scheme as compared with conventional scheme in which setpoints were chosen based on experience. From simulation studies, the one-layer scheme was also determined to outperform the two-layer RTO-APC approach.

For more demanding applications, RTO and APC strategies can be executed dynamically at a fast sampling rate and thus avoiding the issue of inconsistencies between process models. This type of integrated framework of RTO-APC gives rise to a dynamic optimization problem. In a pioneering work, Helbig et al. (2000) attempted to solve this problem simultaneously and repetitively at each control interval. This strategy corresponds to a single-level optimal control problem. For large-scale and highly nonlinear processes, this strategy faces computational difficulties in finding feasible solutions within a reasonable control interval. The computational load issue is compounded by uncertainties in process model, time-varying disturbance and unknown initial conditions. The issue of uncertainties may be alleviated by updating process model with current measurements of process variables. However, some important variables such as temperature and pressure in the middle of a distillation column are only measured sparingly or not at all due to cost savings. As

such, suitable estimation techniques like extended Kalman filter (EKF) may be employed for state and disturbance updates (Lee and Ricker, 1994).

In a related work, Kadam et al. (2002) employed a multirate EKF for estimation of state variables and parameters in a two-level strategy of integrated framework of RTO and MPC. This problem may be viewed as a quasi dynamic optimization problem because RTO calculation is performed at a much lower frequency as compared with MPC calculation. At the higher level, RTO is subjected to external disturbances such as economic factors and environmental conditions whereas MPC is subjected to operational disturbances at the lower level. The decision for triggering RTO calculation is made at a time-scale separation block connecting these two levels. The trigger is based on sensitivity analysis of the optimal reference trajectories.

To be more systematic on the triggering mechanism, Srinivasan et al. (2003) proposed a tracking scheme that is derived from necessary conditions of optimality (NCO). This NCO-tracking scheme relies on a solution model that is used to manipulate inputs. The solution model is obtained by dissecting optimal input profiles and relating these profiles to various parts of the NCO. Throughout the solution horizon, optimal input profiles are typically discontinuous from one interval to the next at the so-called switching times. However, they are continuous and differentiable within one or more intervals called arcs (Bryson and Ho, 1975). To leverage on these properties within the arcs, Schlegel and Marquardt (2004) proposed a method that automatically detects the switching times. The optimal solution is found in three steps namely:

1. parameterization of input variables using a discretized *B*-spline representation or, more recently, using a wavelet transformation technique (Schlegel and Marquardt, 2006),
2. reformulation of the integrated dynamic optimization problem as multi-stage NLP problem, with each stage corresponds to a potential arc, and

3. solution of the NLP problem using SNOPT, which is an efficient active-set SQP algorithm (Gill et al., 1998, 2005) and LIMEX as a numerical integrator (Schlegel et al., 2004).

The NLP problem can also be treated with a barrier or an interior-point method. Here, differential state variables, algebraic state variables and manipulated variables are grouped as unknown variables (Kameswaran and Biegler, 2006). These bound constraints are replaced by two logarithmic terms comprising differences between the unknown variables and their respective lower bounds as well as differences between the unknown variables and their respective upper bounds. Each logarithmic term is multiplied by a nonnegative barrier parameter. These logarithmic barrier terms are added to the NLP objective function. The augmented objective function and Karush-Kuhn-Tucker (KKT) conditions are discretized using the method of orthogonal collocation over finite elements. They are then solved simultaneously subject to a set of equality constraints.

A local solution is found within an interior point of the specified lower and upper bounds of the unknown variables. The local solution converges to that of the original NLP problem as the barrier parameter approaches zero (Forsgren et al., 2002). An efficient barrier-method solver called Interior-Point OPTimizer (IPOPT) has been developed by Wachter (2002) and later improved by Wachter and Biegler (2006). Efficacy of the barrier method has been illustrated in many industrial case studies such as low-density polyethylene (LDPE) process at high pressure and temperature (Cervantes et al., 2002), Tennessee Eastman challenge (Jockenhovel et al., 2003), and polymerization in CSTR with recycle loop (Lang and Biegler, 2007).

2.1.3 Integration between Top and Middle Decision-making Levels

In addition to the integrated frameworks discussed above, integration of scheduling and RTO can bring further economic benefits to the plant (Figure 2.3). However, only a few researchers have published work in this subject (Nystrom et al., 2006; Terrazas-Moreno et al., 2008; Prata et al., 2008). The main reason is due to difficulties in combining different modeling approaches that are formulated from scheduling and

RTO problems. The integrated model can be massive and lead to computationally intractable solution strategies.

Recall that scheduling is a decision-making process that answers the collective questions of when, where and how to make and deliver a series of products (Floudas and Lin, 2004). The scheduling constraints are typically delivery times, limited resources in terms of raw materials and equipment utilization, and different processing recipes. It is normal that a scheduling problem involves discrete decisions in, for example, equipment assignments and task allocations. Therefore, most scheduling problems are often formulated as MIP. On the other hand, RTO is concerned with minimizing or maximizing an economic objective function that is directly related to a rigorous steady-state plant model. Constraints on economic and operational parameters are common. Steady-state RTO problems can be formulated as NLP and solved using efficient SQP algorithms based on active-set or barrier methods.

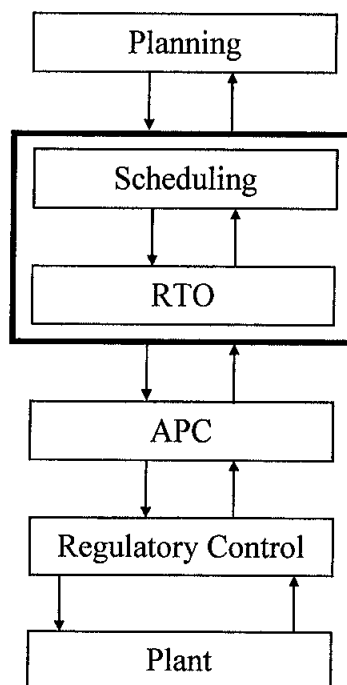


Figure 2.3: Integrated scheduling and RTO

There are cases, for example in polymerization processes, where RTO problems are formulated using dynamic process models. This type of RTO problem is referred

to as a dynamic optimization problem. If scheduling and dynamic RTO are integrated, a mixed integer dynamic optimization (MIDO) problem arises. The MIDO problem is mostly non-convex and thus may become intractable for large-scale nonlinear processes. A pioneering attempt on this subject can be seen in Tousain (2002), and subsequently, in Tousain and Bosgra (2006). The authors studied MIDO problems on an HDPE production plant. In an iterative approach, the scheduling problem was formulated as MILP and solved with branch and bound method using GAMS/CPLEX solver. The highly nonlinear dynamic optimization problem was solved using SQP algorithm developed by van der Schot et al. (1999).

In another work, Chatzidoukas et al. (2003) studied integrated scheduling and optimal grade transition for a catalytic gas-phase polyolefin fluidized bed reactor. Modeling was carried out under gPROMS environment. Production and transition stages are treated separately, thus forming master and primal subproblems, respectively. The master subproblem was formulated as MILP and solved using GAMS/CPLEX algorithm based on Bender decomposition method. The primal subproblem was solved using gOPT optimizer.

2.2 Concluding Remarks

This chapter provides a critical review of relevant work on integration of levels in process automation hierarchy. A full integration of all levels into a single-level control is the ultimate objective of PSE researchers. As such, an area such as integrated framework of planning and scheduling that traditionally belongs to OR domain is currently being pursued. The objective, however, is difficult to realize due to multi-temporal nature of the activities at each of these levels.

Advances in mathematical modeling and large-scale solution techniques as well as information and communication technology give optimism that the single-level control objective can be achieved in the near future. Parts of the work with practical examples are already published in literature. Lately, the subject of an integrated RTO-MPC scheme receives notable attention. Much of the work in this area revolves around dynamic optimization of reaction or distillation processes of a small plant. It appears that plantwide applications have yet to be demonstrated in literature. The

main reason could be due to difficulty in developing and integrating dynamic models of large equipment in a single flowsheet.

More recently, integration of scheduling and RTO problems becomes a popular research topic in PSE. Due to presence of binary variables in scheduling decisions and use of dynamic models in RTO, the integrated problem gives rise to a MIDO problem. The solution to the MIDO problem may be computationally intractable when handling complex equipment such as liquefied natural gas (LNG) heat exchangers, fluidized-bed catalytic cracker and reactive distillation column. This difficulty could be alleviated with the use of a steady-state RTO model. If the needs for having binary variables are removed in the scheduling problems, the integrated scheduling-RTO framework can be formulated as a large-scale NLP problem. This type of problem can be solved using a standard SQP algorithm.

CHAPTER 3

RGP MODELING AND CONTROL

3.1 Introduction

Simulation based on first-principle steady-state and dynamic models have been recognized as a valuable tool in engineering. Its usage becomes more widespread as personal computers become more powerful. In general, simulation methods are divided into two broad categories: 1) equation oriented, and 2) modular approaches. Notable examples of equation oriented simulators are DIVA (Holl et al., 1988; Kröner et al., 1990) and DYN SIM (Sorensen et al., 1990; Gani et al., 1992; Perregaard et al., 1992). Both simulators contain standard thermodynamic correlations and physical properties that can be employed to develop steady-state and dynamic models.

The open-form approach offers more robust models. However, this is achieved at the expense of ease-of-use since users need to be technically adept in writing and solving mathematical models. Steady-state models involve solution of a problem comprising mainly algebraic equations. Dynamic models include presence of temporal but not spatial element; hence gives rise to a problem of ordinary differential equations. Since thermodynamic relations contain algebraic equations, dynamic models deal with a problem of differential-algebraic equations.

Another modeling approach is close-form modular simulation, which is more attractive for industrial practitioners. This approach entails attachment of one solved flowsheet to another. In the latest generation of commercial simulators like HYSYS, AspenPlus and iCON, unsolved flowsheets may be linked up and solved through both forward and backward calculations. Two major advantages of using the modular approach are:

1. Reduces modeling time and efforts: Prebuilt objects of logical operations and major equipment are readily available. Almost no mathematical modeling effort is required. However, users need to have good knowledge in engineering subjects such as thermodynamics, reaction engineering, as well as transport and separation processes.

2. Shorter on-the-job training period: Young engineers have learned to use commercial simulators at the university level, especially in executing their final year projects. Once they become familiar with plant operations, these engineers will be able to develop steady-state and dynamic models using available plant information.

Successful industrial applications on using dynamic models for control purposes are aplenty. Schad (1998) and Altena et al. (1998) used PROSIM to pre-estimate process gains for developing multivariable control of a turboexpander plant. More recently, Alsop and Ferrer (2006) successfully employed a dynamic model of propane/propylene splitter in HYSYS to skip plant step testing completely. DMCPlus was used to design and implement the model predictive control (MPC) schemes in the real plant. Several refinery cases are also available. For examples, Mantelli et al. (2005) and Pannocchia et al. (2006) designed MPC schemes for crude distillation unit and vacuum distillation unit based on dynamic simulation models.

The aforementioned works provide evidence that first-principle dynamic models can be utilized as an alternative to running plant test. A dynamic model may be considered as a virtual plant for step testing purposes. This way, traditional practice of conducting step test on actual plant may be reduced or totally circumvented. Worries about product quality giveaways and/or off-specifications may be alleviated. In addition, dynamic models may also be utilized to train personnel and troubleshoot plant problems offline.

In subsequent sections, developments of steady-state and dynamic models of a refrigerated gas plant (RGP) are discussed. Steady-state model of RGP is validated against actual plant data. The steady-state model is used as a basis for developing a dynamic model, which serves as a virtual plant throughout this work. Major control philosophies are presented independently according to their purposes. Development of an APC strategy in the form of MPC scheme is also discussed.

3.2 Process Description

Key operating values are calibrated with the data collected from a real gas processing plant (Figure 3.1). Feeds to the RGP come from three main streams A, B and C. Another feed gas stream D is also available at a much smaller quantity. The feed gas compositions vary as listed in Table 3.1. The values fall within the approximate range of typical natural gas compositions found across the world (NaturalGas.Org).

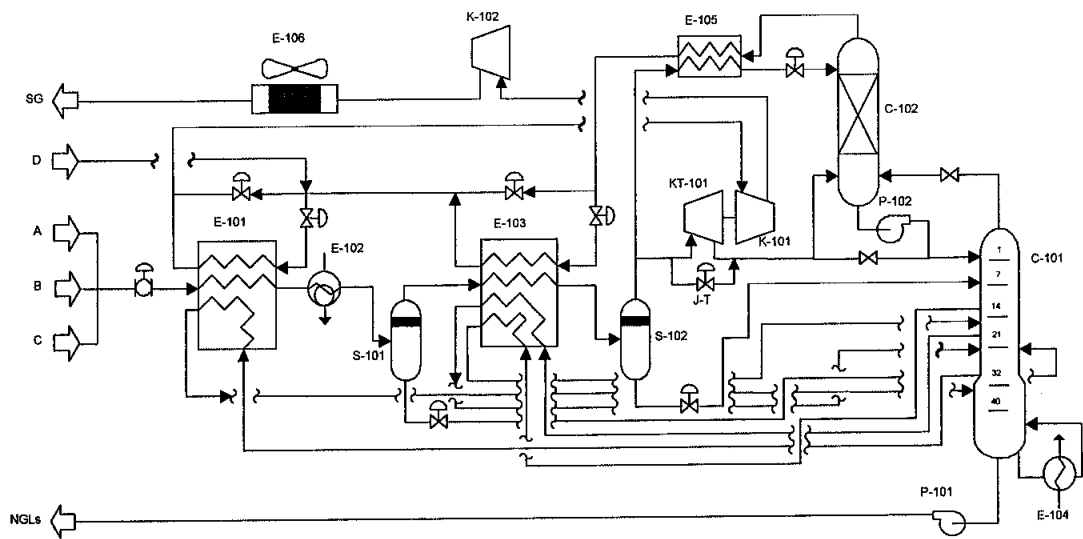


Figure 3.1: Process flow diagram of RGP. E=heat transfer equipment (non-fired); S=separator; KT=turboexpander; K=compressor; P=pump; C=column; J-T=Joule-Thompson valve

Table 3.1: Compositions of feed gas streams

Component	A	B	C	D
Methane	0.8865	0.7587	0.6797	0.7604
Ethane	0.0622	0.0836	0.1056	0.1581
Propane	0.0286	0.0535	0.0905	0.0441
i-Butane	0.0102	0.0097	0.0302	0.0080
n- Butane	0.0059	0.0194	0.0402	0.0051
i-Pentane	0.0003	0.0058	0.0121	0.0000
n-Pentane	0.0002	0.0068	0.0101	0.0000
n-Hexane	0.0001	0.0002	0.0028	0.0000
Nitrogen	0.0039	0.0043	0.0012	0.0177
Carbon Dioxide	0.0020	0.0580	0.0276	0.0066

Water, sulfur and mercury are assumed to be absent when feed gas streams enter the RGP. In other words, all feed gas streams are assumed to be sweet, dry gas with

varying richness and carbon dioxide levels. At normal operation, the RGP processes mixed feed gas at a plant throughput of 280 ton/h. Feed gas at 20 °C and 60 bar is cooled by exchanging heat with sales gas in three coldboxes (E-101, E-103, E-105), a propane refrigeration cooler (E-102) and an air cooler (E-106). To enhance vapor-liquid separation, feed gas is flashed in two stages. Most vapor is expanded in turboexpander (KT-101) whereas some in Joule-Thompson valve depending on throughput level. Liquids are fed to various stages of a demethanizer (C-101). Top product of demethanizer and that from expansion process are sent to an absorber in gas subcooled process (GSP) unit to improve recovery of natural gas liquids. Bottom product of demethanizer is further processed to separate the liquids into ethane, propane, butane and condensates. Top product of absorber containing sales gas is recompressed twice to meet minimum specification of 30 bar.

3.3 Modeling

The refrigerated gas plant (RGP) is simulated under HYSYS 2006 CP5 (6729) environment. Thermodynamic properties of the vapors and liquids are estimated by the Peng-Robinson equation of state (Appendix A). Feed gas components in Table 3.1 are entered individually with their respective compositions even though hydrocarbons heavier than pentane are grouped as condensates. In other words, there is no hypothetical component listed in the simulation model.

3.3.1 Steady-state Modeling

Simulation work starts with steady-state model development. In general, unit operations and streams are installed in HYSYS process flow diagram (PFD) from left to right and bottom upwards as shown in Figure 3.1. Accuracy of the simulation model is generally good. Simulated values of key process conditions closely resemble (around 95%) those of the normal operating conditions as shown in Table 3.2. Two largest deviations from normality are observed at coldbox E-101 side draw no. 3 (SD3) outlet temperature and air cooler E-106 inlet temperature with corresponding values of 19.5 and 11.6%. The former is attributed to the removal of ethane product stream from the model. In actual plant, this stream absorbs heat brought into coldbox E-101 by the feed gas and thereby reduces the SD3 outlet temperature. The other large deviation is caused by omission of booster compressor R-151, which was

decommissioned for economic reasons. As a result, outlet of compressor K-101, which is the inlet to coldbox E-106, undergoes a small expansion process at the bypass valve causing its temperature and pressure to drop a little when compared against plant data.

In steady-state modeling, three coldboxes (E-101, E-103 and E-105) are simulated as liquefied natural gas (LNG) heat exchangers. In coldbox E-101, the hot side is feed gas stream and the cold sides are sales gas and SD3 streams. In coldbox E-103, the hot side is processed gas stream and the three cold sides are the sales gas, side draw no. 1 (SD1) and side draw no. 2 (SD2) streams. In coldbox E-105, only two streams are involved in the heat exchange. The hot and cold sides are processed gas and sales gas streams, respectively. Effectiveness of the coldboxes may be assessed by observing their respective hot and cold composite curves (Figure 3.2).

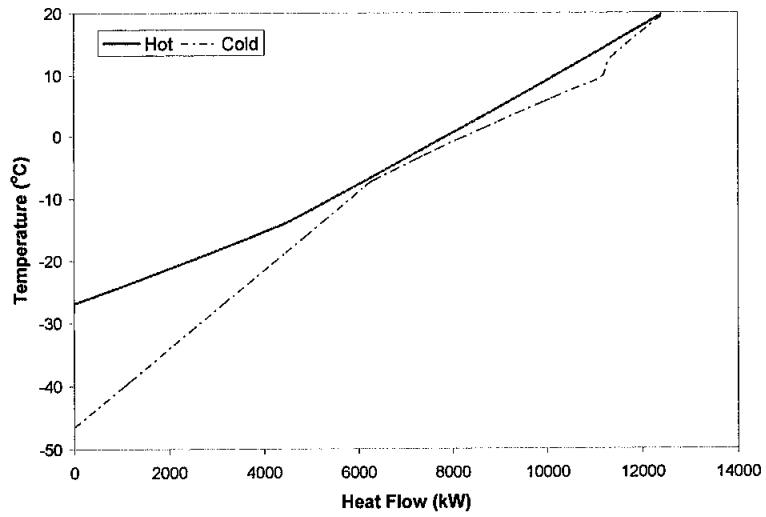
The large initial gaps between the hot and cold composite curves illustrate the tremendous amount of heat that is exchanged in the first two coldboxes. Except for coldbox E-105, the gaps in coldboxes E-101 and E-103 narrow down to above $0.2\text{ }^{\circ}\text{C}$ towards the end of the process rendering these coldboxes effectively utilized. In simulation of all three coldboxes, no temperature cross phenomenon is observed. The log mean temperature differences are 1.7, 18.0 and $16.7\text{ }^{\circ}\text{C}$ for coldboxes E-101, E-103 and E-105, respectively. On the other hand, the propane refrigeration cooler E-102 and the air-cooler E-106 are modeled as simple chillers with 'Direct Q' heat duty. This simplification is necessary in order to reduce the computational load at the dynamic modeling stage later.

Modeling of demethanizer C-101 requires special attention because it is the main fractionator in RGP. The actual column comprises 40 valve trays and 3 chimney trays. However, the chimney trays are ignored in simulation since their purpose is only to collect liquids resulting in zero separation efficiency. The bottom of demethanizer C-101 is heated by low-low pressure steam on the shell side of a thermosiphon reboiler E-104. The reboiler is simulated as a simple heater with 'Direct Q' duty source.

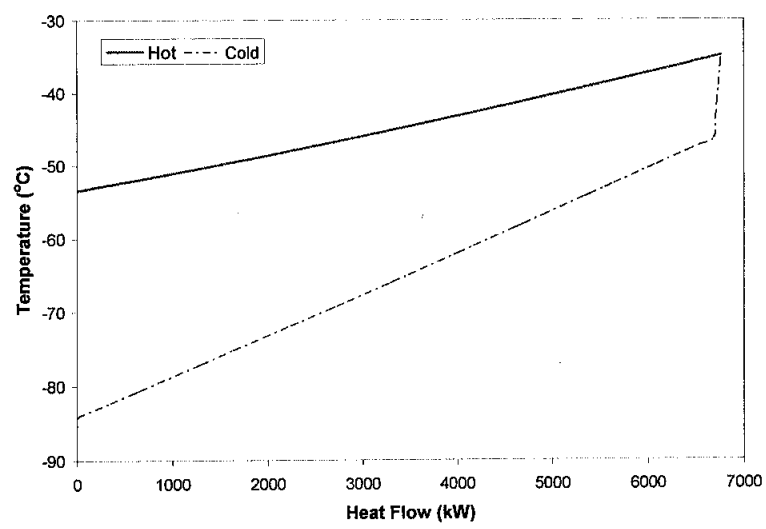
Table 3.2: Steady-state specifications and normal operating conditions (NOC) around major equipment

Equipment	Variable	Unit	Simulation	NOC	Deviation (%)
E-101	FG T_{in}	°C	19.7	20.7	4.8
	FG T_{out}	°C	-26.9	-26.9	0
	SG T_{in}	°C	-46.8*	-49.7	5.8
	SG T_{out}	°C	19.5	19.5	0
	SD3 T_{out}	°C	13.5*	11.3	19.5
	FG P_{in}	barg	56.0	56.0	0
	FG ΔP	barg	0.632	0.632	0
	SG ΔP	barg	0.733	0.733	0
E-102	FG T_{out}	°C	-34.9	-37.0	5.7
	FG ΔP	barg	0.5	NA	NA
S-101	ΔP	barg	0	0	0
E-103	PG T_{out}	°C	-53.4	-52.1	2.5
	SD1 T_{out}	°C	-36.3	-36.3	0
	SD2 T_{out}	°C	-35.0	-34.1	2.6
	SG T_{out}	°C	-47.1*	-49.7	5.2
	PG ΔP	barg	1.08	1.08	0
	SD1 ΔP	barg	0	NA	NA
	SD2 ΔP	barg	0	NA	NA
	SG ΔP	barg	0.80	NA	NA
S-102	ΔP	barg	0	0	0
KT-101	T_{out}	°C	-87.3*	-88.6	1.5
	P_{in}	barg	53.8*	55.0	2.2
	P_{out}	barg	20.9	21.0	0.5
K-101	P_{in}	barg	19.0*	19.3	1.6
	P_{out}	barg	22.7*	22.8	0.4
C-101	T_{top}	°C	-90.1*	-86.7	3.9
	T_{bot}	°C	27.3*	28.3	3.5
	P_{top}	barg	20.5	20.5	0
	P_{bot}	barg	22.0	NA	NA
	T_{35}	°C	5.3	5.3	0
	SD1 rate	ton/h	30.0	NA	NA
	SD2 rate	ton/h	3.3	NA	NA
	SD3 rate	ton/h	9.1	NA	NA
K-102	P_{out}	barg	32.9	33.6	2.1
E-106	T_{in}	°C	69.5*	62.3	11.6
	T_{out}	°C	43.0	43.2	0.5

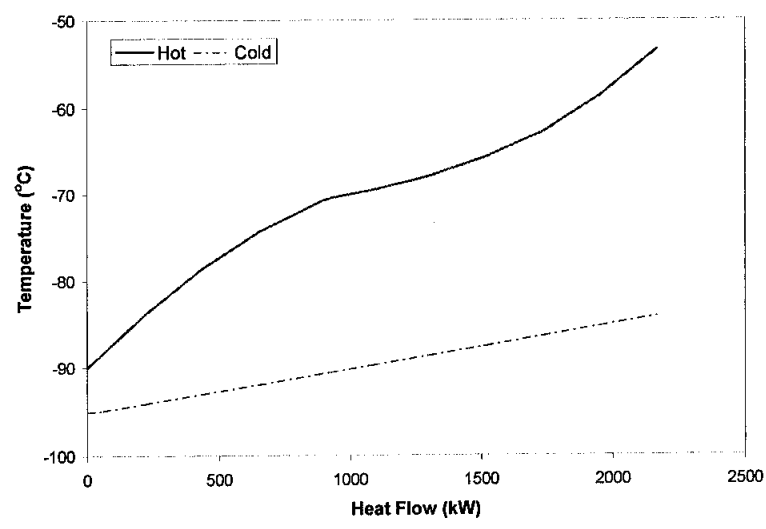
Note: * represents the flowsheet simulated values. NOC = normal operating condition based on average plant data after Ethane Extraction Improvement project (22-23 August 2005). NA = not applicable/available; FG = feed gas; SG = sales gas; PG = processed gas; SD = side draw; ΔP = pressure drop; T_{35} = demethanizer tray 35 temperature.



(a) E-101 composite curves



(b) E-103 composite curves



(c) E-105 composite curves

Figure 3.2: Composite curves at the coldboxes

Feeds to demethanizer C-101 come from three major sources at various locations of the column. They are:

1. Absorber C-102 bottom entering at tray 1.
2. Condensed liquid from separator no. 2 (S-102) entering at tray 7.
3. Condensed liquid from separator no. 1 (S-101) entering at tray 21.

Besides the above feed sources, internal liquids at trays 14, 21 and 32 are drawn off and returned at the same locations after being reboiled at coldboxes E-101 and E-103. These side draws serve two purposes: 1) to reduce methane losses at the bottom of demethanizer C-101, and 2) to cool the feed gas and processed gas. The temperature profile inside demethanizer C-101 is quite steep ranging from about -90 at the top to above 25 °C at the reboiler. The simulated values closely resemble plant data as illustrated in Figure 3.3. Internal pressure gradient is assumed linear from 20.5 (top) to 22.0 barg (bottom) because only one point (top pressure) is available for validation.

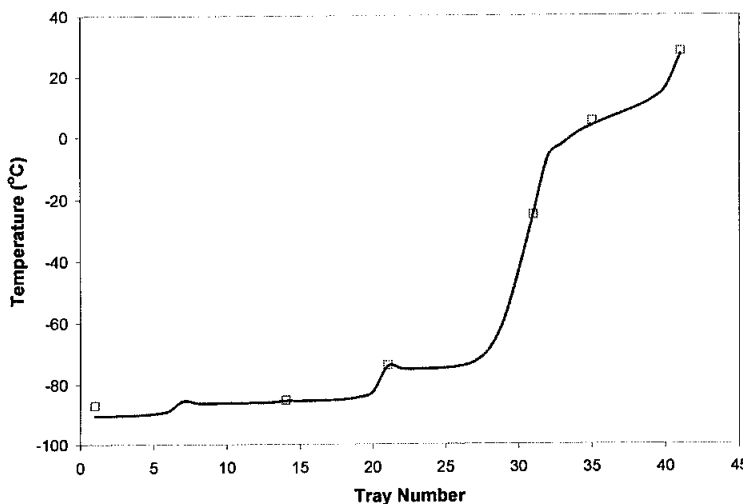


Figure 3.3: Temperature profile of demethanizer C-101. Square markers denote plant data. Solid line represents simulated values

Absorber C-102 is initially simulated as a 7-tray column for simplicity. Other specifications are top and bottom pressures at 20.8 and 20.9 barg, respectively. Liquid at bottom of absorber C-102 is refluxed to top of demethanizer C-101. On the contrary, vapor stream (overhead) leaving top of demethanizer C-101 is forwarded to bottom of absorber C-102. This looping condition increases modeling complexity

since absorber C-102 is acting like a condenser to demethanizer C-101. As a solution, a 'Recycle' operator is added to demethanizer C-101 overhead in order to solve both demethanizer C-101 and absorber C-102 flowsheets, simultaneously.

There are five turbo machineries simulated for RGP model. Two are combined as a turboexpander-compressor (KT/K-101). Major function of turboexpander KT-101 is to expand processed gas isentropically. As a result, the processed gas temperature and pressure reduce drastically by about 36 °C and 33 barg, respectively. The turboexpander KT-101 outlet is a two phase stream with 11% condensed liquid. It flows to the bottom section of absorber C-102 in order to enhance recovery of natural gas liquids. Energy produced from the processed gas expansion is utilized to drive shaft of the booster compressor K-101.

To be realistic, about 20% energy loss is estimated in this mechanical process. This is carried out by setting booster compressor K-101 duty to be 80% that of turboexpander KT-101 in HYSYS 'Set' operator. Booster compressor K-101 discharges sales gas stream at 22.7 barg. Sales gas pressure is further increased to 32.9 barg at another compressor K-102 in order to meet pipeline specification. The remaining turbo machineries are demethanizer bottom pump P-101 and absorber bottom pump P-102. Both pumps are assumed to work at 75% efficiency adiabatically. Outlet stream pressure of pumps P-101 and P-102 are specified as 30.1 and 24.9 barg, respectively.

During steady-state model development, there are three main concerns that require special attention:

1. Inadequate capacity of demethanizer reboiler E-104
2. Dry ice formation at top of absorber C-102
3. Temperature crosses at coldboxes E-101, E-103, E-105

The first concern relate to composition of feed gas streams. The higher the content of natural gas liquids in feed gas streams, the more energy is required to reboil the bottom of demethanizer C-101. As a result, reboiler E-104 outlet temperature will decrease at excessive presence of natural gas liquids if the steam flow rate (HYSYS

'Direct Q' duty) remains constant. The second concern relates to amount of carbon dioxide in feed gas streams. Dry ice (solid carbon dioxide) formation is favored at high carbon dioxide level and subzero temperature. This is undesirable because dry ice can clog packings of absorber C-102 and layers inside coldboxes E-101, E-103 and E-105. If this happens, C-102 absorption capacity will decrease due to reduction in the mass transfer area. Similarly, heat transfer areas of the coldboxes will be reduced rendering them ineffective. The most critical part within RGP is the top feed of absorber C-102 since it is the coldest stream (about -101°C) in the plant. However, no formation of dry ice is detected here by HYSYS built-in 'Carbon Dioxide Freeze Out' utility.

Temperature cross is another major concern because it can take place in any one of the three coldboxes E-101, E-103 and E-105. Temperature cross occurs when the hot pinch temperature is lower than the cold pinch temperature. This condition entails the transfer of heat from the cold stream to the hot stream, which violates the second law of thermodynamics. One way to circumvent this situation is to specify a minimum difference of 5°C between the cold and hot pinch temperatures. If this approach is inadequate, flow rates of by-passed streams should be reduced.

3.3.2 Dynamic Modeling

Once a high fidelity steady-state model is set up, three additional steps are required to be taken in order to prepare the model for dynamic simulation. These steps are: 1) sizing of unit operations, 2) specification of pressure or flow condition at boundary streams, and 3) installation of controller. As a first step, all unit operations need to be sized accordingly. If plant data are available, these values are used for sizing information. This is preferable in order to produce a more realistic dynamic model. In some circumstances, the plant data are missing or outdated due to ongoing rejuvenation and revamp projects. In HYSYS, an alternative sizing procedure may be used. Vessels such as condensers, separators and reboilers should be able to hold 5-15 minutes of liquid accumulation. The vessel volumes may be quickly estimated by dividing the steady-state values of the entering liquid flow rates from the holdup time.

For a column, only the internal section needs to be sized. This is accomplished by specifying the tray/packing type and dimensions. Types of trays available in HYSYS are sieve, valve, bubble cap, chimney and sump. Tray must be specified with at least the following dimensions: 1) tray diameter, 2) tray spacing, 3) weir length, and 4) weir height. For a packed column, there are a number of packing types to choose from. Most of the packing comes with the pre-specified properties such as void fraction and surface area. The minimum dimension need to be entered is the packing volume or packing height and column diameter. Design specifications for demethanizer C-101 and absorber C-102 are presented in Tables 3.3 and 3.4, respectively.

Table 3.3: Sizing of demethanizer C-101 column and reboiler E-104

Parameter	Value
Tray Space (m)	0.550
Tray Diameter (m)	2.450
Tray Type	Valve
Tray efficiency (%)	90
Weir Height (mm)	48
Weir Length (m)	2.009
Flow Paths	2
Weeping Factor	1.000
Tray Thickness (mm)	3.175
Foaming Factor	1
Maximum Pressure Drop (mm of liquid)	152.4
Maximum Flooding (%)	85
Valve Material Density (kg/m^3)	8220
Valve Material Thickness (mm)	1.524
Hole Area (% of active area)	15.3
Valve Orifice Type	Straight
Valve Design Method	Glitsch
Side Weir Type	Straight
Maximum Weir Loading ($\text{m}^3/\text{h-m}$)	89.42
Downcomer Volume (m^3)	0.3019
Downcomer Type	Vertical
Downcomer Clearance (mm)	38
Max Downcomer Backup (%)	50
Side Downcomer Top Width (mm)	304.8
Side Downcomer Bottom Width (mm)	304.8
Center Downcomer Top Width (mm)	330.2
Center Downcomer Bottom Width (mm)	330.2
Reboiler Diameter (m)	3.5
Reboiler Length (m)	9.3
Reboiler Orientation	Horizontal

Table 3.4: Sizing of absorber C-102 column

Section	1	2	3	4	5
Internal Type	Chimney	Packed Cascade	Packed Cascade	Chimney	Sump
Packing Type	-	MiniRing (Metal) No. 3	MiniRing (Metal, Random) No. 2	-	-
Height (m)	0.6	1.829	3.657	0.765	4.304
Diameter (m)	3.2	3.2	3.2	3.2	3.2
Weir Height (mm)	227.2	-	-	227.2	-
Weir Length (m)	2.56	-	-	2.56	-

For heat exchangers, each holdup system is sized with a k -value. This value is a constant representing the inverse resistance to flow as shown in Equation 3.1 (Aspentech, 2006):

$$F = k\sqrt{\Delta P} \quad (3.1)$$

where,

F = flow rate

k = conductance or reciprocal of resistance

ΔP = frictional pressure loss, which is pressure drop minus static head

The k -value may be calculated by HYSYS using the converged solution of the steady-state model. For practical purposes, only one heat transfer zone is required for refrigeration cooler E-102 and the air-cooler E-106. Refrigeration cooler E-102 is initially supplied with the duty obtained from steady-state model. During simulation, this duty varies in order to meet controller TC-101 setpoint. Air cooler E-106 is equipped with two fans. Each fan is designed to handle 3600 actual m³/h of air at maximum speed of 60 rpm. Air enters cooler E-106 at 28 °C and atmospheric condition. Internally, air cooler E-106 is configured with two tube rows and two passes that can deliver 500 kW/°C of convective heat transfer capacity (UA value). Additional specifications for coolers E-102 and E-106 are presented in Table 3.5.

Table 3.5: Sizing of refrigeration cooler E-102 and air cooler E-106

	E-102	E-106
Zones	1	-
Volume (m ³)	17	430
<i>k</i> -value	1.544	3.503

Simulation of coldboxes E-101, E-103 and E-105 is more challenging as they are modeled as LNG heat exchangers. Sizing is required for each zone and layer. A zone refers to horizontal segmentation of a coldbox. Higher number of zones increases modeling accuracy at the expense of higher computational effort. Similarly, a layer refers to vertical segmentation of a coldbox. Each layer carries fluids only from one stream. Thus number of layers is equal to number of streams entering or leaving the coldboxes. Mixing of fluids across layers is prohibited to preserve composition of individual streams. The allowable modes of heat transfer are through conduction between layers and convection by fins. For practical purposes, number of zones in the coldboxes is limited to three. In each zone, geometry, metal properties and a few sets of layers are specified according to mechanical design databook of the actual plant (Table 3.6). On each layer, plate and fin properties are entered as default values. The UA values are taken as constants from steady-state model, and specified in each zone and layer. The *k*-values are initialized from steady-state model and then modified to minimize error between actual plant and simulated data.

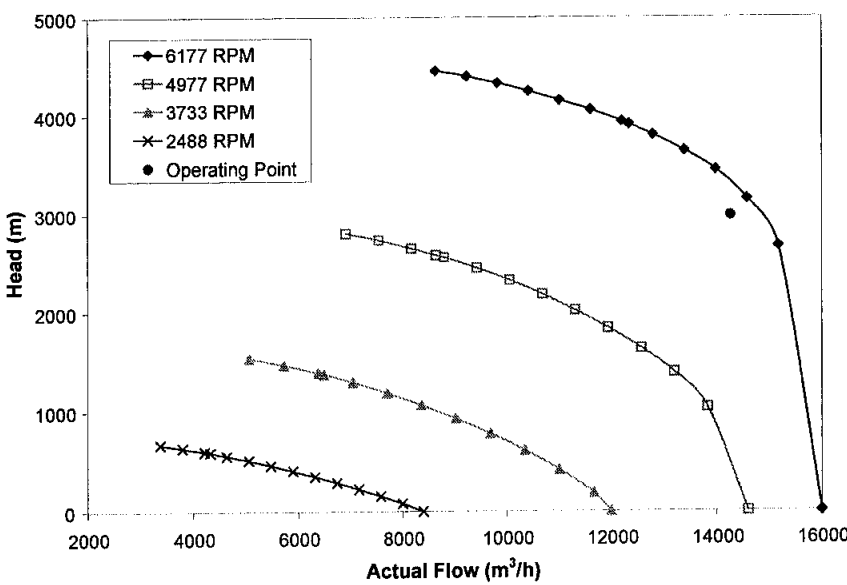
Equipment with negligible holdup are easily modeled in dynamic mode. For example, dynamic pressure specification for a mixer is always set to 'Equalize all'. This setup avoids backflow condition, in which one of the inlet streams with the lowest pressure carries a negative flow rate and thus flows away from the mixer. A tee split stream specification may be selected as constant values at the initial stage. However, this is not recommended for final simulation since flows of the splitter outlets are governed by the differences in the upstream and downstream pressures. If flow of one of the outlet streams is specified, the rate should be regulated by a split-range controller. Flows of fluid across valves are governed by an equation similar to Equation 3.1. In this case, the *k*-value is substituted with the valve sizing coefficient, C_v , to be consistent with the literature. The valve is sized with a 50% valve opening and 15-30 kPa pressure drop at a typical flow rate. Calculation of a C_v value is performed based on the current steady-state profile.

Table 3.6: Dynamic specifications of coldboxes E-101, E-103 and E-105

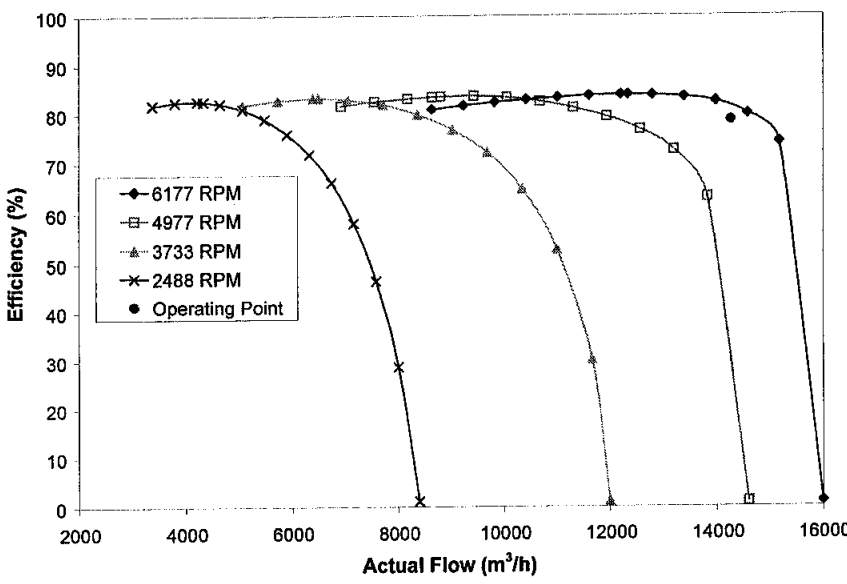
	E-101	E-103	E-105
Zone Geometry			
• Width (m)	1.05	1.05	1.05
• Height (m)	1.281	1.281	1.281
Zone Metal Properties			
• Thermal cond (W/m-°C)	180	180	180
• C_p (kJ/kg-°C)	0.88	0.88	0.88
• Density (kg/m ³)	2748	2748	2748
Zone Layers			
• Number of Layers in Set	3	4	2
• Repeated Sets	12	6	5
Plate and Fin Properties			
• Perforation (%)	0	0	0
• Height (mm)	6.73	6.73	6.73
• Pitch, fins/m	530	530	530
• Fin thickness (mm)	0.419	0.419	0.419
• Plate thickness (mm)	1.22	1.22	1.22
Convective UA (kW/°C)			
• Layer 1	1881.172	242.563	84.190
• Layer 2	1982.556	275.894	84.190
• Layer 3	101.385	7.479	-
• Layer 4	-	25.852	-
Conductance (k-value)			
<i>Zone 1</i>			
• Layer 1	0.289	0.215	0.220
• Layer 2	0.115	0.106	0.016
• Layer 3	0.320	0.080	-
• Layer 4	-	0.200	-
<i>Zone 2</i>			
• Layer 1	0.325	0.260	0.230
• Layer 2	0.139	0.119	0.014
• Layer 3	0.408	0.102	-
• Layer 4	-	0.160	-
<i>Zone 3</i>			
• Layer 1	-	-	0.200
• Layer 2	-	-	0.014

Turbo machineries such as pumps, compressors and expanders may be simulated in a rigorous manner. The main requirement is availability of the characteristic curves of individual equipment. A complete characteristic curve must consist of head and efficiency curves. In HYSYS, pump curves can be generated automatically based on designated pump speeds and steady-state conditions. This feature reduces modeling effort since a realistic pump can be installed based on current flowsheet conditions. However, automatic curve generator is unavailable for compressors and

turboexpanders. The characteristic curves need to be added at the ‘Rating-Curves’ page in order to enhance rigor of dynamic model. Compressors and turboexpanders may also be modeled based on steady-state duty, and adiabatic or polytropic efficiency specifications. For pumps, only the power and static head are required. This simplification is only recommended to ease the transition from steady-state to dynamic mode or to force a more difficult model to converge.



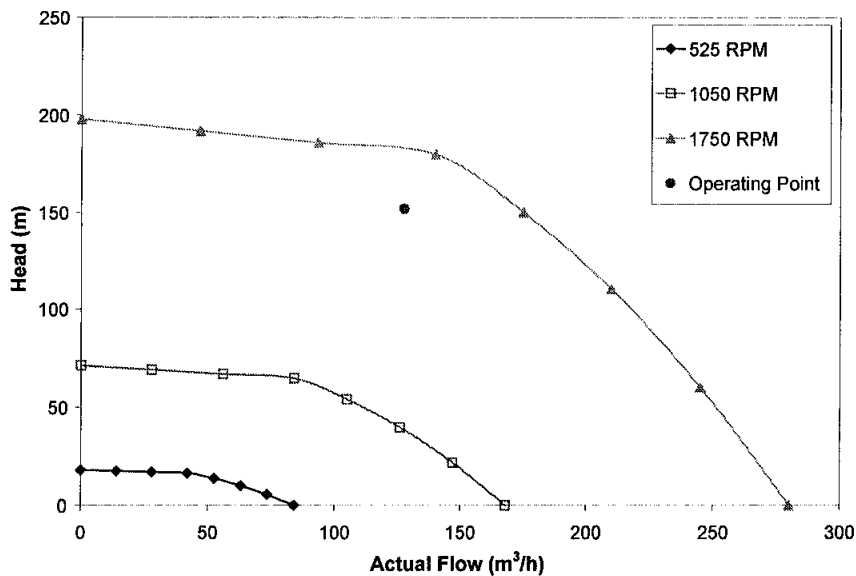
(a)



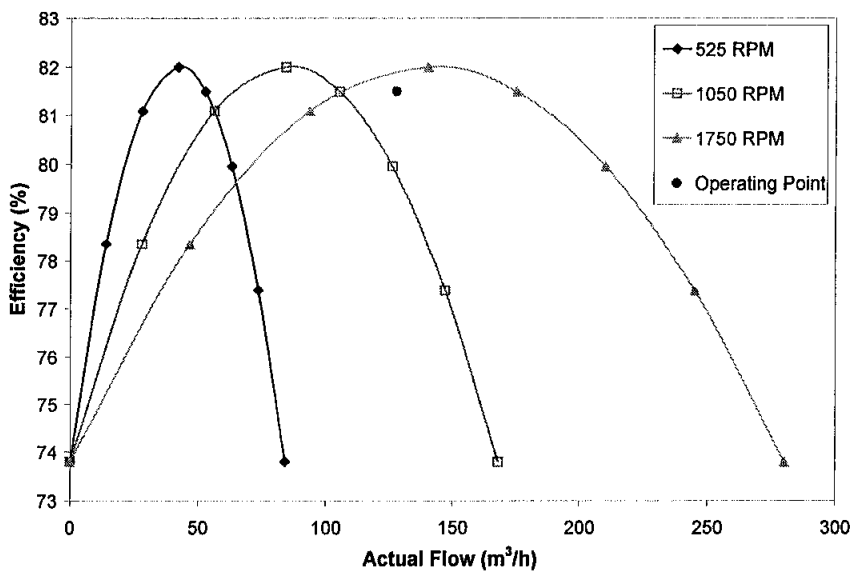
(b)

Figure 3.4: Head (a) and efficiency (b) curves of booster compressor K-102. Current operating point is shown as a solid circle.

In the current work, turboexpander-compressor K/KT-101 is modeled in this manner since their characteristic curves are unavailable. On the other hand, booster compressor K-102, demethanizer bottom pump P-101 and absorber bottom pump P-102 are modeled using corresponding curves as illustrated in Figures 3.4 to 3.6. Multispeed design characteristics of compressor K-102 and pump P-101 are necessary because these units are manipulated by PI controllers to maintain setpoints of PC-101 and LC-103, respectively (Figure 3.4).

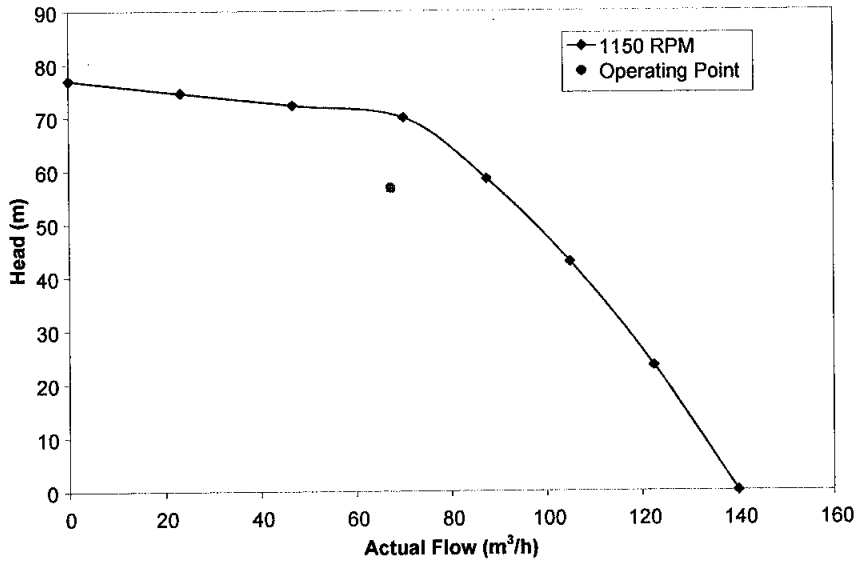


(a)

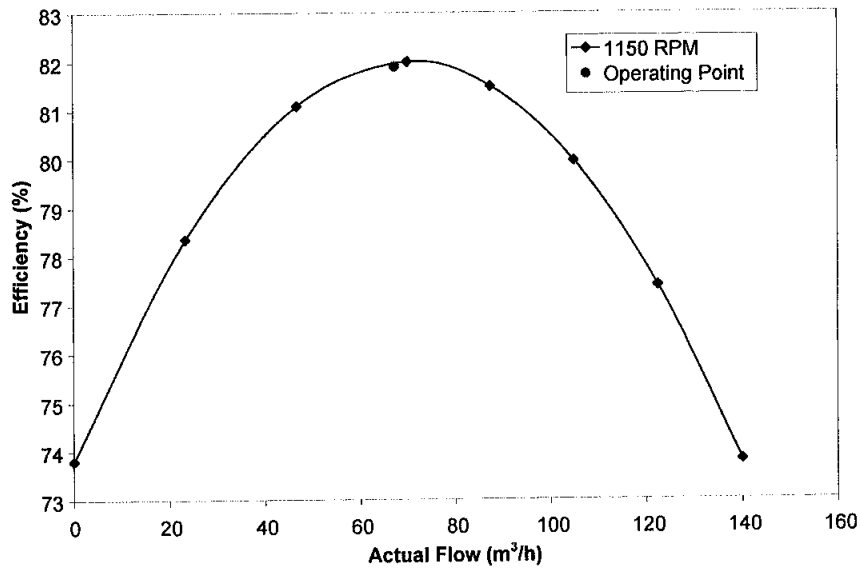


(b)

Figure 3.5: Head (a) and efficiency (b) curves of demethanizer bottom pump P-101. Current operating point is shown as a solid circle.



(a)



(b)

Figure 3.6: Head (a) and efficiency (b) curves of absorber bottom pump P-102. Current operating point is shown as a solid circle.

The second step in the transition from steady-state to dynamic model is to enter a pressure or flow condition at all boundary streams. This pressure-flow specification is important because pressure and material flows are solved simultaneously in HYSYS. Any inconsistency will stop the 'Integrator' due to convergence failure. In addition, compositions and temperatures of all feed streams at the flowsheet boundary must be input *a priori*. Physical properties of other streams are then calculated sequentially at each downstream unit operation based on the specified holdup model values (k and C_v). In the current simulation work, all boundary streams are specified with pressure

values. The feed streams enter RGP at 56.0 barg. The exiting streams are the NGL stream at 28.5 barg and the SG stream at 33.5 barg. Flow specification is avoided since inlet stream flows can be governed by regulatory controllers and outlet streams flows are dictated by separation processes in the RGP.

The final step is installation of regulatory controllers. In most cases, basic regulatory controllers are sufficient for stabilizing a plant model. However, advanced regulatory controllers such as cascade, ratio, split range and surge controllers are required to handle more difficult control problems. In this work, the RGP is equipped with the following controller schemes:

1. Three PI flow controllers at plant inlets to control individual flow rates of feed gas streams.
2. Two PI temperature controllers to control refrigeration cooler E-102 outlet stream temperature and demethanizer C-101 tray 35 temperature.
3. Two PI level controllers to control reboiler E-104 level and absorber C-102 bottom level.
4. Two cascade controllers to control separator no. 1 (S-101) and separator no. 2 (S-102) levels by manipulating the liquid flow rates at the outlets of the respective separators. Each cascade controller consists of a primary level controller and a secondary flow controller.
5. Three split range controllers (SRC), one to regulate top pressure of separator no. 2 (S-102) and the other two are employed to control feed gas temperature at coldbox E-101 outlet and processed temperature at coldbox E-103 outlet.
6. A ratio controller to regulate flow of stream that flows to gas subcooled process (GSP) unit over that to turboexpander KT-101.

7. A surge controller at booster compressor K-102 to prevent compressor blade damage.
8. A digital on-off controller to control air cooler E-106 outlet temperature.

Locations of these controllers are shown in Figure 3.7. The controllers are tagged based on their orders of installation. Starting values of PID controller tuning parameters follow those suggested by Svrcek et al. (2006). These values as listed in Table 3.7 are optimized for a quarter decay ratio criterion and recommended to be used as the initial steady-state. Fine tuning should be performed for sluggish controllers. For extremely fast acting controllers, a setpoint ramping procedure may be imposed to enhance realism and to stabilize plant. In general, increasing the controller gain will result in faster closed loop response while decreasing it will cause a slower but more stable response. The integral action in PI control should be applied to eliminate the controlled variable offset from the setpoint. The derivative action in the PID control scheme serves as the lead term. Thus a PID controller is capable to reduce the oscillation period of the PI controller due to its ability in predicting the error direction. On the other hand, HYSYS 'Autotuner' feature may also be used to calculate the controller gain as well as the integral and/or derivative times. However, the dynamic model must be stabilized *a priori* before this feature is enabled. In the next section, final tuning parameter values are presented and major control philosophies are discussed.

Table 3.7: Suggested tuning parameter settings (Svrcek et al., 2006)

Controller	K_c	τ_i (min)	τ_d (min)
FC	0.4-0.65	0.05-0.25	-
PC (l)	0.5-2	0.1-0.25	-
PC (v)	2-10	2-10	-
LC	2-10	1-5	-
TC	2-10	2-10	0-5

Note: FC=flow controller; PC=pressure controller; LC=level controller; TC=temperature controller. For PC, (l) = liquid; (v) vapor; K_c =controller gain; τ_i =integral time; τ_d =derivative time.

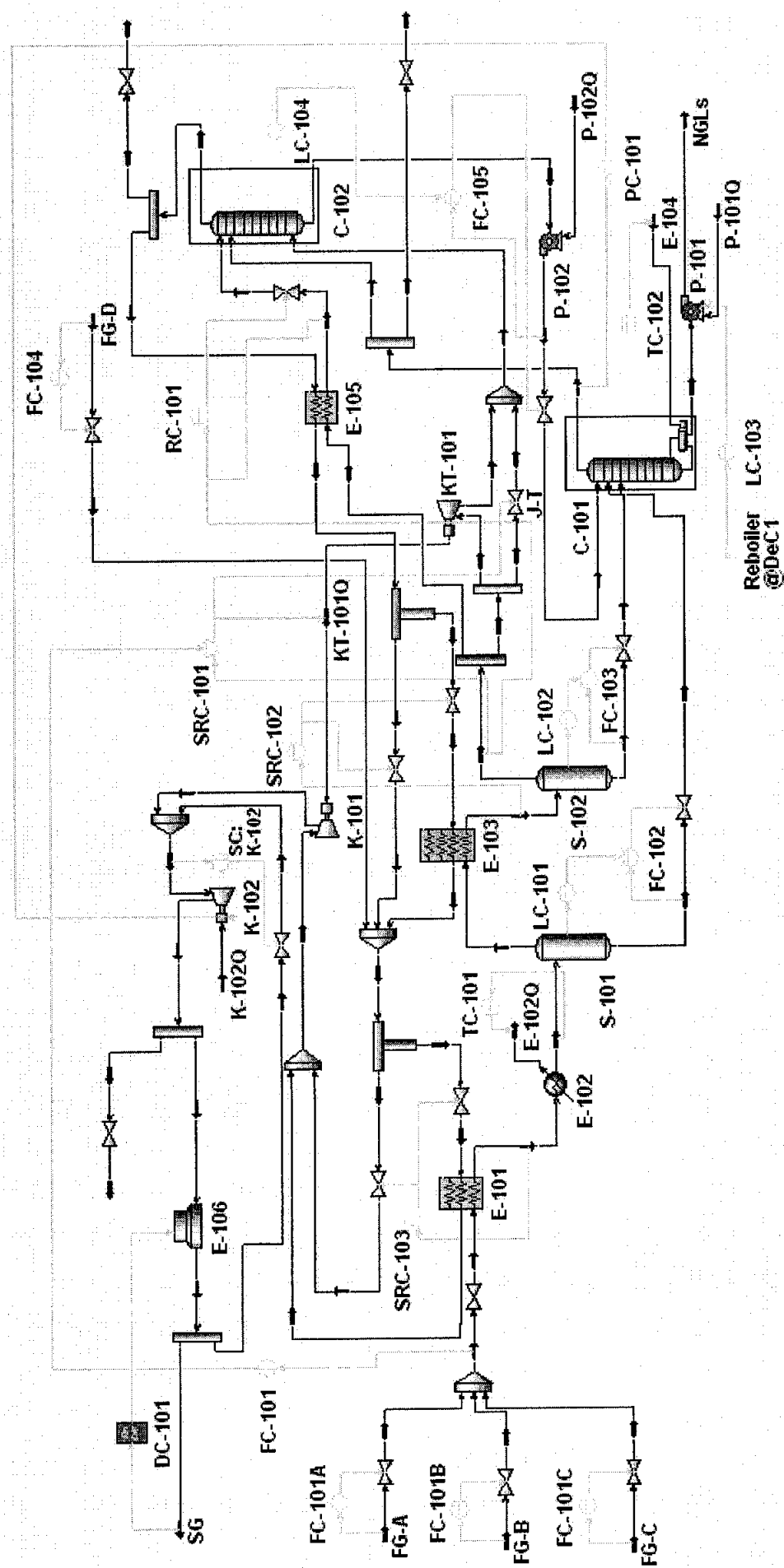


Figure 3.7: Process and instrumentation diagram of RGP

3.4 RGP Control Philosophies

There are four major control schemes adopted in RGP namely: 1) plant load control, 2) demethanizer overhead pressure control, 3) sales gas quality control, and 4) plant temperature control. The first control scheme is used mainly during load scheduling. The remaining three schemes are employed during mode scheduling. Philosophies behind these control schemes are presented in this section.

3.4.1 Plant load control

The purpose of this loop is to control flow of mixed feed gas or plant load (Figure 3.8). At normal condition, plant load is maintained at 280 ton/h by flow controller FC101. This is achieved by regulating separator S-102 pressure via split-range operation of controller SRC101. Setpoint of split-range controller SRC101 is sent remotely by flow controller FC101. Both FC101 and SRC101 are reverse-acting controllers. This configuration renders controller output to decrease when process value is higher than target specification.

Split range control is executed by manipulation of inlet guide vanes of turboexpander KT-101 and/or Joule-Thompson (J-T) valve through parallel operation (Figure 3.9). The inlet guide vanes are simulated as a 'Control Valve' of turboexpander KT-101 duty, which is designed to fully close at 4 mA and fully open at 12 mA. On the other hand, Joule-Thompson valve is modeled as a linear valve with C_v value of 100 US gallon/min. The J-T valve is designed to only open after turboexpander KT-101 duty reaches a maximum value of 3000 kW. Important plant load control parameters and their corresponding values are shown in Table 3.8.

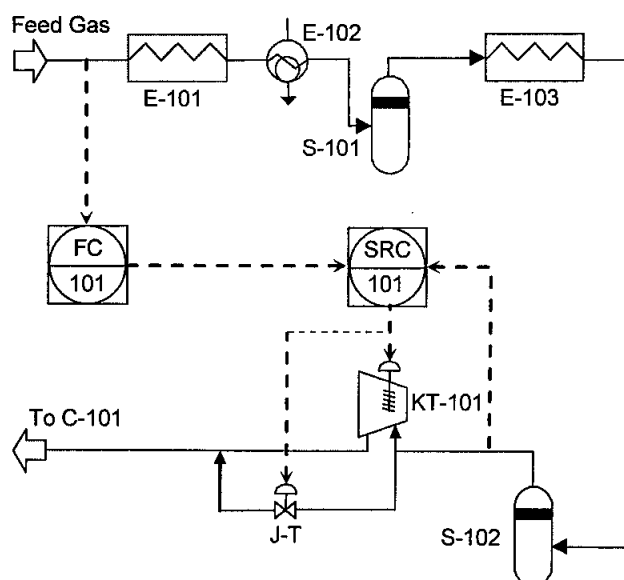


Figure 3.8: Plant load control scheme

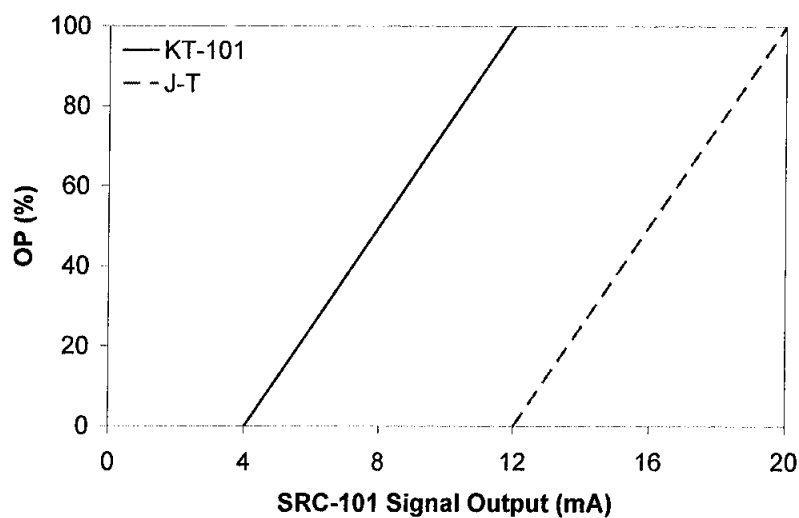


Figure 3.9: SRC-101 split range setup

Table 3.8: Control and tuning parameters

	FC101	SRC101
Action	Reverse	Reverse
Mode	Auto	CAS
Range	0 to 400 ton/h	0 to 100 barg
SP	280.0 ton/h	51.8 barg
K_c	2.4	2.0
τ_i	2.7	2.0

3.4.2 Demethanizer overhead pressure control

Demethanizer C-101 overhead pressure is controlled by varying compressor K-102 speed through pressure controller PC101 (Figure 3.10). Pressure controller PC101 is a direct-acting controller, which increases its output when process value is higher than setpoint (Table 3.9a). Increasing output of pressure controller PC101 increases compressor K-102 speed. Higher speed of compressor K-102 reduces its suction pressure and thus overhead pressure of demethanizer C-101.

In the event of low suction volume, potential surge of compressor K-102 is prevented through opening of a kickback valve by reverse-acting controller SC101. Surge control parameters A, B and C (Table 3.9b) are calculated based on the lowest values of compressor K-102 head curves (Figure 3.4). Control and surge lines as well as quick-opening action of surge controller SC101 are standard design decisions.

An important function of pressure controller PC101 is to provide means for changing RGP operation mode. Change of plant mode from natural gas liquids to sales gas increases demethanizer C-101 overhead pressure from 22 to 24 barg. Indirectly, sales gas final temperature is also increased. The final temperature of sales gas is regulated by on-off controller TC103, which fully opens when process value rises above 34 °C and fully closes when process value drops below 28 °C via a latch mechanism.

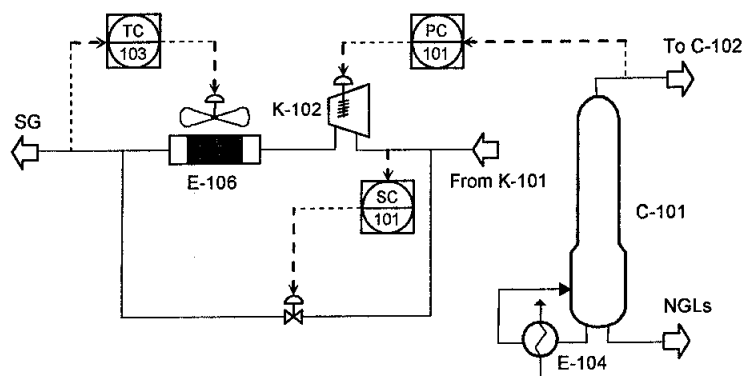


Figure 3.10: Demethanizer overhead pressure control scheme

Table 3.9 a: Control and tuning parameters

	PC-101	SC-101	TC-103
Action	Direct	Reverse	Latch
Mode	Auto	Auto	Auto
Range	0 to 60 barg	1000 to 20,000 m ³ /h	0 to 60 °C
SP	22 barg (24 barg)	6723 m ³ /h	28≤SP≤34 °C
K _c	2.0	2.0	N/A
τ _i	2.0	2.0	N/A

Note: (·) = SG recovery mode; N/A=not applicable.

Table 3.9b: Surge control parameters

	SC-101
Parameter A, m	1606.5
Parameter B, m/(m ³ /s)	-1782.3
Parameter C, m/(m ³ /s) ²	2130.6
Control line, %	10.0
Backup line, %	5.0
Quick opening, %/s	3.0

3.4.3 Sales Gas Quality Control

Quality of sales gas is measured by its composition. A high level of carbon dioxide in sales gas is undesirable due to environmental concerns. This issue is fortunately resolved in a section upstream of RGP. On the other hand, higher contents of ethane and heavier hydrocarbons, termed natural gas liquids, increase gross heating value (GHV) of the sales gas. Low GHV indicates lean sales gas whereas high GHV denotes losses of natural gas liquids. Since separation of natural gas is a pseudo-binary cut process, sales gas quality is controlled by specifying its ethane content.

During natural gas liquids mode, ethane content in absorber C-102 overhead is specified at 2.0 mole % (Table 3.10). This is achieved by regulating temperature of processed gas exiting coldbox E-103 through split-range controller SRC102 (Figure 3.11). Division of sales gas entering or bypassing coldbox E-103 is carried out via cross setup of valves A and B (Figure 3.12). Valve A opens linearly from 4 to 20 mA signal whereas valve B closes linearly within the same range.

During sales gas mode, the ethane content is set at 5.0 mole %. A higher cut percentage is crucial in preventing excessive condensation in separator S-102 and bottom of absorber C-102. Liquid level at separator S-102 is regulated by cascading signal from level controller LC102 to flow controller FC103. Similarly, liquid level at bottom of absorber C-102 is controlled by a cascade controller consisting of level controller LC104 and flow controller FC105.

Recovery of natural gas liquids is improved by increasing the ratio of processed gas flowing to absorber C-102 over that to turboexpander KT-101. The ratio is specified at 0.005 for sales gas mode and 0.15 for natural gas liquids mode. High limit of controller RC101 ratio is dictated by maximum flow rate of processed gas to absorber C-102, which is 40 ton/h by design. Low limit is set to ensure convergence of coldbox E-105 model during steady-state and dynamic simulations.

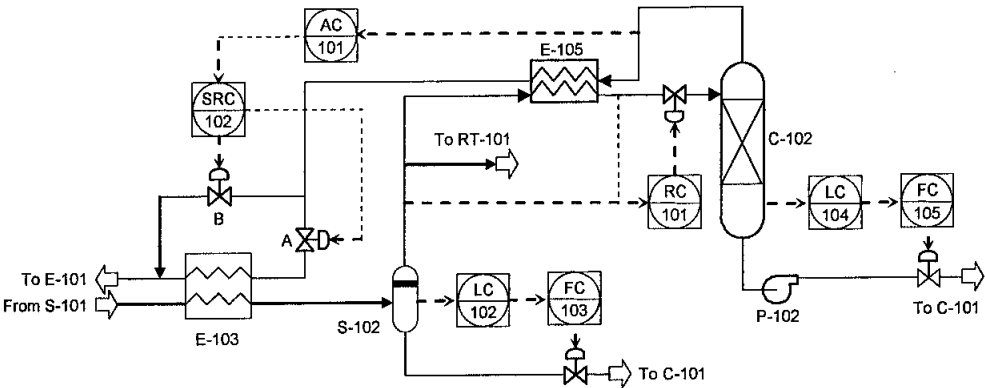


Figure 3.11: Sales gas quality control scheme

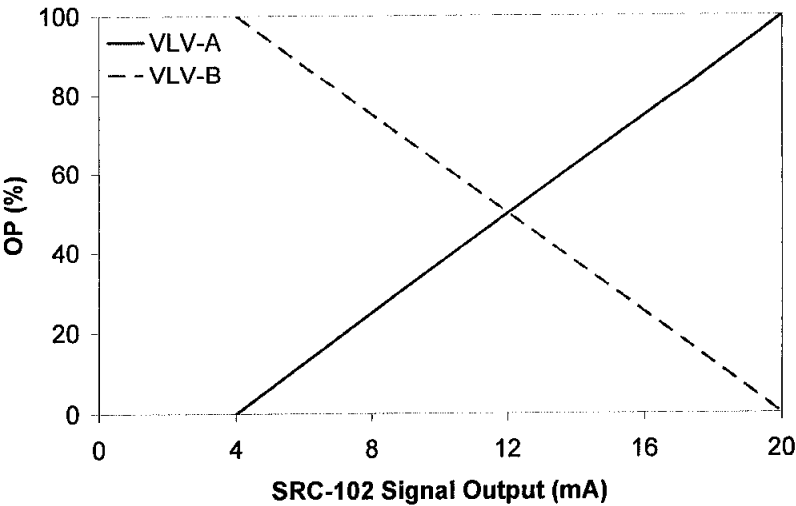


Figure 3.12: SRC-102 split range setup

Table 3.10: Control and tuning parameters

	AC-101	SRC-102	LC-102	FC-103
Action	Reverse	Direct	Direct	Reverse
Mode	Auto	CAS	Auto	CAS
Range	0 to 10 mol %	-100 to 0 °C	0 to 100 %	0 to 60 ton/h
SP	2.0 % (5.0%)	-53.9 °C (-43.3 °C)	50 %	19.9 ton/h (17.0 ton/h)
K_c	1.0	2.0	1.8	0.25
τ_i	0.1	2.0	32.1	0.1

	RC-101	LC-104	FC-105
Action	Reverse	Direct	Reverse
Mode	Auto	Auto	CAS
Range	0 to 40 ton/h	0 to 100 %	0 to 60 ton/h
SP	0.15 (0.005)	50 %	35.0 ton/h (26.1 ton/h)
K_c	0.2	1.8	0.25
τ_i	0.2	32.1	0.1

Note: (·) = SG recovery mode; CAS=cascade mode.

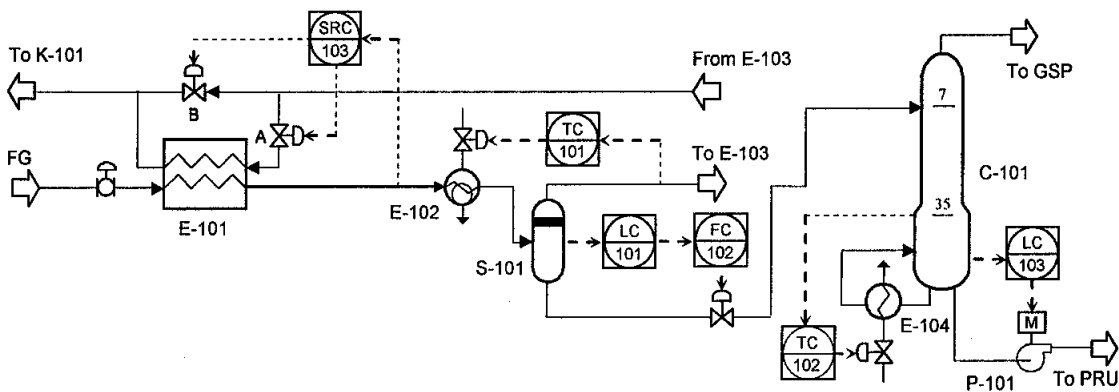
3.4.4 Plant Temperature Control

Operating condition of RGP is indicated in two places. The primary location is at top of absorber C-102. Temperature reaches -90 °C or lower during natural gas liquid mode and around -70 °C during sales gas mode. However, temperature swing at this location can only be achieved through a sequence of events termed mode scheduling. In other words, the primary indicator of RGP state cannot be controlled directly.

Another location signifying RGP condition is at refrigeration cooler E-102 outlet. Here, feed gas is chilled in two stages (Figure 3.13). The first stage is at coldbox E-101 and the second stage at cooler E-102. Temperature of feed gas exiting coldbox E-101 is regulated by reverse-acting split-range controller SRC103. The split of sales gas flow is governed by cross configuration of valves A and B as explained previously (Figure 3.14). Larger amount of sales gas entering coldbox E-101 results in cooler feed gas temperature. Setpoints for natural gas liquids and sales gas modes are -30.5 and -25.1 °C, respectively (Table 3.11).

In the second stage, feed gas is further chilled by refrigeration cooler E-102. The chilling process is regulated by direct-acting temperature controller TC101. This setup compels the controller output to increase when process value is higher than setpoint.

Sufficient heat is required for good separation of sales gas from natural gas liquids in demethanizer C-101. Control objective is to maintain tray 35 temperature at 5 °C in both modes. This is achieved by manipulating reboiler E-104 duty through temperature controller TC102. In the event of excessive boiling, liquid level at demethanizer C-101 bottom is regulated by level controller LC103. The controller output is speed of pump P-101 with multiple head and efficiency curves (Figure 3.5).



The graph shows the relationship between SRC-103 Signal Output (mA) on the x-axis and OP (%) on the y-axis. The x-axis ranges from 0 to 20 mA with major ticks every 4 units. The y-axis ranges from 0 to 100% with major ticks every 20 units. Two lines are plotted: VLV-A (solid line) and VLV-B (dashed line). VLV-A starts at (4, 0) and increases linearly to (20, 100). VLV-B starts at (4, 100) and decreases linearly to (20, 0). The two lines intersect at (12, 50).

SRC-103 Signal Output (mA)	VLV-A OP (%)	VLV-B OP (%)
4	0	100
8	25	75
12	50	50
16	75	25
20	100	0

Figure 3.14: SRC-103 split range setup

Table 3.11: Control and tuning parameters

	TC-101	SRC-103	TC-102
Action	Direct	Reverse	Reverse
Mode	Auto	Auto	Auto
Range	-70 to -10 °C	-100 to 0 °C	-30 to 20 °C
SP	-40.0 °C (-30.6 °C)	-30.5 °C (-25.1 °C)	5.0 °C
Kc	0.31	1.0	0.91
Ti	0.32	1.0	9.7

	LC-101	FC-102	LC-103
Action	Direct	Reverse	Direct
Mode	Auto	CAS	Auto
Range	0 to 100 %	0 to 60 ton/h	0 to 100 %
SP	50 %	30.4 ton/h (15.4 ton/h)	50 %
Kc	1.8	0.25	2.0
Ti	23.6	0.1	0.3

Note: (·)=SG recovery mode; CAS=cascade mode.

Up to this point, only regulatory control of RGP is discussed. Given challenges such as feed disturbance, rising operational costs and fluctuating prices of natural gas liquids, sustaining production at an optimum cost is crucial to the RGP. These challenges may be alleviated by implementing an MPC scheme in replacement of the current regulatory control schemes. Discussion on MPC development is the subject of the next section.

3.5 Model Predictive Control

Model predictive control (MPC) refers to a cluster of advanced control algorithms that employ a process model to make prediction of future plant state. Applications of MPC technology are widely spread out in areas such as refining, petrochemical, gas processing, polymer, pulp and paper, automotive, and aerospace industries (Qin and Badgwell, 2003). In general, MPC algorithms are classified as linear or nonlinear depending upon the type of process model used. A process model is obtained through empirical or first-principle modeling.

A first-principle model is derived from material and energy balances of an actual plant. Parameters such as hold-up coefficients (k), valve coefficients (C_v), overall heat transfer coefficients (U) and reaction kinetic constants (k_R) are either estimated from

off-line modeling or adjusted on-line using extended Kalman filter. The first-principle model is generally written in discrete-time implicit form as:

$$\mathbf{x}_{k+1} = \mathbf{f}(\mathbf{x}_k, \mathbf{u}_k, \mathbf{v}_k, \mathbf{w}_k) \quad (3.2a)$$

$$\mathbf{y}_k = \mathbf{g}(\mathbf{x}_k, \mathbf{u}_k) + \boldsymbol{\xi}_k \quad (3.2b)$$

where $\mathbf{x} \in \mathcal{R}^n$ is a vector of state variables, $\mathbf{u} \in \mathcal{R}^{m_u}$ is a vector of manipulated variables or inputs, $\mathbf{y} \in \mathcal{R}^{m_y}$ is a vector of controlled variables or outputs, $\mathbf{v} \in \mathcal{R}^{m_v}$ is a vector of measured disturbance variables or input noise, $\mathbf{w} \in \mathcal{R}^{m_w}$ is a vector of unmeasured disturbance variables or process noise, and $\boldsymbol{\xi} \in \mathcal{R}^{m_\xi}$ is a vector of measurement noise. In most circumstances, Equation 3.2 is highly nonlinear to reflect the true process. However, linearization of process model around operating conditions is also a common practice. Nonlinear MPC utilizes nonlinear form of Equation 3.2 to predict future responses of the process. In-depth discussion on nonlinear MPC is beyond the scope of this work. Comprehensive overview of nonlinear MPC can be found in Allgower et al. (1999).

An empirical model is developed from input-output information of a plant that is excited with a sequence of systematic testing signals. Common process models are FIR/FSR, transfer functions, auto-regressive with exogenous inputs (ARX) and state-space models. Transfer function models are traditionally employed by process control engineers due to several reasons namely: 1) simplicity of models, 2) familiarity with model structures, and 3) ability to relate model parameters with physical elements. The simplest form of transfer function is first-order model (Seborg et al., 2004):

$$\frac{y(s)}{u(s)} = \frac{K_p}{\tau_p s + 1} \quad (3.3)$$

which relates output $y(s)$ to input $u(s)$ through process gain K_p and time constant τ_p . Transfer function models are written in Laplace domain as denoted by transformed variable s . First-order and second-order models with or without time delay are typically used. Often lead-lag models are also utilized to describe more complex processes.

To be useful, the continuous-time transfer function models need to be transformed because modern MPC algorithms are based on discrete-time models. An ARX model can be written in an equivalent matrix form of discrete-time transfer function as (Kailath, 1980):

$$\mathbf{y}_k = \Phi_y(q^{-1})\mathbf{y}_k + \Phi_u(q^{-1})\mathbf{u}_k + \Phi_v(q^{-1})\mathbf{v}_k + \Phi_w(q^{-1})\mathbf{w}_k + \zeta_k \quad (3.4a)$$

where

$$\zeta_k = [\mathbf{I} - \Phi_y(q^{-1})]\xi_k \quad (3.4b)$$

A notable feature of ARX model is backward-shift operator q^{-1} that represents difference terms compactly. The difference terms appear in Equation 3.4 when transfer function models are discretized at sampling time Δt . For example, the term $\Phi_u(q^{-1})\mathbf{u}_k$ can be represented in two-term polynomial series as $b_1q^{-1}\mathbf{u}_k + b_2q^{-2}\mathbf{u}_k$ and expanded as $b_1\mathbf{u}_{k-\Delta t} + b_2\mathbf{u}_{k-2\Delta t}$. A general form of ARX polynomial model can thus be written as:

$$\mathbf{A}\mathbf{y}_k = \mathbf{B}\mathbf{u}_k + \zeta_k \quad (3.5)$$

where \mathbf{A} and \mathbf{B} , respectively, are matrices of output and input coefficients with appropriate sizes. For convenience, measured \mathbf{v} and unmeasured \mathbf{w} disturbance variables are grouped as inputs to the process. Noise ζ can be colored even though measurement noise ξ is white or Gaussian.

Another type of process model is state-space model, which is derived from a set of first-order ordinary differential equations. State variables \mathbf{x} need not have physical meanings because they may be constructed in arbitrary order from input-output testing data. Linear state-space model is obtained by rearranging ARX model with single delay as:

$$\mathbf{x}_{k+1} = \mathbf{A}\mathbf{x}_k + \mathbf{B}_u\mathbf{u}_k + \mathbf{B}_v\mathbf{v}_k + \mathbf{B}_w\mathbf{w}_k \quad (3.6a)$$

$$\mathbf{y}_k = \mathbf{C}\mathbf{x}_k + \mathbf{D}\mathbf{u}_k + \xi_k \quad (3.6b)$$

where \mathbf{A} , \mathbf{B} , \mathbf{C} and \mathbf{D} are coefficient matrices of corresponding variables with appropriate sizes. Nonlinear state-space model include a nonlinear term $\mathbf{N}(\mathbf{x}_k, \mathbf{u}_k)$ in

its output (Equation 3.6b). Function $\mathbf{N}(\mathbf{x}_k, \mathbf{u}_k)$ may be obtained, for example, from neural network or block-oriented models such as Wiener or Hammerstein model. If a neural network model is used, extrapolation beyond the range of learning data sets may be unreliable. On the other hand, a Wiener/Hammerstein model may be used to approximate any nonlinear process (Sentoni et al., 1998).

3.5.1 System Identification

System identification refers to a technique of obtaining process model through input-output testing data. Process inputs may be stepped independently with various magnitudes or excited simultaneously via pseudo-random-binary-sequence (PRBS) signals. In this section, process models are developed from open-loop step and PRBS tests.

3.5.1.1 Step Test

The first step in setting up MPC controller is to obtain a process model. Here, a traditional approach of open-loop step testing is initially implemented. Two main requirements are imposed during step testing: 1) tuning of regulatory controllers is prohibited, and 2) if operator intervention is required to uphold plant safety or maintaining product quality, synchronizing or correlated input moves are disallowed (Qin and Badgwell, 2003).

Responses of outputs \mathbf{y} : $\mathbf{y}=[y_1 \ y_2]$, where outputs y_1 is after cooler E-102 stream temperature and y_2 is demethanizer C-101 tray 35 temperature, due to inputs \mathbf{u} : $\mathbf{u}=[u_1 \ u_2]$, where input u_1 is cooler E-102 duty and input u_2 is reboiler E-104 duty, are plotted in Figures 3.15 and 3.16. The inputs are moved by increasing and decreasing certain percentages of the valve opening according to the values in Tables 3.7 and 3.8. In each test, an input is stepped after 100 min simulation time, returned to the nominal condition after 500 min and maintained there for another 500 min. In essence, a total of 1100 min is taken for each of the twenty step tests. The long duration ensures that steady-state output values are reached in each step test. Outputs are measured simultaneously during each input move in order to capture their dynamic responses due to that particular input. For small step changes in inputs, all responses resemble a first order plus time delay (FOPTD) model:

$$g_{ij} = \frac{K_{p,ij} e^{-\tau_{d,ij}s}}{\tau_{p,ij}s + 1} \tag{3.7}$$

Notation g_{ij} refers to the transfer function relating output y_i to input u_j . $K_{p,ij}$ and $\tau_{p,ij}$ are process gain and time constant, respectively. Time delay is given by $\tau_{d,ij}$.

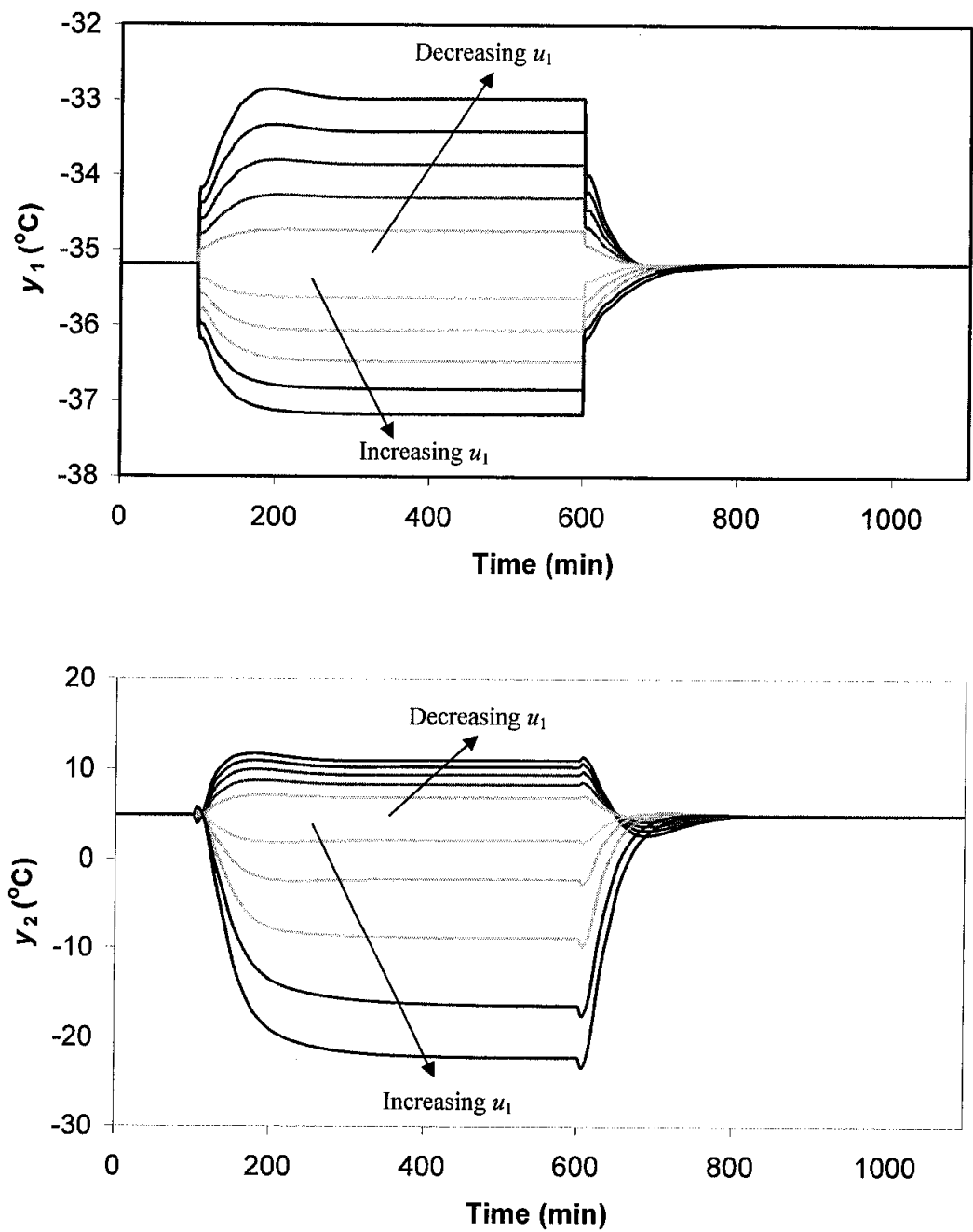


Figure 3.15: Open-loop step responses of outputs y_1 (top) and y_2 (bottom) due to various moves of input u_1

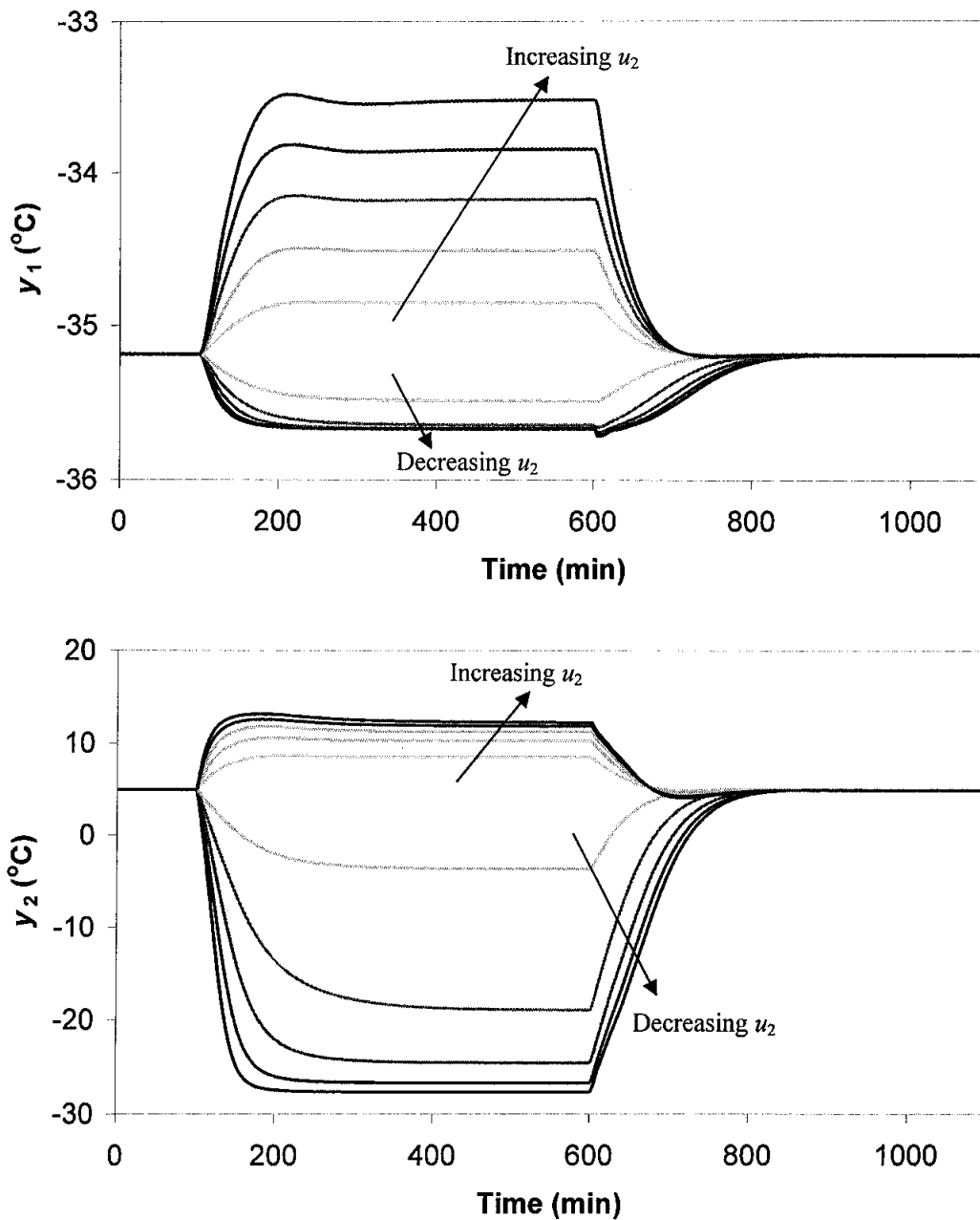


Figure 3.16: Open-loop step responses of outputs y_1 (top) and y_2 (bottom) due to various moves of input u_2

Responses from larger step changes reveal lead behaviors and varying gains for step changes of equal magnitude but in the opposite direction. Nonlinearity is expected due to the presence of large equipment such as a distillation column, liquefied natural gas heat exchangers and absorber in the process. For simplicity, lead term is ignored and step testing data are fitted with FOPTD model (Equation 3.7). Process models are identified using prediction error method. All identified models can explain about 90% of the experimental data.

Table 3.12: Open-loop responses with u_1 move

Case	($\% \Delta u_1$)	Input Moves		Output SS Values	
		u_1 (%)	u_1 (kW)	y_1 ($^{\circ}\text{C}$)	y_2 ($^{\circ}\text{C}$)
Nom.	0	85.0	3570.0	-35.2	5.0
A1	2	86.7	3641.4	-35.6	2.1
B1	4	88.4	3712.8	-36.1	-2.2
C1	6	91.1	3784.2	-36.5	-8.8
D1	8	91.8	3855.6	-36.8	-16.5
E1	10	93.5	3927.0	-37.2	-22.2
F1	-2	83.3	3498.6	-34.7	6.9
G1	-4	81.6	3427.2	-34.3	8.3
H1	-6	79.9	3355.8	-33.9	9.4
I1	-8	78.2	3284.4	-33.2	10.3
J1	-10	76.5	3213.0	-33.0	11.0

Nom. = nominal value; SS = steady-state.

Table 3.13: Open-loop responses with u_2 move

Case	($\% \Delta u_2$)	Input Moves		Output SS Values	
		u_2 (%)	u_2 (kW)	y_1 ($^{\circ}\text{C}$)	y_2 ($^{\circ}\text{C}$)
Nom.	0	67.0	3015.0	-35.2	5.0
A2	2	68.3	3075.3	-34.8	8.5
B2	4	69.7	3135.6	-34.5	10.3
C2	6	71.0	3195.9	-34.2	11.3
D2	8	72.4	3256.2	-33.8	11.9
E2	10	73.7	3316.5	-33.5	12.2
F2	-2	65.7	2954.7	-35.5	-3.6
G2	-4	64.3	2894.4	-35.6	-18.9
H2	-6	63.0	2834.1	-35.7	-24.5
I2	-8	61.6	2773.8	-35.7	-26.6
J2	-10	60.3	2713.5	-35.7	-27.6

Nom. = nominal value; SS = steady-state.

Figures 3.17 to 3.19 show the variations of the process gains, time constants and time delays. Preliminary visual inspection suggests that the process should be shifted to another operating condition (-4% u_2 move). This condition results in the highest gain ($K_{p,22} = 9.1$ $^{\circ}\text{C}/\%$), thus making it easier to control output y_2 by manipulating input u_2 . It should be noted, however, that this move entails significant deviation from the desired value of $y_2 = 5$ $^{\circ}\text{C}$. The resulting new value of $y_2 = -18.9$ $^{\circ}\text{C}$ is quite close to the tray weeping limit of approximately -20 $^{\circ}\text{C}$. To maintain good separation of sales gas from natural gas liquids, plant state remains at nominal conditions.

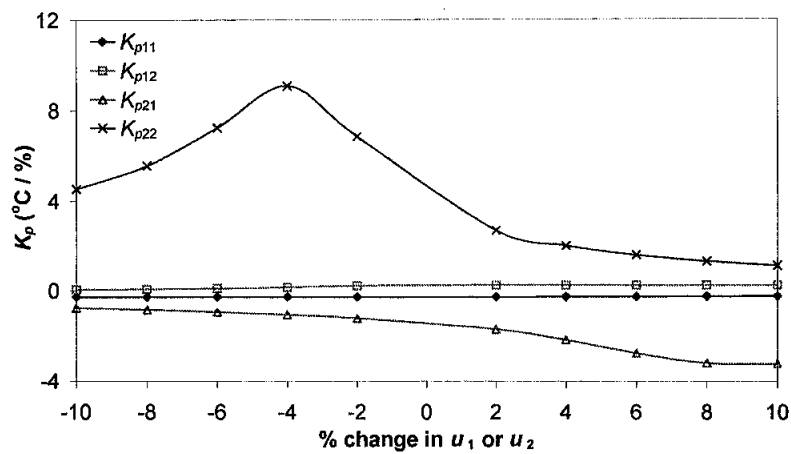


Figure 3.17: Variation of process gains (K_p) with respect to changes in cooler duty (u_1) and reboiler duty (u_2) from nominal value.

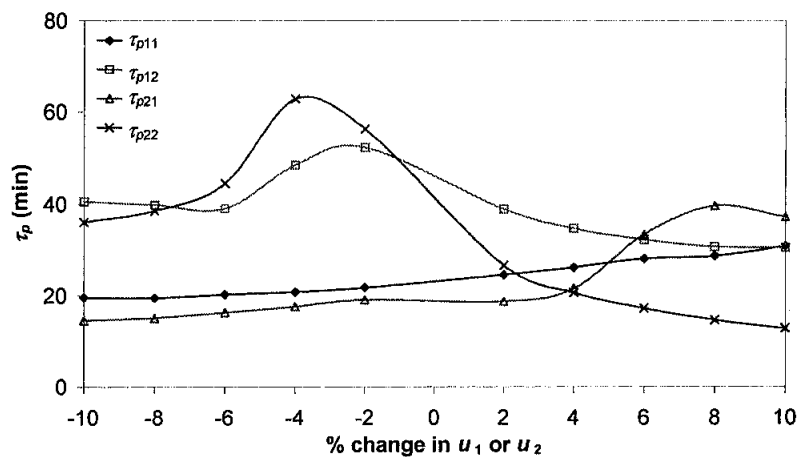


Figure 3.18: Variation of process time constants (τ_p) with respect to changes in cooler duty (u_1) and reboiler duty (u_2) from nominal value.

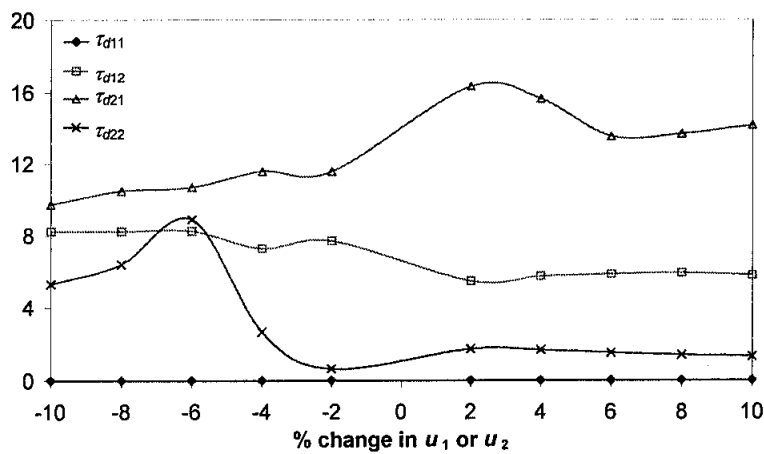


Figure 3.19: Variation of process time delays (τ_d) with respect to changes in cooler duty (u_1) and reboiler duty (u_2) from nominal value.

Nonlinearity of process gains $K_{p,21}$ and $K_{p,22}$ suggest that an adaptive controller such as gain scheduling approach is more appropriate for estimating output y_2 . However, the FOPTD model (Equation 3.7) could still be applied since these gains behave linearly within a small range of $[-2\%, +2\%]$ of moves for both inputs u_1 and u_2 . In addition, the other two gains $K_{p,11}$ and $K_{p,12}$ are constant throughout entire range of the step tests. On the other hand, nonlinearity in both time constants and time delays may be attributed to modeling uncertainty and errors. Mismatch between actual process and model is resolved in the MPC formulation via feedback mechanism. Discussion on this issue is deferred to later section of this chapter. An approximate process model is obtained after experimental tuning of MPC parameters following the approach by Khaledi and Young (2005). Final values of process gains, time constants and time delays obtained from step testing are presented in Table 3.14.

Table 3.14: FOPTD model parameters

Transfer Function	Model Parameters		
	K_p ($^{\circ}\text{C}/\%$)	τ_p (min)	τ_d (min)
g_{11}	-0.26	24.5	0
g_{12}	0.26	38.9	5.5
g_{21}	-1.70	18.8	16.4
g_{22}	2.69	26.6	1.7

3.5.1.2 PRBS Test

The traditional approach of performing step tests to obtain process models is time consuming because each input has to be moved 8 to 15 times while other variables are fixed at their steady-state values. The step tests are run continuously until all relevant inputs are stepped. In addition, linearity assumption must hold for input moves at equal magnitude but in opposite direction. One way to alleviate drawbacks of step testing is through multivariable plant testing using pseudo-random-binary-sequence (PRBS) input signals.

PRBS signals are generated using shift registers and Boolean algebra (Godfrey, 1993). Attributes of a PRBS signal depends on two parameters namely: 1) number of shift registers n_r , and 2) switching time t_{sw} . Plenty of guidelines for designing these parameters are available in literature. For example, Gaikwad and Rivera (1996) propose the following guidelines for a MIMO system comprising n_u number of inputs and n_y number of outputs:

$$t_{sw} \leq \frac{2.8\tau_{dom}^L}{\alpha_s} \quad (3.8)$$

$$N_s^{(1)} \geq \frac{2\pi\alpha_s\beta_s\tau_{dom}^H}{t_{sw}} \quad (3.9)$$

where τ_{dom} are estimates for the lowest (with superscript L) and highest (with superscript H) dominant time constants for the process, α_s is a multiplier between closed-loop and open-loop response times, and β_s is a factor representing frequency of an input that provides information up to a certain percentage of open-loop settling time of the process. These factors are used to define frequency (ω) bandwidth as follows:

$$\frac{1}{\beta_s\tau_{dom}^H} \leq \omega \leq \frac{\alpha_s}{\tau_{dom}^L} \quad (3.10)$$

Factor $N_s^{(1)} = 2^{n_r} - 1$ in Equation 3.9 relates to the period of PRBS signals in such a way that the sequence repeats itself after a period $P_s = N_s t_{sw}$.

A key requirement of MIMO PRBS signals is that there must be a sufficient lack of cross-correlation among all generated signals. One way to realize this requirement is by using delayed versions of the same signal for the remaining inputs. In other words, inputs 2 to n_u of a MIMO system is delayed by a factor D , which is defined as:

$$D = \frac{t_{OLST}^{\max}}{t_{sw}} \quad (3.11)$$

where t_{OLST}^{\max} is the maximum open-loop settling time after considering all SISO transfer functions estimated during pre-step tests. Delayed factor D may also be used to estimate N_s :

$$N_s^{(2)} \geq n_u D \quad (3.12)$$

Final value of N_s is taken as the higher value between those calculated in Equations 3.9 and 3.12.

$$N_s = \max(N_s^{(1)}, N_s^{(2)}) \quad (3.13)$$

Magnitudes of PRBS inputs are decided by APC engineers after discussion with plant operators. Guidelines for input magnitudes are unavailable because: 1) model gains requires *a priori* process knowledge as they are plant specific, and 2) plant constraints must be respected to maintain safety and product quality. In this work, changes of $\pm 5\%$ are selected for both inputs. Other PRBS design parameters are estimated from results of step tests (Table 3.14) and presented in Table 3.15. Recall that during step test, large input moves yield nonlinear responses making it difficult to estimate process gains (Figures 3.15 to 3.17). During PRBS test, nonlinearity is accounted for in the design of input signals.

Table 3.15: Design parameters of PRBS inputs

Parameters	Values	Remarks
Factor α_s	2	Close-loop response is twice as fast as open-loop response.
Factor β_s	5	Signal frequency corresponds to about 99% OLSST.
τ_{dom}^L (min)	19	$\tau_{p,21}$ (Table 3.14)
τ_{dom}^H (min)	39	$\tau_{p,12}$ (Table 3.14)
t_{OLST}^{\max}	200	About five times $\tau_{p,12}$
t_{sw} (min)	26	Calculated from Equation 3.8
ω bandwidth (min^{-1})	[0.0051, 0.1053]	Calculated from Equation 3.10
N_s	48	Calculated from Equation 3.13
P_s (min)	1248	Period $P_s = N_s T_{sw}$

Figures 3.20 and 3.21, respectively, show input moves and output responses from PRBS test. Recall that input u_1 is cooler E-102 duty whereas input u_2 is reboiler E-104 duty. The third input is load disturbance measured during the test. Outputs y_1 is after cooler E-102 stream temperature and y_2 is demethanizer C-101 tray 35 temperature. Fewer oscillations are found in output y_2 due to slow dynamics of rectifying section of the demethanizer C-101. Process is modeled using ARX and state-space structures. Low-order ARX model is chosen due to: 1) better representation of the 2x2 system in study, and 2) marginal improvements of higher-order ARX models. Numbers of

parameters A and B are two whereas delay is one. For state-space structure, a fourth-order model is selected for the same reasons as those of ARX model. Both ARX and state-space models can estimate about 70 and 50 % of outputs y_1 and y_2 , respectively. These results are expected due to highly nonlinear nature of the process.

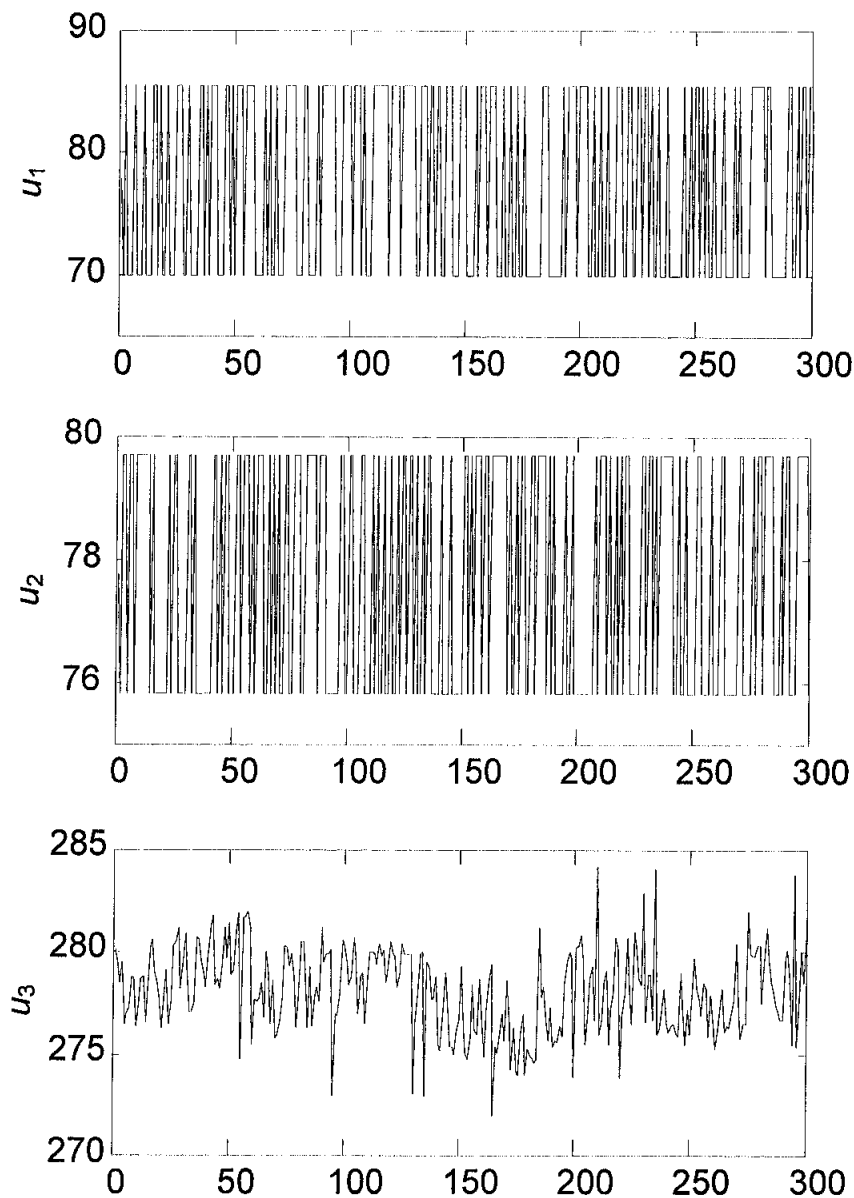


Figure 3.20: PRBS signals on inputs u_1 (cooler E-102 duty) and u_2 (reboiler E-104 duty), as well as measured input disturbance u_3 (plant load). Only the first 300 out of 1248 samples are illustrated for clarity.

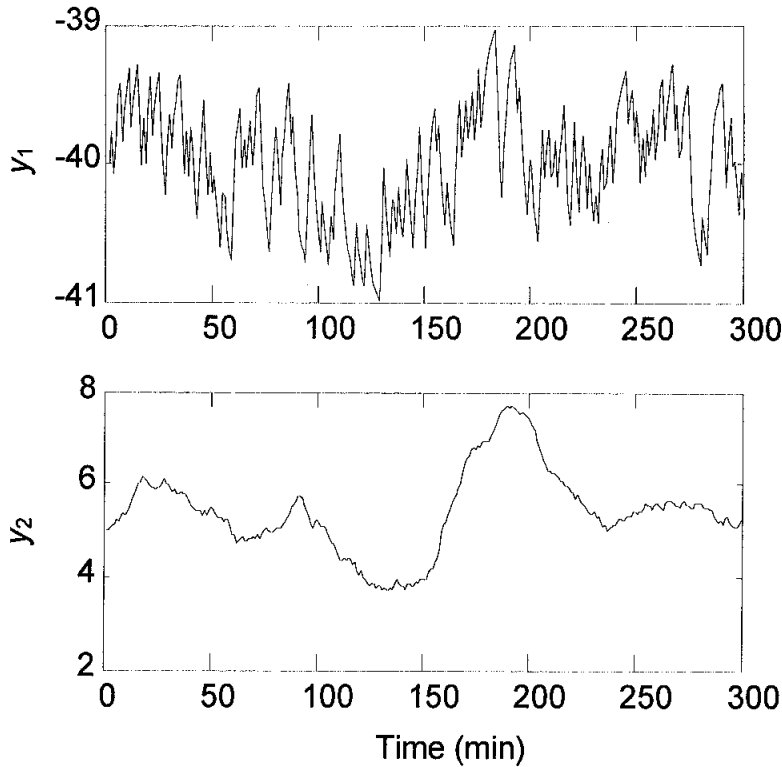


Figure 3.21: Responses of outputs y_1 (after cooler E-102 stream temperature) and y_2 (demethanizer tray 35 temperature) due to PRBS signals. Only the first 300 out of 1248 samples are illustrated for clarity.

Figure 3.22 illustrates output responses of ARX and state-space models due to a unit step of corresponding inputs. Directionality of gains of both ARX and state-space models is consistent with that estimated from FOPTD model (Table 3.14). On the other hand, magnitude of gains of ARX model due to input u_2 appears to be larger than those of state-space model. From control point of view, this condition makes it easier to regulate outputs y_1 and y_2 by smaller u_2 move. However, open-loop settling times for ARX model exceed 200 min, which is the maximum value estimated from step tests. In the next section, performance of MPC scheme using ARX and state-space models is studied in order to select the better process model.

Table 3.16: Process gains K_p of FOPTD, ARX and state-space (SS) models.

Transfer Function	K_p ($^{\circ}\text{C}/\%$)		
	FOPTD	ARX	SS
g_{11}	-0.26	-0.17	-0.15
g_{12}	0.26	0.10	0.04
g_{21}	-1.70	-2.72	-2.56
g_{22}	2.69	6.36	3.78

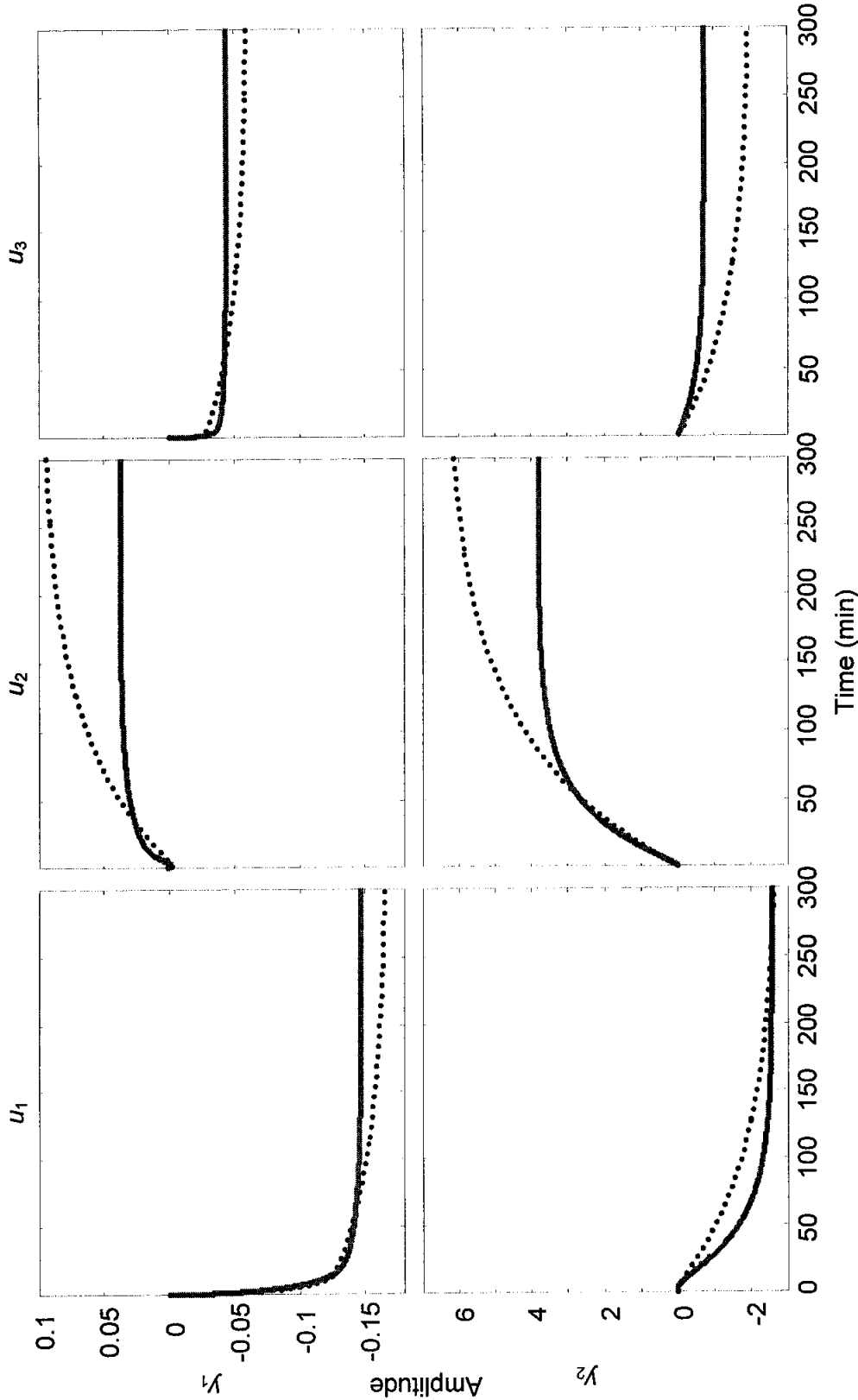


Figure 3.22: Step responses of process models: ARX (dotted) and state-space (solid)

3.5.2 MPC Design

MPC controller is designed by specifying: 1) a discrete process model to represent an actual plant, and 2) design and tuning parameters. Identification of process model has been discussed in the previous section. Discussion on design and tuning of MPC parameters is presented in this section. Performance of MPC schemes based on ARX and state-space models is compared in several cases of setpoint tracking in order to select the better model.

3.5.2.1 MPC Formulation

The objective of MPC scheme is to minimize a quadratic function written in the following compact form (Qin and Badgwell, 2003):

$$\min_{\Delta \mathbf{u}^M} \left\{ \mathbf{J} = \sum_{j=1}^P \|\mathbf{e}_{k+j}^y\|_{\mathbf{Q}}^2 + \sum_{j=0}^{M-1} [\|\Delta \mathbf{u}_{k+j}\|_{\mathbf{R}}^2 + \|\mathbf{e}_{k+j}^u\|_{\mathbf{S}}^2] \right\} \quad (3.14)$$

subject to model equations and inequality constraints:

$$\mathbf{y}_{\min} \leq \mathbf{y}_{k+j} \leq \mathbf{y}_{\max}, \quad \forall j=1, \dots, P \quad (3.15a)$$

$$\Delta \mathbf{u}_{\min} \leq \Delta \mathbf{u}_{k+j} \leq \Delta \mathbf{u}_{\max}, \quad \forall j=0, \dots, M-1 \quad (3.15b)$$

$$\mathbf{u}_{\min} \leq \mathbf{u}_{k+j} \leq \mathbf{u}_{\max}, \quad \forall j=0, \dots, M-1 \quad (3.15c)$$

where \mathbf{e}_{k+j}^y are deviations of future model output \mathbf{y}_{k+j} from reference trajectory \mathbf{y}_{k+j}^r over a prediction horizon of length P , $\Delta \mathbf{u}_{k+j}$ are predicted input moves over control horizon of length M , \mathbf{e}_{k+j}^u are deviations of future input \mathbf{u}_{k+j} from desired steady-state input \mathbf{u}^s over control horizon of length M . The conflicting terms in Equation 3.14 are assigned relative importance through positive semi-definite weighting matrices \mathbf{Q} , \mathbf{R} and \mathbf{S} . The more important terms are indicated by higher diagonal values of weighting matrices. Reference trajectory is modeled in the filtered setpoint form as:

$$\mathbf{y}_{k+j}^r = \alpha^j \mathbf{y}_k^m + (1 - \alpha^j) \mathbf{y}_k^{sp}, \quad \forall j=1, \dots, P \quad (3.16)$$

This approach offers several advantages: 1) degrees of freedom of MPC controller are enhanced through filter constant $\alpha = [0 \ 1]$, where higher α value means slower control

action to reach setpoint y_k^{sp} , and 2) a feedback mechanism is added through measured output y_k^m at current time instant k to reduce plant-model mismatch. Solution to the optimization problem is a sequence of M input moves:

$$\Delta \mathbf{U}^M = [\Delta \mathbf{u}_k, \Delta \mathbf{u}_{k+1}, \dots, \Delta \mathbf{u}_{k+M-1}] \quad (3.17)$$

In practice, however, only the first input move $\Delta \mathbf{u}_k$ is implemented at each control action. The remaining calculated moves $[\Delta \mathbf{u}_{k+1}, \dots, \Delta \mathbf{u}_{k+M-1}]$ are discarded. In subsequent control actions, this process is repeated at each time step.

3.5.2.2 Design and Tuning Parameters

Table 3.17 shows MPC design and tuning parameters. MPC controller is built on top of two decentralized PI controllers, TC101 and TC102, which are previously employed to regulate duties of refrigeration cooler E-102 and reboiler E-104. Parameters are selected after performing several closed-loop simulation studies under different process conditions. The decision of 1-minute control interval is made so that actual process does not deviate too much from model prediction before the next MPC action. Control horizon of length 2 indicates less aggressive MPC actions. Long prediction horizon of 120 is sufficient to bring process to a new steady-state. Output weights \mathbf{Q} are ten times larger than input rate weights \mathbf{R} indicating heavier penalties are imposed on deviation from targets rather than input moves. No penalty is imposed on deviation from nominal input values as shown by zero input weights \mathbf{S} .

Table 3.17: MPC design and tuning parameters

Parameters	Values
Control interval, Δt	1 min
Control horizon, M	2
Prediction horizon, P	120
Weighting matrices:	
• Output, \mathbf{Q}	diag[1 1]
• Input rate, \mathbf{R}	diag[0.1 0.1]
• Input, \mathbf{S}	diag[0 0]
Constraints:	
• Output, \mathbf{y}	[-20 20; -20 20]
• Input rate, $\Delta \mathbf{u}$	[-5 5; -5 5]
• Input, \mathbf{u}	[]

The inputs \mathbf{u} are left unconstrained in MPC scheme as denoted by empty square matrix \square . However, physical constraints of the inputs \mathbf{u} are enforced at plant level since duties of refrigeration cooler E-102 and reboiler E-104 are bounded. Outputs \mathbf{y} are loosely constrained at $\pm 20^\circ\text{C}$ to account for adequate temperature swing during changes of plant operating mode. Input rates $\Delta \mathbf{u}$ are capped at $\pm 5\%$ to ensure that actual process is taken from one state to another within reasonable movements of inputs.

3.5.2.3 Setpoint Tracking

A good controller should be able to bring an output from its nominal value to another state smoothly. This process is termed setpoint tracking. Performance of MPC controller is measured using integral of squared error (ISE) for output changes and total duties for input moves. Nominal input and output values are given in Table 3.18. Relationship between controller output value (%) and actual duty (kW) is assumed linear within ranges presented in Table 3.19. Total simulation time for all cases of setpoint tracking is 100 min.

Table 3.18: Nominal input and output values

Index	Input (%)	Output ($^\circ\text{C}$)
1	77.7	-33.8
2	64.4	4.8

Table 3.19: Ranges of actual input duty values

Input	Minimum (kW)	Maximum (kW)
u_1	0	4200
u_2	0	4500

Three case studies are carried out to determine the performance and costs of setpoint tracking by MPC and PI controllers. Case 1 is a change in setpoint of y_1 by -1°C . Downward movement in y_1 will result in increasing duty of u_1 . On the other hand, Case 2 is a change in setpoint of y_2 by $+1^\circ\text{C}$, which will increase duty of u_2 . Cases 1 and 2 are typically encountered when RGP receives rich feed gases. This condition forces RGP to utilize more energy in order to process more natural gas liquids. In both Cases 1 and 2, y_1 and y_2 are tracked independently. In Case 3, both y_1 and y_2 are simultaneously stepped by -1 and $+1^\circ\text{C}$, respectively. Since y_1 and y_2 move

in the opposite directions, Case 3 depicts response of the MPC controllers due to process interaction.

Figures 3.23 to 3.25 compare closed-loop responses of MPC controller using ARX (MPC-ARX) and state-space (MPC-SS) process models for Cases 1, 2 and 3. In all three cases, outputs y_1 and y_2 are brought to new steady-states by coordinated moves of both inputs u_1 and u_2 . In Cases 1 and 3, smaller output deviations from respective targets are observed for MPC-ARX controller actions. This trend is reversed in Case 2. Table 3.20 affirms this preliminary visual inspection through comparison of ISE values of the responses. To reach new setpoints, MPC-ARX controller seems to deploy smaller input moves especially on u_2 . Recall that ARX model has larger gains than state-space model (Table 3.16). A large model gain enables the MPC controller to predict future behavior of outputs with less effort. Based on average input duties, however, only marginal energy savings within a range of 0.2 to 1.9 kW/min are realized from using MPC-ARX controller (Table 3.21). These savings may translate into thousands on Ringgit Malaysia (RM) per annum for a large plant such as RGP. Discussion on economics of RGP operation is the subject of the next chapter.

Table 3.20: Integral of Squared Errors (ISEs) [$(^{\circ}\text{C})^2 \cdot \text{min}$] for different setpoint changes

Output	Case 1		Case 2		Case 3	
	ARX	SS	ARX	SS	ARX	SS
y_1	2.65	2.66	0.10	0.05	2.67	2.71
y_2	0.48	1.34	3.21	3.17	4.13	7.16

Table 3.21: Average input duties (kW/min) for different setpoint changes

Input	Case 1		Case 2		Case 3	
	ARX	SS	ARX	SS	ARX	SS
u_1	3577.5	3578.2	3256.5	3258.4	3580.8	3582.0
u_2	3005.8	3006.0	2917.9	2918.7	3028.4	3029.8

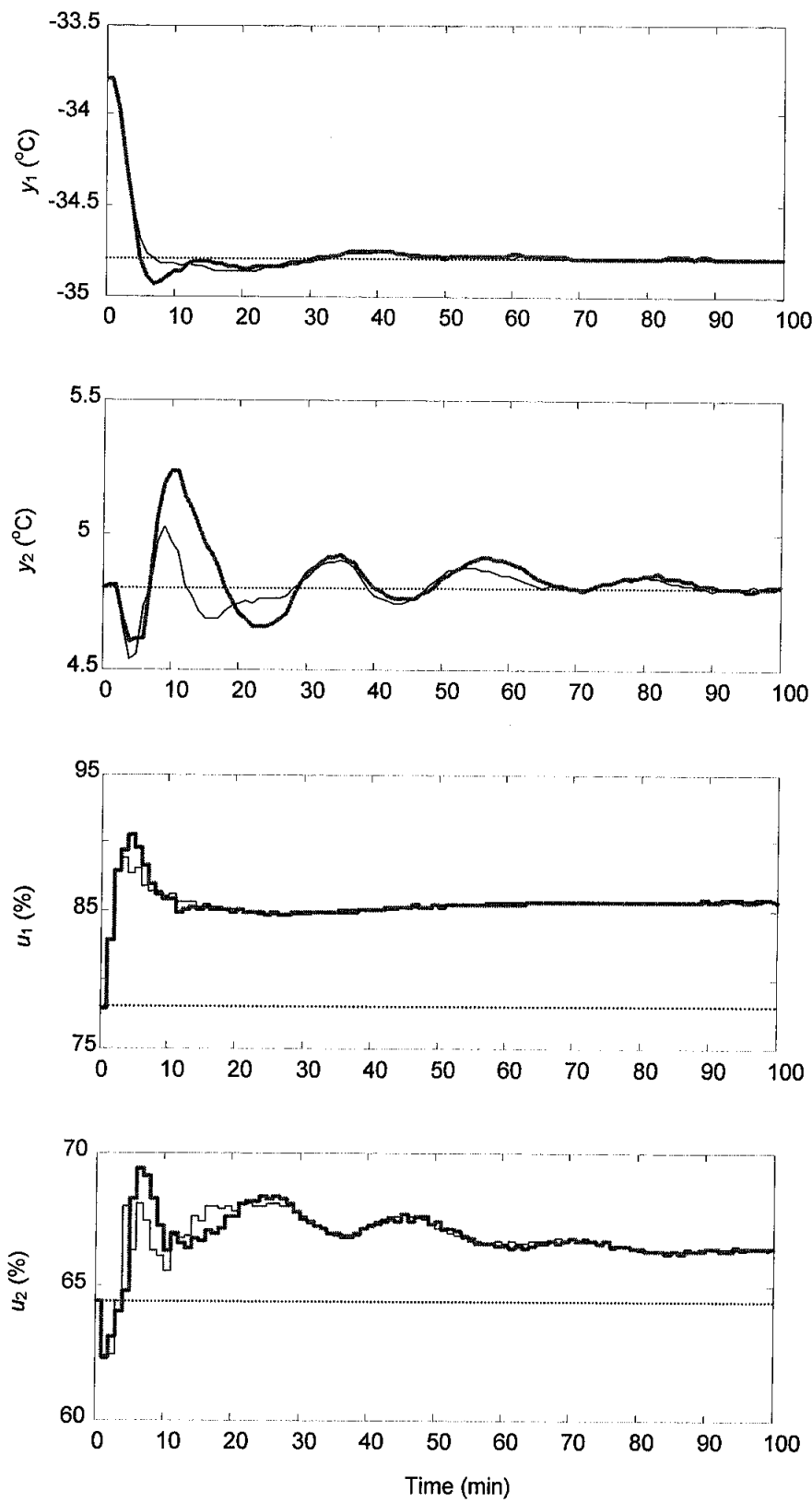


Figure 3.23: Closed-loop responses for a change in y_1 (Case 1) using ARX (thin line) and state-space (thick line) models as compared with output setpoints and input nominal values (dotted line)

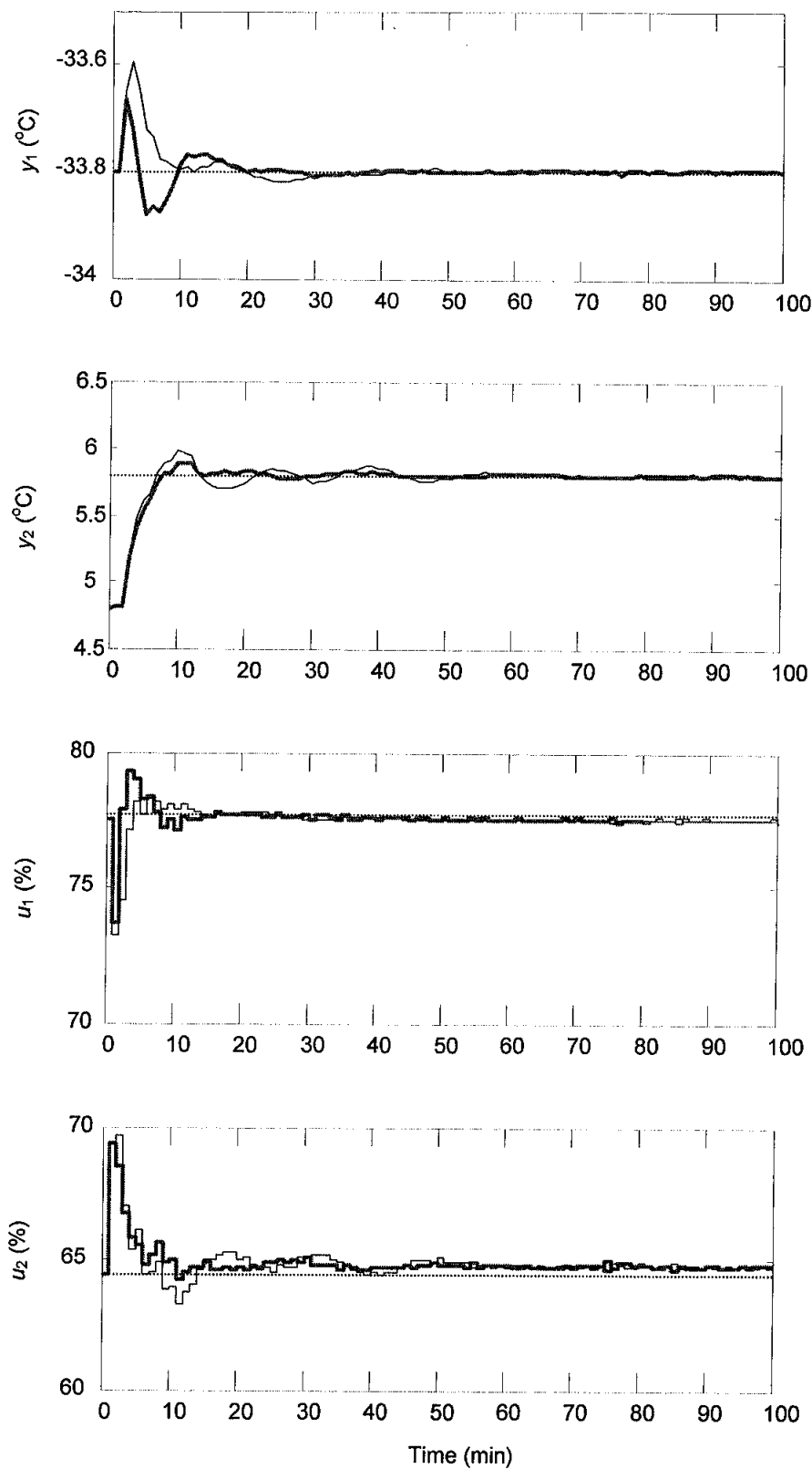


Figure 3.24: Closed-loop responses for a change in y_2 (Case 2) using ARX (thin line) and state-space (thick line) models as compared with output setpoints and input nominal values (dotted line)

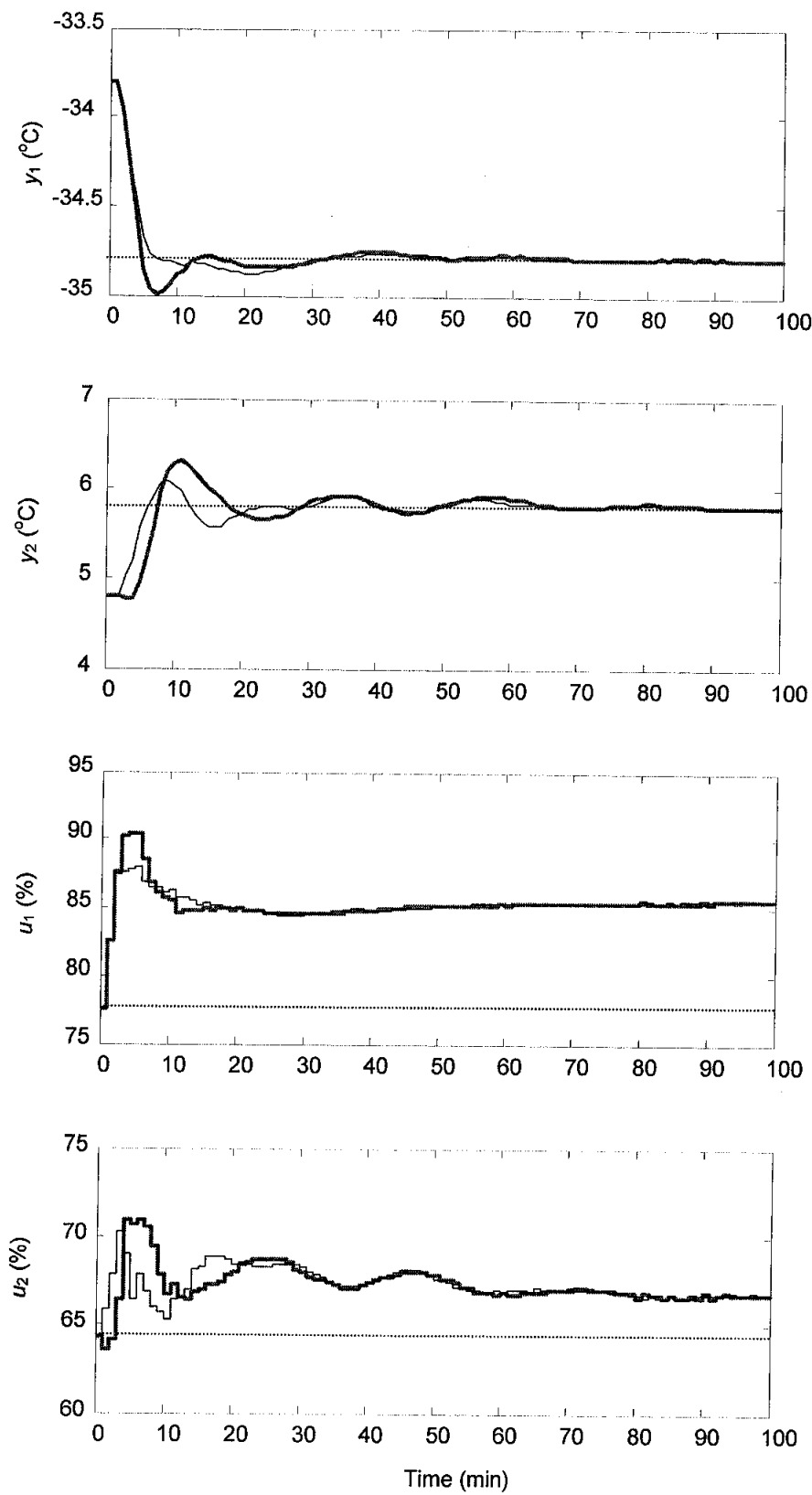


Figure 3.25: Closed-loop responses for simultaneous changes in y_1 and y_2 (Case 3) using ARX (thin line) and state-space (thick line) models as compared with output setpoints and input nominal values (dotted line)

3.6 Concluding Remarks

Developments of steady-state and dynamic models of RGP are presented in this chapter. An accuracy of close to 95% is achieved when the steady-state model is validated against actual plant data. The plant data are averaged *a priori* over a 48-hour continuous period during the natural gas liquids mode of operation. The dynamic model is initialized and developed based on the steady-state model. Regulatory controllers are installed to stabilize RGP and maintain product qualities. To better handle operational and economic challenges, a two-output-by-three-input constrained MPC scheme is employed in RGP. This MPC scheme is developed based on step and PRBS tests. Process model is approximated by linear parametric models in the forms of ARX and state-space models. ARX model is selected due to smaller ISEs on output variables in several cases of setpoint tracking.

CHAPTER 4

REAL-TIME OPTIMIZATION

4.1 Introduction

Natural gas has recently emerged as an important source of clean energy. Improving operational efficiency of a refrigerated gas plant (RGP) may significantly increase its profit margin. One way to increase efficiency is through frequent updates of RGP operating conditions. This proves to be a challenging task due to time-varying nature of feed gas flow rates and compositions. At the plant outlet, product values may also fluctuate at frequent intervals depending on market conditions. Such challenges in operation and economics are typically handled by employing advanced process control (APC) and real-time optimization (RTO), respectively.

Development of APC scheme in the form of model predictive control (MPC) is discussed in the previous chapter. The MPC scheme is commissioned on top of PI controllers for stabilizing and maintaining product qualities. Here, MPC actions can reduce operating costs by coordinating and adjusting input moves optimally (Huang and Riggs, 2002). A reduction in operating cost may increase RGP profit if all else remain the same. Maximization of profit is performed at RTO layer. This procedure requires a plantwide, preferably first-principle, model of RGP. Steady-state RGP model may be used for solving the RTO problem due to highly complex and nonlinear nature of the process.

4.2 RTO Problem Formulation

The goal of real-time optimization (RTO) is to maximize RGP profit while respecting certain plant constraints, and contractual obligations to both producers and customers. This is generally carried out through maximization of product throughputs and/or minimization of feed gas and operating costs. The RTO problem can be written in the following form:

$$\max_{u^{ss}, y^{ss}} f_E \quad (4.1a)$$

subject to:

$$g_E(\mathbf{u}^{ss}, \mathbf{y}^{ss}, \mathbf{z}^{ss}, \mathbf{p}) \leq 0 \tag{4.1b}$$

$$\mathbf{y}^{ss} = f_m(\mathbf{u}^{ss}, \mathbf{z}^{ss}, \mathbf{p}) \tag{4.1c}$$

$$\mathbf{y}_{\min} \leq \mathbf{y}^{ss} \leq \mathbf{y}_{\max} \tag{4.1d}$$

$$\mathbf{u}_{\min} \leq \mathbf{u}^{ss} \leq \mathbf{u}_{\max} \tag{4.1e}$$

where f_E is an economic objective function and g_E is a set of inequality constraints. Steady-state process outputs \mathbf{y}^{ss} and inputs \mathbf{u}^{ss} are bounded within their corresponding minimum and maximum values. Algebraic state variables \mathbf{z}^{ss} are updated via steady-state RGP model f_m using constant plant parameters \mathbf{p} . The optimization problem is solved using a HYSYS built-in sequential quadratic programming (SQP) algorithm with constraints (Chamberlain and Powell, 1982). The procedure starts with formulation of the RTO problem (Figure 4.1). It is stopped when one of the following conditions is achieved:

1. The SQP algorithm reaches convergence, or
2. A new state with higher profit value is attained for non-convergence cases.

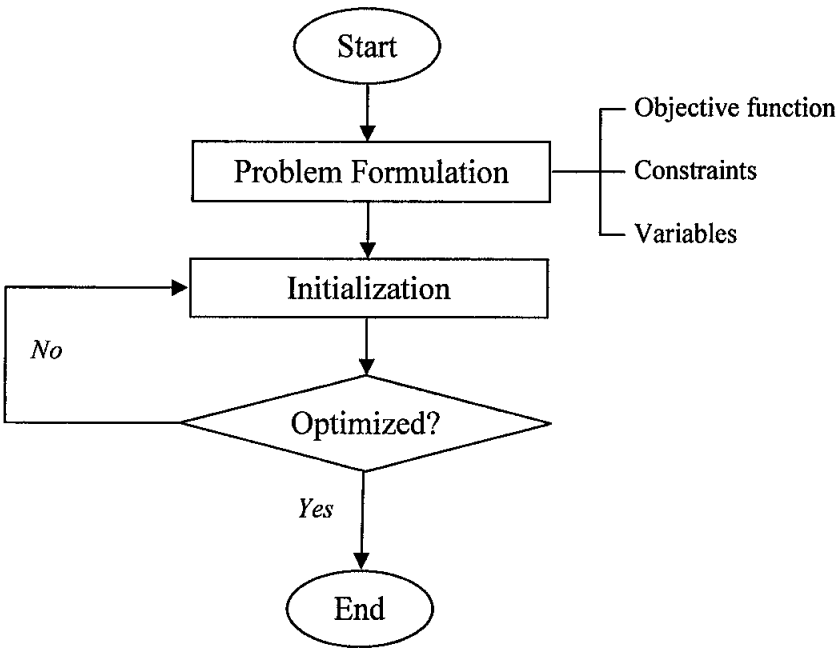


Figure 4.1: Optimization process flowchart

RTO problem formulation involves three main steps of defining: 1) an objective function, 2) process constraints, and 3) optimization variables. The objective function as written in Equation 4.1a is further defined as:

$$P = \sum_{i=1}^I R_i - \sum_{j=1}^J E_j \quad (4.2)$$

where P is profit, R_i ($I=5$) are revenues and E_j ($J=10$) are expenses. In other words, the objective function is specially formulated as an economic expression of product values and operational expenses. Valuable products are sales gas and natural gas liquids comprising ethane, propane, butane and condensates. Revenues are calculated based on flow rates of respective products. Operational expenses are mainly due to costs of feed gas and utilities in the forms of refrigeration cooler duty (E-102Q), demethanizer reboiler duty (E-104Q), compressor fuel gas consumption (K-102Q), turboexpander-compressor maintenance (KT/K-101Q) and electricity usage for pumping actions (P-101Q and P-102Q). Prices and corresponding units of each component of revenues and expenses are shown in Table 4.1.

Table 4.1: Economic data

Component	Price	Unit
Feed gas A	6.0	RM/MMBtu
Feed gas B	5.5	RM/MMBtu
Feed gas C	5.0	RM/MMBtu
Feed gas D	7.0	RM/MMBtu
Sales gas	14.4	RM/MMBtu
Ethane	304.0	RM/ton
Propane	569.0	RM/ton
Butane	908.0	RM/ton
Condensates	673.8	RM/ton
Refrigeration	169.0	RM/MWh
Steam duty	89.9	RM/MWh
Compressor duty	84.5	RM/MWh
Turboexpander duty	42.3	RM/MWh
Electricity	233.3	RM/MWh

Source: Personal correspondence with an engineer working at a GPP

For practical reasons, only inequality constraints are specified. This way, feasible solution can be obtained faster or within RTO sampling interval of 200 min. The long duration of sampling interval is necessary to match the open-loop settling time of

MPC controller. Total number of constraints is thirty four including specifications on product qualities as well as limits in plant throughput, equipment and processes (Table 4.2).

Table 4.2: Values and bounds of constraint variables

Variable	Unit	Min	Max	Description
c_1	ton/h	100.0	310.0	Flow of mixed feed gas
c_2	MJ/m ³	35.1	48.1	Gross heating value of sales gas
c_3	-	-	0.75	Specific gravity of sales gas
c_4	mol%	-	2.00	Carbon dioxide content in sales gas
c_5	ton/h	205.0	-	Flow of sales gas
c_6	bar	30.0	-	Pressure of sales gas
c_7	°C	-	50.0	Temperature of sales gas
c_8	kW/°C	-	2000	Coldbox E-101 capacity
c_9	°C	5.0	-	Coldbox E-101 LMTD
c_{10}	kW/°C	-	800	Coldbox E-103 capacity
c_{11}	°C	5.0	-	Coldbox E-103 LMTD
c_{12}	kW/°C	-	400	Coldbox E-105 capacity
c_{13}	°C	5.0	-	Coldbox E-105 log LMTD
c_{14}	kW	0	4000	Cooler E-102 duty
c_{15}	kW	0	4700	Demethanizer C-101 reboiler duty
c_{16}	kW	0	4000	Turboexpander KT-101 duty
c_{17}	kW	0	4700	Compressor K-102 duty
c_{18}	kW	0	30.0	Pump P-101 duty
c_{19}	kW	0	15.0	Pump P-102 duty
c_{20}	%	25.0	85.0	Flooding at Section 1 of demethanizer
c_{21}	%	25.0	85.0	Flooding at Section 2 of demethanizer
c_{22}	%	25.0	85.0	Flooding at Section 3 of demethanizer
c_{23}	%	25.0	85.0	Flooding at Section 4 of demethanizer
c_{24}	%	10.0	50.0	DC backup at Section 1 of demethanizer
c_{25}	%	10.0	50.0	DC backup at Section 2 of demethanizer
c_{26}	%	10.0	50.0	DC backup at Section 3 of demethanizer
c_{27}	%	10.0	50.0	DC backup at Section 4 of demethanizer
c_{28}	%	25.0	85.0	Flooding in absorber C-102
c_{29}	%	10.0	50.0	DC backup in absorber C-102
c_{30}	°C	5.0	-	Air cooler LMTD
c_{31}	-	0.50	1.00	Ratio of gas to expander over that to JT valve
c_{32}	-	0.50	1.00	Ratio of gas to coldbox E-103 to that bypasses it
c_{33}	-	0.50	1.00	Ratio of gas to coldbox E-101 to that bypasses it
c_{34}	-	0.005	0.150	Fraction of gas to gas subcooled process section

Note: LMTD=log mean temperature difference; JT=Joule-Thompson;
DC=downcomer

Significance of the constraints can be explained as follows. The feed gas flow rate of 310 ton/h represents the maximum load that RGP can process at a given time. Constraints on sales gas are as specified by the customers. Specifically, the constraints

on gross heating value and specific gravity are to ensure quality of the sales gas. Maximum carbon dioxide content of less than 2.0 mol % is to adhere to environmental regulation imposed by major customers. Minimum sales gas flow rate of 205 ton/h is the load demanded by the customers. Minimum pressure of 30 bar and maximum temperature of 50 °C are offsite specifications. Flooding and downcomer backup constraints on demethanizer C-101 are to ensure good separation of sales gas from natural gas liquids. Similar constraints on absorber C-102 represent surrogates to flooding in absorber bed and chimney trays.

Maximum heat exchange capacities in three cold boxes E-101, E-103 and E-105 are taken as per design. The same reason goes to maximum duties of cooler E-102, reboiler E-104, turboexpander KT-101, compressor K-102 and pumps P-101 and P-102. Log-mean temperature difference (LMTD) of greater than 5 °C is to prevent temperature cross violation at the cold boxes as well as air cooler E-106. Physical constraints on ratios of gas flowing to certain streams are imposed to avoid dealing with negative flow rate in one of the other split streams. Minimum fraction of gas flowing to gas subcooled process section are enforced to prevent total shutdown of this section. On the other hand, maximum fraction corresponding to the highest gas flow rate of about 40 ton/h is based on design conditions.

The last step in RTO problem formulation is the definition of variables. This challenging task must be performed properly because there are many potential variables to be selected. It should be noted that solution to the steady-state RTO problem (Equation 4.1) is a set of targets that are passed to dynamic control layer for implementation. A dynamic model of RGP is already developed in Chapter 3. Process and instrumentation diagram (P&ID) of this model is illustrated in Figure 3.7. Two product streams, namely SG and NGLs, contain sales gas and natural gas liquids, respectively. Feed gas streams A, B, C and D comprises different levels of carbon dioxide but similar compositions of hydrocarbons (Table 4.3).

It should be noted that compositions of feed gas streams other than feed gas stream D differ from those given in Table 3.1. This is due to nature of Taguchi method that requires simultaneous changes of all variable values at each run. For example, an abrupt change of lean feed gas stream A to very rich feed gas stream C

flowing at 280 ton/h will cause RGP dynamic model to crash. On the other hand, the dynamic model can handle a sudden change of flow of rich feed gas stream D from 0 to 2 ton/h due to its much smaller rate. It should be noted that the altered compositions of feed gas streams A, B and C cause no loss of generality when it comes to parametric design of RGP.

Table 4.3: Compositions of feed gas streams used for parametric design

Component	A	B	C	D
Methane	0.8956	0.8790	0.8465	0.7604
Ethane	0.0525	0.0516	0.0497	0.1581
Propane	0.0289	0.0284	0.0273	0.0441
<i>i</i> -Butane	0.0103	0.0101	0.0098	0.0080
<i>n</i> - Butane	0.0060	0.0059	0.0057	0.0051
<i>i</i> -Pentane	0.0003	0.0003	0.0003	0.0000
<i>n</i> -Pentane	0.0002	0.0002	0.0002	0.0000
<i>n</i> -Hexane	0.0001	0.0001	0.0001	0.0000
Nitrogen	0.0040	0.0039	0.0037	0.0177
Carbon Dioxide	0.0020	0.0206	0.0567	0.0066

In the P&ID, controllers and energy streams are numbered systematically. However, numbering for most material streams is omitted for reading clarity. The large dynamic model of RGP contains 770 state variables and 21 regulatory control loops. This implies that hundreds of variables are available for manipulation. In practice, however, only several variables are considered important. These variables are constantly monitored and regulated by manipulating controller outputs.

Key controllers are: (a) split range controller SRC103 that regulates feed gas stream temperature after coldbox E-101, (b) temperature controller TC101 that regulates cooler E-102 outlet temperature, (c) split range controller SRC102 that regulates feed gas stream temperature after coldbox E-103, (d) Ratio controller RC101 that regulates flow of gas to absorber C-102 over that to turboexpander KT-101, (e) flow controller FC104 that regulates flow of feed gas stream D, which is mainly used to increase sales gas gross heating values, (f) pressure controller PC101 that regulates demethanizer C-101 overhead pressure, (g) temperature controller TC102 that regulates demethanizer tray 35 temperature, and (h) flow controller FC101 that regulates plant load. For MPC and RTO purposes, manipulated variables and/or setpoints of these controllers are selected as optimization variables.

Significance of these variables is analyzed using Taguchi design of parameters, which is simply termed parametric design.

4.3 Parametric Design

Parametric design through Taguchi method was successfully applied in many engineering disciplines. For example, Cheng et al. (2008) studied thermal chemical vapor decomposition of silicon film by integrating computational fluid dynamic codes in FLUENT and a dynamic model of Taguchi method with L_{18} ($2^1 \times 3^7$) orthogonal arrays. They found that thickness deviation of silicon film could be reduced by up to 11% from 36% previously. Engin et al. (2008) employed L_{16} ($4^2 \times 2^2$) arrays to investigate color removal from textile dyebath effluents in a zeolite fixed-bed reactor. A surfactant called hexadecyl-trimethyl-ammonium bromide (HTAB, $C_{19}H_{42}BrN$) was added to increase absorption capacity of the zeolite. Experimental results indicated that HTAB concentration, zeolite bed height and wastewater flowrate were important parameters, whereas HTAB flowrate was insignificant parameter.

In another application, Chiang (2005) studied cooling performance of parallel-plain fin heat sink module using L_{18} ($2^1 \times 3^7$) arrays. Through analysis of variance (ANOVA), four out of eight variables were found to exhibit significant contribution to the cooling process. The significant variables are number of opening slots (34.8%), surface area of copper base (22.7%), fan capacity (13.6%) and height of fin flake (8.7%). By utilizing an optimal configuration of these variables in simulated environment, a 15% improvement in cooling performance was achieved. Lee and Kim (2000) proposed a controller gain tuning technique for multi-axis PID control system. The test bed was a parallel-mechanism machine tool containing eight servodrivers. Each servodriver has four controller gains, thus a total of 32 gains needed to be tuned simultaneously. By utilizing L_9 (3^4) orthogonal arrays, robust controller gains were obtained. A performance indicator namely the index of average position and velocity errors was reduced by 61.4%. In addition, average signal-to-noise ratio (*SNR*) was increased by 8.5 dB to attain better control of the machine tool.

In the current work, Taguchi method for design of parameters is applied to accomplish the following objectives (Roy, 1990):

1. To identify and rate optimization variables under the influence of disturbance variables.
2. To determine optimum configurations of optimization and disturbance variables.
3. To estimate and validate maximum RGP profit within specific constraints of all variables.

Cross-array experiments employing $L_{27} (3^7)$ and $L_9 (3^2)$ internal and external arrays, respectively, are performed on RGP dynamic model to investigate effects of seven optimization variables and two disturbance variables at 3 levels each on to RGP profit.

4.3.1 Taguchi Method

Taguchi method can be illustrated with the help of a flow diagram (Figure 4.2). The procedure employed in the current work is modified from that presented by Yang et al. (2007). It is more compact and includes a failure loop for invalidated design of experiment.

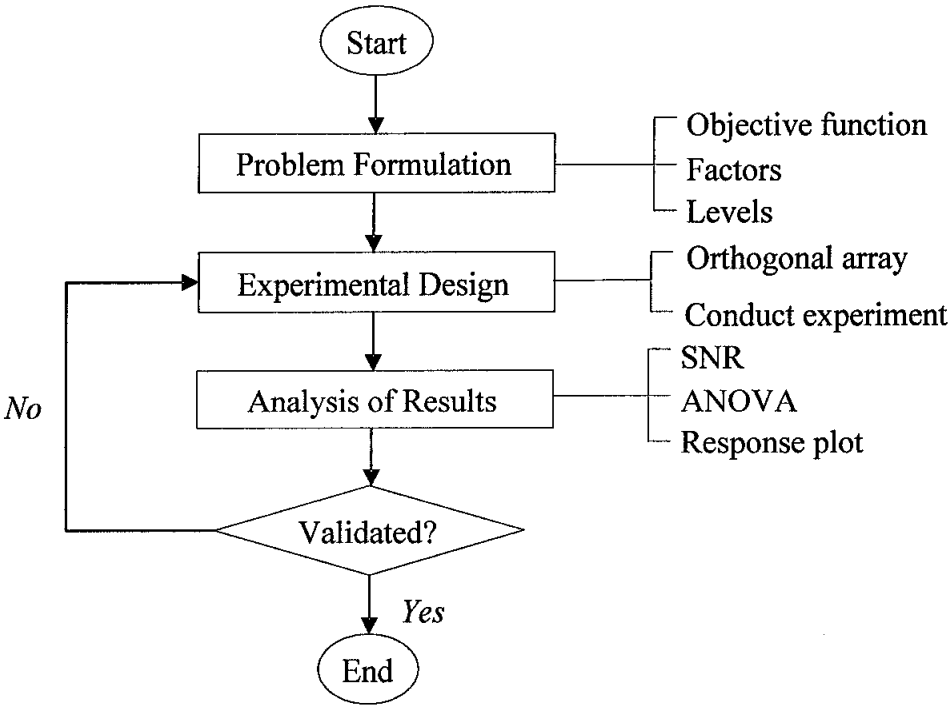


Figure 4.2: Flow diagram of Taguchi method

Step 1 involves problem formulation, which requires definitions of an objective function, factors and levels. This step entails an in-depth knowledge of the process of interest. In case of RGP, inputs from experienced operators are essential in determining potential optimization and disturbance variables, as well as their normal, high and low values (Table 4.4). Optimization and disturbance variables are called controllable and noise factors, respectively, in Taguchi-related literature. Limits of high and low values are called levels. Median, and lower and upper quartiles of the limits may also be included to augment experimental design configurations.

Controllable factors *A* to *G* are set up in an L_{27} (3^7) internal array whereas noise factors *H* and *I* in an L_9 (3^2) external array. Cross-array experiments between external and internal arrays are conducted to include the effect of noise on controllable factors (Taguchi and Konishi, 1987). Outputs from running these experiments are profit values obtained from an objective function (Equation 4.2). Since RGP dynamic model is developed based on first principles, significance of optimization and disturbance variables can be systematically established through Taguchi method.

Table 4.4: Description of factors and levels for RGP

Factors	L_1	L_2	L_3	Units	Description
<i>A</i>	90	95	100	%	Split range controller SRC103 output
<i>B</i>	30	40	50	%	Temperature controller TC101 output
<i>C</i>	90	95	100	%	Split range controller SRC102 output
<i>D</i>	0.005	0.075	0.15	-	Ratio controller RC101 ratio
<i>E</i>	0	25	50	%	Flow controller FC104 output
<i>F</i>	22	23	24	barg	Demethanizer C-101 overhead pressure
<i>G</i>	70	85	100	%	Temperature controller TC102 output
<i>H</i>	250	280	310	ton/h	Feed gas flow rate
<i>I</i>	6.0	5.5	5.0	RM/MMBtu	Feed gas prices

Note: L =level; subscript denotes level number.

Step 2 involves designing and conducting experiments. Numbers of factors and levels have an effect on selection of standard orthogonal arrays. For 7 controllable factors at 3 levels such as the one in this study, an L_{27} array consisting of 27 rows and 13 columns is appropriate. The rows and columns represent experimental runs and factors, respectively. Since there are only 7 controllable factors used to calculate RGP profit, the remaining 6 columns on far right of the array are ignored. Similarly, an L_9 array consisting of 9 rows and 4 columns is selected for 2 noise factors at 3 levels.

Only the first 2 columns are used in this study. Reduced arrays are shown in Tables 4.5 and 4.6. It should be noted that, in order to capture adequate responses of all 7 controllable factors towards the objective function, only 27 experiments from an internal array need to be conducted for each of the 9 runs from an external array. Hence a total of 243 (=27*9) experiments need to be performed. This is more appealing than running 19,683 (3^9) experiments under full factorial design approach.

Table 4.5: Taguchi internal array showing levels of controllable factors

Run	Factors						
	<i>A</i>	<i>B</i>	<i>C</i>	<i>D</i>	<i>E</i>	<i>F</i>	<i>G</i>
1	1	1	1	1	1	1	1
2	1	1	1	1	2	2	2
3	1	1	1	1	3	3	3
4	1	2	2	2	1	1	1
5	1	2	2	2	2	2	2
6	1	2	2	2	3	3	3
7	1	3	3	3	1	1	1
8	1	3	3	3	2	2	2
9	1	3	3	3	3	3	3
10	2	1	2	3	1	2	3
11	2	1	2	3	2	3	1
12	2	1	2	3	3	1	2
13	2	2	3	1	1	2	3
14	2	2	3	1	2	3	1
15	2	2	3	1	3	1	2
16	2	3	1	2	1	2	3
17	2	3	1	2	2	3	1
18	2	3	1	2	3	1	2
19	3	1	3	2	1	3	2
20	3	1	3	2	2	1	3
21	3	1	3	2	3	2	1
22	3	2	1	3	1	3	2
23	3	2	1	3	2	1	3
24	3	2	1	3	3	2	1
25	3	3	2	1	1	3	2
26	3	3	2	1	2	1	3
27	3	3	2	1	3	2	1

Table 4.6: Taguchi external array showing levels of noise factors

Factor	Run								
	1	2	3	4	5	6	7	8	9
<i>H</i>	1	1	1	2	2	2	3	3	3
<i>I</i>	1	2	3	1	2	3	1	2	3

Step 3 deals with analysis of results. Three major statistical tools commonly applied in Taguchi method are signal-to-noise ratio (SNR), analysis of means (ANOM) and analysis of variance (ANOVA). SNR for each run n is defined as:

$$(SNR)^n = -10 \log(MSD)^n; \forall n=1, \dots, N \quad (4.3)$$

where $N=27$ is the number of experiments in the internal array. Since RGP profit is chosen as the objective function in this work, mean squared deviation (MSD) is defined to uphold “the-larger-the-better” quality principle as follows:

$$(MSD)^n = \frac{1}{M} \sum_{m=1}^M \frac{1}{(x^{mn} - \bar{x}^m)^2}; \forall n=1, \dots, N \quad (4.4)$$

where $M=9$ is the number of experiments in the external array. Equation 4.3 is slightly modified from the one presented by Roy (1990). This is necessary to avoid dealing with large absolute values of RGP profit. In the current work, deviational values of profit are obtained from the spread around means \bar{x}^m of respective cases.

For ANOM and ANOVA, two averages must be calculated *a priori*. Average of factor k at level l in case m , \bar{x}_{kl}^m , is taken as sum of respective factorial values divided by number of repeated level, N_R .

$$\bar{x}_{kl}^m = \frac{1}{N_R} \sum_{n=1}^{N_R} x_{kl}^{mn}; \forall k=1, \dots, K; \forall l=1, \dots, L; \forall m=1, \dots, M \quad (4.5)$$

where $N_R=9$, $K=7$ and $L=3$ are correspondingly numbers of repeated level, factors and levels. It should be noted that in Equation 4.4, n is an index referring to run numbers in L_{27} array that correspond to unique configurations of factorial levels. This means that $n=1, \dots, N_R$ may not follow a sequence from 1 to N_R . For example, index $n=1$ may refer to the tenth row in L_{27} array containing the first output of a particular factor at level 2. After determining average of factor k at level l , average of factor k over all levels L in each case m , \bar{x}_k^m is calculated as below:

$$\bar{x}_k^m = \frac{1}{L} \sum_{l=1}^L \bar{x}_{kl}^m; \forall k=1, \dots, K \quad (4.6)$$

These two averages are used to calculate variance V_k^m which has two contributors. The numerator is the sum of squares between two averages of factor k (\bar{x}_{kl}^m and \bar{x}_k^m). The denominator is called degrees of freedom of factor k over all levels L in case m , $(DOF)_k^m$.

$$V_k^m = \frac{\sum_{l=1}^L (\bar{x}_{kl}^m - \bar{x}_k^m)^2}{L_k^m - 1}; \forall k=1, \dots, K \quad (4.7)$$

Percentage contribution C_k^m is obtained by dividing individual variance of factor k , V_k^m from total variance of all factors and multiplying the result with 100.

$$C_k^m = \frac{100V_k^m}{\sum_{k=1}^K V_k^m}; \forall k=1, \dots, K \quad (4.8)$$

Step 4 is validation of experiment. For each run in external array, there are 27 experimental runs in internal array. By design, only one run will yield the highest profit margin. Preliminary visual inspection of trends of each factor average contributions at all levels can be made through a response plot. Here, average values of profit and SNR of factor k at levels $l=1, \dots, L$ ($L=3$) are plotted against corresponding factors. The response plot may be used to locate optimal design configuration for the purpose of verifying results. Additional experiments with 9 runs are required to compare both experimental and calculated values of profit. The calculated optimum profit x_{opt}^m in case m is obtained by summing up mean \bar{x}^m for the same case with maximum deviations of average values of factor k at level l , \bar{x}_{kl}^m from the corresponding average values at all levels, \bar{x}_k^m .

$$x_{opt}^m = \bar{x}^m + \left(\sum_{k=1}^K \max(\bar{x}_{kl}^m) - \bar{x}_k^m \right); \forall l=1, \dots, L \quad (4.9)$$

where

$$\bar{x}^m = \bar{x}_k^m; \forall k=1, \dots, K \quad (4.10)$$

Equation 4.9 implies that average of factor k over all levels, \bar{x}_k^m equals to mean \bar{x}^m of the respective case m . This is true since Taguchi design of experiment is unbiased by construction.

4.3.2 Analyses of Taguchi Results

All experiments are conducted using RGP dynamic model developed under HYSYS environment. Profit (Equation 4.1) is calculated online in a built-in spreadsheet. Material and energy units are converted *a priori* to be consistent with the basis of one-minute interval calculation. To ensure repeatability, HYSYS 2006 SP5 running on Windows XP Professional operating system is employed. This process simulator is installed in a standard Dell Optiplex GX520. Reproducibility is also ensured because experimental steps are pre-configured in 'Event Scheduler'. Changes on levels of all factors are set to run in parallel.

Experiments are stopped after all factors reach steady-state at 420 min simulation time. In most experiments, profit values level off after 360 min but in some runs, the values slightly fluctuate towards the end. For these runs, the last 60 values are averaged out. Only one profit value is required for each run. Major results are presented in Table 4.7. For convenience, profit is denoted as x^{mn} where m ($m=1, \dots, 9$) and n ($n=1, \dots, 27$) are indices of external and internal runs, respectively. Cases 1 to 9 refer to the corresponding values of index m . In the following discussion, Cases 1-3, 4-6 and 7-9 are categorized as Groups I, II and III due to similarity in configuration of noise factor H (plant load) and sequence of noise factor I (feed gas prices).

Table 4.7: Results of Taguchi crossed-orthogonal-array experiments

Run	Profits (RM/min)										\bar{x}^n
	x^{1n}	x^{2n}	x^{3n}	x^{4n}	x^{5n}	x^{6n}	x^{7n}	x^{8n}	x^{9n}		
1	1742.94	1785.86	1741.67	1773.24	2007.01	1947.93	2189.85	2225.79	2160.85	1975.01	
2	1764.03	1805.35	1755.75	1996.33	2026.64	1965.99	2213.38	2249.27	2179.83	1995.18	
3	1798.38	1832.00	1777.96	2019.41	2038.59	1977.41	2230.85	2260.46	2192.79	2014.21	
4	1731.30	1778.85	1735.15	1957.65	1991.79	1942.41	2177.60	2212.26	2150.55	1964.17	
5	1754.64	1800.10	1751.35	1982.67	2015.66	1959.77	2201.50	2238.52	2169.87	1986.01	
6	1777.01	1817.79	1760.46	2002.25	2030.58	1973.66	2222.27	2253.86	2185.60	2002.61	
7	1723.50	1773.30	1729.05	1950.23	1985.75	1936.35	2161.30	2198.99	2143.29	1955.75	
8	1747.93	1794.78	1748.01	1974.82	2009.52	1955.43	2186.93	2224.65	2163.69	1978.42	
9	1763.72	1808.65	1757.94	1996.29	2027.19	1970.67	2209.06	2243.64	2180.47	1995.29	
10	1760.99	1802.53	1746.53	1982.39	2013.95	1958.16	2199.29	2232.72	2166.66	1984.80	
11	1744.46	1791.71	1743.56	1969.70	2005.60	1951.41	2179.52	2218.32	2160.46	1973.86	
12	1759.31	1805.31	1758.48	1982.90	2019.01	1965.31	2199.07	2237.94	2173.00	1988.92	
13	1738.38	1786.61	1740.90	1969.89	2001.48	1948.91	2186.01	2222.60	2159.27	1972.67	
14	1728.07	1778.10	1734.41	1951.93	1988.02	1939.62	2161.86	2201.19	2148.40	1959.07	
15	1742.37	1791.84	1749.59	1968.70	2003.45	1955.76	2186.88	2225.69	2166.81	1976.79	
16	1732.66	1782.34	1736.92	1960.44	1996.18	1944.51	2175.24	2212.85	2151.70	1965.87	
17	1720.47	1770.57	1728.48	1944.59	1981.31	1934.02	2155.48	2195.28	2142.96	1952.57	
18	1733.46	1785.18	1743.70	1959.46	1996.17	1950.31	2175.49	2213.85	2158.20	1968.42	
19	1730.56	1779.28	1737.60	1952.84	1992.14	1941.69	2162.20	2203.57	2150.47	1961.15	
20	1739.71	1789.44	1745.09	1965.75	2001.44	1953.61	2181.14	2221.69	2160.53	1973.16	
21	1728.68	1779.92	1737.27	1948.20	1986.54	1941.44	2157.78	2199.03	2149.73	1958.73	
22	1723.58	1774.15	1731.25	1948.44	1987.44	1938.21	2156.62	2199.82	2147.33	1956.32	
23	1733.20	1784.63	1741.88	1959.36	1997.94	1949.52	2167.50	2210.99	2155.37	1966.71	
24	1720.77	1770.29	1732.80	1942.57	1981.62	1937.03	2153.45	2195.00	2145.96	1953.28	
25	1706.99	1760.48	1722.91	1930.70	1970.28	1927.69	2139.05	2181.13	2130.81	1941.12	
26	1717.47	1773.86	1735.39	1942.55	1983.44	1940.31	2154.70	2196.45	2146.72	1954.54	
27	1705.45	1758.57	1723.00	1929.39	1969.82	1928.74	2138.05	2181.83	2136.44	1941.25	
Means=	1739.63	1787.46	1742.48	1965.28	2000.32	1949.48	2178.59	2216.94	2158.44	1970.96	

Note: Superscript n refers to experimental run number in internal arrays.

4.3.2.1 Effect of Noise Factors

Means for Cases 1, 2 and 3 (Group I) are respectively 1739.63, 1787.46 and 1742.48 in the unit of RM/min. For convenience, the unit RM/min is omitted in subsequent discussions. For Cases 4, 5 and 6 (Group II), means are 1965.28, 2000.32 and 1949.48. In the last three cases (Group III), the values are 2178.59, 2216.94 and 2158.44. The means for Groups I, II and III can be calculated as 1756.53, 1971.69 and 2184.66, respectively. A gap of about 200 is noticed between Groups I and II as well as between Groups II and III. This discrepancy is caused by the presence of noise factor H , which is plant load. Increasing plant load increases amount of feed gas and thus RGP profit due to additional productions of sales gas and natural gas liquids. However, it should be noted that RGP was designed to process a maximum of 310 ton/h of feed gas. Any amount higher than this value will push equipment loads towards upper constraints. On the other hand, RGP load can be reduced to 100 ton/h of feed gas without the need for total plant shutdown. However, under-loading is undesirable since RGP profit will also diminish.

Similarly, effect of noise factor I on RGP profit can be deduced. The highest values of average profit in each Groups I, II and III are generated from I_2 (factor I , level 2) configuration. As clearly shown in Cases 2, 5 and 7, the average profits are respectively 1787.46, 2000.32 and 2178.59. This is attributed to different economic values of feed gas streams A, B and C due to different values of carbon dioxide contents (Table 4.3). Highly priced feed gas stream A erodes RGP profit while the cheaper feed gas stream C increases it.

4.3.2.2 Average Profit Analysis

To study relative significance of factors quantitatively, ranking of factors is initially performed using analysis of mean (ANOM). Table 4.8 shows ANOM results for RGP profit. Equations 4.4 and 4.5 are applied to calculate averages of factor k . For RGP profit analysis, values of profit from Cases 1-9 are averaged out in a row-by-row basis as implemented by Yang et al. (2007). This approach is consistent with the general procedures of Taguchi method that deals with average values. Superscript m referring to run number in the external arrays may be omitted in this section. Hence, an average

value of profit at certain level is denoted as \bar{x}_{kl} . As an example, averages of factor A at levels 1, 2 and 3 are (Equation 4.4):

$$\bar{x}_{A1} = \frac{1}{9} \begin{pmatrix} 1975.01 + 1995.18 + 2014.21 \\ + 1964.17 + 1986.01 + 2002.61 \\ + 1955.75 + 1978.42 + 1995.29 \end{pmatrix} = 1985.18; n=1, \dots, 9.$$

$$\bar{x}_{A2} = \frac{1}{9} \begin{pmatrix} 1984.80 + 1973.86 + 1988.92 \\ + 1972.67 + 1959.07 + 1976.79 \\ + 1965.87 + 1952.57 + 1968.42 \end{pmatrix} = 1971.44; n=10, \dots, 18.$$

$$\bar{x}_{A3} = \frac{1}{9} \begin{pmatrix} 1961.15 + 1973.16 + 1958.73 \\ + 1956.32 + 1966.71 + 1953.28 \\ + 1941.12 + 1954.54 + 1941.25 \end{pmatrix} = 1956.25; n=19, \dots, 27.$$

where \bar{x}_{Al} denotes average of profit due to factor A at level l ($l=1, \dots, 3$). Similarly, average of factor A at all three levels is (Equation 4.5):

$$\bar{x}_A = \frac{1}{3} (1985.18 + 1971.44 + 1956.25) = 1970.96$$

By design, average of factor A is the same as those of other factors as shown in Table 4.8. This factorial average value is also the same as the global mean value of 1970.96 as presented in Table 4.7 and implied by Equation 4.10.

Table 4.8: Analysis of means for average profit

	\bar{x}_{Al}	\bar{x}_{Bl}	\bar{x}_{Cl}	\bar{x}_{Dl}	\bar{x}_{El}	\bar{x}_{Fl}	\bar{x}_{Gl}
Level 1	1985.18	1980.56	1971.95	1969.98	1964.10	1969.28	1959.30
Level 2	1971.44	1970.85	1970.81	1970.30	1971.06	1970.69	1972.48
Level 3	1956.25	1961.47	1970.11	1972.59	1977.72	1972.91	1981.10
\bar{x}_k	1970.96	1970.96	1970.96	1970.96	1970.96	1970.96	1970.96
E_k	28.93	19.09	1.84	2.61	13.63	3.63	21.80
R_k	1	3	7	6	4	5	2

Note: k =factor number; l =level number

Ranking is initially determined from ANOM, which shows deviation of the highest value from the lowest value of average of factor k at level l : $l=1,\dots,L$ ($L=3$). This deviation is denoted as E_k . The highest ranking is assigned to a factor carrying the highest E_k value. In case of 7 controllable factors that affect RGP profit, the descending order of importance is *AGBEFDC* (Table 4.8). This implies that factor *A* is the most significance while factor *C* is the least significance. Ranking from ANOM is verified with ranking from ANOVA (Table 4.9). In the latter analysis, averages of factor k at level l and at all levels L are used to determined sum of squares of factor k . For example, sum of squares of factor *A* is:

$$S_A = 27 * \left[\begin{array}{l} (1985.18-1970.96)^2 \\ + (1971.44-1970.96)^2 \\ + (1956.25-1970.96)^2 \end{array} \right] = 11310.14$$

Table 4.9: Analysis of variance for average profit

	<i>A</i>	<i>B</i>	<i>C</i>	<i>D</i>	<i>E</i>	<i>F</i>	<i>G</i>
S_k	11310.14	4918.75	46.51	109.73	2507.23	181.24	6507.04
$(DOF)_k$	2	2	2	2	2	2	2
V_k	5655.07	2459.37	23.26	54.86	1253.61	90.62	3253.52
C_k	44.21	19.23	0.18	0.43	9.80	0.71	25.44
R_k	1	3	7	6	4	5	2

Note: k =factor number

In general, an S_k value represents spread of experimental results of factor k from data average. A large value such as the one obtained here indicates significant contribution of that particular factor towards output (RGP profit). On the other hand, a factor is deemed unimportant if its S_k value approaches zero. Since S_k values are unbounded at the higher end, it is convenient to denote relative importance of a factor k in term of its percentage contribution, C_k (Equation 4.7). Before calculating C_k , a quantity called general variance of factor k , V_k needs to be determined. This quantity differs from population variance σ^2 , which could only have been obtained if all 19,683 (3^9) possible experiments had been conducted. The V_k value is obtained from Equation 4.6 where degree of freedom of factor k , $(DOF)_k$ is one less its number of levels. For example, variance of factor *A* is thus:

$$V_A = \frac{11310.14}{3-1} = 5655.07$$

Finally, percentage contribution of factor A is:

$$C_A = \frac{100(5655.07)}{\left[\begin{array}{l} 5655.07 + 2459.37 + 23.26 + 54.86 \\ + 1253.61 + 90.62 + 3253.52 \end{array} \right]} = 44.21\%$$

Ranking of factor k , R_k from ANOVA is presented in Table 4.9 above. The descending order of importance of 7 controllable factors is *AGBEFDC*. This result is strikingly similar to the one from ANOM. Factor A (split range controller SRC103 output) is a major contributor with 44.2%. This factor regulates temperature of feed gas exiting coldbox E-101 that could influence refrigeration cooler duty (temperature controller TC101 output). Lower feed gas temperature means less cooler E-102 duty is required to maintain the same separation and thus higher RGP profit. Contribution of factor B (temperature controller TC101 output) at 19.2% is slightly less than that of factor G (temperature controller TC102 output) at 25.4%. Both factors B and G play an important role in plant energy balance. Hence an increase in temperature controller TC101 output that further reduces RGP temperature must be accompanied by a similar raise in temperature controller TC102 output. Disproportionate contribution of factors B and G is attributed to presence of factor A .

The effect of factor E (flow controller FC104 output) is also significant with 9.8% contribution. Flow controller FC104 output regulates re-injection of rich hydrocarbon to boost sales gas gross heating value. An increase in flow controller FC104 output increases sales gas production. Due to large gap between prices of sales gas and feed gas stream D (Table 4.1), a lift in sales gas rate increases RGP profit. However, it should be noted that only 10 ton/h of feed gas stream D is available for this purpose. Contribution of factor F (pressure controller PC101 that regulates demethanizer overhead pressure) is about four times as large as factor C (split range controller SRC102 output). Both factors C and F are mainly used to regulate demethanizer overhead quality. Since installation of gas subcooled process (GSP) section in RGP, influence of split range controller SRC102 controller on demethanizer overhead quality has been drastically reduced and taken over by pressure controller PC101.

Contribution of factor D (RC101 controller ratio) is minor at 0.4%. This factor regulates split of processed gas going into GSP section and/or turbo-expander. A higher value of RC101 controller ratio promotes more recovery of ethane and heavier hydrocarbons at GSP section. In other words, factor D is useful in improving ethane recovery but only slightly significant in increasing RGP profit due to lower price of ethane as compared with other natural gas liquids and sales gas values.

4.3.2.3 Signal-to-Noise Ratio (SNR) Analysis

RGP profit is determined by independently setting 7 controllable and 2 noise factors in Taguchi arrays. $L_{27} (3^7)$ internal arrays are selected for controllable factors and $L_9 (3^2)$ external arrays for noise factors. This means that each experimental run from internal arrays (Table 4.5) needs to be repeated 9 times under different configuration of external arrays (Table 4.6). In the previous section, significance of controllable factors in maximizing RGP profit has been discussed with moderated influence of noise factors. In this section, significance of controllable factors is investigated using signal-to-noise ratio (SNR) approach. Qualitative principle in the form of “the-larger-the-better” SNR is selected for this analysis. A high value of SNR in a particular run indicates minimum effects of noise factors on outputs. SNR values for all runs are presented in Table 4.10. They are calculated using Equations 4.2 and 4.3. Taking run array $mn=13$ (runs 1 and 3 in external and internal arrays, respectively) for example, mean standard deviation (MSD)¹³ can be calculated as:

$$(MSD)^{13} = \frac{1}{9} \left[\begin{aligned} &(1798.38-1739.63)^{-2} + (1832.00-1787.46)^{-2} + (1777.96-1742.48)^{-2} \\ &+ (2019.41-1965.28)^{-2} + (2038.59-2000.32)^{-2} + (1977.41-1949.48)^{-2} \\ &+ (2230.85-2178.59)^{-2} + (2260.46-2216.94)^{-2} + (2192.79-2158.44)^{-2} \end{aligned} \right] = 0.2940$$

Signal-to-noise ratio (SNR)¹³ is:

$$(SNR)^{13} = -10 * \log(0.2940) = 5.32$$

Table 4.10: Results of signal-to-noise ratio (SNR) analysis

Run	$(SNR)^n$	$(SNR)_{Adj}^n$
1	5.32	23.37
2	26.40	44.46
3	32.03	50.09
4	8.89	26.95
5	22.37	40.43
6	29.11	47.17
7	23.51	41.57
8	16.88	34.94
9	27.15	45.21
10	19.09	37.15
11	4.43	22.49
12	24.91	42.96
13	0.58	18.64
14	20.83	38.89
15	12.91	30.97
16	13.49	31.54
17	24.95	43.00
18	-3.51	14.54
19	18.34	36.39
20	-12.84	5.22
21	19.31	37.37
22	22.69	40.74
23	-18.06	0.00
24	23.72	41.78
25	28.86	46.91
26	22.06	40.11
27	28.63	46.68

Since an SNR value may be negative when MSD rises above 1, a bias is added to all SNR values. The bias is chosen as the minimum value of SNR across all case studies. In essence, an adjusted SNR is defined as:

$$(SNR)_{Adj}^{mn} = (SNR)^{mn} - \min(SNR)^m \quad (4.11)$$

In this case, the adjusted SNR for run array $mn=13$ is:

$$(SNR)_{Adj}^{13} = 32.03 - (-18.06) = 50.09$$

In subsequent discussions, the word 'adjusted' is omitted for convenience. All *SNR* values refer to adjusted *SNR* values. These values are used to determine ranking of controllable factors that can minimize effects of noise factors.

Ranking is performed using a similar method employed in average profit analysis. However, *SNR* values instead of average values of profit are used in carrying out ANOM and ANOVA. For ANOM, averages of *SNR* of factor *k* at levels 1, 2 and 3 are initially calculated before determining the corresponding E_k values. For example, *SNR* averages of factor *A* are:

$$(\overline{SNR})_{A1} = \frac{1}{9} \begin{pmatrix} 23.37+44.46+50.09 \\ +26.95+40.43+47.17 \\ +41.57+34.94+45.21 \end{pmatrix} = 39.35$$

$$(\overline{SNR})_{A2} = \frac{1}{9} \begin{pmatrix} 37.15+22.49+42.96 \\ +18.64+38.89+30.97 \\ +31.54+43.00+14.54 \end{pmatrix} = 31.13$$

$$(\overline{SNR})_{A3} = \frac{1}{9} \begin{pmatrix} 36.39+5.22+37.37 \\ +40.74+0.00+41.78 \\ +46.91+40.11+46.68 \end{pmatrix} = 32.80$$

where $(\overline{SNR})_{Al}$ denotes average of *SNR* due to factor *A* at level *l*: $l=1, \dots, 3$. Thus, average of *SNR* due to factor *A* at all three levels is:

$$(\overline{SNR})_A = \frac{1}{3}(39.35+31.13+32.80) = 34.43$$

Other average *SNR* values of factor *k* are calculated using the same procedure and presented in Table 4.11. Ranking of 7 controllable factors in descending order of importance is *FEACBDG*. This shows that factors *F* and *G* are respectively the most and least important factors. However, it is important to note that *SNR* results disagree with the ones based on average profit. Interpretation of results from *SNR* analysis is differed until after discussion on ANOVA, which is utilized to verify results from ANOM.

Table 4.11: Analysis of means (ANOM) for SNR

	$(\overline{SNR})_{Al}$	$(\overline{SNR})_{Bl}$	$(\overline{SNR})_{Cl}$	$(\overline{SNR})_{Dl}$	$(\overline{SNR})_{El}$	$(\overline{SNR})_{Fl}$	$(\overline{SNR})_{Gl}$
Level 1	39.35	33.28	32.17	37.79	33.70	25.08	35.79
Level 2	31.13	31.73	38.98	31.40	29.95	37.00	36.93
Level 3	32.80	38.28	32.13	34.09	39.64	41.21	30.57
\bar{x}_k	34.43	34.43	34.43	34.43	34.43	34.43	34.43
E_k	8.22	6.55	6.85	6.39	9.69	16.13	6.36
R_k	3	5	4	6	2	1	7

Note: k =factor number; l =level number

The main objective of ANOVA is to calculate percentage contributions of factor k , C_k in influencing RGP profit. Ranking of factors may also be determined from C_k values. A factor with the highest C_k value is the most significance. The procedure for calculating C_k values are presented previously in the case of average profit analysis and thus will not be repeated here. The descending order of importance from ANOVA is *FEACBGD* (Table 4.12). The order is similar to that from ANOM except for the last two, in which factors D and G switch places. Since ANOVA is a second order statistical analysis, its results are more reliable than those of ANOM.

Table 4.12: Analysis of variance (ANOVA) for SNR

	A	B	C	D	E	F	G
S_k	1019.78	633.06	840.08	555.96	1289.81	3781.63	620.73
$(DOF)_k$	2	2	2	2	2	2	2
V_k	509.89	316.53	420.04	277.98	644.90	1890.82	310.36
C_k	11.67	7.24	9.61	6.36	14.76	43.26	7.10
R_k	3	5	4	7	2	1	6

Note: k =factor number

It is evident that ranking orders for statistical analyses using average profit and SNR values differ markedly. Factor A (split range controller SRC103 output) with 44.2% contribution is the most significance in maximizing RGP profit. On the other hand, factor F (pressure controller PC101 setpoint) with 43.3% is the most important in minimizing effects of noise factors through SNR analysis. PC101 is a pressure controller responsible for maintaining demethanizer overhead pressure. Raising pressure controller PC101 setpoint from 22 to 24 bar increases demethanizer top column temperature by about 5 °C. This action induces losses of ethane and propane in sales gas product stream. On the other hand, a low value of pressure controller

PC101 setpoint at 22 bar helps to improve recovery of natural gas liquids due to cooler condition at enriching part of demethanizer. Given fluctuating disturbances in the forms of noise factors H (plant load) and I (feed gas prices), pressure controller PC101 should be set at appropriate level to stabilize demethanizer.

Factor E (flow controller FC104 output) at 14.8% contribution is the next important factor. Flow controller FC104 regulates rich hydrocarbon (feed gas stream D) injection to sales gas product stream. In the event of low plant load, flow controller FC104 output is increased to boost sales gas flow rate and gross heating values. This practice will drive revenue upwards due to large gap between prices of sales gas and feed gas stream D. Factor A (split range controller SRC103 output) with 11.7% contribution is also significant. Split range controller SRC103 output regulates amount of processed gas entering and bypassing coldbox E-101. A high value of split range controller SRC103 output at 100% means no bypass. As a result, the hotter feed gas exchanges more heat with the much cooler processed gas and leaves coldbox E-101 at lower temperature. This will have a positive effect on recovery of natural gas liquids and thus RGP profit. A stream with high carbon dioxide content contains lower quantity of hydrocarbon (termed leaner) to be processed. Since carbon dioxide has zero heating value, leaner feed gas requires less energy to be cooled and/or heated in order to achieve the same separation as the richer one. Thus split range controller SRC103 output value needs to be adjusted accordingly to handle either feed gas streams A, B or C.

Explanation for significance of Factor C (split range controller SRC102 output) with 9.6% contribution is similar to that of Factor A (split range controller SRC103 output). The only difference between the two factors is in regulating split of sales gas flow at coldbox E-103 instead of E-101. Contributions from factors B (temperature controller TC101 output) and G (temperature controller TC102 output) are about the same at 7.2% and 7.1%, respectively. Temperature controller TC101 output regulates propane refrigeration cooler duty while temperature controller TC102 output regulates demethanizer reboiler duty. Both variables control the amount of energy leaving or entering RGP. A high value of plant load requires additional load on temperature controller TC101 duty to maintain the same recovery of natural gas liquids. Increasing value of temperature controller TC101 output must be matched by the same amount in

temperature controller TC102 output. With close to zero contribution, factor D (RC101 controller ratio) is the least significant factor in regulating external disturbances. RC101 is a ratio controller that regulates amount of feed gas entering turboexpander and GSP section of RGP. A high value of RC101 controller ratio improves recovery of natural gas liquids. However, RC101 controller ratio can hardly be employed to minimize the effects of fluctuations in feed gas flow and prices on to RGP profit.

Besides determining significance of factors responsible for stabilizing disturbance, SNR results may also be employed to locate optimal configuration of factors to yield maximum RGP profit. This configuration is found based on ‘the-higher-the-better’ qualitative principle. From Table 4.10, the highest SNR value of 50.1 comes from run 3 with configuration $A_1B_1C_1D_1E_3F_3G_3$. This configuration consistently gives the highest profit values in all Cases 1-9 as shown by results across the same row. In fact, profit value of 2260.46 in Case 8 is the maximum one found from all 243 experiments.

On the other hand, zero SNR value implies that configuration $A_3B_2C_1D_3E_2F_1G_3$ in run 23 yields the lowest profit. However, it is found that average profit value of 1966.71 at this run is closer to the overall mean value of 1970.96 than to the minimum value of 1941.42. This result confirms that SNR principle employed in this study is only valid in determining the highest value but not the lowest value of RGP profit. In general, maximum and minimum values of profit can only be ascertained after running the entire 19,683 (3^9) experiments under full factorial design approach. It is possible that profit values derived from Taguchi method do not even reach either side of the extremities. For this reason, it is important to estimate and validate maximum value of profit by running another set of experiments under optimal configurations of both controllable and noise factors.

4.3.3 Validation

The final step in Taguchi method is validation of results. RGP profits obtained from conducting HYSYS experiments are compared with those calculated based on ANOM. In this case, ANOM results are obtained for individual Cases 1-9 as opposed

to the one discussed previously where ANOM is performed using average values of profit from all 9 cases. This is necessary because the latter lacks configuration of noise factors to be assigned in HYSYS 'Event Scheduler'. ANOM profit values are obtained from Equation 4.8, which contains two terms namely means and maximum differences of averages of factor $k : k=1,...,K$ ($K=7$) for the corresponding cases $m=1,...,9$. An example on how to calculate ANOM profit is shown below:

$$x_{opt}^1 = 1739.63 + (16.31 + 12.49 + 1.42 + 2.31 + 8.05 + 4.06 + 11.65) = 1795.92$$

where superscript value of optimum output x_{opt}^1 denotes Case 1. The mean value for Case 1 is 1739.63 (Table 4.7). Values in parenthesis are maximum differences between individual averages of factor k at level $l=1,...,L$ ($L=3$) and their means at respective Cases 1-9 (Table 4.13).

Table 4.13: Maximum differences of averages of controllable factors for Cases 1 to 9

Case	A	B	C	D	E	F	G
1	16.31	12.49	1.42	2.31	8.05	4.06	11.65
2	12.17	9.36	0.36	2.02	6.93	2.84	10.08
3	8.33	6.84	0.89	0.79	6.54	1.36	6.74
4	18.37	11.47	1.81	2.13	6.85	3.18	12.31
5	14.43	9.78	1.12	2.79	5.57	2.03	9.77
6	9.37	6.41	0.24	1.87	6.12	1.01	7.94
7	20.60	11.75	1.17	0.60	7.28	1.06	13.19
8	17.22	10.70	1.21	1.07	6.54	0.53	11.42
9	11.23	7.60	1.01	1.15	7.01	1.49	8.13

Optimal configurations of controllable factors can be determined from a response plot of average values of factor k at respective levels against output values. In this work, the outputs are profit and *SNR* values. Two qualitative observations can be made from this plot: 1) significance of individual factors can be established from steepness of factorial graph slopes, and 2) levels of individual factors yielding maximum RGP profits and *SNR* can be visually determined. In the first observation, the steeper the slope of a factorial graph, the more significant the factor is. This deduction can complement percentage contributions of factors, C_k as discussed previously. As an example, split range controller SRC102 (factor C) output may be varied between 90 and 100% without affecting much of RGP profit. For split range controller SRC102 output values below 90%, a decrease by 1% in controller output

increases demethanizer top temperature by about 0.2 °C. This eventually leads to losses in ethane and propane products by about 0.90 and 2.25%, respectively. On the other hand, a controller output value above 100% is not allowed due to violation in physical constraint. Similar deductions can be made on the effects of factor D (RC101 controller ratio) and factor F (pressure controller PC101 setpoint) on the RGP profit.

The second observation is important in estimating and validating experimental results. A configuration of optimal levels of factors should yield a maximum value of RGP profit. In analysis that uses average values of profit, it is clear that maximum profit could be obtained from configuration $A_1B_1C_1D_3E_3F_3G_3$ (Figure 4.3). Values of this optimal configuration are set up in HYSYS 'Event Scheduler' and run for 420 min. RGP profit is calculated automatically using built-in spreadsheet to prevent round-off error. Profit values of 1813.67, 1840.20, 1791.35, 2009.59, 2037.80, 1981.95, 2229.17, 2259.73 and 2192.06 are obtained for Cases 1-9, respectively. Assuming that HYSYS experimental results are the correct ones, deviation from these values are termed error, E^m for cases $m=1,\dots,9$. For example, an E^m value can be calculated as:

$$E^1 = 100 \frac{(1795.92 - 1813.67)}{1813.67} = -0.98\%$$

where superscript 1 in error term E^1 denotes Case 1. Positive E^m values indicate that HYSYS experimental results are lower than those obtained from ANOM. In this work small E^m values of less than 1% for all cases are obtained (Table 4.14). This means that optimal configurations of controllable factors for all cases have been found.

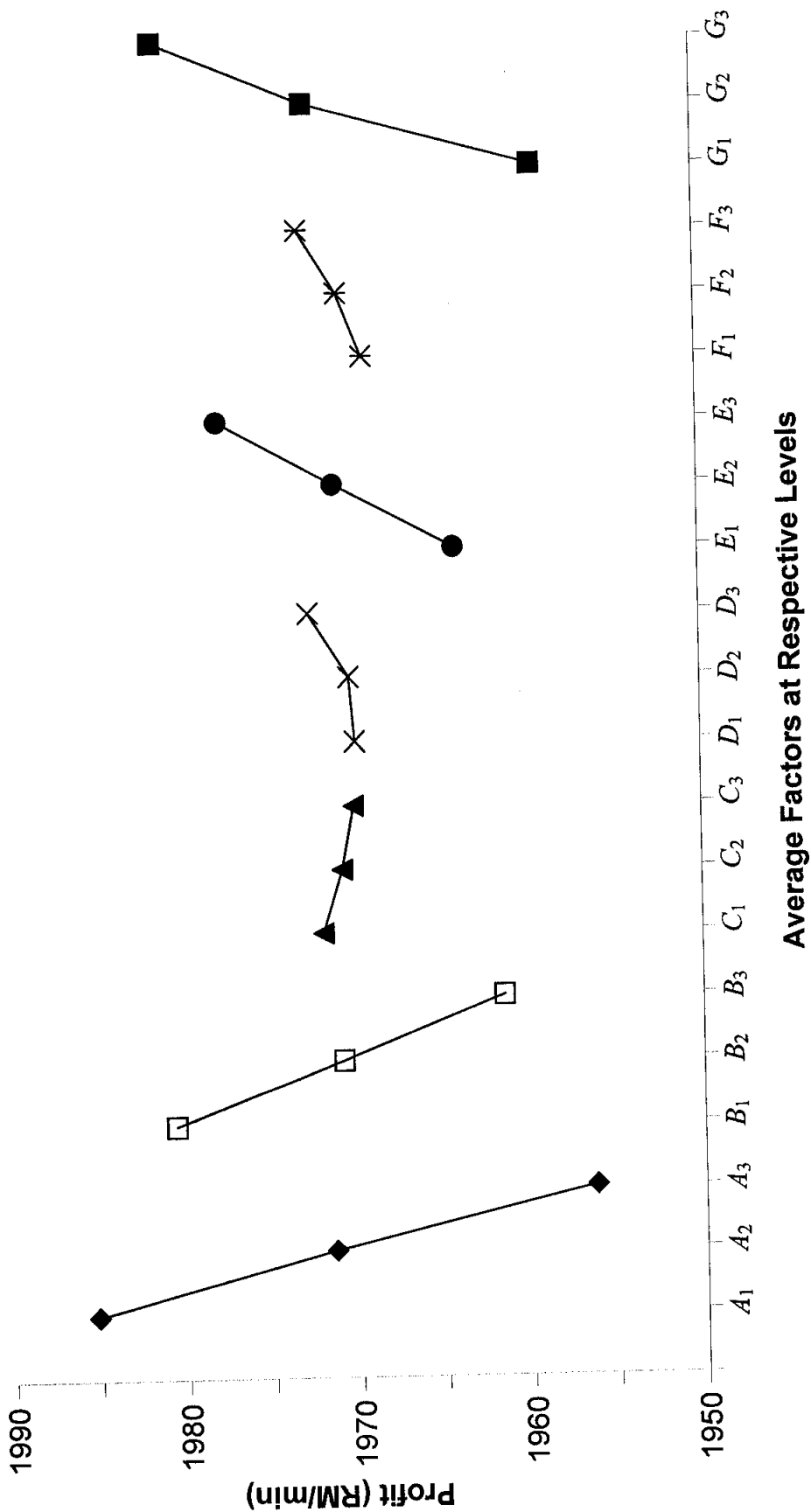


Figure 4.3: Response plot for average profit analysis

Optimal configurations of noise factors can be determined from means of profit in Cases 1-9 (Table 4.7). A minimum value of 1739.63 is obtained from Case 1 with configurations H_1I_1 . On the other hand, configurations H_3I_2 in Case 8 yield a maximum value of 2216.94. This shows that optimum configurations of noise factors have been found in Case 8. If combined with the previous result, optimal configurations of controllable and noise factors are $A_1B_1C_1D_3E_3F_3G_3H_3I_2$. When run in HYSYS, these configurations yield a profit value of 2259.73. A comparison with ANOM result yields a small E^m value of 0.3% confirming that this configuration is optimum. In addition, the profit value obtained from running optimal configuration of factors is close to the maximum profit value of 2260.46 obtained from run 3 in Case 8 with configuration $A_1B_1C_1D_3E_3F_3G_3H_3I_2$.

Table 4.14: RGP profit values from experiments (HYSYS) and Taguchi method (ANOM) at optimal conditions

Case	HYSYS (RM/min)	ANOM (RM/min)	Deviation (%)
1	1813.67	1795.92	-0.98
2	1840.20	1831.21	-0.49
3	1791.35	1773.98	-0.97
4	2009.59	2021.39	0.59
5	2037.80	2045.82	0.39
6	1981.95	1982.43	0.02
7	2229.17	2234.24	0.23
8	2259.73	2265.63	0.26
9	2192.06	2196.05	0.18

Figure 4.4 shows a response plot based on SNR analysis. Configuration $A_1B_3C_2D_1E_3F_3G_2$ seems optimal because SNR values of each factor are the highest. Another run in HYSYS with this configuration coupled with H_3I_2 configuration on noise factors yields profit value of 2233.75. This value is 1.2% lower than the one found based on average profit analysis. When optimal configurations based on average profit and SNR values are compared, agreements are only found on levels of factors A , E and F . Differences in optimal levels of factors B , C , D and G are found to be responsible for lowering profit. This result shows that an optimal configuration of factors cannot be determined from SNR response plot. Instead, the optimal configuration can be found from the response plot based on average profit values of all 9 cases as discussed earlier.

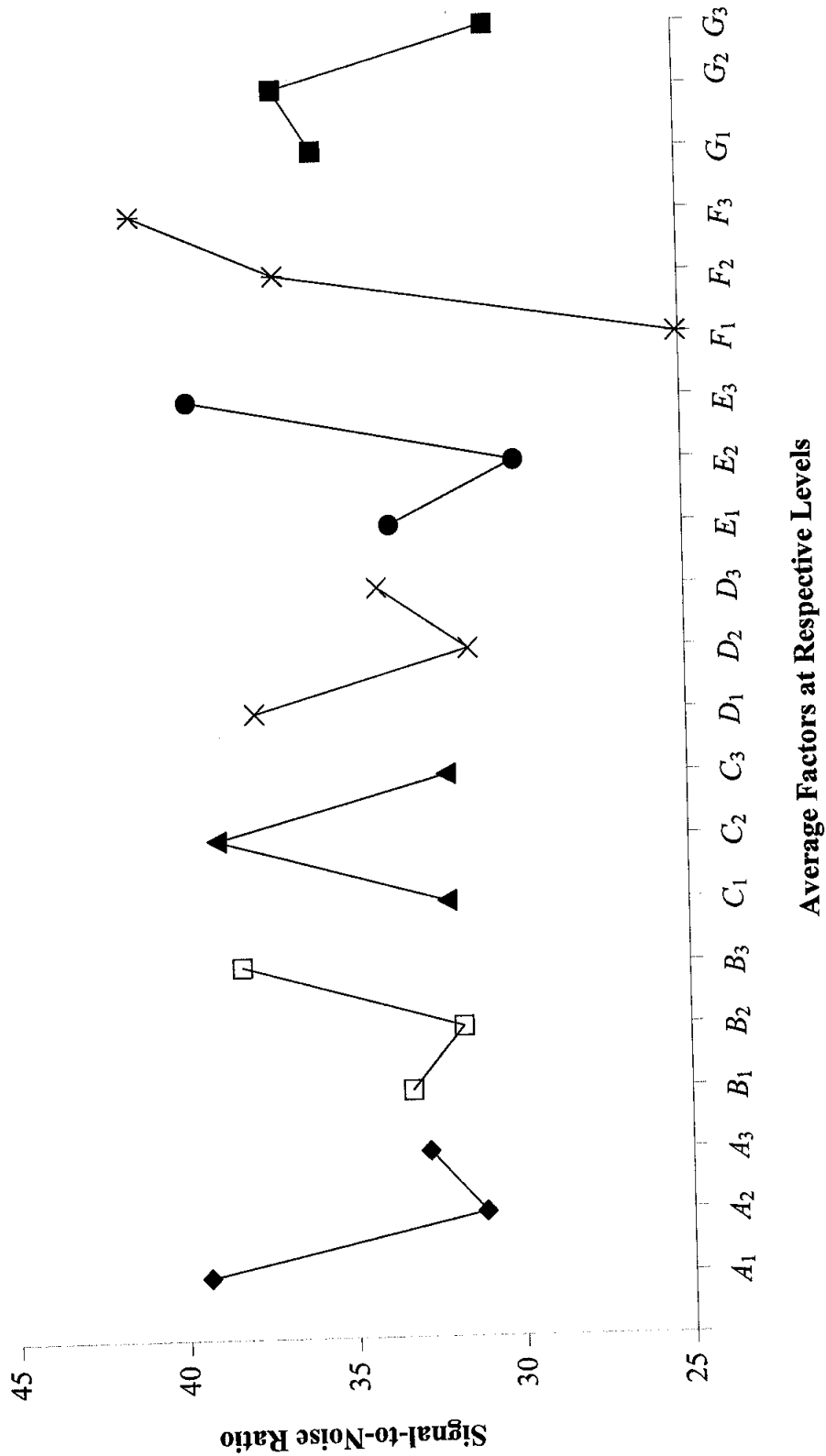


Figure 4.4: Response plot for SNR analysis

When the optimal configuration based on average profits is run in HYSYS, dynamic responses and final steady-state levels for Cases 1 to 9 can be plotted to illuminate several interesting points (Figure 4.5). Highly fluctuating trends in the early part of simulation time reflect difficulties faced by RGP to maintain stability due to changes in levels of all factors. After initial rise in profit values, trough is clearly noticed after about 10 min of simulation effort for all 9 cases. For the last three cases, additional fluctuations are noticed after 30 min of simulation time.

In general, the trough phenomenon is caused by inadequacy of cooling for separation of natural gas liquids from sales gas when feed gas flow is raised from 250 to 280 ton/h. This corresponds to changes in factor *H* from level 1 to 2. Recall that feed gas is cooled by increasing levels of factors *A* (split range controller SRC103 output), *B* (temperature controller TC101 output) and *C* (split range controller SRC102 output). However, these factors are set at their lowest levels under optimal conditions causing profit values to initially drop. After occurrence of trough, sharp rise in RGP profit margins is caused by increasing level of factor *D* (RC101 controller ratio) from level 1 to 3. Raising RC101 controller ratio from 0.003 to 0.15 increases feed gas flow to GSP section from about 1.1 to 34.2 ton/h. This action improves recovery of valuable natural gas liquids and thus RGP profit.

In Cases 1-3 (Group I), profit trends produce the deepest trough and settle at the lowest margins due to low value of feed gas flow at 250 ton/h. Mild oscillations in Group I results are caused by changes in factors *D*, *E*, *F*, *G* from level 1 to 3 and variations in factor *I* (feed gas prices) at all three levels. Profit trends in Cases 4-6 (Group II) settle above Group I steady-state values. Higher settling trends of Group II profit are caused by increase in feed gas flow from 250 to 280 ton/h. Raising feed gas flow by additional 30 ton/h also causes similar trough occurrences as in Group I due to insufficient cooling. On the other hand, profit trends in Cases 7-9 (Group III) generate the shallowest trough among the three groups. Major fluctuation of profit trends is seen after 30 min of simulation time. This phenomenon is attributed to equivalent delay in switching time of level of factor *D* (RC101 controller ratio) from levels 1 to 3. The delay is required to prevent instability of RGP dynamic model when changes on other factors are imposed simultaneously. Trends of Group III settle at the highest levels as compared with trends of the other two groups. Results from this

observation indicate that factor H (plant load) at level 3 yields the highest profit margins. Slight differences of steady-state values are caused by variations in levels of factor I . The highest profit margin obtained in Case 8 reveals that I_2 (feed gas stream B with moderate carbon dioxide content) configuration is optimum although price of feed gas stream B is in between those of feed gas streams A and C.

4.3.4 Summary of Parametric Design

Significance of 7 controllable and 2 noise factors affecting RGP profit is studied by conducting 243 experiments in a cross-orthogonal-array set up. Three controllable factors handling RGP energy consumption top the ranked list. A combined effect of factors A (split range controller SRC103 output) and B (temperature controller TC101 output) controls the entire plant temperature. Higher values of these factors cool the plant and thus enhancing recovery of natural gas liquids. In a balancing move, energy intake through factor G (temperature controller TC102 output) is vital in ensuring smooth separation of feed gas in demethanizer C-101.

RGP profit can also be improved by setting higher level of factor E (flow controller FC104 output). This action increases amount of hydrocarbon injection to sales gas product, and thus boosting sales gas gross heating value and flow. Contributions from factors C (split range controller SRC102 output), D (RC101 controller ratio) and F (pressure controller PC101 setpoint) are found to be slightly significant in optimizing RGP profit. These controllable factors play more important roles in minimizing the effects of noise factors as shown in ANOM and ANOVA results of SNR values. Among the two noise factors, factor H (plant load) is more significant than factor I (feed gas prices). Higher plant load increases amount of feed gas to be processed, which in turn produces more sales gas and natural gas liquids products.

Maximum RGP profit is derived from an optimal configuration of both controllable and noise factors. This unique configuration of low, medium or high levels of individual factors was selected based on a response plot of average profit values. The optimal configuration of factors is set in HYSYS for validation. For all Cases 1 to 9, results from HYSYS experiments are compared against those from

ANOM. Remarkable agreements found in all cases verify the optimality of factorial configuration.

It should be noted that optimization via Taguchi method is only valid over certain pre-set levels and ranges of controllable and noise factors. In reality, plant states move constantly due to time-varying nature of feed gas flow and compositions as well as existing dynamics inside the plant. Therefore, frequent updates of factorial values within and sometime outside the pre-set ranges may be necessary to locate global optimality. Restricting factorial levels at a fixed configuration all the time may not always work. For example, low levels of factor *A* (split range controller SRC103 output) and factor *B* (temperature controller TC101 output) at optimal configuration are inadequate for handling rich feed gases. In fact, compositions of feed gas streams A, B and C specified for Taguchi design of experiment studied here differ only in carbon dioxide but not in hydrocarbon contents. This is done to avoid systematic crash of dynamic RGP model used in the experiments. The crash can happen when compositions of a mixed feed gas stream flowing at 280 ton/h are suddenly changed from lean to rich and vice-versa as required by Taguchi method.

The current specification of feed gas compositions is applied without loss of generality because the main objective of Taguchi approach is to verify suitability of key factors for control and/or optimization purposes. All 7 controllable factors are found suitable at varying degrees of contribution to RGP profit. As a matter of decision, two factors namely factor *B* (temperature controller TC101 output) and factor *G* (temperature controller TC102 output) are selected as manipulated variables for MPC scheme. These two factors function as sink and source terms, respectively, in overall balance of plant energy. The remaining factors are employed in RTO studies of RGP in the next section.

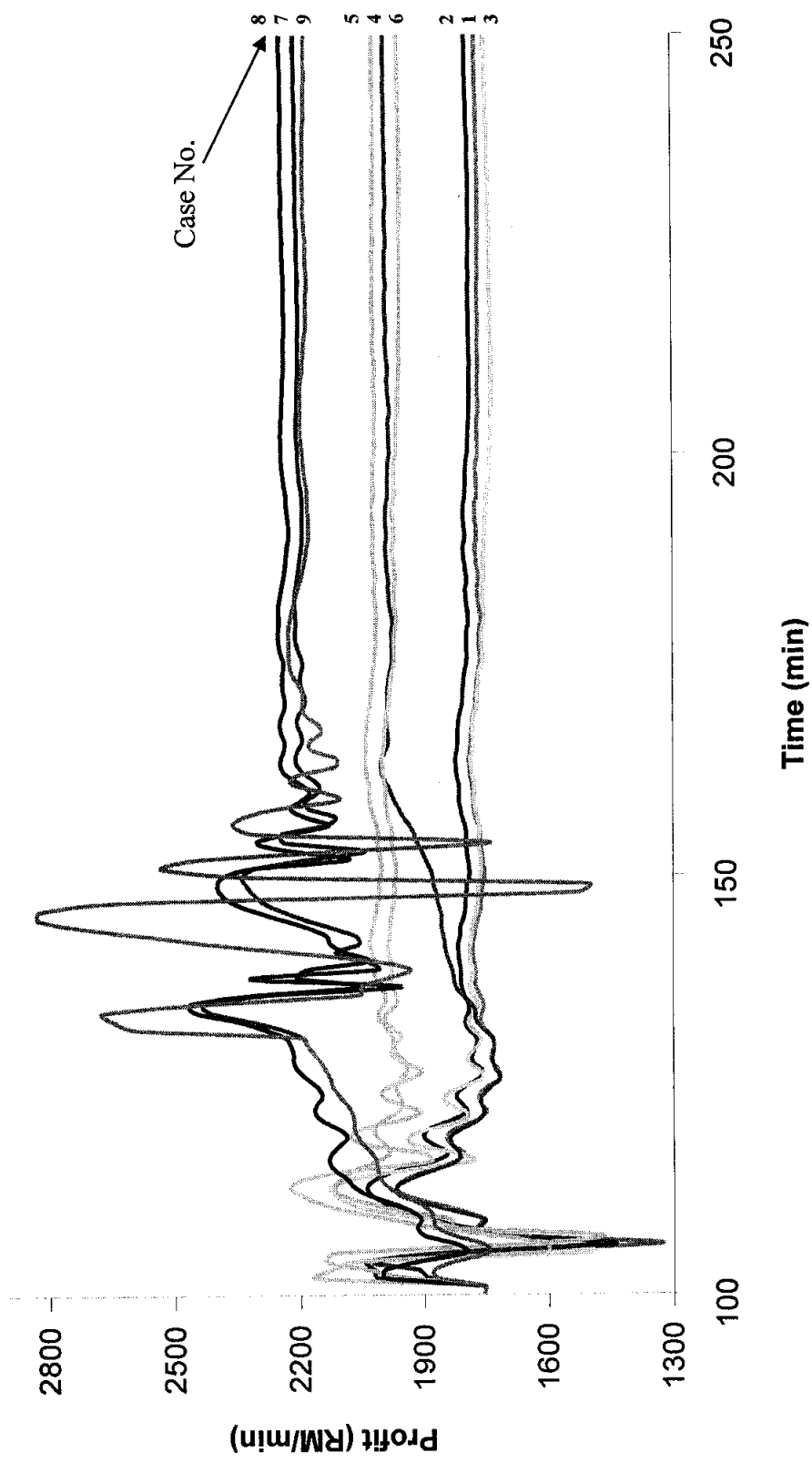


Figure 4.5: RGP profits under optimal configurations for Cases 1 to 9

4.4 RTO Case Study

Benefits of employing RTO in maximizing RGP profit are illustrated in a case study. The case study centers on balancing flow rates of three feed gas streams with different compositions and prices. Higher composition of natural gas liquids in a feed gas stream increases its richness and thus makes gas processing more difficult. This is because a richer stream requires more cooling and reboiling energy to achieve good separation of sales gas from natural gas liquids. However, energy is limited and plant is constrained to certain ranges of operating conditions. Acceptance to process richer off-gas streams can be interpreted as social contribution to reduce flaring at a crude oil terminal and a slug catcher. This situation is unique in the case of RGP because it lacks a product recovery unit comprising deethanizer, depropanizer and debutanizer. As a result, RGP is reluctant to process the richer streams despite the fact that they are cheaper than the lean feed gas stream. Such scenario of feed gas prices is only valid for this case study. In another scenario, a different type of gas processing plant may find better economic advantages to process the richer streams. The caveat is that the price structure is reverse where richer feed gas streams are more expensive than leaner streams. An RTO study on this kind of price structure requires a dynamic model of the product recovery unit and thus beyond the scope of the current work.

In this work, the RTO study is based on price structure as presented in Table 4.1. Ten variables are selected as optimization variables. Descriptions and bounds of these variables are shown in Table 4.15. Parallels of the optimization variables with factors of the previous parametric design study are:

1. Variable u_1 is flow rate of sales gas that goes into coldbox E-101. It is used to manipulate temperature of feed gas exiting the same coldbox. This variable is a surrogate to factor A , which is split range controller SRC103 output.
2. Variable u_2 is temperature of feed gas stream (factor B) exiting cooler E-102. Its initial value is required for solving cooler E-102 flowsheet and thus convergence of the entire steady-state model. This variable is the controlled variable of temperature controller TC101. Since it is selected as optimization

variable, the manipulated variable of TC101, which is cooler E-102 duty, is constrained between 0 and 4200 kW.

3. Variable u_3 is flow rate of sales gas that goes into coldbox E-103. It is used to manipulate temperature of feed gas exiting the same coldbox. This variable is surrogate to factor C , which is split range controller SRC102 output.
4. Variable u_4 is flow rate of processed gas to gas subcooled process section. This variable is numerator of RC101 controller ratio (factor D). Low value of u_4 contributes to less recovery of natural gas liquids.
5. Variable u_5 is flow rate of processed gas to turboexpander KT-101. High value of this variable means less or no flow of processed gas to Joule-Thompson bypass valve. Value of u_5 is proportional to flow rate of mixed feed gas stream at RGP inlet. This is because u_5 is the resulting output of split-range controller SRC101, which serves as a slave to flow controller FC101.
6. Variable u_6 is demethanizer tray 35 temperature (factor G), which is one of the specifications used for solving demethanizer C-101 flowsheet. This variable is the controlled variable of temperature controller TC102. Since variable u_6 is selected as optimization variable, the manipulated variable of TC102, which is reboiler E-104 duty, is constrained between 0 and 4500 kW.
7. Variable u_7 is temperature of processed gas exiting coldbox E-105. When solving steady-state optimization problem, value of u_7 must vary with RGP overall temperature to reflect upstream events.
8. Variables u_8 , u_9 and u_{10} are flow rates (factor H) of feed gas streams A, B and C. Prices of these streams are reflected by factor I . Thus effects of both factors H and I are reflected by behaviors of these three variables.

Table 4.15: Bounds and description of optimization variables

Var.	Factor	Unit	Bounds		Description
			Lower	Upper	
u_1	A	ton/h	0	300.0	Flow of sales gas to coldbox E-101
u_2	B	°C	-42.0	0.0	Temperature of feed gas exiting cooler E-102
u_3	C	ton/h	0	300.0	Flow of sales gas to coldbox E-103
u_4	D	ton/h	0	40.0	Flow of PG to GSP section
u_5	H	ton/h	0	300.0	Flow of PG to turboexpander KT-101
u_6	G	°C	0	20.0	Temperature of demethanizer C-101 tray 35
u_7	G	°C	-100.0	-50.0	Temperature of PG exiting coldbox E-105
u_8	$H \& I$	ton/h	100.0	310.0	Flow of feed gas stream A
u_9	$H \& I$	ton/h	0	150.0	Flow of feed gas stream B
u_{10}	$H \& I$	ton/h	0	100.0	Flow of feed gas stream C

Note: SG=sales gas; PG=processed gas; GSP=gas subcooled process

It should be noted that factors E and F are excluded in the current RTO study. The former factor, a surrogate to flow rate of feed gas stream D , is only used to boost gross heating value of sales gas. Its role is taken care of by feed gas streams B and C . On the other hand, the latter factor is dropped because: 1) an abrupt change in overhead pressure of demethanizer C-101 will cause instability for the entire plant operation, and 2) balancing flow rates of feed gas streams A , B and C is performed at natural gas liquids mode, which requires the overhead pressure of demethanizer C-101 to remain constant at 22 barg. Decision of which feed gas streams and their respective quantities to be processed is the focus of current RTO study.

4.4.1 RTO Results and Discussion

This section is divided into two parts. The first part deals with economic issues. In the latter part, operational matters are discussed.

4.4.1.1 Economics

Recall that the RTO objective function is profit margin of RGP. This is because profit is the bottom line of any plant business consideration. Higher profit can be obtained by increasing revenues, decreasing expenses or both at the same time. In this work, economic calculations are based on RGP operation in a fixed regime environment. Supply of feed gas streams and demand for products are agreed on long-term contract bases. Hence prices of feed gas, sales gas and natural gas liquids do not fluctuate as those in the daily spot market. Even the utility costs remain unchanged in the

cost overrun since feed gas and product values as well as operational expenses (OPEX) are precisely known *a priori*.

Table 4.16: Values (RM/min) of economic parameters for base and RTO case studies

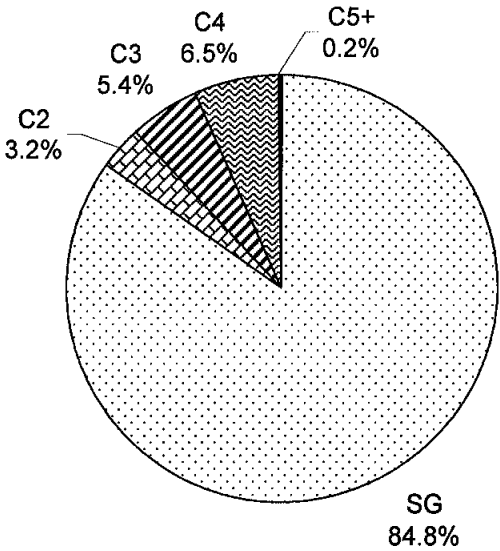
Parameter	Case Study	
	Base	RTO
Revenue	3320.50	3745.27
Cost of feed gas	1435.56	1550.94
OPEX	23.98	14.41
Profit	1860.95	2179.92

Table 4.16 shows results from the RTO study in comparison with the base case. Revenue is upped by 12.8% from 3320.50 to 3745.27 RM/min. Cost of feed gas increases by 8.0% from 1435.6 to 1550.9 RM/min. Conversely, OPEX decreases by 39.9% from 23.98 to 14.41 RM/min. In the end, RGP profit jumps to 2179.92 from 1860.95, or up by 17.1%, amid increments in both revenue and cost of feed gas.

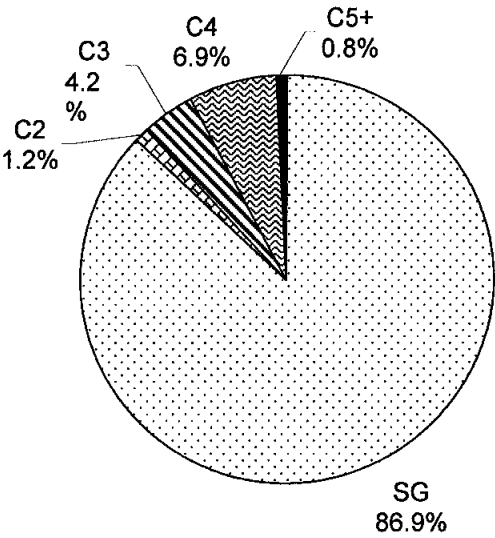
Breakdown of revenue is presented in Figure 4.6. For the base case, sales gas takes up 84.8% of total revenue, ethane 3.2%, propane 5.4%, butane 6.5% and condensates 0.2%. Large contribution from sales gas is attributed to the following facts: 1) sales gas is a major product whereas natural gas liquids are the by-products, 2) feed gas stream A is a lean gas containing 88.6 mole % methane and 11.4% natural gas liquids, and 3) price of sales gas is more than double that of feed gas. Similar result is shown in the RTO case whereby the contributions of revenue from sales gas is 86.9%, ethane 1.2%, propane 4.2%, butane 6.9% and condensates 0.8%. In a word, contributions from sales gas, butane and condensates increase by 2.1, 0.4 and 0.6%, respectively. However, contributions from ethane and propane reduce by 2.4 and 1.2%, respectively. These results reveal that the RTO strategy in maximizing RGP profit is to induce losses of ethane and propane in sales gas product stream whilst recovering more butane and condensates in natural gas liquids product stream.

RGP expenses are presented in Figure 4.7. For the base case, cost of feed gas stream A represents 98.4% of total expenses. Out of 1.6% contribution from OPEX, the combined cost of refrigeration cooler (E-102Q) and reboiler (E-104Q) makes up 1.0%. The remaining costs are derived from compressor fuel gas K-102Q (0.4%) and maintenance of turboexpander KT-101Q (0.2%). Costs of pumping actions P-101Q

and P102Q are too small to be illustrated in the pie chart and thus neglected here. For the RTO case, portion of feed gas stream A is reduced by 8.4% to give way to contributions from feed gas streams B (4.2%) and C (4.9%). This is necessary to recover more natural gas liquids. At the same time, OPEX decreases by 0.7% from the base case portion. Contribution of cooler duty E-102Q shrinks by 0.5% when OPEX components are further analyzed. On the other hand, negligible changes are detected from the other contributions of OPEX components.



(a) Base case



(b) RTO case

Figure 4.6: RGP revenue due to sales gas (SG), ethane (C2), propane (C3), butane (C4) and condensates (C5+)

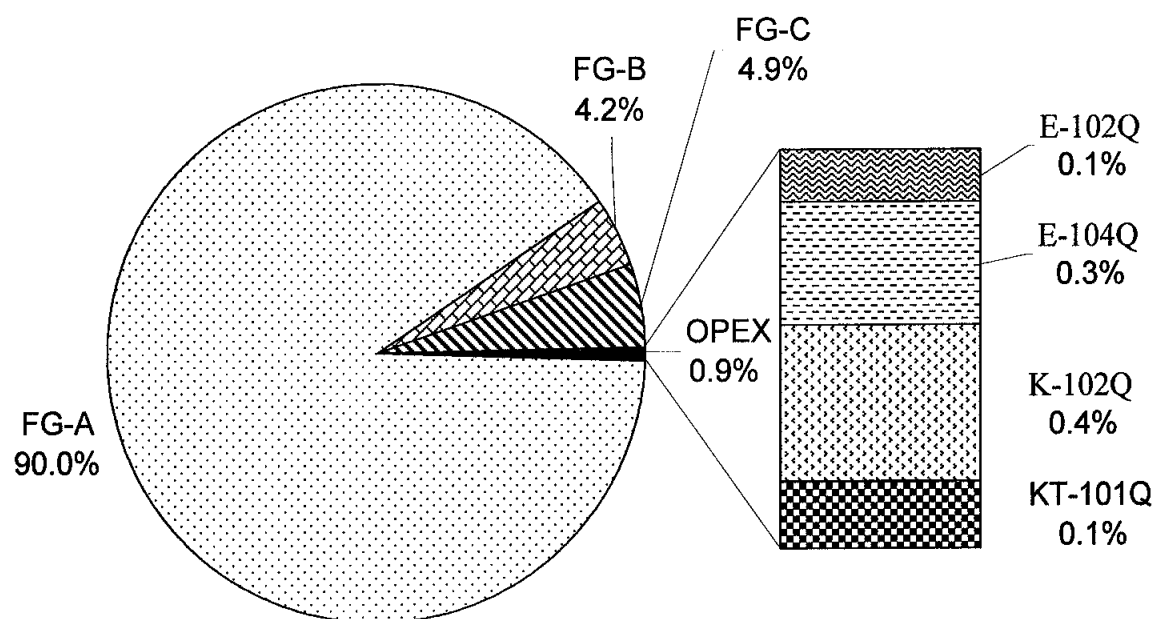
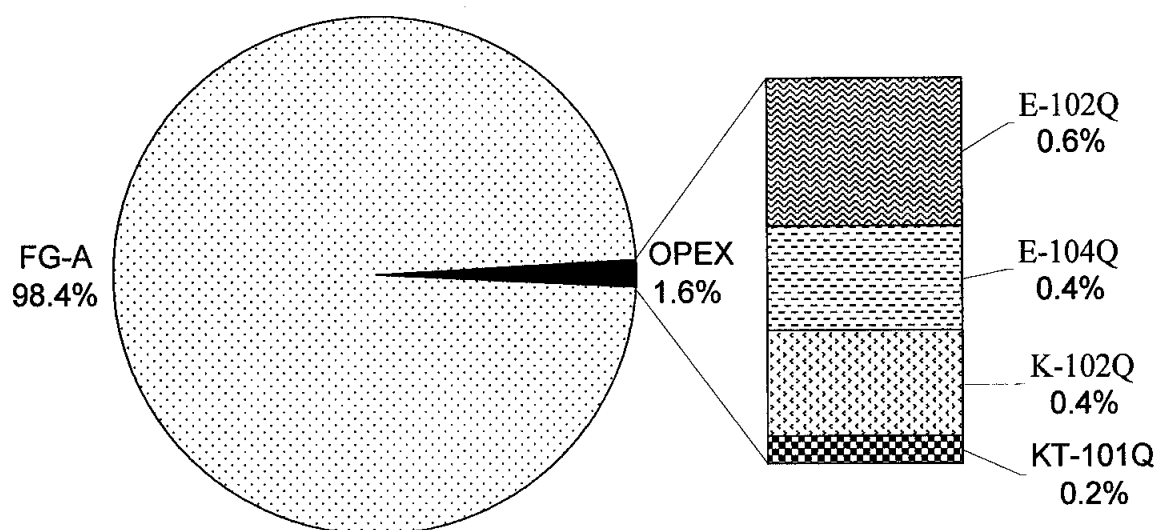


Figure 4.7: RGP expenses due to costs of feed gas (FG) streams A, B and C, and duties of cooler E-102Q, demethanizer reboiler E-104Q, compressor K-102Q and turboexpander KT-101Q

4.4.1.2 Process

While economics is the bottom line of RGP business, safety is an important aspect in its operation. For this reason, buffers are often created to ensure reliability and smooth operation of the plant. The buffers are beneficial and can be turned into opportunities for enhancing plant performance. These opportunities may entail some of the RGP assets to “sweat” as certain variables and constraints may be forced to move closer to their respective lower and/or upper bounds. Table 4.17 shows the moves of optimization variables in an attempt to shrink these buffers. These moves on RTO case study are obtained while satisfying plant limits on process, equipment and throughput capacity (Table 4.18).

Table 4.17: Values of optimization variables for base and RTO case studies

Var.	Unit	Case Study		Description
		Base	RTO	
u_1	ton/h	224.3	217.0	Flow of sales gas to coldbox E-101
u_2	°C	-40.0	-17.7	Temperature of feed gas exiting cooler E-102
u_3	ton/h	170.6	225.8	Flow of sales gas to coldbox E-103
u_4	ton/h	34.5	24.6	Flow of PG to GSP section
u_5	ton/h	194.1	228.6	Flow of PG to turboexpander KT-101
u_6	°C	5.0	10.9	Temperature of demethanizer C-101 tray 35
u_7	°C	-80.9	-58.5	Temperature of PG exiting coldbox E-105
u_8	ton/h	280.0	274.7	Flow of feed gas stream A
u_9	ton/h	0	15.0	Flow of feed gas stream B
u_{10}	ton/h	0	20.3	Flow of feed gas stream C

Note: PG=processed gas; GSP=gas subcooled process

Recall that the base case reflects RGP condition during natural gas liquids mode. At this mode, overall temperature of RGP is colder than that during sales gas mode. This condition favors recovery of natural gas liquids from feed gas stream A whose composition of hydrocarbon is lean. To optimize profit, RGP needs to overcome this deficiency by mixing feed gas stream A with richer feed gas streams B and C. Results from Tables 4.17 and 4.18 indicate that the balancing act is obtained by slightly decreasing flow rate of feed gas stream A whilst adding a right combination of feed gas streams B and C. These changes effectively increase total mixed feed gas intake to the maximum throughput of 310 ton/h.

Table 4.18: Values of constraint variables for base and RTO case studies

Variable	Unit	Case Study		Description
		Base	RTO	
c_1	ton/h	280.0	310.0	Flow of mixed feed gas
c_2	MJ/m ³	38.1	39.6	Gross heating value of sales gas
c_3	-	0.57	0.60	Specific gravity of sales gas
c_4	mol%	0.14	0.55	Carbon dioxide content in sales gas
c_5	ton/h	225.1	264.6	Flow of sales gas
c_6	bar	33.5	33.5	Pressure of sales gas
c_7	°C	35.6	34.2	Temperature of sales gas
c_8	kW/°C	1443	762	Coldbox E-101 capacity
c_9	°C	8.3	11.1	Coldbox E-101 LMTD
c_{10}	kW/°C	347	131	Coldbox E-103 capacity
c_{11}	°C	13.4	24.3	Coldbox E-103 LMTD
c_{12}	kW/°C	136	87	Coldbox E-105 capacity
c_{13}	°C	18.7	11.7	Coldbox E-105 log LMTD
c_{14}	kW	3291	689	Cooler E-102 duty
c_{15}	kW	4294	2951	Demethanizer C-101 reboiler duty
c_{16}	kW	2234	3291	Turboexpander KT-101 duty
c_{17}	kW	4661	3989	Compressor K-102 duty
c_{18}	kW	27.7	22.5	Pump P-101 duty
c_{19}	kW	8.9	5.4	Pump P-102 duty
c_{20}	%	60.0	27.8	Flooding at Section 1 of demethanizer
c_{21}	%	52.3	26.3	Flooding at Section 2 of demethanizer
c_{22}	%	46.6	26.7	Flooding at Section 3 of demethanizer
c_{23}	%	69.2	52.8	Flooding at Section 4 of demethanizer
c_{24}	%	30.9	25.1	DC backup at Section 1 of demethanizer
c_{25}	%	30.6	25.9	DC backup at Section 2 of demethanizer
c_{26}	%	33.8	27.6	DC backup at Section 3 of demethanizer
c_{27}	%	40.1	32.6	DC backup at Section 4 of demethanizer
c_{28}	%	67.9	74.2	Flooding in absorber C-102
c_{29}	%	17.6	17.5	DC backup in absorber C-102
c_{30}	°C	12.0	8.2	Air cooler LMTD
c_{31}	-	1.00	0.88	Fraction of PG to expander over that to JT valve
c_{32}	-	1.00	0.82	Fraction of sales gas to coldbox E-101
c_{33}	-	0.76	0.85	Fraction of sales gas to coldbox E-103
c_{34}	-	0.151	0.086	Ratio of PG to gas subcooled process section

Note: LMTD=log mean temperature difference; JT=Joule-Thompson;
DC=downcomer; PG=processed gas;

Due to presence of richer stream of mixed feed gas, overall RGP temperature is raised to prevent excessive condensation at separator S-101. Recall from summary of parametric design study (Section 4.3.4) that overall RGP temperature is mainly “controlled” at two locations: 1) feed gas stream exiting coldbox E-101, and 2) feed gas stream exiting cooler E-102. Increasing temperature of both streams will indirectly increase temperature of other streams in RGP. From Table 4.19,

temperature of feed gas stream exiting coldbox E-101 increases almost twice the former value from -30.3 to -15.5 °C. This is achieved partly by reducing flow of sales gas to the same coldbox by 3.3% from 224.3 to 217.0 ton/h (Table 4.17). As a result, flow of liquid exiting separator S-101 reduces drastically by 64.2% from 30.7 to 11.0 ton/h. Further down the stream, temperature of feed gas stream exiting cooler E-102 rises from -40.0 to -17.7 °C due to reduction in this cooler duty by 79.1% from 3291 to 689 kW. Consequently, temperature of processed gas exiting coldbox E-105 moves upward from -80.9 to -58.5 °C. This move substantially increases overhead temperature of absorber C-102, which is the main indicator of RGP state, from -94.4 to -62.8 °C.

Table 4.19: Values of selected plant model outputs for base and RTO case studies

Var.	Unit	Case Study		Description
		Base	RTO	
y ₁	°C	-30.3	-15.5	Temperature of feed gas exiting coldbox E-101
y ₂	ton/h	30.7	11.0	Flow of liquid exiting separator S-101
y ₃	°C	-53.9	-27.7	Temperature of PG exiting coldbox E-103
y ₄	ton/h	20.7	13.7	Flow of liquid exiting separator S-102
y ₅	°C	-94.4	-62.8	Overhead temperature of absorber C-102
y ₆	ton/h	54.9	45.4	Flow of natural gas liquids

Note: PG=processed gas

In the middle of RGP, temperature of processed gas stream exiting coldbox E-103 increases from -53.9 to -27.7 °C in parallel with upward temperature adjustments in other parts of RGP. The temperature increase would have been much higher if flow of sales gas to the same coldbox had not been increased by 32.4% from 170.6 to 225.8 ton/h. A higher temperature means a smaller portion of processed gas condenses at separator S-102. This premise holds truth since flow of liquid exiting the separator decreases from 20.7 to 13.7 ton/h. The liquefied processed gas is forwarded to demethanizer C-101 for recovery of natural gas liquids.

At demethanizer C-101, temperature of tray 35 is doubled from 5.0 to 10.9 °C despite a decrease in reboiler E-104 duty from 4294 to 2951 kW. All four sections of demethanizer C-101 show downward trends in flooding suggesting reduced internal traffics of vapor and liquid. The incident arises from lower feed rates to this distillation column and from drop in reboiler E-104 duty. Slight reduction in

downcomer backup is also observed at all four sections. However, this reduction still exceeds the minimum limit of 10%, which is required to maintain vapor-liquid equilibrium at high temperature. Warmer state of demethanizer C-101 promotes losses of lighter but not heavier components of natural gas liquids as shown by: 1) increase in flooding at absorber C-102 from 67.9 to 74.2%, and 2) reduction in flow of natural gas liquids from 54.9 to 45.4 ton/h. Analyzing breakdown of RGP revenue (Figure 4.6) verifies the fact that contributions from sales gas, butane and condensate increase at the expense of those from ethane and propane.

Warmer conditions in RGP result in less heat transfer from the hotter feed gas and/or processed gas streams to the colder sales gas streams in coldboxes. Here, heat exchange capacities or ' UA ' values of coldboxes E-101, E-103 and E-105 are reduced by 47.2, 62.2 and 36.0%, respectively. The ' UA ' values are calculated based on a general heat transfer relation (GPSA, 2004):

$$Q = UA * LMTD \quad (4.12)$$

where Q is duty or amount of heat that is transferred from hot to cold streams inside a coldbox and $LMTD$ denotes corrected log-mean-temperature-difference. Reduction of ' UA ' values in the above manner is due to: 1) decrease in duties of coldboxes E-101, E-103 and E-105 correspondingly by 29.4, 31.5 and 59.7% from base values of 11955, 4651 and 2540 kW, 2) increase in $LMTD$ of coldboxes E-101 and E-103 by 33.7 and 81.3%, respectively, and 3) decrease in $LMTD$ of coldbox E-105 by 37.4%. Had the latter share an upward $LMTD$ trend as shown in coldboxes E-101 and E-103, the ' UA ' value of coldbox E-105 would have dropped much lower.

At the major product stream, quantity of sales gas increases from 225.1 to 264.6 ton/h, way above its minimum specification of 205 ton/h. Quality of sales gas is never compromised despite increment in its flow rate. The reason that gross heating value and specific gravity of sales gas increase by 3.9 and 5.3%, respectively, is due to higher compositions of ethane and propane in sales gas product stream. Carbon dioxide content in sales gas product stream is quadrupled from 0.14 to 0.55 mol % as a result of processing feed gas streams B and C. This increase, however, is still below the upper limit of 2.00 mol %.

Pressure of sales gas remains unchanged because RGP is operating under natural gas liquids mode, in which overhead pressure of demethanizer C-101 stays constant at 22 barg. On the other hand, temperature of sales gas decreases by 1.4 °C as a result of reduction in booster compressor K-102 duty from 4661 to 3989 kW. The reduction in compressor K-102 duty is because of lower pressure difference between its suction and discharge sides. This happens after turboexpander KT-101 duty is *a priori* raised from 2234 to 3291 kW due to increase in processed gas flow rate by 17.8% from 194.1 to 228.6 ton/h. The additional expansion work at turboexpander KT-101 further drives up its mechanically link compressor K-101 duty, which in turn discharges sales gas at a higher pressure.

4.5 Concluding Remarks

This chapter discusses a procedure on maximization of RGP profit through real-time optimization (RTO). Profit of RGP is obtained from the difference between revenues and expenses. Revenues are calculated based on values of sales gas and natural gas liquids. The former is a major product whereas the latter is further processed to recover individual components of the natural gas liquids. Expenses are due to costs of feed gas and operation.

As a case study, three feed gas streams A, B and C are considered to be processed. These streams represent lean, rich and very rich gas with varying levels of carbon dioxide. Balancing flow rates of these streams is necessary given plant limits on process, equipment and throughput capacity. A high-fidelity steady-state model of RGP developed in Chapter 3 is employed in order to minimize uncertainties due to complexity of the process (Yip and Marlin, 2004). A solution to the RTO problem is obtained by manipulating ten optimization variables, including three feed gas stream flow rates, while satisfying thirty-four constraints.

Values of these optimization variables (Table 4.17) and/or the corresponding model outputs (Table 4.19) may be passed to control layer for implementation. Either regulatory controllers or model predictive control (MPC) scheme can be employed to move plant states to the new targets. The MPC scheme is preferred due to its ability in

predicting future outputs and moving inputs optimally, thus reduces operating cost. The implementation of setpoints entails rigorous data transfer from steady-state RTO layer to dynamic scheduling layer, which is subject of the next chapter.

CHAPTER 5

INTEGRATED APPROACH FOR SCHEDULING AND RTO

5.1 Introduction

A refrigerated gas plant (RGP) faces challenges on three fronts namely: 1) at plant inlet, multiple streams of feed gas from various producers are mixed causing fluctuation in feed gas flow rate and composition; 2) within RGP, unscheduled shutdowns due to regular equipment malfunction; 3) at RGP outlet, strict specifications of several products are regularly enforced by its customers where penalty will be imposed if these specifications are violated (Bullin, 1999). In business aspect, RGP enters into diverse agreements with gas producers. As a result, prices of feed gas vary depending, among others, on quality of gas and tenure of the contracts. In contrast, price of sales gas is tightly regulated by government. Prices of liquids namely ethane, propane, butane and condensates are floated to market values.

These challenges force RGP to improve its operational efficiency in order to maintain profitability. An identified area of improvement is during change of plant operating mode. The change of plant mode poses a short-term (weeks) and continuous scheduling problem in which pre-configured set points are directly implemented by regulatory controllers. While this practice has been accepted in the past, efforts are currently undertaken to improve it. This type of problem differs from batch scheduling, which receives considerable attention in operations research. Excellent reviews of batch scheduling have been published by Floudas and Lin (2004) and by Mendez et al. (2006).

In contrast, continuous scheduling is often integrated with control to give rise to mixed integer dynamic optimization (MIDO) problem. An example can be found in Chatzidoukas et al. (2003) who formulate a MIDO problem on gas-phase copolymerization in fluidized bed reactor. The authors simultaneously optimize grade transition time of a copolymer and schemes of feedforward-feedback control. In another related work on polymerization, Kadam et al. (2007) integrate real-time optimization (RTO) with model predictive control (MPC) within a dynamic

framework of grade transition problem. A method of tracking the necessary conditions of optimality with a solution model is employed to preserve a feasible and optimal operation under uncertainty. The addition of RTO layer between scheduling and control layers is necessary in order to improve plant economics, production or other suitable objectives. Since scheduling is normally performed at a much larger time-scale (days to weeks) as compared to RTO (hours to days) and MPC (seconds to minutes), integration of the three automation layers to enhance economic benefits is difficult.

The current work proposes a potential means to address this issue through an integrated approach of scheduling and RTO. This way, setpoints are re-calculated based on current plant conditions. Optimal setpoints may be implemented using regulatory or advanced controllers such as MPC scheme. RGP is employed as a test bed. Steady-state and dynamic models of RGP are simulated under HYSYS environment as presented in Chapter 3. MPC actions are calculated using MATLAB. Communication between HYSYS and MATLAB is executed via component object module (COM) technology (Beronich et al., 2005).

5.2 Integration of Scheduling and RTO

In a typical scheduling scenario, new plant set points are pre-determined from early design specifications or heuristics. The set points are manually adjusted by experienced personnel to the desired levels. This practice has several drawbacks: 1) current state of the plant may change due to sustained large disturbance or major revamp activities and thus invalidate design set points, and 2) manual adjustment of set points may lead to excessive energy utilization especially if target trajectory is not optimal. One way to overcome these drawbacks is to integrate scheduling tasks with real-time optimization (RTO) before passing set points to control layer. The proposed approach is illustrated in Figure 5.1.

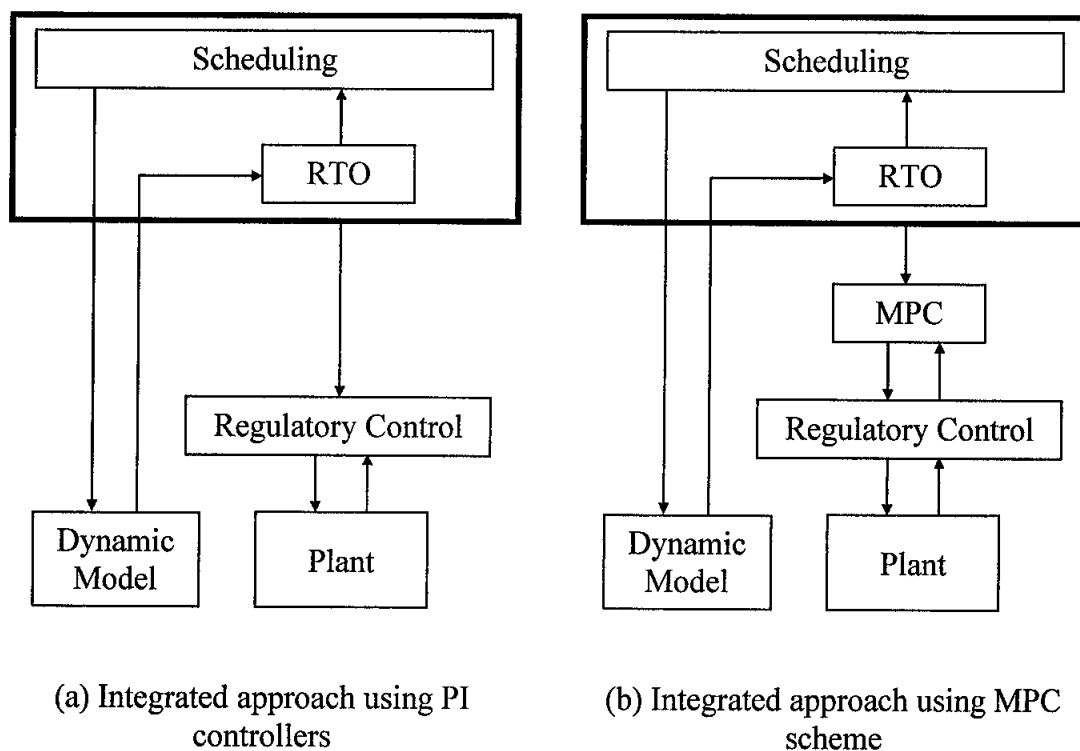


Figure 5.1: Structure of integrated scheduling and real-time optimization (RTO) approach. Set points may be implemented via model predictive control (MPC) scheme or, alternatively, regulatory controllers.

The new methodology leverages on availability of first-principle models in both steady-state and dynamic modes. This is necessary to maintain accuracy when data are transferred between the two models. In particular, scheduling is carried out using a dynamic model until a new steady-state is reached. Data from the dynamic model are passed to the steady-state model for target optimization task. For practical reasons, only several values of key variables are exchanged to minimize mismatch between dynamic and steady-state models.

Number of variables sent from dynamic to steady-state model is 49, which includes stream flow rates, temperatures and pressures. In contrast, only six to eight variables are forwarded from steady-state to dynamic model as setpoints. This is to ensure that: 1) rigorous steady-state model is used for solving optimization problems at RTO layer, and 2) feasible setpoints are passed to controllers for implementation of optimal setpoints at the plant. For the second purpose, another dynamic model is used

to represent an actual plant. The only difference between the dynamic model and the plant is that the latter is at the state prior to scheduling.

Nonlinear dynamic model of a plant can be described implicitly by the following set of differential-algebraic equations:

$$\left(\frac{d\mathbf{x}}{dt}\right) = f_m(\mathbf{x}, \mathbf{y}, \mathbf{z}, \mathbf{p}, t), \quad t \in [t_0, t_f] \quad (5.1a)$$

$$0 = g_m(\mathbf{x}, \mathbf{y}, \mathbf{z}, \mathbf{p}, t), \quad t \in [t_0, t_f] \quad (5.1b)$$

$$\mathbf{x}(t_0) = \mathbf{x}_0 \quad (5.1c)$$

where \mathbf{x} and \mathbf{z} are differential and algebraic state variables, respectively. Process output is denoted by \mathbf{y} whereas model and design parameters by \mathbf{p} . Equation 5.1 is solved simultaneously over fixed time horizon for given \mathbf{y} , \mathbf{p} and initial conditions \mathbf{x}_0 . This dynamic model is used for scheduling and control implementation. On the other hand, RTO is performed based on steady-state model that can be represented by Equations 5.1a and 5.1b without the transient term.

During simulation of a scheduling problem, designed and optimal set points are only introduced to the plant after 30 min to show that the plant is previously at steady-state level. At the end of experiments, new steady-states are reached. Economic benefits are calculated online using a built-in spreadsheet to prevent round-off error. For fair comparison of different control procedures, instantaneous values of economic parameters are averaged out over the entire simulation time as (Ferrer-Nadal et al., 2007):

$$\bar{F}_E(t) = \frac{1}{t_f - t_0} \int_{t_0}^{t_f} F_E(t) dt \quad (5.2)$$

where F_E and \bar{F}_E , respectively, denote values of instantaneous and average economic parameters namely profit, revenues and expenses over time horizon $[t_0, t_f]$. Profit is taken as a function of revenues and expenses (Equation 4.2). Revenues are derived from the values of sales gas and natural gas liquids. Expenses are due to costs of feed

gas and operation. The operational costs include those emanate from refrigeration and reboiler duties, compressor fuel gas, turboexpander maintenance and pumping actions.

Efficacy of the proposed approach is illustrated in several types of scheduling problems namely: 1) mode, 2) load, and 3) input. Input scheduling refers to mixing of certain fractions of lean and rich feed gas streams at normal plant load of 280 ton/h. Load scheduling refers to variations of flow rate of lean feed gas stream by ± 30 ton/h. Mode scheduling refers to change of plant operating mode from sales gas to natural gas liquids, and vice-versa.

5.3 Mode Scheduling

Four studies are performed in the case of scheduling of RGP operation mode from natural gas liquids to sales gas as given below (Case A):

1. Mode scheduling with PI controllers (base case)
2. Mode scheduling with MPC controllers
3. Integration of mode scheduling and RTO with PI controllers
4. Integration of mode scheduling and RTO with MPC controllers

The above studies are repeated for mode scheduling of sales gas to natural gas liquids (Case B). In total, eight case studies are conducted. Each case is simulated for 510 min. For clarity, process description of each mode scheduling is presented in subsequent sections.

5.3.1 Scheduling from Natural Gas Liquids to Sales Gas Mode (Case A)

5.3.1.1 Process

In case of scheduling from natural gas liquids to sales gas mode, RGP temperature as indicated by top of absorber increases by more than 20 °C from a nominal value of -94.4 °C (Table 4.19). A higher plant temperature is achieved by diverting flow of sales gas streams away from both coldboxes E-101 and E-103, and thus reducing heat transfer from the hotter feed gas stream. Cooler E-102 duty is also decreased allowing

temperature of feed gas stream to rise to -30.6°C (Table 5.1). In addition, pressure at top of demethanizer C-101 is increased to 24 barg. Since turboexpander KT-101 discharges at about the same pressure, more processed gas stream bypasses it to undergo an expansion process at Joule-Thompson valve. This is carried out to prevent overload of booster compressor (K-101) and sales gas compressor (K-102) while meeting pressure specification at sales gas product stream. Recovery of natural gas liquids at gas subcooled process (GSP) section is lowered due to reduction of processed gas flow. As a result, more ethane and propane are lost in sales gas product stream causing value of sales gas to increase.

Table 5.1: Values of target variables for base and RTO cases in sales gas mode

Var.	Unit	Case Study		Description
		Base	RTO	
y_1	$^{\circ}\text{C}$	-22.0	-25.1	Temperature of feed gas exiting coldbox E-101
y_2	$^{\circ}\text{C}$	-30.6	-30.2	Temperature of feed gas exiting cooler E-102
y_3	$^{\circ}\text{C}$	-42.6	-38.9	Temperature of PG exiting coldbox E-103
y_4	$^{\circ}\text{C}$	5.0	15.2	Temperature of demethanizer C-101 tray 35
y_5	barg	24	24	Pressure of demethanizer C-101 overhead
y_6	ton/h	1.2	9.0	Flow of PG to GSP section

Note: PG=processed gas; GSP=gas subcooled process

Figure 5.2 illustrates closed-loop responses of two important target variables namely: 1) temperature of feed gas stream exiting cooler E-102 (output y_2) and, 2) temperature of demethanizer C-101 tray 35 (output y_4). Trajectories of these variables depend mainly on the types of controllers employed. Preliminary visual inspection indicates that both PI controllers and MPC scheme manage to track the setpoints. This task is performed by manipulating duty of cooler E-102 (input u_2) and duty of reboiler E-104 (input u_4). Here, MPC moves are well-coordinated as shown by quicker and deeper downward adjustments of inputs u_2 and u_4 before they stabilized at new levels. In actual fact, optimal MPC moves reduce offset duration in output y_4 in approximately 80 min.

For the integrated approach, scheduling setpoints (Table 5.1) are optimized *a priori* at the current plant state before implemented by the controllers. Values of optimization and constraint variables are shown in Tables B.1 and B.2, respectively. Significance of variable moves is analogous to those presented in Chapter 4 and thus

will not be elaborated. In essence, pre-cooling of feed gas has been shifted more heavily on coldbox E-101 with its exit stream temperature decreases by 3.1 °C. Load on cooler E-102 reduces a little due to higher setpoint at its exit stream temperature by 0.4 °C. Similarly, feed gas vapor entering coldbox E-103 is subjected to less cooling. The vapor is now exiting the coldbox by 3.7 °C hotter. This phenomenon causes temperature of demethanizer C-101 tray 35 to rise considerably to 15.2 °C from its previous condition at 5 °C.

Tracking outputs y_2 and y_4 to their respective optimal setpoints is a challenging task for PI controllers namely: 1) temperature controller TC101 that regulates output y_2 by manipulating input u_2 , and 2) temperature controller TC102 that regulates output y_4 by manipulating input u_4 . From closed-loop trajectories shown in Figure 5.3, output y_4 regulated by TC102 settles at a much longer time when compared with that controlled by MPC scheme. This poor performance is caused by the nature of PI controllers, in which inputs are moved independently to satisfy target criteria of various outputs.

For example, large input u_4 moves at the early stage result in sudden increase in output y_4 . When the output trajectory exceed y_4 target, integral action of temperature controller TC102 kicks in to eliminate the offset. At the same time, input u_2 is adjusted in sharp downward direction to raise output y_2 temperature from -40.0 to -30.2 °C. This action consequently moves downstream temperatures upward making it harder to control output y_4 . On the other hand, MPC scheme manages to bring outputs y_2 and y_4 to the respective targets faster due to its excellent predictive capability.

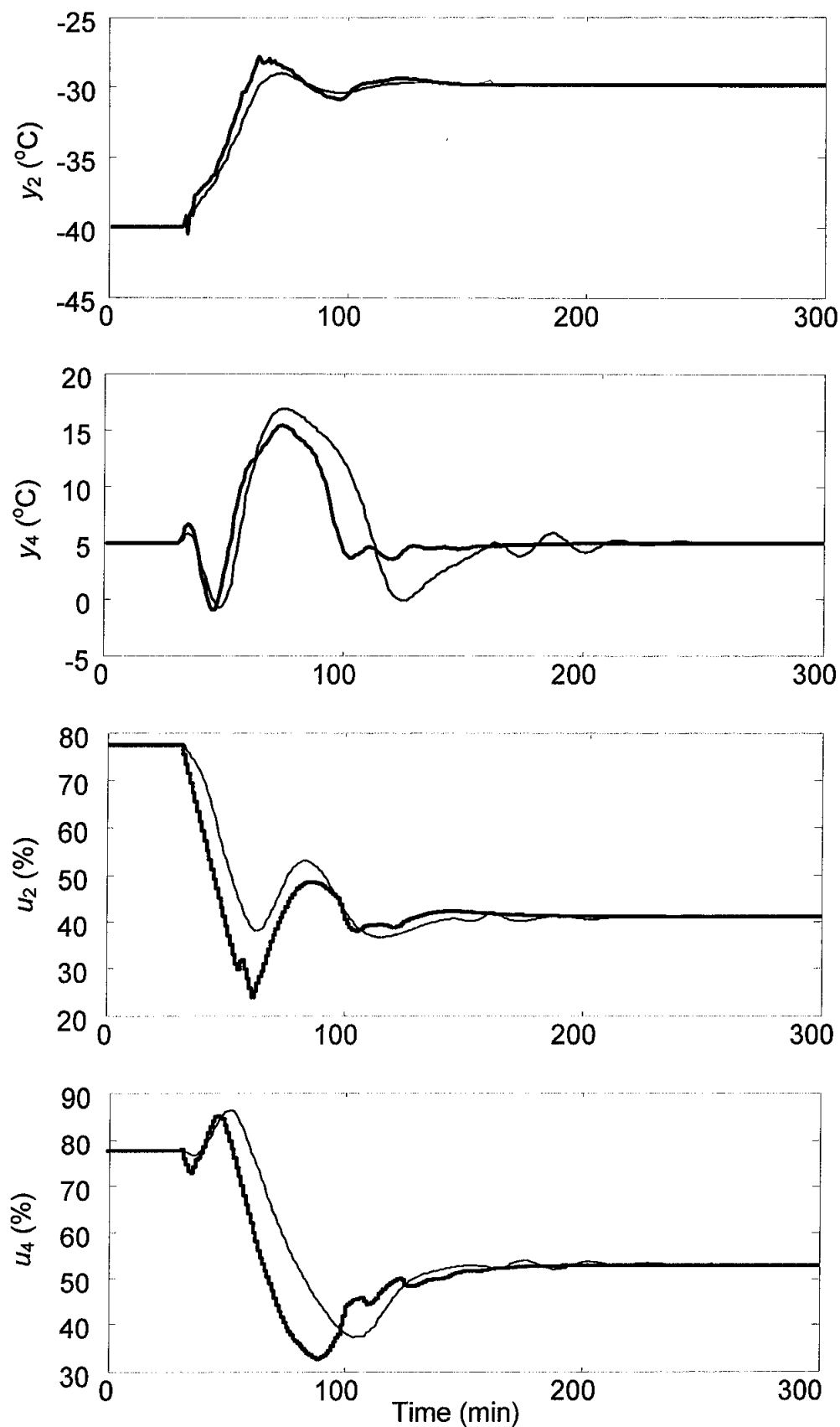


Figure 5.2: Closed-loop responses of PI (thin line) and MPC (thick line) controllers on temperature of feed gas stream exiting cooler E-102 (y_2) and temperature of demethanizer C-101 tray 35 (y_4) for Cases A1 and A2 (scheduling only); u_2 =cooler E-102 duty in %; u_4 =reboiler E-104 duty in %

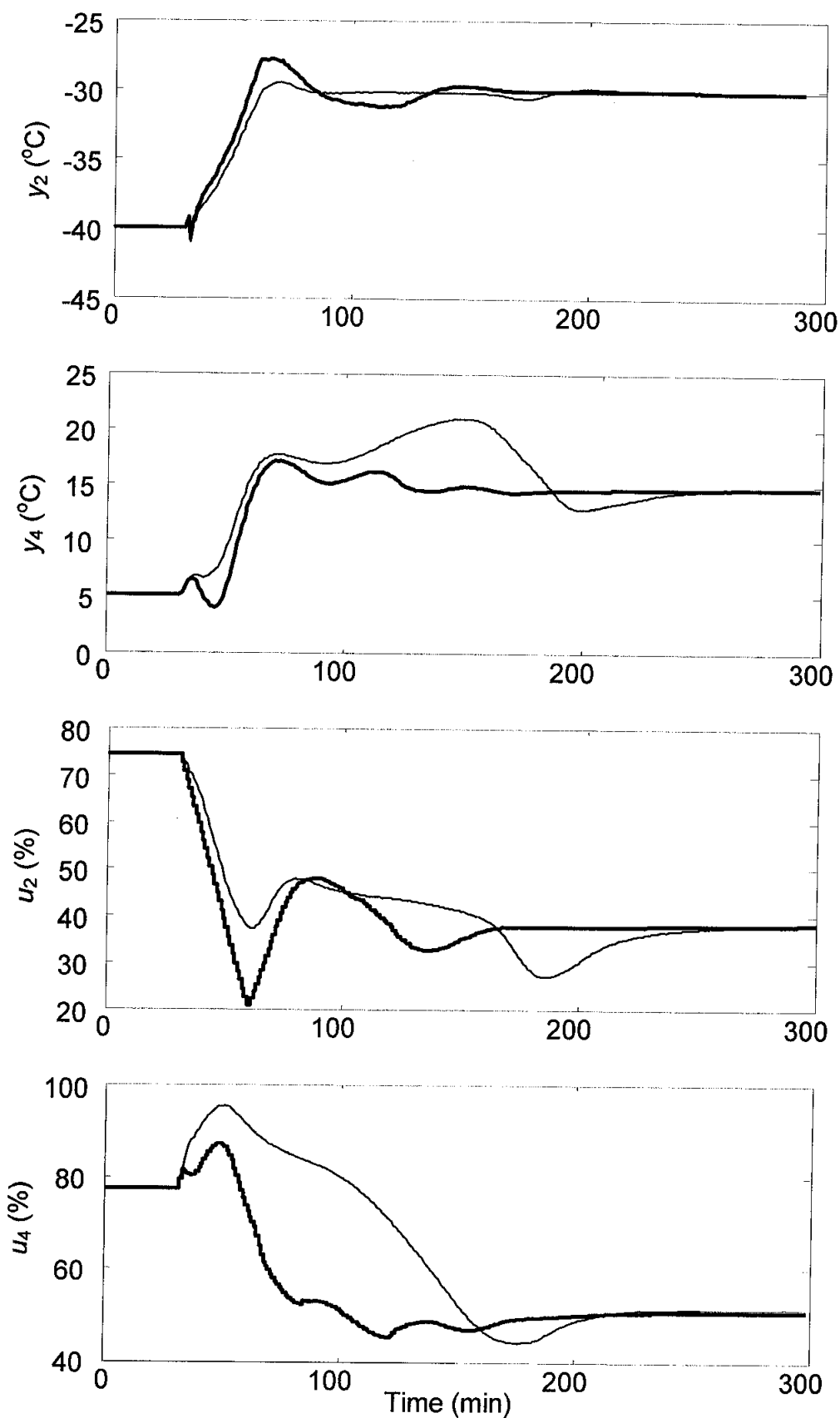


Figure 5.3: Closed-loop responses of PI (thin line) and MPC (thick line) controllers on temperature of feed gas stream exiting cooler E-102 (y_2) and temperature of demethanizer C-101 tray 35 (y_4) for Cases A3 and A4 (integrated approach); u_2 =cooler E-102 duty in %; u_4 =reboiler E-104 duty in %

5.3.1.2 Economics

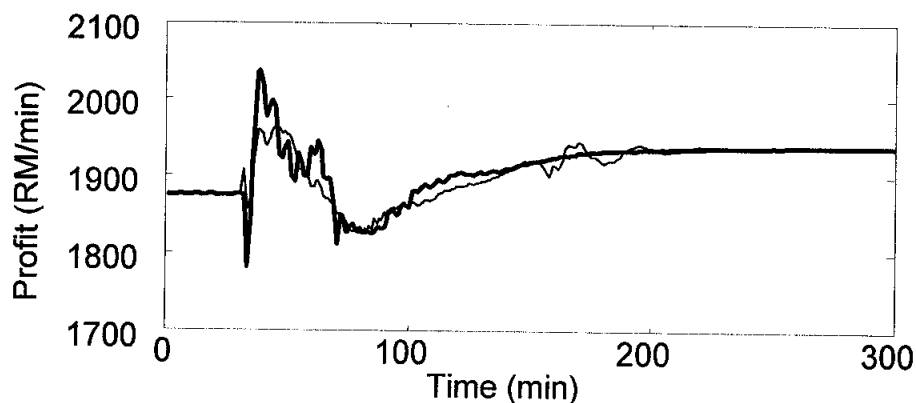
Four studies are performed in the case of mode scheduling from natural gas liquids to sales gas mode. Case A1 is the base case where scheduling setpoints are implemented by PI controllers. If the same setpoints are executed by MPC scheme as in Case A2, RGP profit increases by 0.1% (Table 5.2). This is achieved due to increase in revenue from sales gas by the same quantum but decrease in revenue from liquids by 0.5%. At the same time, operational expenses decrease by 1.3% due to efficiency of MPC controller in bringing plant to a new state optimally. Dynamic trajectories of RGP profit are illustrated in Figure 5.4. For both Cases A1 and A2, large peaks in profit trajectories correspond to the period of increase in flowrate of sales gas product stream due to losses of ethane and propane. The cause of these losses is a brief period of temperature rises at demethanizer C-101 tray 35 temperature (output y_4) way above the setpoint value of 5 °C. When output y_4 returns to its setpoint, trough in profit trajectories is noticed due to concurrent drop in revenue from natural gas liquids. When this effect stabilizes, RGP profit slowly rises towards a new steady-state level higher than the previous value.

Table 5.2: Average values (RM/min) of economic parameters over 510 min simulation time

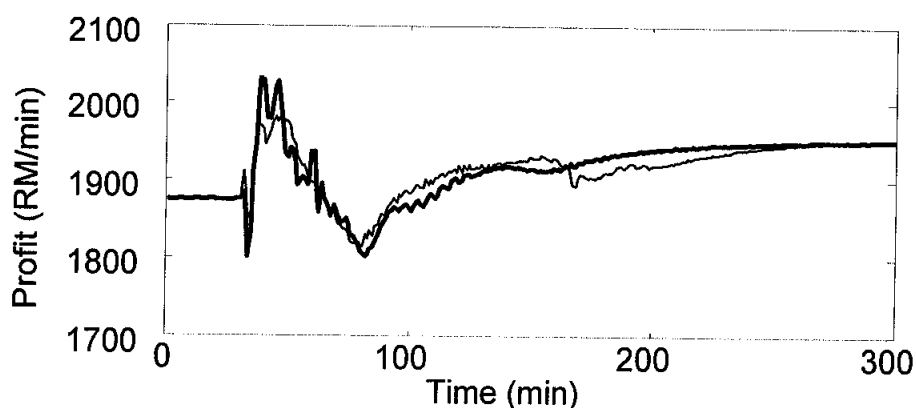
Case	Profit	Revenues		Expenses	
		Sales Gas	Liquids	Feed Gas	Operation
A1	1921.75	2954.99	417.24	1435.55	14.93
A2	1923.35	2958.38	415.27	1435.57	14.73
A3	1929.70	2982.02	398.03	1435.61	14.74
A4	1930.58	2982.76	397.60	1435.50	14.28

Additional benefits can be achieved if scheduling setpoints are optimized at RTO layer before they are implemented by controllers. For Cases A3 and A4, RGP profit increases by 0.4 and 0.5%, respectively (Table 5.2). Revenue from sales gas increases by 0.9% in both cases. However, sharp declines in revenue from liquids are noticed at 4.6 and 4.7% for Cases A3 and A4, respectively. In terms of operating expenses, PI controllers manage to obtain reduction by 1.3% whereas MPC scheme by 4.4%. Trajectories of RGP profit are similar to those in the first two cases (Figure 5.4). A noticeable difference is when profit trajectory of Case A3 lies above that of Case A4 for about 100 min. The reason is again due to losses of ethane and propane in the sales

gas product stream. This occurs when temperature controller TC102 performs poorly in controlling temperature of demethanizer C-101 tray 35 (Figure 5.3).



(a) Scheduling only – Case A1 (thin line) and Case A2 (thick line)



(b) Integrated approach – Case A3 (thin line) and Case A4 (thick line)

Figure 5.4: Dynamic trajectories of RGP profit for Case A

5.3.2 Scheduling from Sales Gas to Natural Gas Liquids Mode (Case B)

5.3.2.1 Process

In case of scheduling from sales gas to natural gas liquids mode, RGP temperature indicator drops to -94.4°C from around -74.3°C . Cooling is achieved partly by lowering temperature of streams exiting all three coldboxes E-101, E-103 and E-105, and cooler E-102 as specified in Table 5.3. Feed gas flow to gas subcooled process section also increases significantly from 1.2 to 34.5 ton/h. In addition, top of demethanizer pressure decreases from 24 to 22 barg. This procedure induces higher recovery of natural gas liquids.

Table 5.3: Values of target variables for base and RTO cases in natural gas liquids mode

Var.	Unit	Case Study		Description
		Base	RTO	
y_1	°C	-30.5	-30.4	Temperature of feed gas exiting coldbox E-101
y_2	°C	-40.0	-39.1	Temperature of feed gas exiting cooler E-102
y_3	°C	-53.9	-52.2	Temperature of PG exiting coldbox E-103
y_4	°C	5.0	0.4	Temperature of demethanizer C-101 tray 35
y_5	barg	22	22	Pressure of demethanizer C-101 overhead
y_6	ton/h	34.5	18.8	Flow of PG to GSP section

Note: PG=processed gas; GSP=gas subcooled process

Figure 5.5 shows closed-loop responses of outputs y_2 and y_4 . Temperature controller TC101 reveals underdamped behavior when it manages to track output y_2 down to -40.0 °C from -30.6 °C. Temperature controller TC102 also manages to maintain setpoint of output y_4 at 5 °C. However, movement of this controller input reaches saturation for about 40 min. This happens despite the fact that temperature controller TC102 employs positional algorithm with auto-reset windup. When output y_4 returns to its setpoint, input u_4 slowly reduces to settle at a new steady-state value. On the other hand, MPC coordinated moves manage to reduce saturation period to only a couple of minutes.

For the RTO case, optimal setpoints are obtained for maximizing value of natural gas liquids while maintaining operational stability at new conditions. Setpoints of streams exiting cooler E-102 and coldbox E-103 are increased by 0.9 and 1.7 °C, respectively. At the same time, setpoint of demethanizer tray 35 temperature is reduced to 0.4 °C from the previous state of 5 °C. This action reduces both cooling and reboiling loads, and thus operational expenses. Flow of processed gas to gas subcooled process section decreases by almost one-half. This is done to reduce heat exchange between processed gas and sales gas at coldbox E-105.

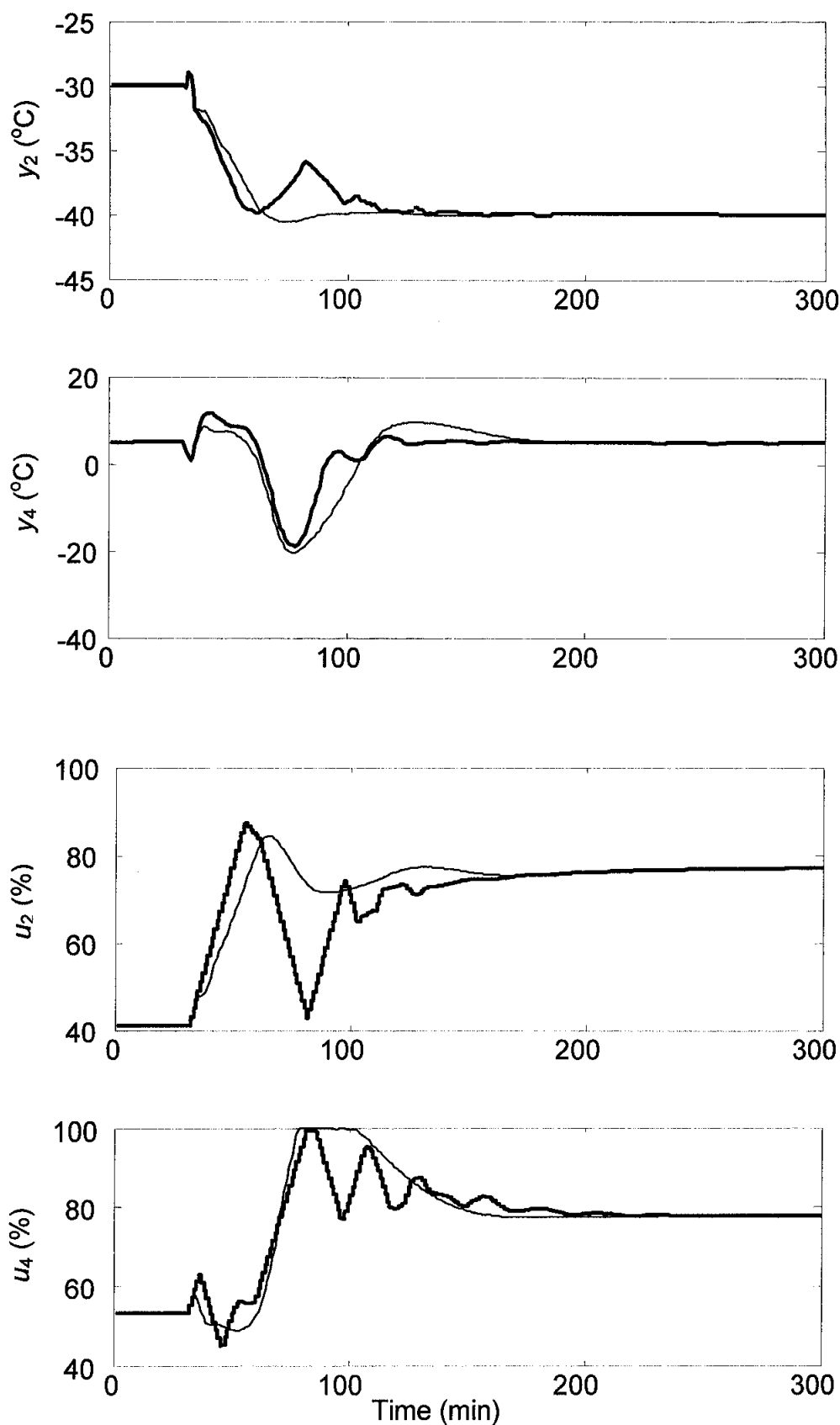


Figure 5.5: Closed-loop responses of PI (thin line) and MPC (thick line) controllers on temperature of feed gas stream exiting cooler E-102 (y_2) and temperature of demethanizer C-101 tray 35 (y_4) for Cases B1 and B2 (scheduling only); E-102Q=cooler E-102 duty in %; E-104Q=reboiler E-104 duty in %

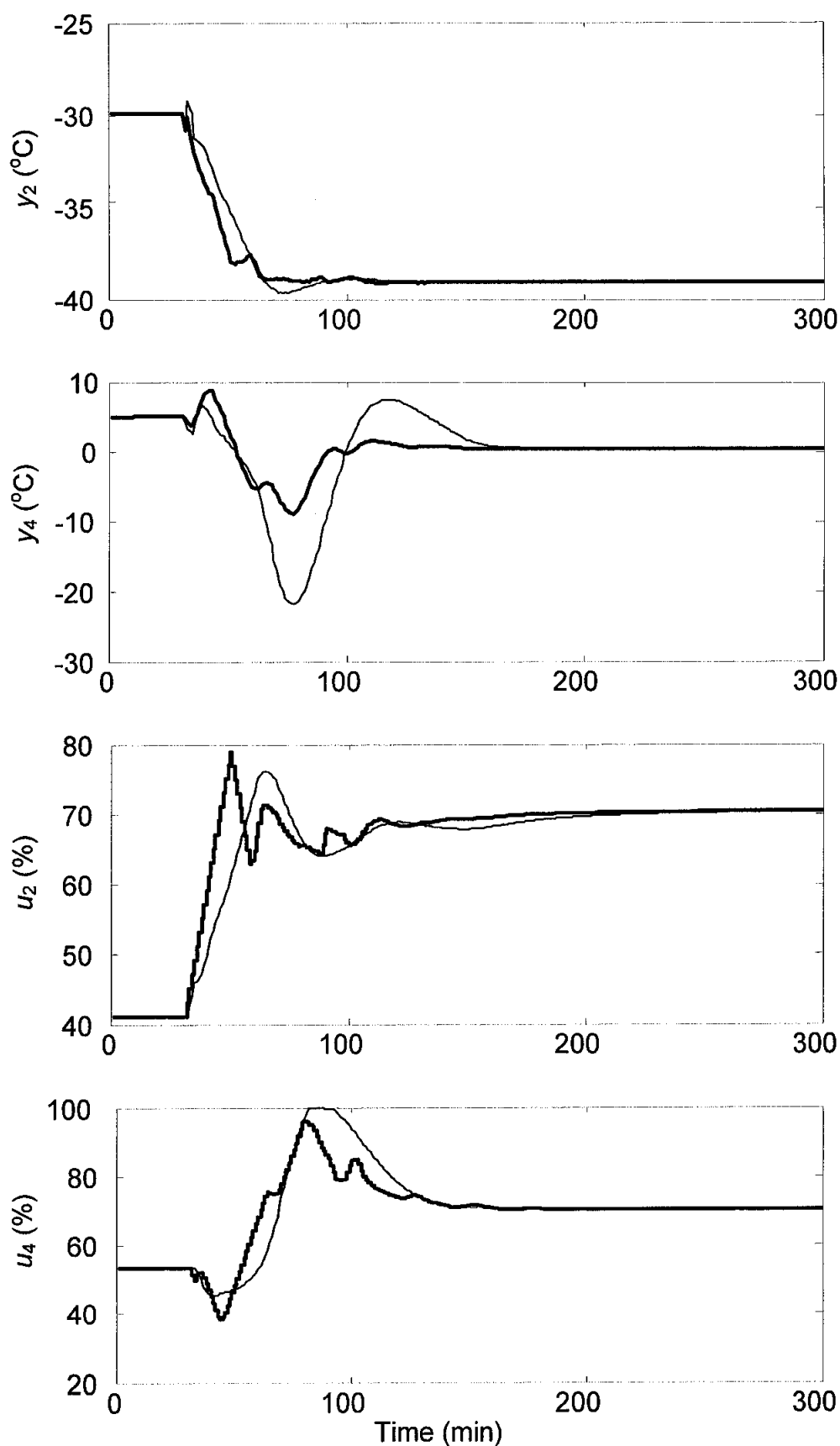


Figure 5.6: Closed-loop responses of PI (thin line) and MPC (thick line) controllers on temperature of feed gas stream exiting cooler E-102 (y_2) and temperature of demethanizer C-101 tray 35 (y_4) for Cases B3 and B4 (integrated approach); E-102Q=cooler E-102 duty in %; E-104Q=reboiler E-104 duty in %

On the other hand, more feed gas flows to turboexpander KT-101 that is mechanically linked to booster compressor K-101. In turn, this action also reduces expenses since operating sales gas compressor K-102 is much more expensive than maintaining turboexpander-compressor K/KT-101. Setpoint tracking for the RTO case is handled poorly by temperature controller TC102 (Figure 5.6). Due to large offset in output y_4 , input u_4 saturation is still a problem albeit at lesser interval. This phenomenon is missing in MPC result. In fact, it can be observed that MPC scheme reveal strategic input adjustments in the following ways: 1) steeper and larger initial move on input u_2 , followed by, 2) deeper initial move on input u_4 to prevent saturation at the upper constraint.

5.3.2.2 Economics

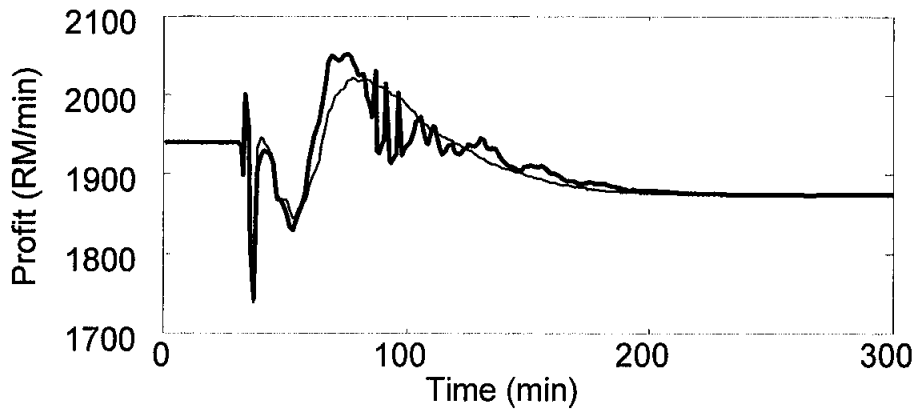
Similar to Case A, four case studies are carried out in Case B. This time, scheduling is performed from sales gas to natural gas liquids mode. Case B1 is used as a basis to be consistent with studies done in Case A. In Case B2, negligible benefit is achieved even though set points are implemented by MPC controller. This happens because economic parameters almost cancel each other out with 0.6% reduction in operating expenses is matched with 0.1% reduction in revenue. Trajectory of RGP profit is shown in Figure 5.7. Except for kinks, which are caused by MPC coordinated actions, profit trajectories for both Cases B1 and B2 closely resemble each other.

Table 5.4: Average values (RM/min) of economic parameters over 510 min simulation time

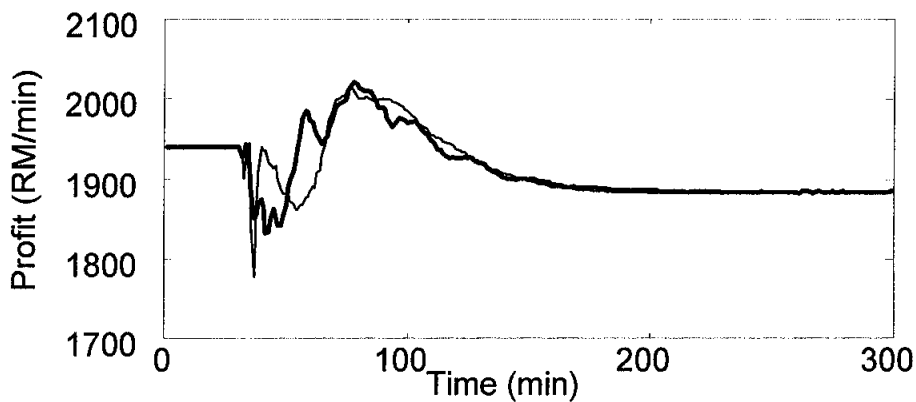
Case	Profit	Revenues		Expenses	
		Sales Gas	Liquids	Feed Gas	Operation
B1	1895.38	2843.57	508.91	1435.55	21.54
B2	1895.70	2844.22	508.45	1435.56	21.41
B3	1900.81	2856.18	500.19	1435.62	19.95
B4	1901.27	2857.68	499.08	1435.58	19.92

Integrated approach of scheduling and RTO are represented in Cases B3 and B4. As compared with the base case (B1), the benefit is 0.3% for both cases. This is achieved at almost similar means by PI and MPC controllers. The former increases value of sales gas by 0.4% whereas the latter by 0.5%. PI and MPC controller actions reduce revenue from liquids by 1.7 and 1.9%, respectively. However, gap between both controllers shrinks to 0.1% in terms of benefit derived from operating expenses.

For this particular case, the small marginal benefit indicates that optimal setpoints calculated by the integrated approach may be equally executed by either PI or MPC controllers. This is because the latter has exhausted all efforts in obtaining optimal trajectory for its manipulated variables.



(a) Scheduling only – Case B1 (thin line) and Case B2 (thick line)



(b) Integrated approach – Case B1 (thin line) and Case B2 (thick line)

Figure 5.7: Dynamic trajectories of RGP profit for Case B

5.4 Load Scheduling

Load scheduling refers to a process of varying flow rate of feed gas stream A by ± 30 ton/h from a regular flow rate of 280 ton/h. In this section, four studies are performed in the case of scheduling of RGP load from 280 to 250 ton/h (Case C):

1. Load scheduling with PI controllers (base case)
2. Load scheduling with MPC controllers

3. Integration of load scheduling and RTO with PI controllers
4. Integration of load scheduling and RTO with MPC controllers

The above studies are repeated for load scheduling from 280 to 310 ton/h (Case D). In total, eight case studies are conducted. Each case is simulated for 510 min. This case study represents flow disturbance in feed gas stream.

5.4.1 Load scheduling from 280 to 250 ton/h (Case C)

5.4.1.1 Process

In the first case of load scheduling, flow rate of feed gas stream A is reduced from 280 to 250 ton/h. RGP is operating at natural gas liquids mode because feed gas stream A is lean. Plant conditions at this base case have been explained in the previous section and thus will not be repeated. In the case of integrated approach, slight changes in operating conditions are necessary to cater for 30 ton/h reduction in feed gas flow rate. These changes are supplied by the RTO layer before being implemented by controllers.

Differences between base and optimal setpoints are presented in Table 5.5. Two target variables, y_1 and y_3 , are maintained at their base values. On the other hand, target variable y_2 drops by 1.8 °C causing cooler E-102 duty to increase by 20.6% from its base value of 2931 kW (Table B.6). This move initially seems counter-intuitive since operating cost due to cooler E-102 rises proportionately. However, an increase in cooler E-102 duty is balanced with 26.0% reduction in reboiler E-104 duty, which directly affects energy level at the stripping section of demethanizer C-101. The reduction in reboiler E-104 duty is an outcome of two factors namely: 1) drop in RGP load by 30 ton/h, and 2) decrease in output y_4 setpoint by 1.8 °C. At the top of demethanizer C-101, pressure is maintained at 22 barg to be consistent with the current plant operating mode. However, flow of processed gas to GSP section is reduced from 34.5 to 11.3 ton/h. This move has a negative implication in recovery of natural gas liquids. At the other end of product stream, sales gas production reduces to 200.5 ton/h (Table B.6). This throughput is slightly below the customer's demand of 205.0 ton/h. As a solution, 9.8 ton/h of hydrocarbon is re-injected to the sales gas product line.

Table 5.5: Values of target variables for base and RTO cases under 250 ton/h load

Var.	Unit	Case Study		Description
		Base	RTO	
y_1	°C	-30.5	-30.5	Temperature of feed gas exiting coldbox E-101
y_2	°C	-40.0	-41.8	Temperature of feed gas exiting cooler E-102
y_3	°C	-53.9	-53.9	Temperature of PG exiting coldbox E-103
y_4	°C	5.0	3.2	Temperature of demethanizer C-101 tray 35
y_5	barg	22	22	Pressure of demethanizer C-101 overhead
y_6	ton/h	34.5	11.3	Flow of PG to GSP section
y_7	ton/h	0	9.8	Flow of hydrocarbon re-injection

Note: PG=processed gas; GSP=gas subcooled process

5.4.1.2 Economics

Four studies are conducted to investigate variations of RGP profit in the first case of load scheduling. In Cases C1 and C2, scheduling targets are implemented by PI and MPC controllers, respectively. Economic results show no additional benefits are achieved by using different controller schemes (Table 5.6). A similar conclusion can be drawn for the integrated approach in Cases C3 and C4 as evidenced by the same values of economic parameters.

A reduction of plant load by 30 ton/h is initially expected to drop RGP production and thus its profit margin. The outcomes from the integrated approach are exactly the opposite. While it is true that natural gas liquids production drops by 1.0%, sales gas production soars by 2.3% from the base level. This quagmire is caused by two factors namely: 1) optimal setpoints favor losses of ethane and propane, and 2) hydrocarbon re-injection has positive effect in boosting flow of sales gas product stream. The first factor causes a rise in operating cost by 4.4%. The second factor inadvertently increases feed gas cost by 1.9%. Despite downward effects in some economic parameters, RGP profit is upped by 1.7% in both Cases C3 and C4.

Table 5.6: Average values (RM/min) of economic parameters over 510 min simulation time

Case	Profit	Revenues		Expenses	
		Sales Gas	Liquids	Feed Gas	Operation
C1	1723.67	2618.30	451.95	1326.76	19.82
C2	1723.68	2618.30	451.94	1326.76	19.80
C3	1753.07	2678.33	447.51	1352.07	20.70
C4	1753.05	2678.30	447.53	1352.06	20.71

5.4.2 Load scheduling from 280 to 310 ton/h (Case D)

5.4.2.1 Process

The second case of load scheduling exhibits challenges in RGP operation at full capacity of 310 ton/h. Plant state deviate a little from the typical conditions at natural gas liquids mode. Pre-cooling of feed gas stream A is carried out by slightly decreasing setpoint of output y_1 from -30.5 to -32.0 °C (Tables 5.5 and 5.7). However, temperature setpoint of feed gas stream exiting cooler E-102 and that of processed gas exiting coldbox E-103 are increased by 2.0 and 8.9 °C, respectively. To cater for an additional load of 30 ton/h, overhead pressure of demethanizer C-101 is raised by 0.5 barg. However, outputs y_4 and y_6 remain at their previous target values.

Table 5.7: Values of target variables for base and RTO cases (Case D)

Var.	Unit	Case Study		Description
		Base	RTO	
y_1	°C	-32.0	-31.2	Temperature of feed gas exiting coldbox E-101
y_2	°C	-38.0	-34.6	Temperature of feed gas exiting cooler E-102
y_3	°C	-45.0	-45.0	Temperature of PG exiting coldbox E-103
y_4	°C	5.0	0	Temperature of demethanizer C-101 tray 35
y_5	barg	22.5	22.5	Pressure of demethanizer C-101 overhead
y_6	ton/h	34.5	22.4	Flow of PG to GSP section
y_7	ton/h	0	0	Flow of hydrocarbon re-injection

Note: PG=processed gas; GSP=gas subcooled process

Optimal setpoints in Table 5.7 reveal an increasing trend of feed gas temperature at pre-cooling stage. Target variables y_1 and y_2 are increased by 0.8 and 3.4 °C, respectively. As a result, cooler E-102 duty drops by almost one-half to 1200 kW (Table B.8). Hotter feed gas condition favors losses of ethane and propane, especially since temperature of processed gas exiting coldbox E-103 is kept at the same level as the base case. This fact is compounded by a decrease in flow of processed gas to GSP section from 34.5 to 22.4 ton/h. To alleviate the current predicament, temperature of demethanizer C-101 tray 35 is reduced from 5.0 to 0 °C.

5.4.2.2 Economics

In the second case of load scheduling, the economic benefits of operating RGP at maximum throughput are examined. Cases D1 and D2 are scheduling without target

optimization. Economic results indicate that scheduling setpoints can be equally implemented by both PI and MPC controllers (Table 5.8). The same deduction is applicable for the integrated approach in Cases D3 and D4. However, RGP achieves a 0.3% increase in profit margin when it is subjected to optimal conditions. This margin comes amid 0.3% rise in sales gas revenue but 1.2% decrease in natural gas liquids revenue. A 10.3% reduction in operating cost also helps in improving RGP profit.

Table 5.8: Average values (RM/min) of economic parameters over 510 min simulation time

Case	Profit	Revenues		Expenses	
		Sales Gas	Liquids	Feed Gas	Operation
D1	2087.18	3191.47	485.89	1571.12	19.06
D2	2087.15	3191.47	485.85	1571.12	19.06
D3	2093.07	3201.36	480.00	1571.19	17.10
D4	2092.93	3201.25	479.95	1571.18	17.08

5.5 Input Scheduling

Input scheduling refers to varying flow rates of feed gas streams. This case is similar to the one presented in Chapter 4 except that flow of mixed feed gas stream is specified at 280 ton/h. In addition, mixing amount of feed gas streams A, B and/or C is pre-determined by the planners based on availability of these gases at the producing sites. As such, four studies are performed in the case of processing feed gas streams A and B flowing at 130 and 150 ton/h, respectively (Case E):

1. Input scheduling with PI controllers (base case)
2. Input scheduling only with MPC controllers
3. Integration of input scheduling and RTO with PI controllers
4. Integration of input scheduling and RTO with MPC controllers

The above studies are repeated for input scheduling of RGP feed gas streams A and C flowing at 180 and 100 ton/h, respectively (Case F). In total, eight case studies are conducted. Each case is simulated for 510 min. This case study represents composition disturbance in mixed feed gas stream.

5.5.1 Input scheduling of feed gas streams A and B (Case E)

5.5.1.1 Process

In this case, RGP processes 130.0 and 150.0 ton/h of feed gas streams A and B, respectively. The presence of richer feed gas stream B forces RGP to increase its overall temperature due to larger composition of heavier hydrocarbons in mixed feed gas stream. This is necessary to ensure good separation of sales gas from natural gas liquids. If temperature setpoints for the base case are higher than those for sales gas mode, the optimal setpoints for Case E are even higher. Target variables y_1 , y_2 and y_3 are all increased by 2.8, 5.5 and 0.4 °C, respectively.

However, flow of processed gas to GSP section reduces from 33.2 to 29.6 ton/h. This move cuts down recovery rate of natural gas liquids. To offset losses of ethane and propane in sales gas product stream, temperature of demethanizer C-101 tray 35 is decreased from 5.0 to 0.3 °C. Overhead pressure of the demethanizer is maintained at 22 barg although there is an option to raise it to 24 barg. This option may be taken if load disturbance is minimal and within control limits in order to avoid stability issue. However, this option is skipped in the current study because the effect of increasing y_5 setpoint has been conducted in the case of scheduling from natural gas liquids to sales gas mode.

Table 5.9: Values of target variables for base and RTO cases (Case E)

Var.	Unit	Case Study		Description
		Base	RTO	
y_1	°C	-14.8	-12.0	Temperature of feed gas exiting coldbox E-101
y_2	°C	-25.6	-20.1	Temperature of feed gas exiting cooler E-102
y_3	°C	-40.1	-39.7	Temperature of PG exiting coldbox E-103
y_4	°C	5.0	0.3	Temperature of demethanizer C-101 tray 35
y_5	barg	22.0	22.0	Pressure of demethanizer C-101 overhead
y_6	ton/h	33.2	29.6	Flow of PG to GSP section
y_7	ton/h	0	0	Flow of hydrocarbon re-injection
y_8	ton/h	130.0	130.0	Flow of feed gas stream A
y_9	ton/h	150.0	150.0	Flow of feed gas stream B
y_{10}	ton/h	0	0	Flow of feed gas stream C

Note: PG=processed gas; GSP=gas subcooled process

5.5.1.2 Economics

Table 5.10 presents economic results for Case E. Results from Cases E1 and E2 indicate remarkable agreement in all economic parameters except for operating expenses. For Case E2, operating expenses drop by 0.9% due to efficiency of MPC scheme in tracking setpoints. The same trend can be seen in Cases E3 and E4 albeit at a smaller benefit of 0.8% differences between the operating expenses. In terms of profit, a 0.4% increase is achieved by implementing RTO targets. The margin is mainly derived from 0.8% increase in sales gas revenue and 12.0% decrease in operating costs. On the other hand, a reduction of 2.4% in natural gas liquids revenue hampers further growth in RGP profit.

Table 5.10: Average values (RM/min) of economic parameters for Case E over 510 min simulation time

Case	Profit	Revenues		Expenses	
		Sales Gas	Liquids	Feed Gas	Operation
E1	1827.03	2536.84	606.22	1295.11	20.92
E2	1827.15	2536.74	606.30	1295.16	20.74
E3	1833.80	2555.90	591.38	1295.05	18.44
E4	1834.43	2556.40	591.33	1295.03	18.27

5.5.2 Input scheduling of feed gas streams A and C (Case F)

5.5.2.1 Process

Feed gas stream C is the richest among the three feed gas streams. Mixing 100.0 ton/h of feed gas stream C with 180.0 ton/h feed gas stream A poses a strong operational challenge. RGP condition is even hotter than that in Case E. For example, temperature of feed gas exiting coldbox E-101 rises from -14.8 to -5.5 °C (Tables 5.9 and 5.11). The same is true for outputs y_2 and y_3 , in which stream temperatures escalate by 9.7 and 13.5 °C, respectively. On the other hand, output y_5 is kept at 5.0 °C to ensure availability of enough energy for separating sales gas from natural gas liquids in demethanizer C-101.

Optimal RGP state in Case F reveals no changes in target variables y_1 and y_3 . However, target variable y_2 is increased by 1.5 °C to yield 15.2% savings in cooler E-102 duty (Table B.8). A reduction of y_4 setpoint from 5.0 to 0 °C helps RGP in two

ways: 1) RGP can further save on operating cost due to reboiler E-104 duty by 7.2%, and 2) flooding in Sections 1 to 3 in demethanizer C-101 is kept above 25% minimum limit. Overhead pressure of demethanizer C-101 is maintained at 22.0 barg based on the same reason as in Case E. On the other hand, flow of processed gas to GSP section increases from 22.2 to 33.3 ton/h. This move has a positive effect in enhancing recovery of natural gas liquids.

Table 5.11: Values of target variables for base and RTO case studies (Case F)

Var.	Unit	Case Study		Description
		Base	RTO	
y ₁	°C	-5.5	-5.5	Temperature of feed gas exiting coldbox E-101
y ₂	°C	-15.9	-14.4	Temperature of feed gas exiting cooler E-102
y ₃	°C	-28.6	-28.6	Temperature of PG exiting coldbox E-103
y ₄	°C	5.0	0	Temperature of demethanizer C-101 tray 35
y ₅	barg	22.0	22.0	Pressure of demethanizer C-101 overhead
y ₆	ton/h	22.2	33.3	Flow of PG to GSP section
y ₇	ton/h	0	0	Flow of hydrocarbon re-injection
y ₈	ton/h	180.0	180.0	Flow of feed gas stream A
y ₉	ton/h	0	0	Flow of feed gas stream B
y ₁₀	ton/h	100.0	100.0	Flow of feed gas stream C

Note: PG=processed gas; GSP=gas subcooled process

5.5.2.2 Economics

Economic results for Case F are presented in Table 5.12. The first two cases are input scheduling as implemented by PI and MPC controllers. A marginal benefit of 0.1% profit is achieved for Case F2 as compared with Case F1. This is due to the same amount of increase in natural gas liquids revenue and 0.8% decrease in operating costs. Results from integrated approach exhibit 0.5% profit growth. This is accomplished at the expense of 3.0% drop in natural gas liquids revenue. However, a 1.1% increase in sales gas revenue and more than 13% savings in operating expenses are enough to offset the cut in revenue. When Cases F3 and F4 are scrutinized, MPC scheme offers 0.5% savings in operating costs as compared with PI controllers.

Table 5.12: Average values (RM/min) of economic parameters over 510 min simulation time

Case	Profit	Revenues		Expenses	
		Sales Gas	Liquids	Feed Gas	Operation
F1	1955.26	2619.11	683.53	1326.59	20.78
F2	1956.25	2619.89	684.05	1327.07	20.62
F3	1965.77	2648.36	662.81	1327.33	18.07
F4	1965.81	2648.14	662.94	1327.28	17.99

5.6 Concluding Remarks

Three types of scheduling problems are studied to verify efficacy of the proposed approach, which is based on integrated framework of scheduling and RTO. The scheduling problems are mode, load and input. Results of mode scheduling are presented and discussed thoroughly in this chapter. However, those of load and input scheduling problems are done partially to avoid repetitions and thus ensure smooth reading of the thesis. For reference, these results are displayed in Appendix B.

In general, change of plant mode from natural gas liquids to sales gas results in higher profit margin. This is because sales gas is more valuable than natural gas liquids. The same fact can be deduced for load and input scheduling cases as evidenced from the economic results. In short, RTO setpoints favor losses of ethane and propane in the sales gas product stream. When these setpoints are implemented at control layer, MPC scheme provides an additional benefit by reducing operational expenses at slightly larger amount than PI controllers do.

CHAPTER 6

CONTRIBUTIONS AND FUTURE RESEARCH AVENUES

The primary motivation of this thesis work is to find a solution for an integrated framework of process scheduling and real-time optimization (RTO), which form the top two layers in the hierarchy of plant automation. Due to multi-temporal nature of these two activities, integration of scheduling and RTO is difficult. This thesis work adds four valuable contributions towards this field of knowledge. The major contributions are divulged in the next section. Future work on the same field is recommended in the latter section of this chapter.

6.1 Contributions

The proposed integrated framework of scheduling and RTO differs from the current ones in the sense that previous work is limited to employing steady-state models on large-scale nonlinear integrated plants or using dynamic models on linearized individual units. In this work, efficacy of the proposed approach is evaluated using a highly interacting nonlinear plant model. Among the challenges faced when integrating scheduling and RTO procedures are: 1) difficulties in developing a rigorous dynamic model consisting of several large units in an integrated plant, 2) difficult connectivity among various applications and dynamic submodels of large individual units into a single process flowsheet, 3) high computational load in executing an online optimization procedure, and 4) concerns on model and process uncertainties. The current work attempts to address the first three limitations.

The first two limitations are addressed in a unified way. A rigorous dynamic model is developed based on the converged solution of a high-fidelity steady-state model. Both models share a Peng-Robinson thermodynamic package and a process flowsheet. This integrated modeling design alleviates the task of moving the simulation from steady-state to dynamic modeling environment. Data transfer between the steady-state and dynamic models is performed automatically by executing a small MATLAB code. Inter-connectivity among submodels of individual unit is established in a single HYSYS simulation platform. Communication between

HYSYS, MATLAB and the third-party software is achieved via component object module (COM) technology. This unified approach certainly facilitates data transfer and thus removes the first two limitations.

The third issue is related to computing power and efficient techniques for online optimization. This is true if a large-scale mixed integer dynamic optimization (MIDO) problem is encountered. It should be noted that there are two aspects to the third limitation. The first aspect, mixed integer problem, is avoided by formulating the scheduling problem as a nonlinear programming (NLP) problem. This can be achieved by treating the scheduling problem as a continuous instead of batch decision-making process. Here, scheduling decisions are enforced using a dynamic model but have yet to be implemented. When the dynamic model is stabilized at a new state, future model outputs are retrieved and forwarded to the RTO layer for target optimization.

The RTO procedure uses a high-fidelity steady-state model, which is *a priori* updated by the dynamic model outputs. The optimal setpoints as passed to a virtual plant for target implementation via either regulatory controllers or MPC scheme. The only difference between the dynamic model and the plant is that the latter is kept at the former state prior to enforcement of scheduling decisions. A combinatorial usage of a dynamic model for enforcing scheduling decisions and a steady-state model for running an RTO procedure can alleviate the difficulty encountered when performing dynamic optimization. This strategy addresses the second aspect of the third issue. Here, the computational load in obtaining a feasible and practical solution of the optimization problem is dramatically reduced to within a stipulated RTO cycle.

Following a discussion of the major thesis work, the detailed contributions are highlighted as follows:

- *Development of steady-state and dynamic models of a refrigerated gas plant (RGP) on a single HYSYS platform to be used as test beds for the proposed approach:* Each RGP model consists of three liquefied natural gas (LNG) heat exchangers, a propane-refrigerated cooler, two flash separators, a distillation

column, an absorber, a turboexpander-compressor, a Joule-Thompson valve, two pumps, a booster compressor and an air cooler. An integrated steady-state model consisting of all operating units is initially developed based on first-principle approach. The relevant model outputs are compared against the actual plant data. Fine-tuning of process and equipment parameters are carried out to ensure that the model reaches about 95% resemblance with the actual plant.

Once a high-fidelity steady-state model is produced, a dynamic model is setup using the current state for initialization purposes. The dynamic model is fairly large containing 770 differential-algebraic equations (DAEs) and 21 regulatory control loops. Sizing of major operating units are based on the plant Mechanical Engineering Handbooks and Technical Datasheets. At the boundary streams, pressures instead of flow rates are specified because the latter can be regulated by controllers. The control philosophies employed in the dynamic model follow those currently applied in the actual plant.

- *Systematic identification of the dynamic model of RGP using step and pseudo-random binary sequence (PRBS) input signals to be deployed in an advanced processed control (APC) strategy:* Plant tests using multi-step input signals results in a 2x2 first-order-plus-time-delay (FOPTD) process model. This model is valuable for estimating magnitude and determining directionality of process gains due to familiarity with its transfer function structure. However, the FOPTD model is vulnerable to process nonlinearity and feed disturbance. This makes it inadequate to be setup as a process model in an APC scheme known as model predictive control (MPC). For this reason, a multiple-input-multiple-output (MIMO) process model with state-space or autoregressive with exogenous input (ARX) structure is more suitable.

These parametric models are developed based on multivariable input-output information obtained simultaneously from the plant tests. Fourth order state-space structure and second order ARX structure can readily replace the FOPTD model to better represent the dynamics of RGP. The latter structure is chosen as the process model because MPC-ARX scheme moves inputs more efficiently for the same case of setpoint tracking. To accommodate the effect of

disturbance, flow rate of mixed feed gas stream is taken as the third input to the process model. This decision augments the MPC-ARX scheme to a two-output-by-three-input scheme.

- *RTO assessment of RGP profit by forcing RGP to consider processing additional feed gas streams.* Optimization is performed using sequential quadratic programming (SQP) algorithm with constraints. RGP profit is taken as the objective function subject to steady-state model convergence and thirty four operational constraints. Ten optimization variables are manipulated to maximize RGP profit. The significance of these optimization variables was established through a series of parametric design of experiments based on Taguchi method. A case study was conducted to evaluate economic feasibility of processing richer feed gas streams B and C. This case is important because RGP prefers to process lean feed gas stream A at a normal throughput of 280 ton/h. The highest profit is earned over two conditions namely: 1) flow rates of feed gas streams A, B and C are properly balanced, and 2) plant throughput is increased to the upper limit of 310 ton/h.
- *Proposition of an integrated framework of scheduling and RTO with realistic applications on three scheduling cases namely: 1) mode, 2) load, and 3) input.* Scheduling is carried out on a dynamic model of RGP. Both MPC and regulatory controllers can be used to implement designed or heuristic setpoints until all key operating variables level off at around 510 min of simulation time. In the integrated approach, another dynamic model (virtual plant) is employed. Setpoints are disjointedly implemented by regulatory and MPC controllers after being optimized at the steady-state RTO layer. In some cases, SQP algorithm faces difficulty in locating global maxima. This causes lack of convergence for a few of the optimization problems. As a remedy, new RGP states with higher profit are accepted as solutions.

Plant-model mismatch is minimized by sending values of 49 major variables from dynamic to steady-state model. These variables consisting of stream flow rates, temperatures and pressures are major specifications in the steady-state

model. On the other hand, only six to eight values of relevant controller setpoints are passed from steady-state to dynamic model. This decision has two advantages namely: 1) it promotes bumpless data transfer between the two models, and 2) it ensures feasible pressure-flow conditions at all streams and unit operations in the dynamic model.

Economic benefits from the integrated approach reach as high as 1.7% in Case C and as low as 0.3% in Cases B and D (Figure 6.1). In Case C, RGP load from feed gas stream A is reduced from 280 to 250 ton/h. As a result, production of sales gas decreases slightly below the load demanded by customers at 205 ton/h. To avoid penalty, a cheaper but richer hydrocarbon stream from another plant is injected into sales gas product line. This action boosts not only flow rate but also gross heating value (GHV) of the sales gas. On the other hand, marginal profit margin of 0.3% each in Cases B and D is mainly caused by warmer plant conditions as compared with corresponding base cases. These conditions result in some losses of ethane and propane into sales gas product stream.

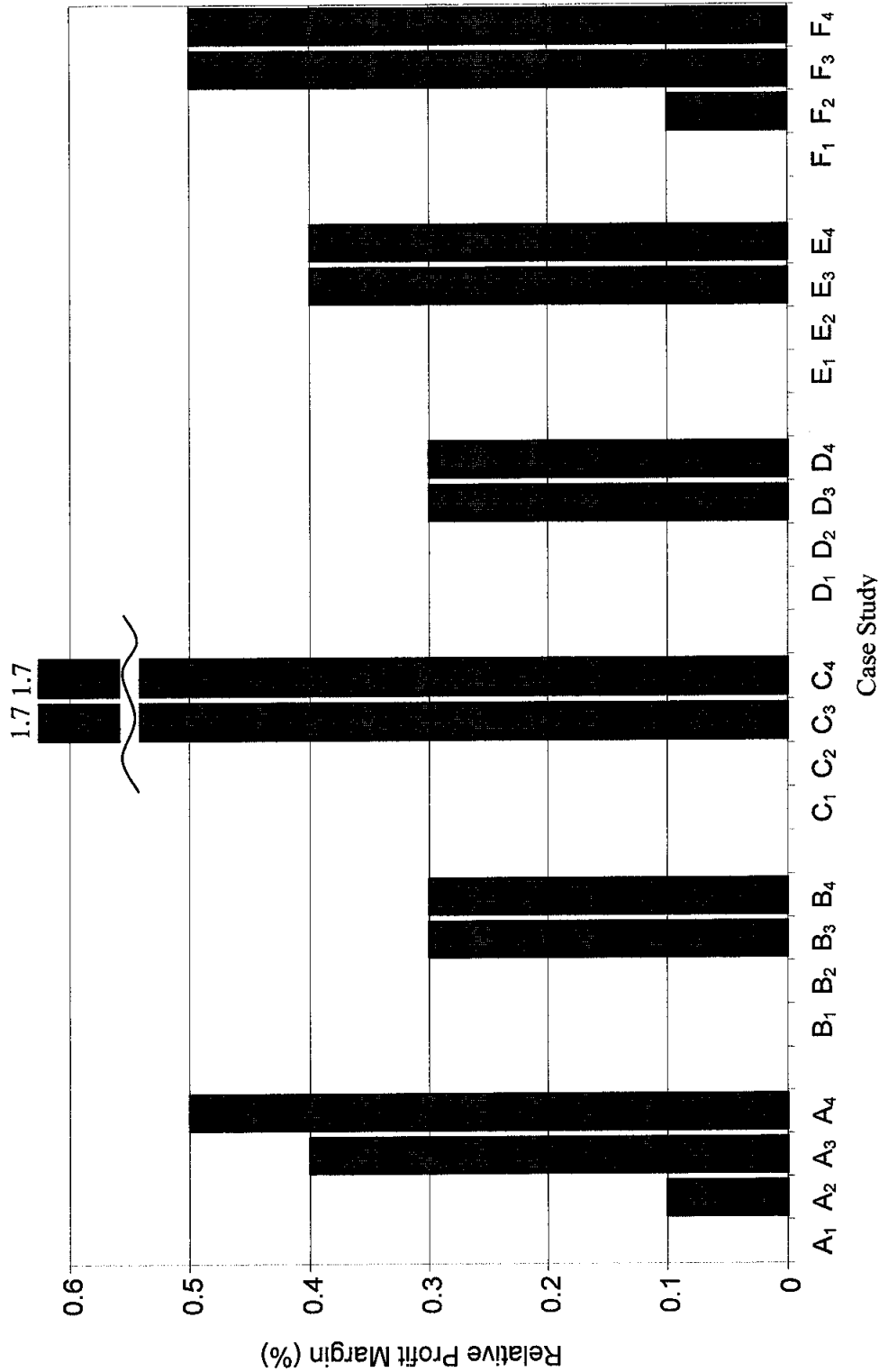


Figure 6.1: Relative profit margins of Cases A to F as compared with respective base cases

Finally, it would be interesting to compare case-average profits from each of the three scheduling problems namely: 1) mode (Cases A and B), 2) load (Cases C and D), and 3) input (Cases E and F). This information is important for RGP to determine which state yields the higher profit on average between two similar cases of scheduling. A case-average profit is defined as sum of profits within the same case study divided by number of sub-cases. A bar chart of case-average profits for all case studies is presented in Figure 6.2. Here, the following trends are observed:

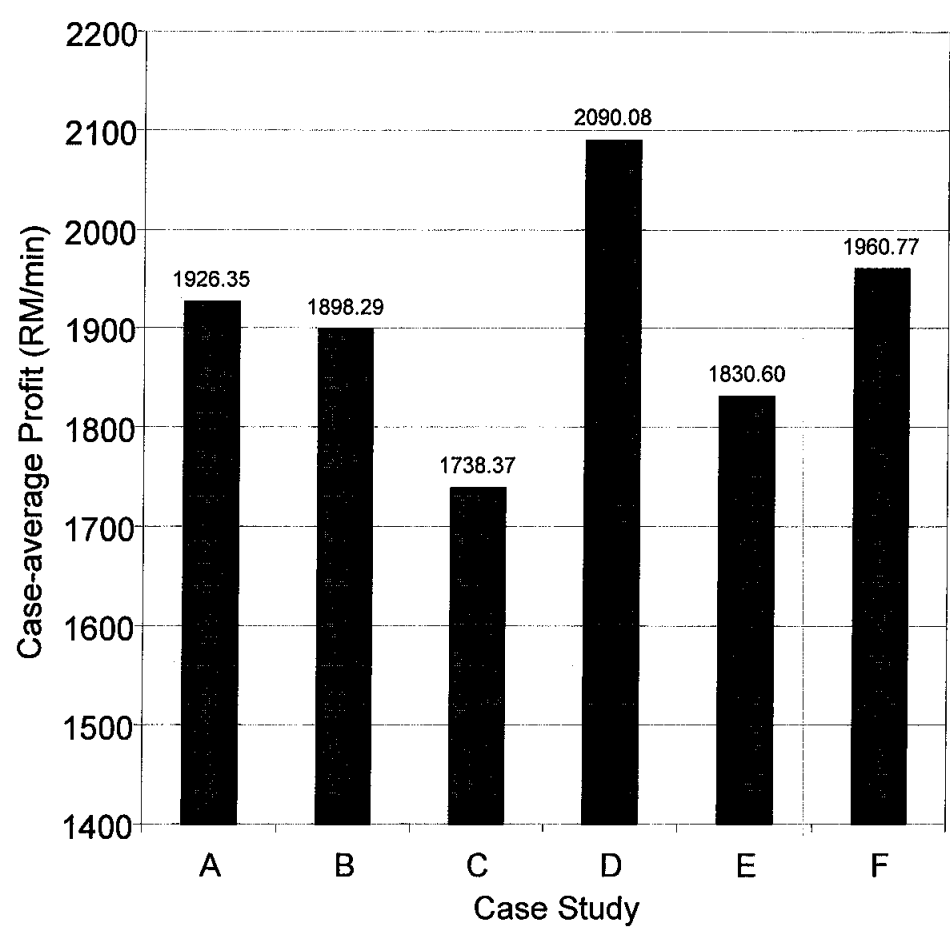


Figure 6.2: Case-average profit values (RM/min) for Cases A to F

1. Mode scheduling in Case B reduces case-average profit by 1.5% or 28.06 RM/min when weighed against that in Case A. Hence RGP should opt for sales gas mode rather than natural gas liquids mode in most of the time. This suggestion is valid as long as prices of sales gas and feed gas are fixed on a long-term basis and the difference between them remains high. In addition, prices of natural gas liquids may be allowed to

fluctuate albeit within a narrow band with long-term average values as presented in Chapter 4. On the other hand, mode scheduling will have to be performed at more frequent intervals if prices of natural gas liquids components namely ethane, propane, butane and condensates float at broader ranges such as those in the daily spot market.

2. Load scheduling favors Case D over Case C with 20.2% or 351.71 RM/min difference in case-average profit. This result indicates that RGP should process lean feed gas stream A at maximum throughput of 310 ton/h. If plant conditions are unfavorable at the upper limit, RGP can decide on reducing its load to between 280 and 310 ton/h. Ultimately, RGP can reap high margin due to large profit difference between the two cases. On the other hand, descent profit can still be made even if RGP is forced to reduce its load to 250 ton/h. The strategy is to boost sales gas production through injection of feed gas stream D. However, flow of this hydrocarbon stream is limited to 10 ton/h.

3. Input scheduling in Case F improves RGP profit by 7.1% or 130.17 RM/min as compared with that in Case E. This result reveals the fact that handling rich hydrocarbon composition in mixed feed gas stream is a desirable challenge for RGP. In the past and at present, RGP prefers to process lean feed gas stream A to avoid “sweating” of its assets. In the future, producers can only deliver rich gas due to depleted content of methane from gas reservoirs. RGP needs to find ways and revamp some assets to prepare for this eventuality. At current state, the best solution in handling rich gas is to warm the plant at an optimal level. This is done to sustain minimum production of sales gas. At the same time, this effort can prevent detrimental conditions such as inadequate duties of cooler E-102 and reboiler E-104, as well as flooding at demethanizer C-101 and absorber C-102.

6.2 Future Research Avenues

While this thesis work has presented several significant contributions on the proposed integrated approach of scheduling and RTO, a few important issues remain to be addressed. For example, the owner of RGP is keen to know whether the proposed approach has reached maturity in terms of technological development. If it does, the next question is whether there are industrial practitioners who have successfully adopted the technology in their plants. Obviously, satisfactory answers to these questions can only be redeemed in years ahead. For now, more research needs to be conducted in order to overcome several technical limitations. The following discussion elaborates these challenges and recommends the next plausible steps in enhancing the proposed integrated approach:

- *Improvement of the MPC process model:* Recall that MPC scheme employs a linear parametric model in the form of ARX structure. This process model is identified using multivariable PRBS input signals that vary $\pm 5\%$ from their respective nominal values. Another type of input signal known as generalized multi-level noise (GMN) may be suitable to handle nonlinearity in the RGP system (Zhu, 2001). The GMN signal is generated from purely random noise with underlying Gaussian distribution. An input is fully characterized by specifying multiple levels and a switching time.

On another issue, nonlinear RGP system can be better represented by Wiener and/or Hammerstein-type models. The resulting nonlinear MPC is expected to perform better than its linear counterpart or regulatory controllers in cases of setpoint tracking and disturbance rejection. While the former case is thoroughly studied in this thesis, the latter is omitted due to difficulty in identifying the disturbance model. Future research should focus on obtaining nonlinear and disturbance models for MPC.

- *Minimization of modeling and operational uncertainties:* In the integrated approach of scheduling and RTO, the former procedure uses a dynamic model whereas the latter a steady-state model. Mismatch between the two models will exist even though efforts are taken to reduce it. In general, data transfer from

dynamic to steady-state model and vice-versa produces errors of the following magnitudes: 1) less than 5% for temperature and pressure of streams and major equipment, and 2) as much as 20% for non-specified flow rates of certain streams.

Small errors in temperature and pressure are credited to sharing of the same Peng-Robinson thermodynamic package in HYSYS. Large errors in stream flow rates are caused by two different fundamental theories used to calculate flow. Steady-state model simultaneously solves material and energy balances while ignoring transient behavior of the process. This is done to expedite calculations for a quick estimate of the current plant state. On the other hand, dynamic model include the accumulation term and relates flow to pressure drop across equipment. The concept used in dynamic model is more realistic and thus can be applied to replicate actual industrial processes. For this reason, it is imperative to simultaneously run RTO and scheduling procedures in the same dynamic model.

- *Adoption of a more sophisticated information technology infrastructure and an efficient optimization algorithm to significantly reduce computational load:* The multi-temporal nature of these procedures poses two technological challenges: 1) hardware limitations especially in computing capabilities such as speed and memory allocation, and 2) underdeveloped dynamic optimization algorithm for solving large-scale constrained nonlinear problems within an RTO sampling interval. It is noted that the first issue can be circumvented by connecting two high-end workstations via an object-link-embedded for process control (OPC) server. With the advent of computing technology, the hardware limitations are expected to be alleviated in the near future.

On the second issue, general purpose optimization codes such as KNITRO (Byrd et al., 1997), LOCO (Vanderber and Shanno, 1997), SOCS (Betts, 2001), SNOPT (Gill et al., 2005) and IPOPT (Wachter and Biegler, 2006) are available for academic usage. These codes are based on direct sparse factorizations that eliminate state variables and linearized equations. The caveat is that users have

to separately deal with the following difficult issues: 1) decomposition of a large-scale nonlinear dynamic model comprising several complex unit operations, 2) coupling of transient material and energy balances with detailed equipment design and other aspects such as operability, controllability and safety, and 3) multi-temporal nature of scheduling and RTO procedures.

REFERENCES

- Allgower F., Badgwell T.A., Qin S.J., Rawlings J.B., and Wright S.J. (1999). Nonlinear predictive control and moving horizon estimation: an introductory overview. In Frank P.M. (Editor), *Advances in Control: Highlights of ECC '99*. Berlin: Springer.
- Alsop N. and Ferrer J.M. (2006). Step-test free APC implementation using dynamic simulation. *AIChE Spring National Meeting*, Orlando, USA.
- Altena D., Howard M., Bullin K. and Cantrell J. (1998). Advanced multivariable control of a turboexpander plant. In the *Proceedings of the Seventy-Seventh GPA Annual Convention*. Tulsa, USA.
- Amaro A.C.S. and Barbosa-Póvoa A.P.F.D. (2008). Planning and scheduling of industrial supply chains with reverse flows: A real pharmaceutical case study. *Computers and Chemical Engineering*, 32 (11), 2606-2625.
- Aspentech (2006), HYSYS 2006 Dynamic modeling guide, Aspen Technology, Cambridge, USA.
- Basak K, Abhilash K.S. Ganguly S. and Saraf, D.N. (2002). On-line optimization of a crude distillation unit with constraints on product properties. *Industrial and Engineering Chemistry Research*, 41(6), 1557-1568.
- Bassett M.H., Dave P., Doyle F.J., Kudva G.K., Pekny J.F. and Reklaitis G.V. (1996). Perspectives on model based integration of process operations. *Computers and Chemical Engineering*, 20 (6-7), 821-844.
- Beronich E., Hawboldt K., Abdi M. (2005), "Linking a process simulator (HYSYS) with MATLAB, a powerful modeling tool for continuous process industry: A tutorial." In the *Proceedings of the 15th IEEE Annual Newfoundland Electrical and Computer Engineering Conference (NECEC 2005)*, St. John's, Canada.

- Birewar D.B. and Grossmann I.E. (1990). Simultaneous production planning and scheduling in multiproduct batch plants. *Industrial and Engineering Chemistry Research*, 29 (4), 570-580.
- Blanco A.M., Masini G., Petracci N. and Bandoni, J.A. (2005). Operations management of a packaging plant in the fruit industry. *Journal of Food Engineering*, 70 (3), 299-307.
- Bryson A. and Ho Y. (1975). *Applied optimal control*. Hemisphere Publishing Co., Washington DC, USA.
- Bullin K.A. (1999). Economic optimization of natural gas processing plants including business aspects. *PhD Dissertation*. Texas A&M University, USA.
- Cervantes A.M., Tonelli S., Brandolin A., Bandoni J.A. and Biegler L.T. (2002). Large-scale dynamic optimization for grade transitions in a low density polyethylene plant. *Computers and Chemical Engineering*, 26 (2), 227-237.
- Chamberlain R.M. and Powell, M.J.D. (1982). The watchdog technique for forcing convergence in algorithms for constrained optimization. *Mathematical Programming Study*, 16, 1-17.
- Chatzidoukas C., Perkins J.D., Pistikopoulos E.N. and Kiparissides C. (2003). Optimal grade transition and selection of closed-loop controllers in a gas-phase olefin polymerization fluidized bed reactor. *Chemical Engineering Science*, 58 (16), 3643-3658.
- Cheng W.T., Li H.C. and Huang C.N. (2008). Simulation and optimization of silicon thermal CVD through CFD integrating Taguchi method. *Chemical Engineering Journal*, 137, 603-613.
- Chiang K-T. (2005). Optimization of the design parameters of Parallel-Plain Fin heat sink module cooling phenomenon based on the Taguchi method. *International Communications in Heat and Mass Transfer*, 32, 1193-1201.

- Cutler C.R. and Perry R.T. (1983). Real time optimization with multivariable control is required to maximize profits. *Computers and Chemical Engineering*, 7 (5), 663-667.
- Darby M.L. and White D.C. (1988). Online optimization of complex process units. *Chemical Engineering Progress*, 84, 51-59.
- Dimitriadis D., Shah N. and Pantelides C.C. (1997). RTN-based rolling horizon algorithms for medium term scheduling of multipurpose plants. *Computers and Chemical Engineering*, 21, S1061–S1066.
- Downs J.J. and Vogel E.F. (1993). A plant-wide industrial process control problem. *Computers and Chemical Engineering*, 17 (3), 245-255.
- Engin A.B. Ozdemir O., Turan M. and Turan A.Z. (2008). Color removal from textile dyebath effluents in a zeolite fixed bed reactor: Determination of optimum process conditions using Taguchi method. *Journal of Hazardous Materials*, 348-353.
- Ferrer-Nadal S., Yélamos-Ruiz I., Graells M. and Puigjaner, L. (2007). An integrated framework for on-line supervised optimization. *Computers and Chemical Engineering*, 31 (5-6), 401-409.
- Floudas C.A. and Lin X. (2004). Continuous-time versus discrete-time approaches for scheduling of chemical processes: A review. *Computers and Chemical Engineering*, 28(11), 2109-2129.
- Forsgren A., Gill P. and Wright M. (2002). Interior methods for nonlinear optimization. *SIAM Review*, 44 (4), 525-597.
- Gaikwad S. and Rivera D. (1996). Control-relevant input signal design for multivariable system identification: Application to high-purity distillation. In the *Proceedings of the 13th IFAC World Congress*, 349-354.

- Gani R., Sorensen E.L. and Perregaard J. (1992), Design and analysis of chemical processes through DYNsim. *Industrial and Engineering Chemistry Research*, 31 (1), 244-254.
- Gill P.E., Murray W. and Saunders M.A. (2005). SNOPT: An SQP algorithm for large-scale constrained optimization. *SIAM Review*, 47 (1), 99-131.
- Gill P.E., Murray W., Saunders M.A. (1998). SNOPT: An SQP algorithm for large-scale constrained optimization, Technical report, Stanford University, USA.
- Godfrey K. (1993). Perturbation signals for system identification. London: Prentice Hall.
- Gonzales R. and Ferrer J.M. (2006), "First-principles dynamic simulation, worth for control engineers? – Depropanizer case study." In the *Proceedings of the Chemical Process Control 7*, Lake Louise, Canada.
- GPSA (2004). GPSA Engineering databook. Gas Processors Supplier Association (*Electronic Version*). Tulsa, USA.
- Grossmann I. (2005). Enterprise-wide optimization: A new frontier in process systems engineering. *AIChE Journal*, 51 (7), 1846-1857.
- Grossmann I.E., Van den Heever S.A. and Harjunkski I. (2002). Discrete optimization methods and their role in the integration of planning and scheduling. *AIChE Symposium Series*, 98, 150.
- Harjunkski I., Nyström R. and Horch A. (2009). Integration of scheduling and control – theory or practice? *Computers and Chemical Engineering*, In Press. doi:10.1016/j.compchemeng.2009.06.016.
- Helbig A, Abel O. and Marquardt W. (2000). Structural concepts for optimization based control of transient processes. In: F. Allgöwer and A. Zheng, Editors, *Progress in Systems and Control Theory*, 26, Birkhauser Verlag, Basel.

- Holl P., Marquardt W. and Gilles E.D. (1988). DIVA - a powerful tool for dynamic process simulation. *Computers and Chemical Engineering*, 12 (5), 421-426.
- Huang H. and Riggs J B. (2002). Comparison of PI and MPC for control of a gas recovery unit. *Journal of Process Control*, 12 (1), 163-173.
- Jockenhövel T., Biegler L.T. and Wächter A. (2003). Dynamic optimization of the Tennessee Eastman process using the OptControlCentre. *Computers and Chemical Engineering*, 27 (11), 1513-1531.
- Kadam J.V., Marquardt W., Srinivasan B. and Bonvin D. (2007). Optimal grade transition in industrial polymerization processes via NCO tracking. *AIChE Journal*, 53 (3), 627-639.
- Kadam J.V., Schlegel M., Marquardt W., Tousain R.L., van Hessem D. H. and van den Berg J. (2002). A two-level strategy of integrated dynamic optimization and control of industrial processes: A case study. *Computer Aided Chemical Engineering*, 10, 511-516.
- Kailath T. (1980). Linear systems. Englewood Cliffs, NJ: Prentice-Hall.
- Kallrath J. (2000). Mixed integer optimization in the chemical process industry: Experience, potential and future perspectives. *Chemical Engineering Research and Design*, 78 (6), 809-822.
- Kallrath J. (2002). Planning and scheduling in the process industry. *OR Spectrum*, 24 (3), 219-250.
- Kameswaran S. and Biegler L.T. (2006). Simultaneous dynamic optimization strategies: Recent advances and challenges. *Computers and Chemical Engineering*, 30 (10-12), 1560-1575.
- Kelly J.D. (2004). Formulating production planning models. *Chemical Engineering Progress*, 100 (1), 43-50.

- Khaledi R. and Young B.R. (2005). Modeling and model predictive control of composition and conversion in an ETBE reactive distillation column. *Industrial and Engineering Chemistry Research*, 44 (9), 3134-3145.
- Knapp H. (1982). Vapor-liquid equilibria for mixtures of low boiling substances. DECHEMA Chemistry Data Series. Frankfurt: Scholium Int.
- Kröner A., Holl P., Marquardt W. and Gilles E.D. (1990). DIVA: an Open Architecture for Dynamic Simulation. *Computers and Chemical Engineering*, 14 (11), 1289-1295.
- Lang Y. and Biegler L.T. (2007). A software environment for simultaneous dynamic optimization. *Computers and Chemical Engineering*, 31 (8), 931-942.
- Lee K. and Kim J. (2000). Controller gain tuning of a simultaneous multi-axis PID control system using the Taguchi method. *Control Engineering Practice*, 8, 949-958.
- Lee J.H. and Ricker N.L. (1994). Extended Kalman Filter Based Nonlinear Model Predictive Control. *Industrial and Engineering Chemistry Research*, 33, 1530-1541
- Lin X, Floudas C.A., Modi S and Juhasz N.M. (2002). Continuous-time optimization approach for medium-range production scheduling of a multiproduct batch plant. *Industrial and Engineering Chemistry Research*, 41, 3884- 3906.
- Mantelli V., Racheli M., Bordieri R., Aloï N, Trivella F. and Masiello A. (2005), Integration of dynamic simulation and APC: a CDU/VDU case study. In the *Proceedings of the European Refining Technology Conference (ERTC)*, Budapest, Hungary.
- Maravelias C.T. and Sung C. (2009). Integration of production planning and scheduling: Overview, challenges and opportunities. *Computers and Chemical Engineering*, In Press, doi:10.1016/j.compchemeng.2009.06.007.

- Méndez C.A., Cerdá, J., Grossmann I.E., Harjunkski I. and Fahl, M. (2006). State-of-the-art review of optimization methods for short-term scheduling of batch processes. *Computers and Chemical Engineering*, 30 (6-7), 913-946.
- Moro L.F.L. (2003). Process technology in the petroleum refining industry - current situation and future trends. *Computers and Chemical Engineering*, 27 (8-9), 1303-1305.
- NaturalGas.org (2009). Available online at <http://www.naturalgas.org>. Last accessed: 8 August 2009.
- Nyström R.H., Harjunkski I. and Kroll A. (2006). Production optimization for continuously operated processes with optimal operation and scheduling of multiple units. *Computers and Chemical Engineering*, 30 (3), 392-406.
- Pannocchia G., Gallinelli L., Brambilla A., Marchetti G. and Trivella F. (2006), Rigorous simulation and model predictive control of a crude distillation unit. In the *Proceedings of the Advances in Chemical Engineering (ADCHEM)*, Gramado, Brazil.
- Papageorgiou L.G. and Pantelides C.C. (1996). Optimal campaign planning-scheduling of multipurpose batch/semicontinuous plants. I. Mathematical formulation. *Industrial and Engineering Chemistry Research*, 35 (2), 488-509.
- Peng D.Y. and Robinson D.B. (1976). A new two-constant equation of state. *Industrial and Engineering Chemistry: Fundamentals*, 15 (1), 59-64.
- Perregaard J., Pedersen B.S. and Gani R. (1992). Steady state and dynamic simulation of complex chemical processes. *Chemical Engineering Research and Design*, 70 (A2), 99-109.
- Pinto J.M., Joly M. and Moro L.F.L. (2000). Planning and scheduling models for refinery operations. *Computers and Chemical Engineering*, 24 (9-10), 2259-2276.

- Pistikopoulos E.N. (1995). Uncertainty in process design and operations. *Computers and Chemical Engineering*, 19 (1), 553-563.
- Poling B.E., Prausnitz J.M. and O'Connell J.P. (2001). *The Properties of Gases and Liquids*. New York: McGraw-Hill.
- Prata A., Oldenburg, J., Kroll, A., and Marquardt, W. (2008). Integrated scheduling and dynamic optimization of grade transitions for a continuous polymerization reactor. *Computers and Chemical Engineering*, 32 (3), 463-476.
- Qin S.J. and Badgwell T. A. (2003). A survey of industrial model predictive control technology. *Control Engineering Practice*, 11 (7), 733-764.
- Rao C.V and Rawlings J.B. (1999). Steady states and constraints in model predictive control. *AIChE Journal*, 45 (6), 1266-1278.
- Roy R.K. (1990). *A Primer of Taguchi Method*. New York: van Nostrand Reinhold
- Sandler S.I. (1999). *Chemical and Engineering Thermodynamics*. New York: Wiley.
- Schad R. (1998). Make the most of process simulation. *Chemical Engineering Progress*, 94 (1), 21.
- Schlegel M. and Marquardt W. (2004). Direct sequential dynamic optimization with automatic switching structure detection. In the *Proceedings of the DYCOPS*, Cambridge, USA.
- Schlegel M. and Marquardt, W. (2006). Detection and exploitation of the control switching structure in the solution of dynamic optimization problems. *Journal of Process Control*, 16 (3), 275-290.
- Schlegel M., Marquardt W., Ehrig R. and Nowak U. (2004). Sensitivity analysis of linearly-implicit differential-algebraic systems by one-step extrapolation. *Applied Numerical Mathematics*, 48 (1), 83-102.

- Seborg D.E, Edgar T.F. and Mellichamp D.A. (2004). Process dynamics and control. New Jersey: Wiley.
- Sentoni G.B., Biegler L.T., Guiver J.B. and Zhao H. (1998). State-space nonlinear process modeling: Identification and universality. *AIChE Journal*, 44 (10), 2229-2239.
- Shah N. (2005). Process industry supply chains: Advances and challenges. *Computers and Chemical Engineering*, 29 (6), 1225-1236.
- Shah N. and Pantelides C.C. (1991). Optimal long-term campaign planning and design of batch operations. *Industrial and Engineering Chemistry Research*, 30 (10), 2308-2321.
- Shobrys D.E. and White D.C. (2000). Planning, scheduling and control systems: Why can they not work together? *Computers and Chemical Engineering*, 24, 163-173.
- Sorensen E.L, Johansen H., Gani R. and Fredenslund A. (1990). Dynamic simulator for design and analysis of chemical processes. In the *Proceedings of the European Symposium on Computer Applications in Chemical Engineering (ComChem)*, 13-18.
- Srinivasan B., Bonvin D., Visser E. and Palanki, S. (2003). Dynamic optimization of batch processes: II. Role of measurements in handling uncertainty. *Computers and Chemical Engineering*, 27 (1), 27-44.
- Stadtler H. (2005). Supply chain management and advanced planning - basics, overview and challenges. *European Journal of Operational Research*, 163 (3), 575-588.
- Svrcek W.Y., Mahoney D.P. and Young B.R. (2006). A real-time approach to process control. New York: Wiley.
- Taguchi G. and Konishi S. (1987). Orthogonal Arrays and Linear Graphs. Dearborn: American Supplier Institute, Inc.

- Tatjewski P. (2008). Advanced control and on-line process optimization in multilayer structures. *Annual Reviews in Control*, 32 (1), 71-85.
- Terrazas-Moreno S., Flores-Tlacuahuac A. and Grossmann, I.E. (2007). Simultaneous design, scheduling, and optimal control of a methyl-methacrylate continuous polymerization reactor. *AIChE Journal*, 54 (12), 3160-3170.
- Tousain R.L. (2002). Dynamic optimization in business-wide process control. *PhD Thesis*, Delft University of Technology, the Netherlands.
- Tousain R.L. and Bosgra O.H. (2006). Market-oriented scheduling and economic optimization of continuous multi-grade chemical processes. *Journal of Process Control*, 16, 291-302.
- van den Heever S.A. and Grossmann I.E. (2003). A strategy for the integration of production planning and reactive scheduling in the optimization of a hydrogen supply network. *Computers and Chemical Engineering*, 27 (12), 1813-1839.
- van der Schot J.J., Tousain R.L., Backx A.C.P.M. and Bosgra O.H. (1999). SSQP for the solution of large-scale dynamic-economic optimization problems, *Computers and Chemical Engineering Supplement*, S507-S510.
- Varma V.A., Reklaitis G.V., Blau G.E. and Pekny J.F. (2007). Enterprise-wide modeling and optimization - An overview of emerging research challenges and opportunities. *Computers and Chemical Engineering*, 31 (5-6), 692-711.
- Wächter A. (2002). An interior point algorithm for large-scale nonlinear optimization with applications in process engineering, *PhD Thesis*, Carnegie Mellon University, USA.
- Wächter A. and Biegler L.T. (2006). On the implementation of an interior-point filter line-search algorithm for large-scale nonlinear programming. *Mathematical Programming*, 106 (1), 25-57.

- Yang K., Teo E-C. and Fuss F.K. (2007). Application of Taguchi method in optimization of cervical ring cage. *Journal of Biomechanics*, 3251-3256.
- Ying C-M and Joseph B. (1999). Performance and stability analysis of LP-MPC and QP-MPC cascade control systems. *AIChE Journal*, 45(7), 1521-1534.
- Yip W.S. and Marlin T.E. (2004). The effect of model fidelity on real-time optimization performance. *Computers and Chemical Engineering*, 28 (1-2), 267-280.
- Zanin A.C., de Gouvêa M.T. and Odloak, D (2002). Integrating real-time optimization into the model predictive controller of the FCC system. *Control Engineering Practice*, 10 (8), 819-831.
- Zanin A.C., de Gouvêa M.T. and Odloak, D. (2000). Industrial implementation of a real-time optimization strategy for maximizing production of LPG in a FCC unit. *Computers and Chemical Engineering*, 24 (2-7), 525-531.

APPENDIX A

PENG-ROBINSON EQUATION OF STATE (EOS)

The Peng and Robinson (1976) EOS relating pressure (P), molar volume (v) and temperature (T) of a pure component is written as:

$$P = \frac{RT}{v-b} - \frac{a(T)}{v(v+b)+b(v-b)}$$

or when rewritten in the form of cubic equation to be solved:

$$Z^3 - (1-B)Z^2 + (A-3B^2-2B)Z - (AB-B^2-B^3) = 0$$

where

$$A = \frac{aP}{(RT)^2}$$

$$B = \frac{bP}{RT}$$

$$Z = \frac{Pv}{RT}$$

with

$$a(T) = a(T_c) \cdot \alpha(T_r, \omega)$$

$$a(T_c) = 0.45724 \frac{(RT_c)^2}{P_c}$$

$$b(T_c) = 0.07780 \frac{RT_c}{P_c}$$

$$\alpha^{1/2} = 1 + \kappa(1 - T_r^{1/2})$$

where R is the universal gas constant at appropriate unit; T_r is the reduced temperature and κ is the characteristic constant for the pure component defined as:

$$T_r = T/T_c$$

$$\kappa = 0.37464 + 1.54226\omega - 0.26992\omega^2$$

The values of acentric factor (ω) of all components studied here may be obtained from, e.g., Poling et al. (2001).

For a mixture containing C number of components, the parameters a and b are obtained from the following mixing and combining rules:

$$a = \sum_{i=1}^C \sum_{j=1}^C x_i x_j a_{ij}$$

$$b = \sum_{i=1}^C x_i b_i$$

$$a_{ij} = (1 - \delta_{ij})(a_i a_j)^{1/2}$$

where $a_{ii}=a_i$ and b_i are the parameters and x_i is the mole fraction for pure component i . The binary interaction parameter (δ_{ij}) is nonzero only when $i \neq j$. Values of δ_{ij} are available at, e.g., Knapp (1982).

At vapor-liquid equilibrium, the fugacity (f_i) for component i must be equal in both phases (for e.g., Sandler, 1999). For Peng-Robinson EOS, the fugacity can be calculated from:

$$\ln \frac{f_i}{x_i P} = \frac{B_i}{B} (Z-1) - \ln(Z-B) - \frac{A}{2\sqrt{2}B} \left(\frac{2 \sum_j x_j A_{ij}}{A} - \frac{B_i}{B} \right) \ln \left(\frac{Z+(1+\sqrt{2})B}{Z+(1-\sqrt{2})B} \right)$$

Another important thermodynamic property is the molar enthalpy, which is used to solve material and energy balances simultaneously. The enthalpy (H) departure from that of an ideal gas (H^{IG}) is:

$$H - H^{IG} = RT(Z-1) + \frac{T}{2\sqrt{2}b} \frac{da}{dT} - a \ln \left(\frac{Z+(1+\sqrt{2})B}{Z+(1-\sqrt{2})B} \right)$$

APPENDIX B **ADDITIONAL RESULTS FROM CHAPTER 5**

Table B.1: Values of optimization variables for Case A

Var.	Unit	Case Study		Description
		Base	RTO	
u_1	ton/h	224.3	197.9	Flow of sales gas to coldbox E-101
u_2	°C	-40.0	-39.1	Temperature of feed gas exiting cooler E-102
u_3	ton/h	170.6	139.2	Flow of sales gas to coldbox E-103
u_4	ton/h	34.5	18.8	Flow of PG to GSP section
u_5	ton/h	194.1	209.8	Flow of PG to turboexpander KT-101
u_6	°C	5.0	0.4	Temperature of demethanizer C-101 tray 35
u_7	°C	-80.9	-70.0	Temperature of PG exiting coldbox E-105

Table B.2: Values of constraint variables for Case A

Variable	Unit	Case Study		Description
		Base	RTO	
c_1	ton/h	280.0	280.0	Flow of mixed feed gas
c_2	MJ/m ³	38.1	38.3	Gross heating value of sales gas
c_3	-	0.57	0.57	Specific gravity of sales gas
c_4	mol%	246.4	161.0	Carbon dioxide content in sales gas
c_5	ton/h	225.1	228.6	Flow of sales gas
c_6	bar	33.5	33.5	Pressure of sales gas
c_7	°C	35.6	33.4	Temperature of sales gas
c_8	kW/°C	1443	1098	Coldbox E-101 capacity
c_9	°C	8.3	10.9	Coldbox E-101 LMTD
c_{10}	kW/°C	347	283	Coldbox E-103 capacity
c_{11}	°C	13.4	15.2	Coldbox E-103 LMTD
c_{12}	kW/°C	136	34.4	Coldbox E-105 capacity
c_{13}	°C	18.7	22.6	Coldbox E-105 log LMTD
c_{14}	kW	3291	2954	Cooler E-102 duty
c_{15}	kW	4294	3359	Demethanizer C-101 reboiler duty
c_{16}	kW	2234	2465	Turboexpander KT-101 duty
c_{17}	kW	4661	4192	Compressor K-102 duty
c_{18}	kW	27.7	25.9	Pump P-101 duty
c_{19}	kW	8.9	7.6	Pump P-102 duty
c_{20}	%	60.0	47.7	Flooding at Section 1 of demethanizer
c_{21}	%	52.3	41.6	Flooding at Section 2 of demethanizer
c_{22}	%	46.6	35.9	Flooding at Section 3 of demethanizer
c_{23}	%	69.2	47.0	Flooding at Section 4 of demethanizer
c_{24}	%	30.9	28.9	DC backup at Section 1 of demethanizer
c_{25}	%	30.6	28.8	DC backup at Section 2 of demethanizer
c_{26}	%	33.8	31.8	DC backup at Section 3 of demethanizer
c_{27}	%	40.1	35.6	DC backup at Section 4 of demethanizer
c_{28}	%	67.9	71.7	Flooding in absorber C-102
c_{29}	%	17.6	17.2	DC backup in absorber C-102
c_{30}	°C	12.0	8.4	Air cooler LMTD
c_{31}	-	1.00	0.98	Fraction of PG to expander over that to JT valve
c_{32}	-	1.00	0.61	Fraction of sales gas to coldbox E-101
c_{33}	-	0.76	0.87	Fraction of sales gas to coldbox E-103
c_{34}	-	0.151	0.081	Ratio of PG to gas subcooled process section

Note: PG=processed gas; GSP=gas subcooled process; LMTD=log mean temperature difference; JT=Joule-Thompson; DC=downcomer

Table B.3: Values of optimization variables for Case B

Var.	Unit	Case Study		Description
		Base	RTO	
u_1	ton/h	183.3	192.0	Flow of sales gas to coldbox E-101
u_2	°C	-30.6	-30.2	Temperature of feed gas exiting cooler E-102
u_3	ton/h	120.6	120.6	Flow of sales gas to coldbox E-103
u_4	ton/h	1.2	9.0	Flow of PG to GSP section
u_5	ton/h	246.4	161.0	Flow of PG to turboexpander KT-101
u_6	°C	5.0	15.2	Temperature of demethanizer C-101 tray 35
u_7	°C	-70.0	-70.0	Temperature of PG exiting coldbox E-105

Table B.4: Values of constraint variables for Case B

Variable	Unit	Case Study		Description
		Base	RTO	
c_1	ton/h	280.0	280.0	Flow of mixed feed gas
c_2	MJ/m ³	38.8	39.2	Gross heating value of sales gas
c_3	-	0.58	0.59	Specific gravity of sales gas
c_4	mol%	0.002	0.002	Carbon dioxide content in sales gas
c_5	ton/h	235.4	241.1	Flow of sales gas
c_6	bar	33.5	33.5	Pressure of sales gas
c_7	°C	28.5	32.2	Temperature of sales gas
c_8	kW/°C	1024	1707	Coldbox E-101 capacity
c_9	°C	10.0	6.0	Coldbox E-101 LMTD
c_{10}	kW/°C	258	155	Coldbox E-103 capacity
c_{11}	°C	15.5	17.0	Coldbox E-103 LMTD
c_{12}	kW/°C	0.7	113.6	Coldbox E-105 capacity
c_{13}	°C	28.2	5.0	Coldbox E-105 log LMTD
c_{14}	kW	1715	1588	Cooler E-102 duty
c_{15}	kW	2525	2362	Demethanizer C-101 reboiler duty
c_{16}	kW	2850	1935	Turboexpander KT-101 duty
c_{17}	kW	2859	3957	Compressor K-102 duty
c_{18}	kW	15.8	13.8	Pump P-101 duty
c_{19}	kW	10.5	8.4	Pump P-102 duty
c_{20}	%	31.2	26.4	Flooding at Section 1 of demethanizer
c_{21}	%	28.4	25.0	Flooding at Section 2 of demethanizer
c_{22}	%	29.1	26.5	Flooding at Section 3 of demethanizer
c_{23}	%	40.1	43.5	Flooding at Section 4 of demethanizer
c_{24}	%	30.8	28.6	DC backup at Section 1 of demethanizer
c_{25}	%	31.7	29.5	DC backup at Section 2 of demethanizer
c_{26}	%	35.4	33.6	DC backup at Section 3 of demethanizer
c_{27}	%	41.1	40.9	DC backup at Section 4 of demethanizer
c_{28}	%	72.3	70.7	Flooding in absorber C-102
c_{29}	%	16.9	16.9	DC backup in absorber C-102
c_{30}	°C	5.4	6.2	Air cooler LMTD
c_{31}	-	1.00	0.66	Fraction of PG to expander over that to JT valve
c_{32}	-	0.51	0.50	Fraction of sales gas to coldbox E-101
c_{33}	-	0.78	0.80	Fraction of sales gas to coldbox E-103
c_{34}	-	0.005	0.035	Ratio of PG to gas subcooled process section

Note: PG=processed gas; GSP=gas subcooled process; LMTD=log mean temperature difference; JT=Joule-Thompson; DC=downcomer

Table B.5: Values of optimization variables for Case C

Var.	Unit	Case Study		Description
		Base	RTO	
u_1	ton/h	207.2	178.8	Flow of sales gas to coldbox E-101
u_2	°C	-40.0	-41.8	Temperature of feed gas exiting cooler E-102
u_3	ton/h	154.4	120.4	Flow of sales gas to coldbox E-103
u_4	ton/h	34.5	11.3	Flow of PG to GSP section
u_5	ton/h	169.6	191.2	Flow of PG to turboexpander KT-101
u_6	°C	5.0	3.2	Temperature of demethanizer C-101 tray 35
u_7	°C	-80.9	-80.9	Temperature of PG exiting coldbox E-105

Table B.6: Values of constraint variables for Case C

Variable	Unit	Case Study		Description
		Base	RTO	
c_1	ton/h	250.0	250.0	Flow of mixed feed gas
c_2	MJ/m ³	38.0	38.6	Gross heating value of sales gas
c_3	-	0.57	0.58	Specific gravity of sales gas
c_4	mol%	0.001	0.002	Carbon dioxide content in sales gas
c_5	ton/h	200.5	213.9	Flow of sales gas
c_6	bar	33.5	33.5	Pressure of sales gas
c_7	°C	34.2	32.2	Temperature of sales gas
c_8	kW/°C	1243.5	1032.5	Coldbox E-101 capacity
c_9	°C	8.6	10.3	Coldbox E-101 LMTD
c_{10}	kW/°C	313.8	243.3	Coldbox E-103 capacity
c_{11}	°C	13.2	14.6	Coldbox E-103 LMTD
c_{12}	kW/°C	134.9	34.1	Coldbox E-105 capacity
c_{13}	°C	18.8	19.2	Coldbox E-105 log LMTD
c_{14}	kW	2931	3536	Cooler E-102 duty
c_{15}	kW	3984	2947	Demethanizer C-101 reboiler duty
c_{16}	kW	1952	2201	Turboexpander KT-101 duty
c_{17}	kW	4219	3899	Compressor K-102 duty
c_{18}	kW	25.1	23.0	Pump P-101 duty
c_{19}	kW	8.6	6.2	Pump P-102 duty
c_{20}	%	56.9	42.4	Flooding at Section 1 of demethanizer
c_{21}	%	49.3	36.8	Flooding at Section 2 of demethanizer
c_{22}	%	44.6	31.6	Flooding at Section 3 of demethanizer
c_{23}	%	65.4	42.4	Flooding at Section 4 of demethanizer
c_{24}	%	30.3	27.1	DC backup at Section 1 of demethanizer
c_{25}	%	29.9	26.8	DC backup at Section 2 of demethanizer
c_{26}	%	32.6	30.1	DC backup at Section 3 of demethanizer
c_{27}	%	38.2	33.6	DC backup at Section 4 of demethanizer
c_{28}	%	66.5	65.1	Flooding in absorber C-102
c_{29}	%	17.6	16.6	DC backup in absorber C-102
c_{30}	°C	11.7	7.3	Air cooler LMTD
c_{31}	-	1.00	0.99	Fraction of PG to expander over that to JT valve
c_{32}	-	0.77	0.59	Fraction of sales gas to coldbox E-101
c_{33}	-	1.00	0.84	Fraction of sales gas to coldbox E-103
c_{34}	-	0.169	0.055	Ratio of PG to gas subcooled process section

Note: PG=processed gas; GSP=gas subcooled process; LMTD=log mean temperature difference; JT=Joule-Thompson; DC=downcomer

Table B.7: Values of optimization variables for Case D

Var.	Unit	Case Study		Description
		Base	RTO	
u_1	ton/h	235.6	253.3	Flow of sales gas to coldbox E-101
u_2	°C	-38.0	-34.6	Temperature of feed gas exiting cooler E-102
u_3	ton/h	96.2	140.6	Flow of sales gas to coldbox E-103
u_4	ton/h	235.7	248.3	Flow of PG to GSP section
u_5	ton/h	34.5	22.5	Flow of PG to turboexpander KT-101
u_6	°C	5.0	0.0	Temperature of demethanizer C-101 tray 35
u_7	°C	-80.9	-70.0	Temperature of PG exiting coldbox E-105

Table B.8: Values of constraint variables for Case D

Variable	Unit	Case Study		Description
		Base	RTO	
c_1	ton/h	310.0	310.0	Flow of mixed feed gas
c_2	MJ/m ³	38.5	38.7	Gross heating value of sales gas
c_3	-	0.57	0.58	Specific gravity of sales gas
c_4	mol%	0.002	0.002	Carbon dioxide content in sales gas
c_5	ton/h	255.4	259.3	Flow of sales gas
c_6	bar	33.5	33.5	Pressure of sales gas
c_7	°C	35.7	37.1	Temperature of sales gas
c_8	kW/°C	1252	1414	Coldbox E-101 capacity
c_9	°C	11.1	9.6	Coldbox E-101 LMTD
c_{10}	kW/°C	160	250	Coldbox E-103 capacity
c_{11}	°C	14.4	14.3	Coldbox E-103 LMTD
c_{12}	kW/°C	195	82	Coldbox E-105 capacity
c_{13}	°C	14.9	14.9	Coldbox E-105 log LMTD
c_{14}	kW	2212	1200.0	Cooler E-102 duty
c_{15}	kW	3685	3180.7	Demethanizer C-101 reboiler duty
c_{16}	kW	2927	3081.5	Turboexpander KT-101 duty
c_{17}	kW	4610	4640.3	Compressor K-102 duty
c_{18}	kW	24.7	23.0	Pump P-101 duty
c_{19}	kW	9.4	8.0	Pump P-102 duty
c_{20}	%	49.7	36.8	Flooding at Section 1 of demethanizer
c_{21}	%	45.8	33.5	Flooding at Section 2 of demethanizer
c_{22}	%	40.7	30.5	Flooding at Section 3 of demethanizer
c_{23}	%	62.9	43.5	Flooding at Section 4 of demethanizer
c_{24}	%	28.8	26.8	DC backup at Section 1 of demethanizer
c_{25}	%	28.7	27.1	DC backup at Section 2 of demethanizer
c_{26}	%	32.8	30.0	DC backup at Section 3 of demethanizer
c_{27}	%	39.0	33.9	DC backup at Section 4 of demethanizer
c_{28}	%	71.8	76.2	Flooding in absorber C-102
c_{29}	%	17.7	17.5	DC backup in absorber C-102
c_{30}	°C	10.3	11.9	Air cooler LMTD
c_{31}	-	1.00	1.00	Fraction of PG to expander over that to JT valve
c_{32}	-	0.38	0.54	Fraction of sales gas to coldbox E-101
c_{33}	-	0.92	0.98	Fraction of sales gas to coldbox E-103
c_{34}	-	0.13	0.08	Ratio of PG to gas subcooled process section

Note: PG=processed gas; GSP=gas subcooled process; LMTD=log mean temperature difference; JT=Joule-Thompson; DC=downcomer

Table B.9: Values of optimization variables for Case E

Var.	Unit	Case Study		Description
		Base	RTO	
u_1	ton/h	214.6	207.5	Flow of sales gas to coldbox E-101
u_2	°C	-25.6	-20.0	Temperature of feed gas exiting cooler E-102
u_3	ton/h	167.7	189.2	Flow of sales gas to coldbox E-103
u_4	ton/h	33.2	29.6	Flow of PG to GSP section
u_5	ton/h	187.8	145.6	Flow of PG to turboexpander KT-101
u_6	°C	5.0	0.3	Temperature of demethanizer C-101 tray 35
u_7	°C	-74.7	-70.9	Temperature of PG exiting coldbox E-105

Table B.10: Values of constraint variables for Case E

Variable	Unit	Case Study		Description
		Base	RTO	
c_1	ton/h	280.0	280.0	Flow of mixed feed gas
c_2	MJ/m ³	37.7	37.9	Gross heating value of sales gas
c_3	-	0.60	0.60	Specific gravity of sales gas
c_4	mol%	0.029	0.026	Carbon dioxide content in sales gas
c_5	ton/h	213.6	213.3	Flow of sales gas
c_6	bar	33.5	33.5	Pressure of sales gas
c_7	°C	30.9	30.8	Temperature of sales gas
c_8	kW/°C	1725	1556	Coldbox E-101 capacity
c_9	°C	5.0	5.0	Coldbox E-101 LMTD
c_{10}	kW/°C	308	413	Coldbox E-103 capacity
c_{11}	°C	12.8	13.4	Coldbox E-103 LMTD
c_{12}	kW/°C	196	158	Coldbox E-105 capacity
c_{13}	°C	13.4	13.5	Coldbox E-105 log LMTD
c_{14}	kW	3351	2429	Cooler E-102 duty
c_{15}	kW	4706	2985	Demethanizer C-101 reboiler duty
c_{16}	kW	2373	1846	Turboexpander KT-101 duty
c_{17}	kW	2986	3492	Compressor K-102 duty
c_{18}	kW	31.9	31.2	Pump P-101 duty
c_{19}	kW	6.6	5.4	Pump P-102 duty
c_{20}	%	42.2	34.2	Flooding at Section 1 of demethanizer
c_{21}	%	45.5	31.3	Flooding at Section 2 of demethanizer
c_{22}	%	62.6	30.3	Flooding at Section 3 of demethanizer
c_{23}	%	60.2	39.8	Flooding at Section 4 of demethanizer
c_{24}	%	26.0	25.7	DC backup at Section 1 of demethanizer
c_{25}	%	27.3	26.7	DC backup at Section 2 of demethanizer
c_{26}	%	36.3	31.4	DC backup at Section 3 of demethanizer
c_{27}	%	37.5	33.9	DC backup at Section 4 of demethanizer
c_{28}	%	60.0	59.3	Flooding in absorber C-102
c_{29}	%	17.2	16.9	DC backup in absorber C-102
c_{30}	°C	11.0	10.8	Air cooler LMTD
c_{31}	-	1.00	0.76	Fraction of PG to expander over that to JT valve
c_{32}	-	0.78	0.89	Fraction of sales gas to coldbox E-101
c_{33}	-	1.00	0.97	Fraction of sales gas to coldbox E-103
c_{34}	-	0.15	0.13	Ratio of PG to gas subcooled process section

Note: PG=processed gas; GSP=gas subcooled process; LMTD=log mean temperature difference; JT=Joule-Thompson; DC=downcomer

Table B.11: Values of optimization variables for Case F

Var.	Unit	Case Study		Description
		Base	RTO	
u_1	ton/h	200.0	200.0	Flow of sales gas to coldbox E-101
u_2	°C	-16.0	-14.4	Temperature of feed gas exiting cooler E-102
u_3	ton/h	117.7	153.6	Flow of sales gas to coldbox E-103
u_4	ton/h	22.2	33.3	Flow of PG to GSP section
u_5	ton/h	199.9	94.7	Flow of PG to turboexpander KT-101
u_6	°C	5.0	0.0	Temperature of demethanizer C-101 tray 35
u_7	°C	-67.5	-52.0	Temperature of PG exiting coldbox E-105

Table B.12: Values of constraint variables for Case F

Variable	Unit	Case Study		Description
		Base	RTO	
c_1	ton/h	280.0	280.0	Flow of mixed feed gas
c_2	MJ/m ³	39.2	39.8	Gross heating value of sales gas
c_3	-	0.60	0.61	Specific gravity of sales gas
c_4	mol%	0.009	0.010	Carbon dioxide content in sales gas
c_5	ton/h	210.4	216.9	Flow of sales gas
c_6	bar	33.5	33.5	Pressure of sales gas
c_7	°C	29.5	31.2	Temperature of sales gas
c_8	kW/°C	332	453	Coldbox E-101 capacity
c_9	°C	16.1	11.8	Coldbox E-101 LMTD
c_{10}	kW/°C	235	295	Coldbox E-103 capacity
c_{11}	°C	13.7	12.5	Coldbox E-103 LMTD
c_{12}	kW/°C	230	66	Coldbox E-105 capacity
c_{13}	°C	6.7	15.1	Coldbox E-105 log LMTD
c_{14}	kW	3229	2733	Cooler E-102 duty
c_{15}	kW	3874	3594	Demethanizer C-101 reboiler duty
c_{16}	kW	2833	1341	Turboexpander KT-101 duty
c_{17}	kW	2366	4119	Compressor K-102 duty
c_{18}	kW	34.3	31.2	Pump P-101 duty
c_{19}	kW	5.0	3.5	Pump P-102 duty
c_{20}	%	31.7	25.1	Flooding at Section 1 of demethanizer
c_{21}	%	31.6	25.1	Flooding at Section 2 of demethanizer
c_{22}	%	27.9	22.7	Flooding at Section 3 of demethanizer
c_{23}	%	46.5	35.1	Flooding at Section 4 of demethanizer
c_{24}	%	24.5	23.1	DC backup at Section 1 of demethanizer
c_{25}	%	25.5	24.3	DC backup at Section 2 of demethanizer
c_{26}	%	31.3	29.9	DC backup at Section 3 of demethanizer
c_{27}	%	35.9	33.3	DC backup at Section 4 of demethanizer
c_{28}	%	58.8	56.6	Flooding in absorber C-102
c_{29}	%	16.6	16.4	DC backup in absorber C-102
c_{30}	°C	2.9	5.7	Air cooler LMTD
c_{31}	-	1.00	0.50	Fraction of PG to expander over that to JT valve
c_{32}	-	0.56	0.71	Fraction of sales gas to coldbox E-101
c_{33}	-	0.95	0.92	Fraction of sales gas to coldbox E-103
c_{34}	-	0.10	0.15	Ratio of PG to gas subcooled process section

Note: PG=processed gas; GSP=gas subcooled process; LMTD=log mean temperature difference; JT=Joule-Thompson; DC=downcomer

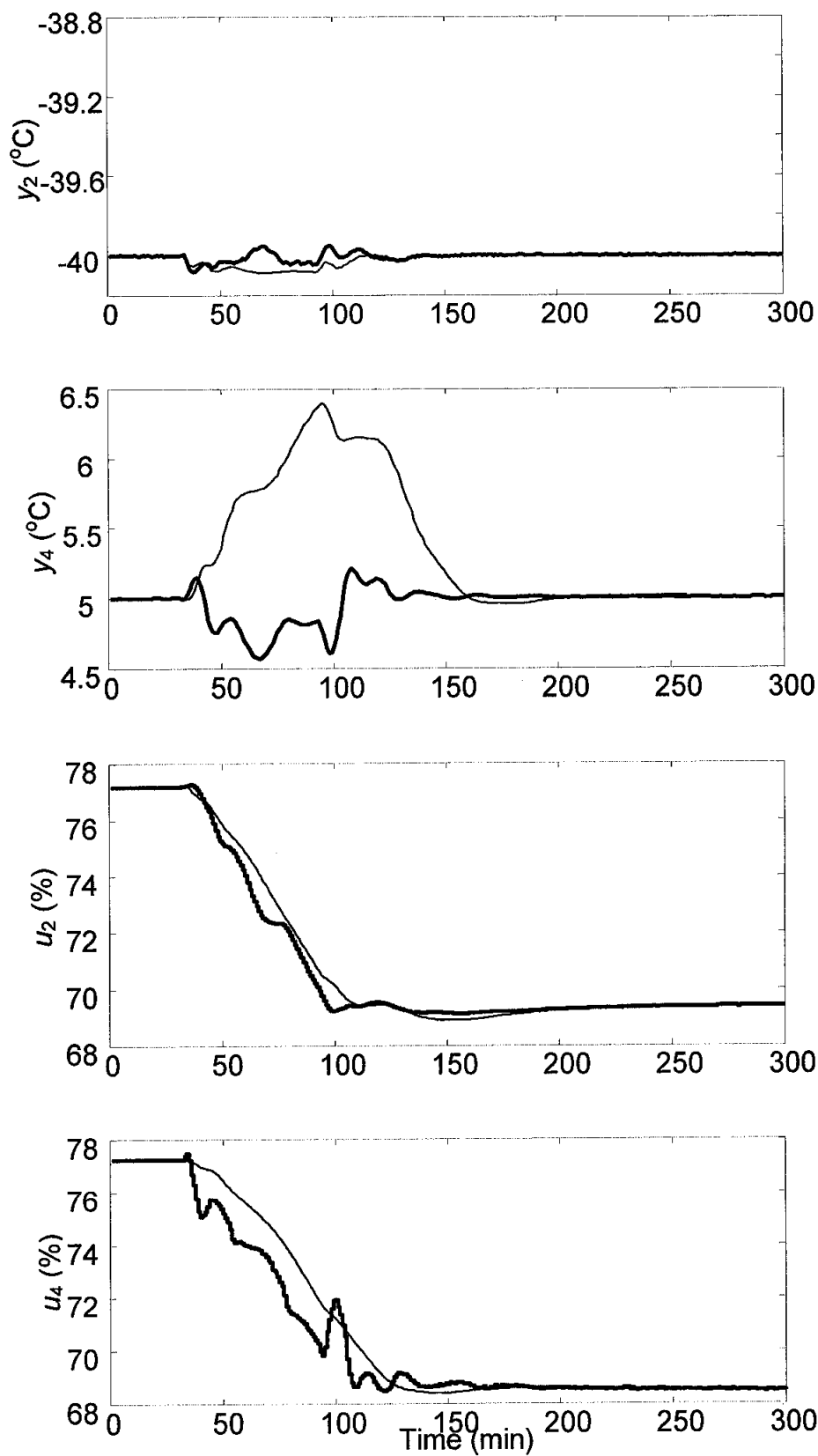


Figure B.1: Closed-loop responses of PI (thin line) and MPC (thick line) controllers on temperature of feed gas stream exiting cooler E-102 (y_2) and temperature of demethanizer C-101 tray 35 (y_4) for Cases C1 and C2 (scheduling only); u_2 =cooler E-102 duty in %; u_4 =reboiler E-104 duty in %

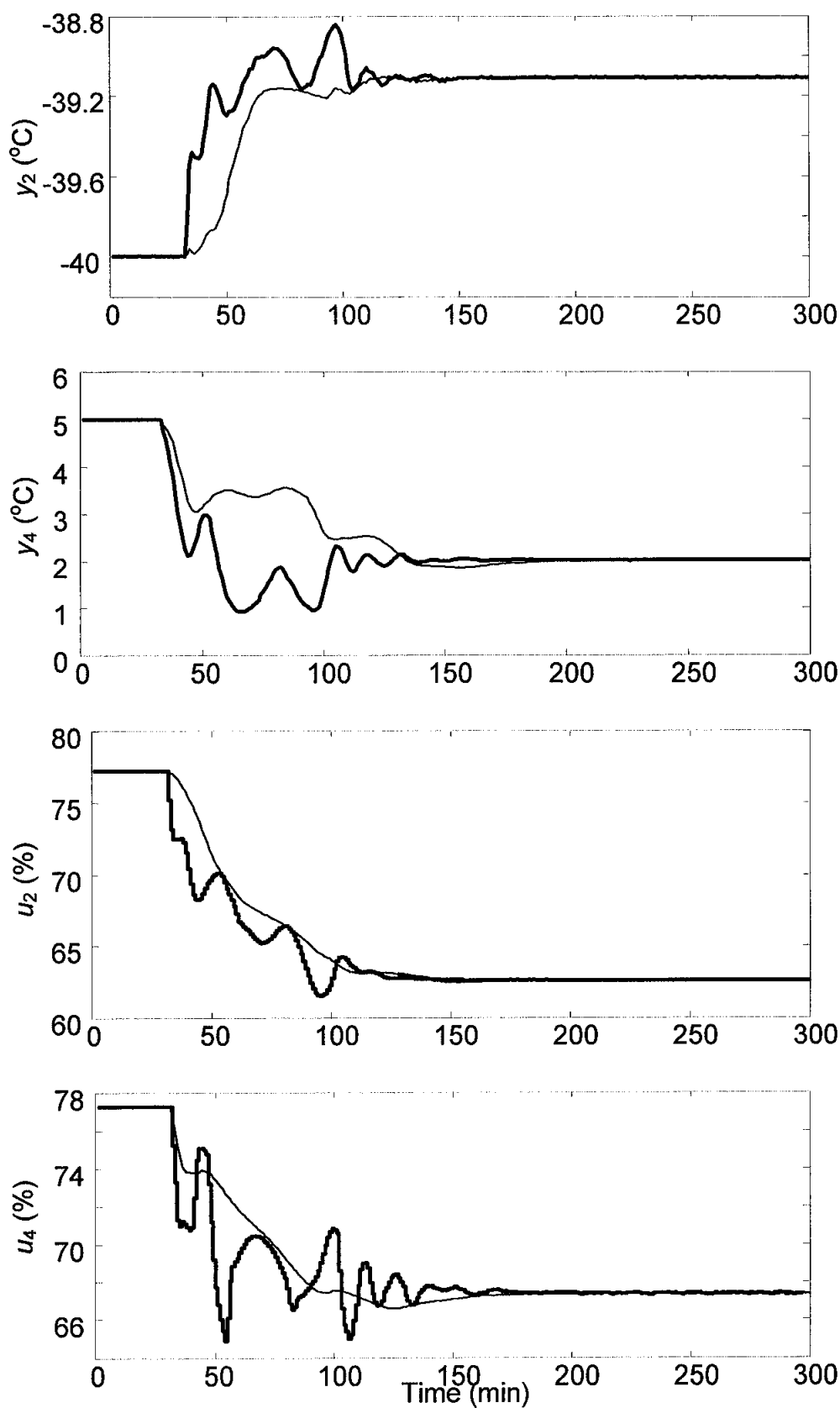


Figure B.2: Closed-loop responses of PI (thin line) and MPC (thick line) controllers on temperature of feed gas stream exiting cooler E-102 (y_2) and temperature of demethanizer C-101 tray 35 (y_4) for Cases C3 and C4 (integrated approach); u_2 =cooler E-102 duty in %; u_4 =reboiler E-104 duty in %

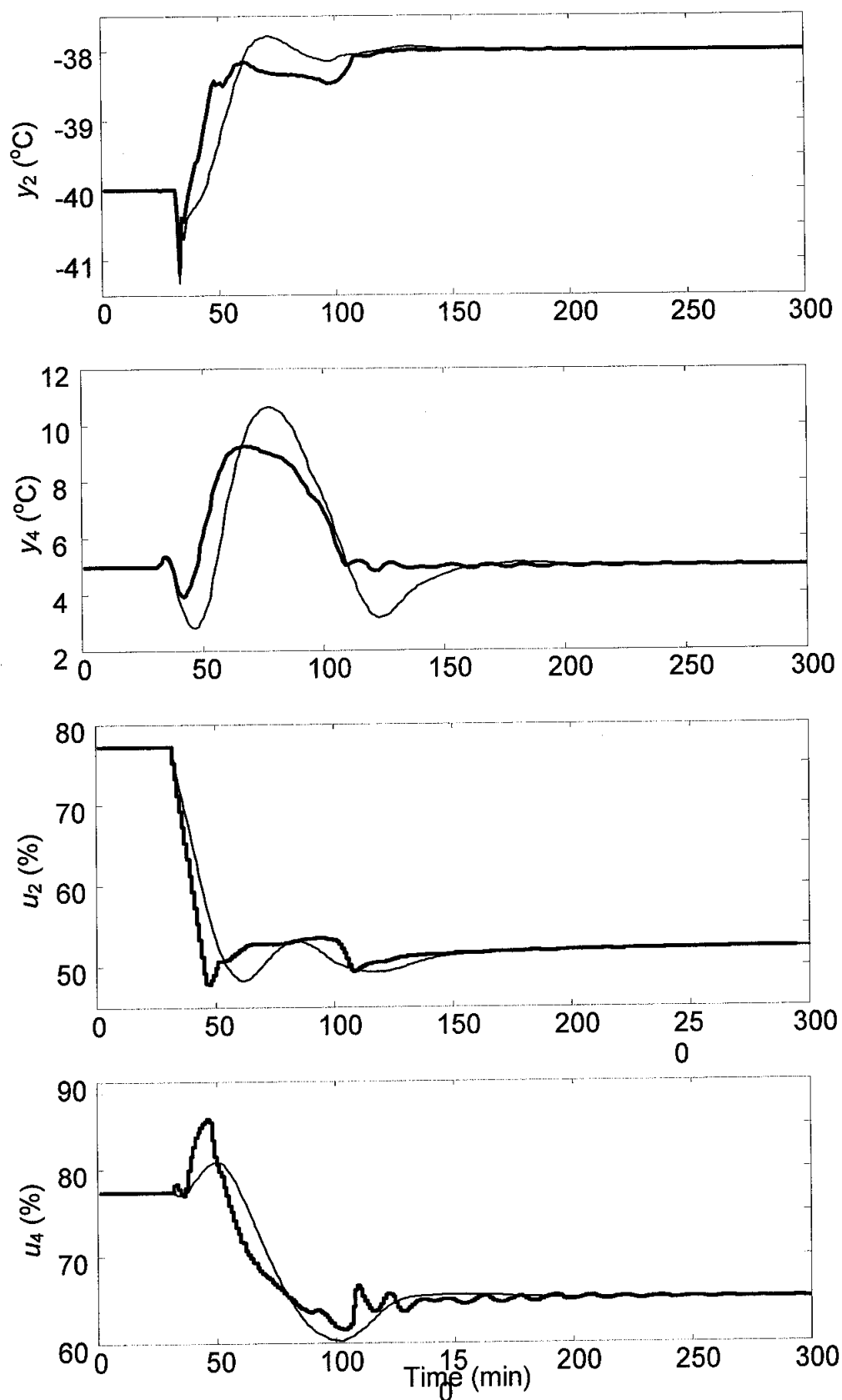


Figure B.3: Closed-loop responses of PI (thin line) and MPC (thick line) controllers on temperature of feed gas stream exiting cooler E-102 (y_2) and temperature of demethanizer C-101 tray 35 (y_4) for Cases D1 and D2 (scheduling only); E-102Q=cooler E-102 duty in %; E-104Q=reboiler E-104 duty in %

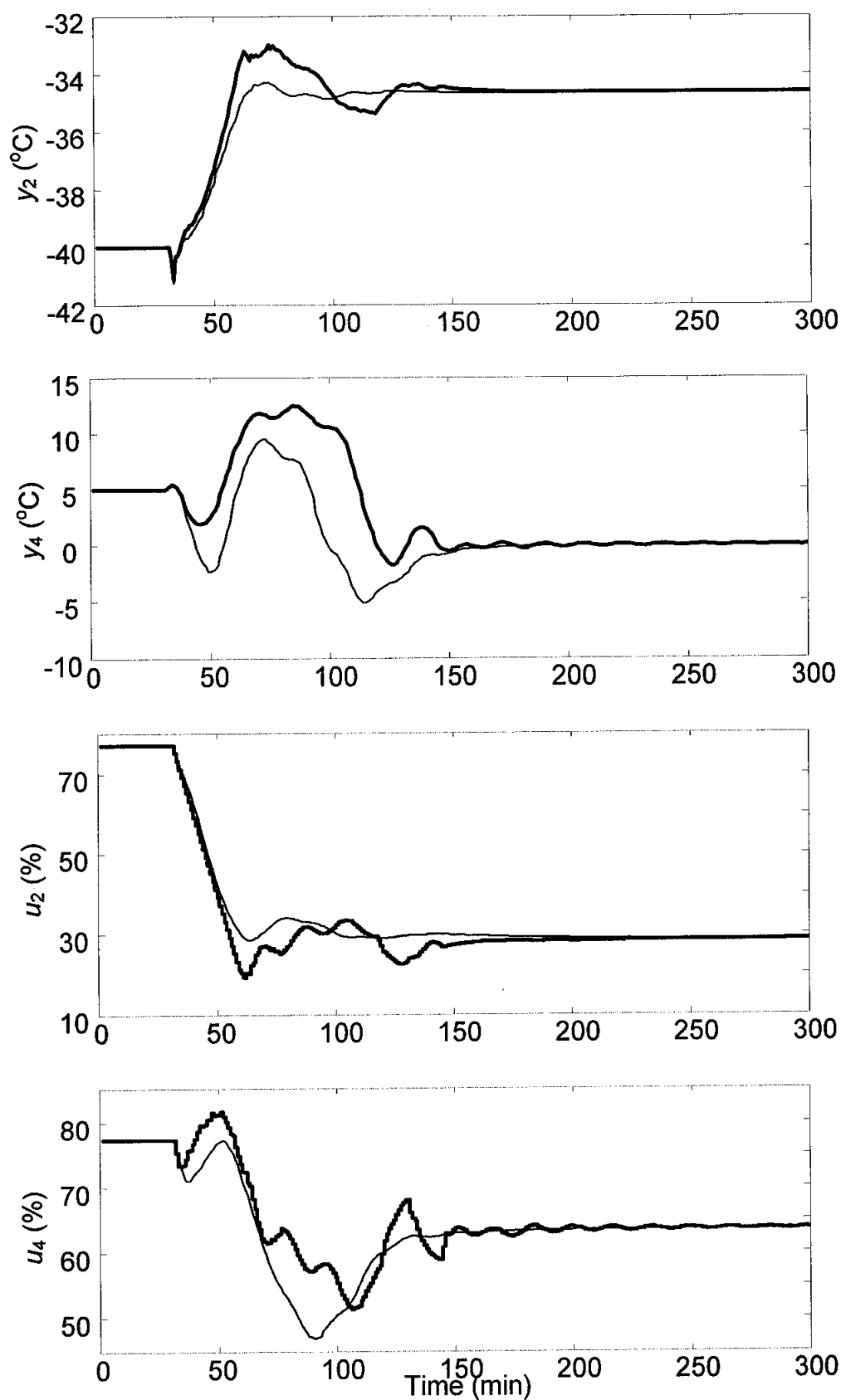


Figure B.4: Closed-loop responses of PI (thin line) and MPC (thick line) controllers on temperature of feed gas stream exiting cooler E-102 (y_2) and temperature of demethanizer C-101 tray 35 (y_4) for Cases D3 and D4 (integrated approach); E-102Q=cooler E-102 duty in %; E-104Q=reboiler E-104 duty in %

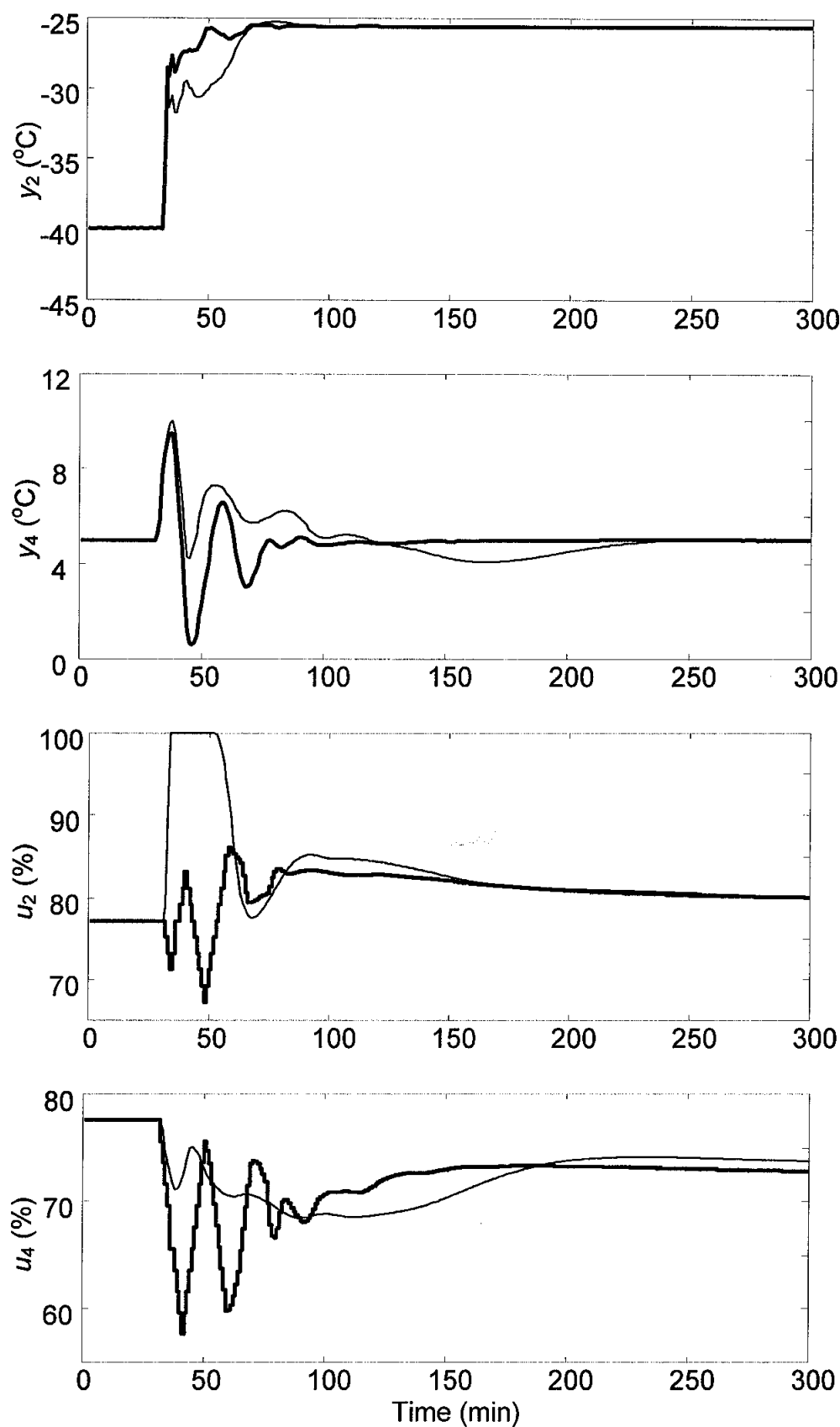


Figure B.5: Closed-loop responses of PI (thin line) and MPC (thick line) controllers on temperature of feed gas stream exiting cooler E-102 (y_2) and temperature of demethanizer C-101 tray 35 (y_4) for Cases E1 and E2 (scheduling only); u_2 =cooler E-102 duty in %; u_4 =reboiler E-104 duty in %

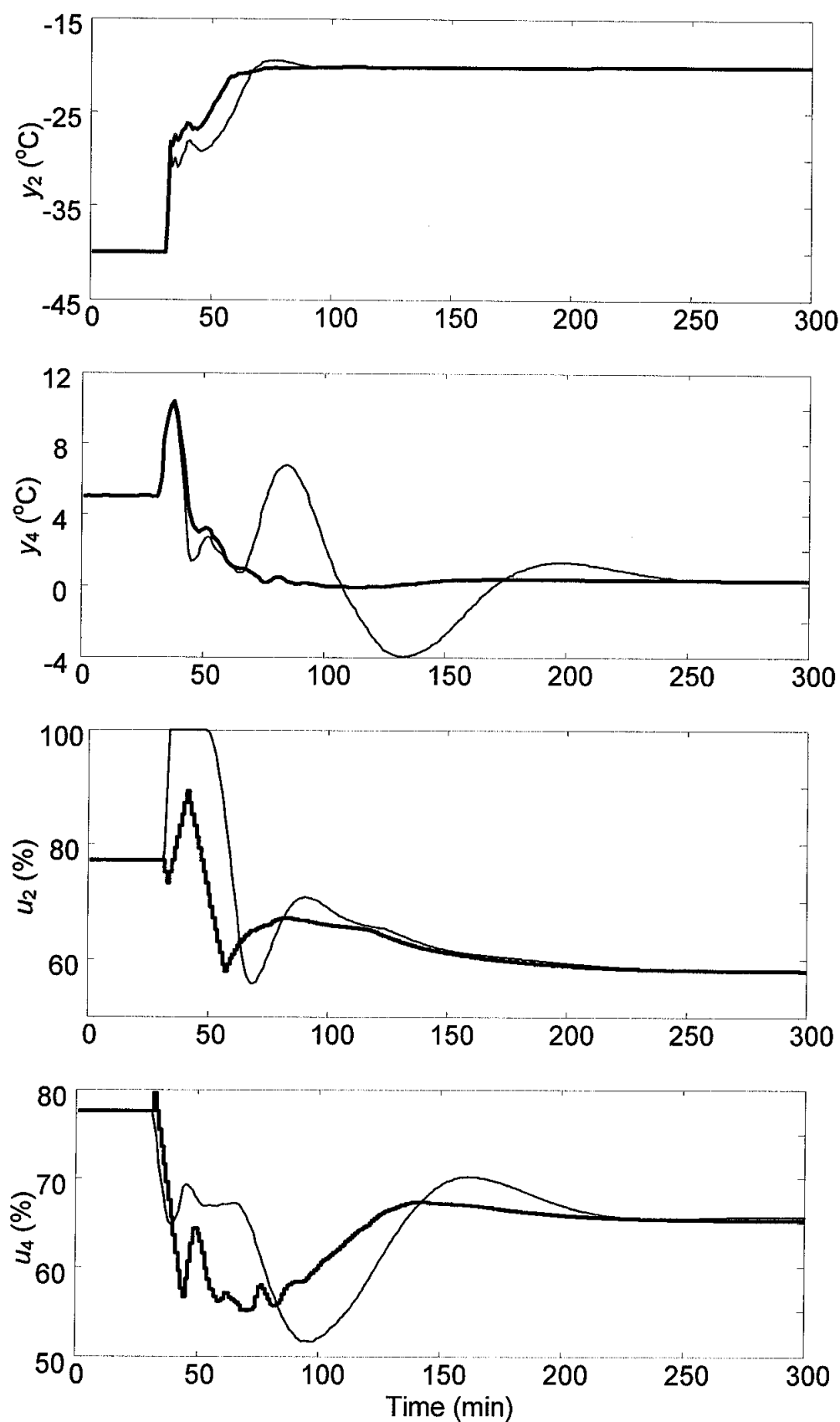


Figure B.6: Closed-loop responses of PI (thin line) and MPC (thick line) controllers on temperature of feed gas stream exiting cooler E-102 (y_2) and temperature of demethanizer C-101 tray 35 (y_4) for Cases E3 and E4 (integrated approach); u_2 =cooler E-102 duty in %; u_4 =reboiler E-104 duty in %

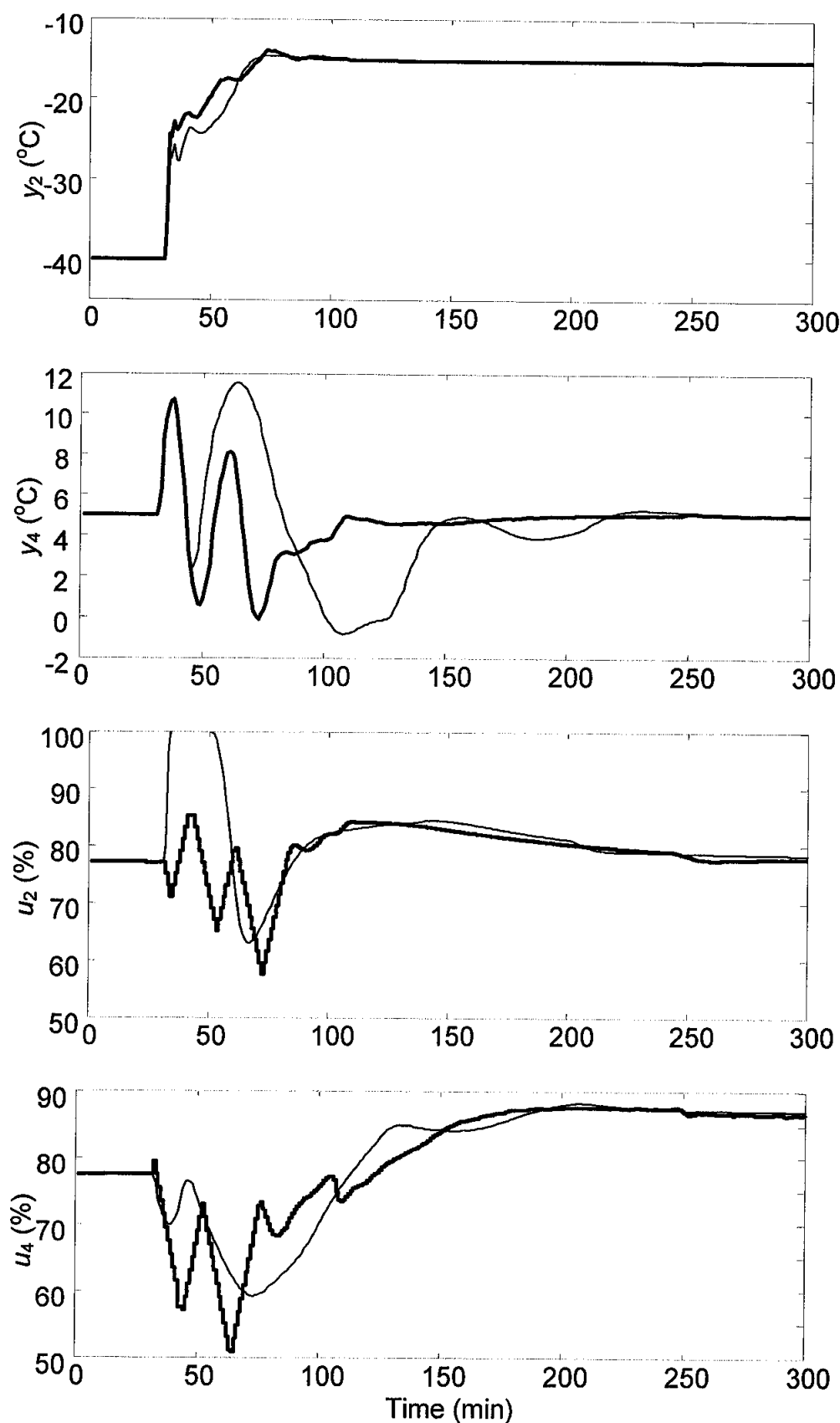


Figure B.7: Closed-loop responses of PI (thin line) and MPC (thick line) controllers on temperature of feed gas stream exiting cooler E-102 (y_2) and temperature of demethanizer C-101 tray 35 (y_4) for Cases F1 and F2 (scheduling only); E-102Q=cooler E-102 duty in %; E-104Q=reboiler E-104 duty in %

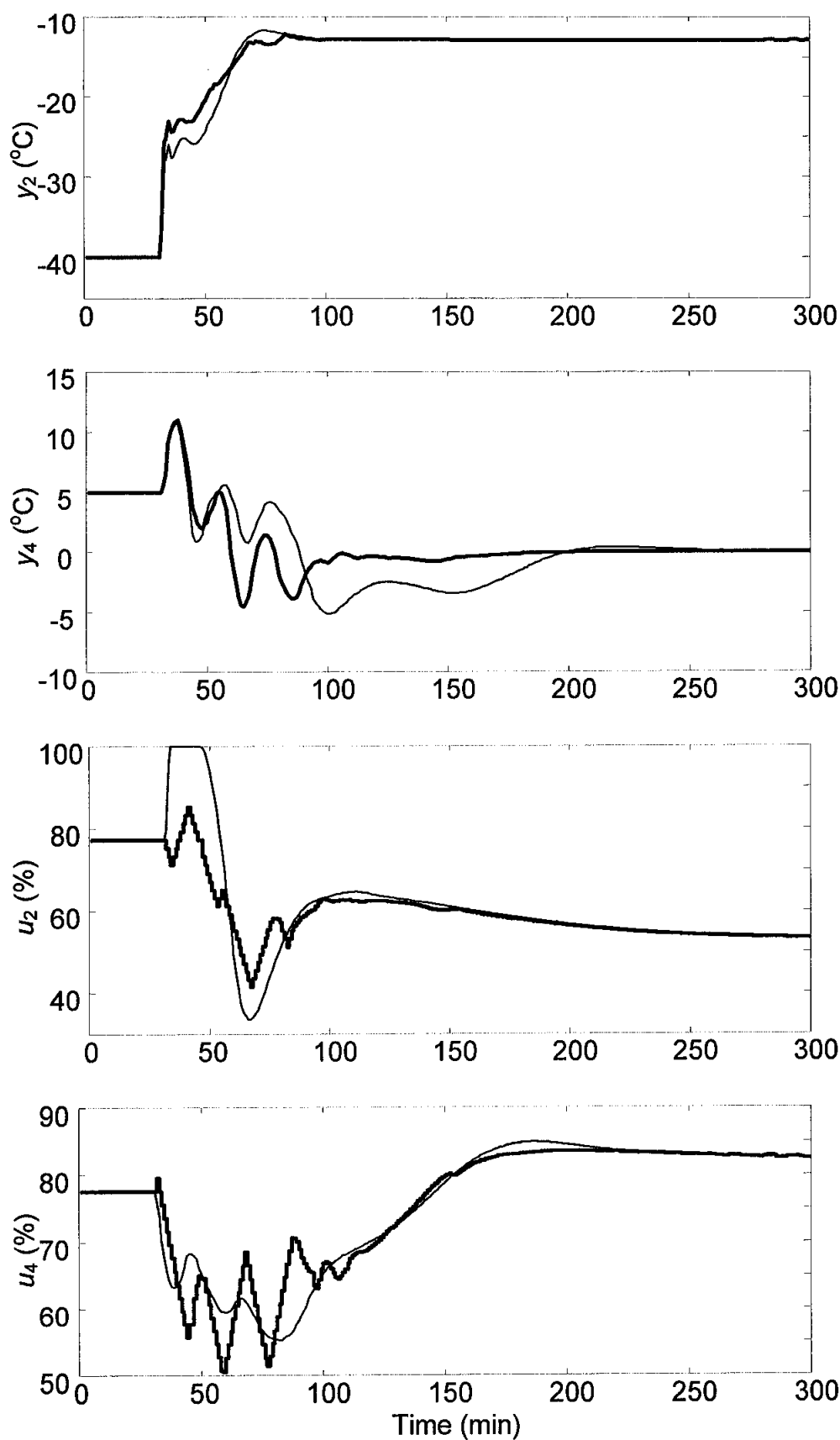
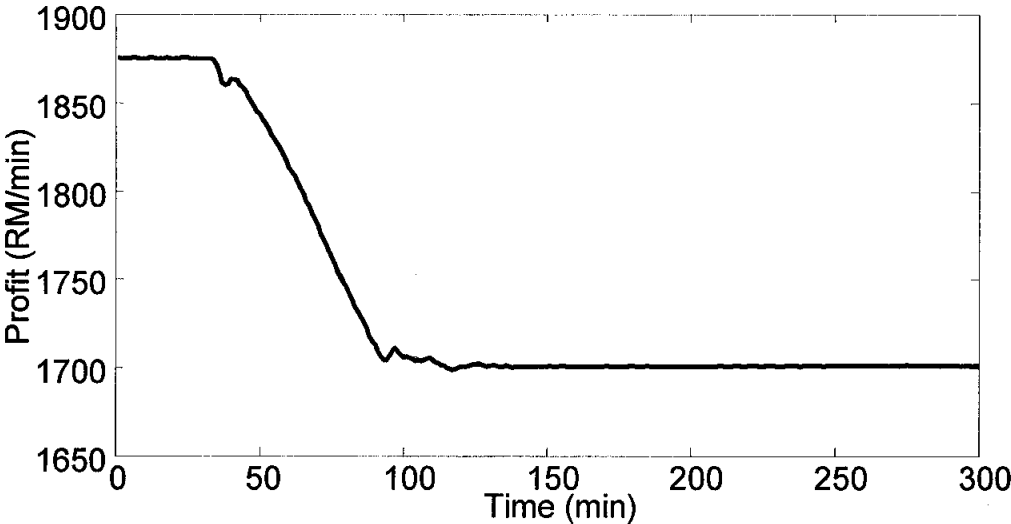
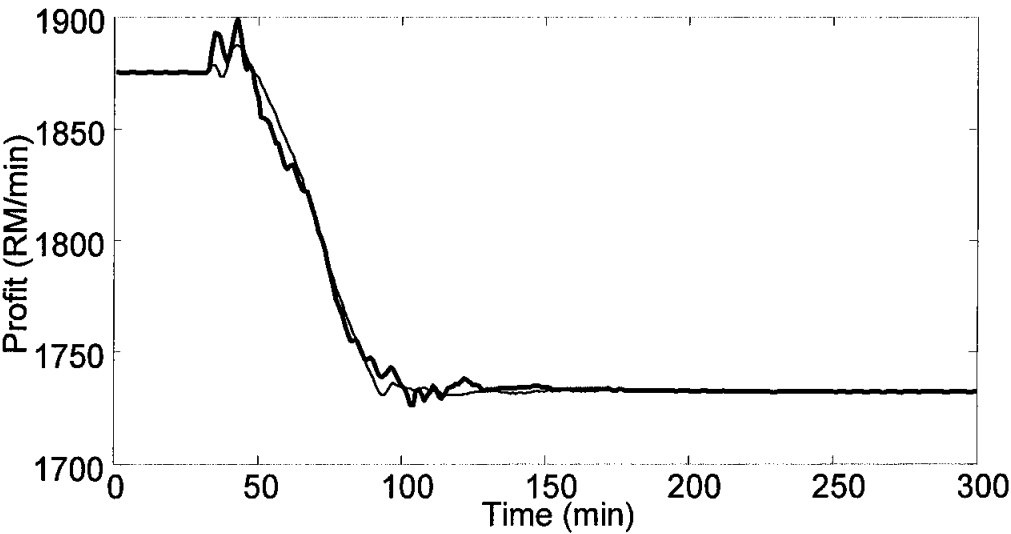


Figure B.8: Closed-loop responses of PI (thin line) and MPC (thick line) controllers on temperature of feed gas stream exiting cooler E-102 (y_2) and temperature of demethanizer C-101 tray 35 (y_4) for Cases F3 and F4 (integrated approach); E-102Q=cooler E-102 duty in %; E-104Q=reboiler E-104 duty in %

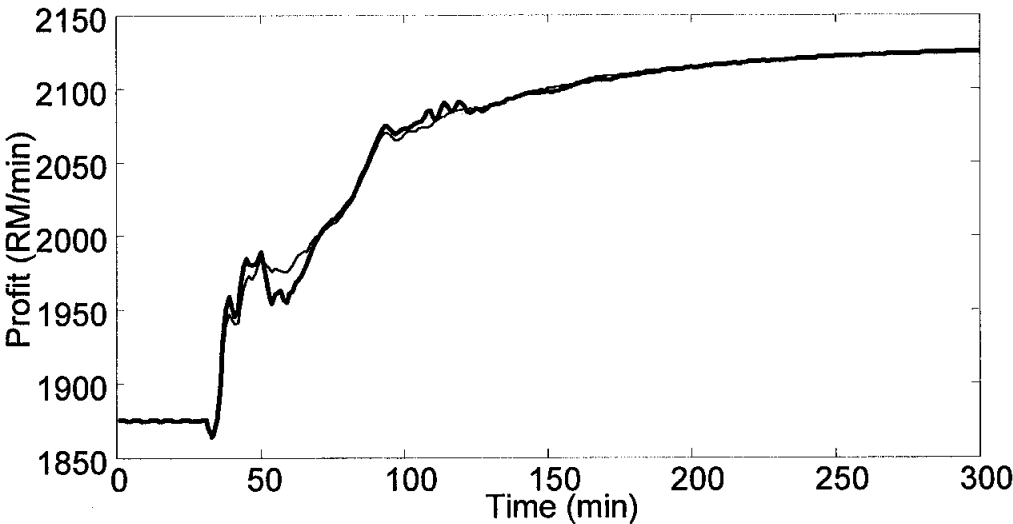


(a) Scheduling only – Case C1 (thin line) and Case C2 (thick line)

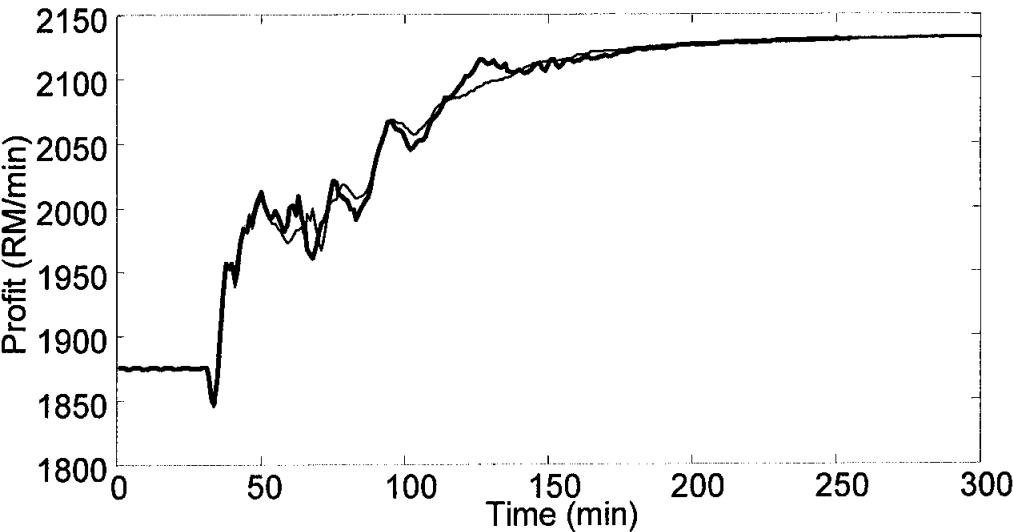


(b) Integrated approach – Case C3 (thin line) and Case C4 (thick line)

Figure B.9: Dynamic trajectories of RGP profit for Case C

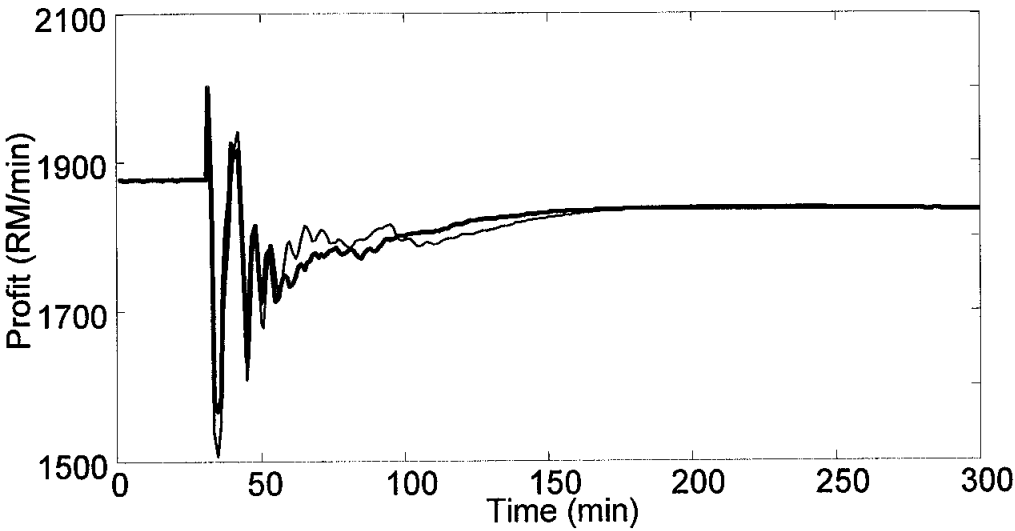


(a) Scheduling only – Case D1 (thin line) and Case D2 (thick line)

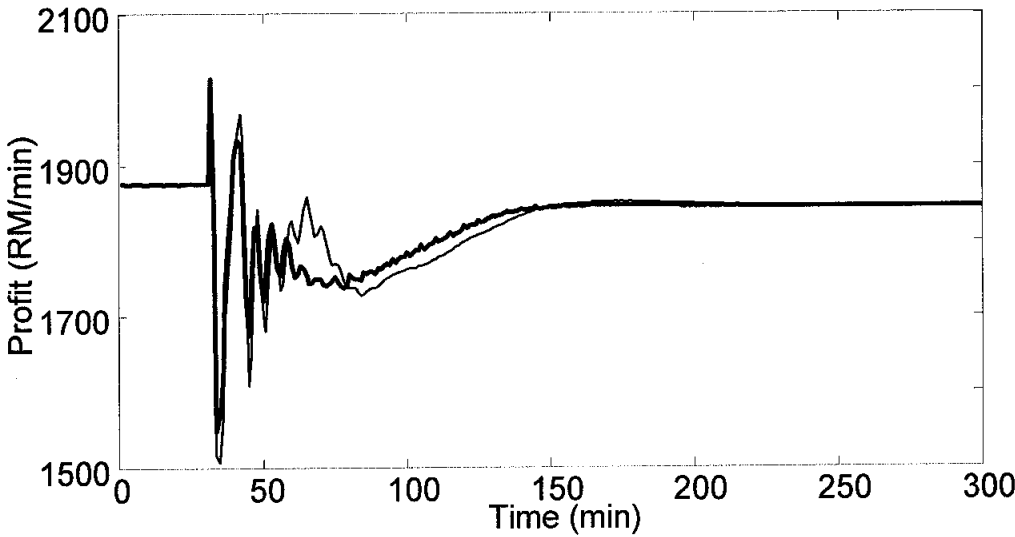


(b) Integrated approach – Case D3 (thin line) and Case D4 (thick line)

Figure B.10: Dynamic trajectories of RGP profit for Case D

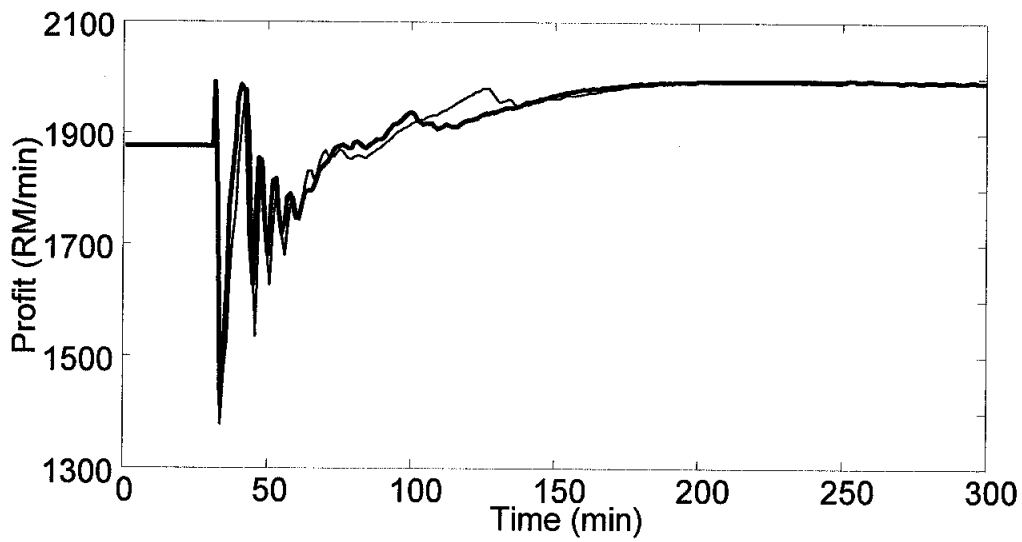


(a) Scheduling only – Case E1 (thin line) and Case E2 (thick line)

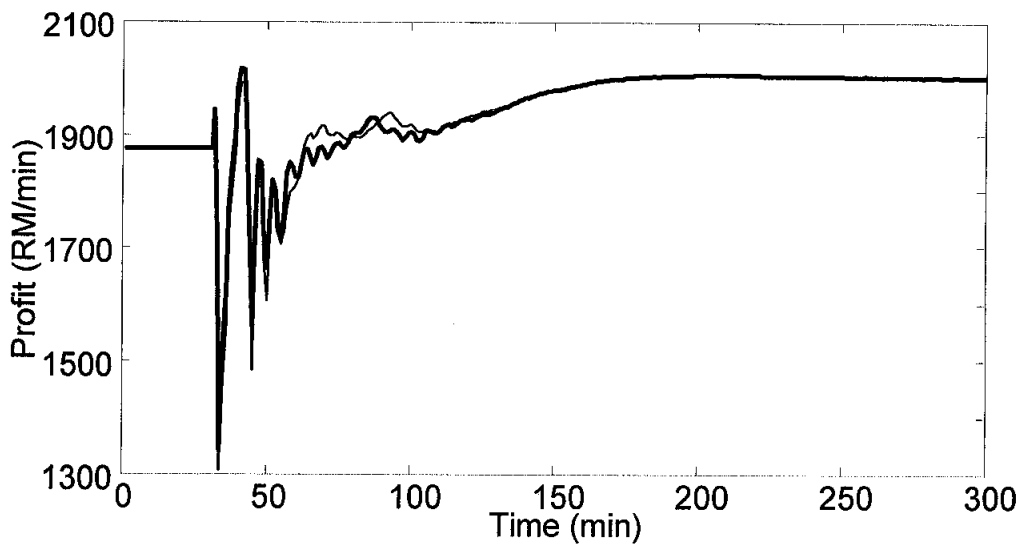


(b) Integrated approach – Case E3 (thin line) and Case E4 (thick line)

Figure B.11: Dynamic trajectories of RGP profit for Case E



(a) Scheduling only – Case F1 (thin line) and Case F2 (thick line)



(b) Integrated approach – Case F3 (thin line) and Case F4 (thick line)

Figure B.12: Dynamic trajectories of RGP profit for Case F

APPENDIX C

LIST OF PUBLICATIONS AND PRESENTATIONS

C.1 Journal

1. Yusoff N. and Ramasamy M. (2009). Integrated Scheduling and RTO of RGP with MPC and PI Controllers. *Journal of Applied Science*, 9 (17), 3027-3033, ISSN 1812-5654.
2. Yusoff N., Ramasamy M. and Yusup S. (2009). Parametric Design of RGP Optimization Variables using Taguchi Method. *Chemical Engineering Research and Design*. Submitted for publication.

C.2 Book Chapter

1. Yusoff N., Ramasamy M. and Yusup S. (2009). Profit Optimization of a Refrigerated Gas Plant. *Energy and Environment: Closing the Loop*, Universiti Malaysia Sarawak. *In press*, September 2009.

C.3 International Conference

1. Yusoff N. and Ramasamy M. (2009). Integrated Scheduling and RTO of RGP with MPC and PI Controllers. In the Proceedings of *International Conference on Chemical and Biochemical Process Engineering (ICCBPE)* in conjunction with *Symposium of Malaysian Chemical Engineers (SOMChE)*, Kota Kinabalu, Sabah, Malaysia. 12-14 August, 2009.
2. Yusoff N. and Ramasamy M. (2009). A Comparison between MPC and PI Controllers Acting on a Refrigerated Gas Plant. In the Proceedings of *International Conference on Control, Instrumentation and Mechatronic Engineering (CIM)*, Melaka, Malaysia, 2-3 June 2009. 470-475.
3. Yusoff N., Ramasamy M. and Yusup S. (2008). A Simulation Study on Dynamics and Control of a Refrigerated Gas Plant. In Proceedings of

International Conference on Foundation of Computer-Aided Process Operations (FOCAPO), Boston, Massachusetts, USA. 29 June – 2 July 2008. 263-266.

C.4 National Conference

1. Yusoff N., Ramasamy M. and Yusup S. (2007). Profit Optimization of a Refrigerated Gas Plant. In the Proceedings of *Engineering Conference on Energy & Environment (ENCON)*, Kuching, Sarawak, Malaysia. 27-28 December 2007.

C.5 Presentation

1. Yusoff N., Ramasamy M. and Yusup S. (2007). Dynamic Simulation and Control of a Gas Processing Plant. *PETRONAS Advanced Process Control Forum*, Kuala Lumpur, Malaysia. 17-18 December 2007.
2. Yusoff N. (2007). Improving GPP Production to Satisfy Power-Hungry Nations. *Shell Inter-Varsity Student Paper Presentation Contest*, Skudai, Johor, Malaysia. 3-4 March 2008.